Light-by-light scattering and muon's anomalous magnetic moment

Dissertation
zur Erlangung des Grades
„ Doktor der Naturwissenschaften “

am Fachbereich Physik, Mathematik und Informatik
der Johannes Gutenberg-Universität Mainz

vorgelegt von

Vladyslav Pauk

geboren in Khust (Ukraine)

Mainz, 2014

Abstract

A study of hadron production by photons opens unique ways to address a number of fundamental problems in strong interaction physics as well as fundamental questions in Quantum Field Theory. In particular, an understanding of two-photon processes is of crucial importance for constraining the hadronic uncertainties in precision measurements and in searches for new physics. The process of $\gamma^*\gamma^*$ fusion (by quasi-real photons γ or virtual photons γ^*) into leptons and hadrons has been observed and studied in detail at nearly all high-energy colliders. From the theoretical point of view two-photon processes are very complicated. One of approaches which may be efficiently used to study non-perturbative features of two-photon production is based on a dispersion theory. Using general properties of relativistic quantum field theory we relate in this work the forward light-by-light scattering to energy weighted integrals of the $\gamma^*\gamma$ fusion cross sections. The first type of new relations derived in this work have the form of exact super-convergence sum rules. The second type involves the effective constants of the low-energy photon-photon interaction and allow to define them in terms of two-photon production cross sections.

We subsequently test and verify these sum rules exactly at tree and one-loop level in scalar and spinor QED. Furthermore, we test the criterium of the tree-level unitarity imposed by the sum rules on the example of the massive spin-1 QED. Next, we apply the sum rules for the forward light-by-light scattering process within the context of the ϕ^4 quantum field theory. Within this theory, we present a stringent causality criterion and apply it to a particular non-perturbative resummation of graphs. Applied to the $\gamma^*\gamma$ production of mesons, the super-convergence sum rules lead to intricate relations between the $\gamma\gamma$ decay widths and the $\gamma^*\gamma$ transition form factors for (pseudo-) scalar, axial-vector and tensor mesons. We discuss the phenomenological implications of these results for mesons in both the light-quark sector and the charm-quark sector.

In the second part of this thesis we develop the formalism to provide an improved estimate for the hadronic light-by-light (HLbL) correction to the muon's anomalous magnetic moment a_μ, by considering single meson contributions beyond the leading pseudo-scalar mesons. This is motivated by the present 3σ deviation between the measurement of a_μ and its estimate in the Standard Model. Furthermore, a forthcoming new experiment at Fermilab aims to improve the experimental precision by a factor of 4 which also requires a similar theoretical improvement. We incorporate available experimental input as well as constraints from light-by-light scattering sum rules to estimate the effects of axial-vector, scalar, and tensor mesons. We give numerical evaluations for the HLbL contribution of these states to a_μ. The presented formalism allows to further improve on these estimates, once new data for such meson states will become available. In the last part of this work, we present a new dispersion formalism developed for the HLbL contribution to a_μ and test the formalism for the case of scalar field theory. The new framework opens a unique possibility for a consistent incorporation of data from e^+e^- colliders for single- as well as multi-meson contributions. Furthermore, it allows to systematically control the HLbL uncertainty in the a_μ which is a crucial step in searches of new physics using this precision quantity.

Zusammenfassung

Die Studie der Hadronproduktion in Photon induzierte Prozesse erlaubt es um eine Reihe fundamentaler Fragestellungen in der starken Wechselwirkung sowie allgemeine Fragen in der Quantenfeldtheorie zu untersuchen. Insbesondere sind die Photon-Photon induzierte Prozesse von wesentlicher Bedeutung um hadronische Korrekturen in Präzisionsmessungen und in der Suche nach neuer Physik jenseits des Standardmodells der Teilchenphysik zu bestimmen. Der Prozess der $\gamma^*\gamma^*$ Fusion durch quasi-reelle (γ) oder virtuelle (γ^*) Photonen in Leptonen und Hadronen wurde an fast allen Hochenergiebeschleunigern vermessen und untersucht. Eine theoretische Beschreibung der zwei-Photon Prozesse ist im allgemeinen kompliziert. Ein Zugang der benutzt werden kann um solche Prozesse im nicht-perturbativen Bereich der starken Wechselwirkung zu beschreiben basiert auf die Dispersionstheorie. Ausgehend von allgemeinen Eigenschaften der relativistischen Quantenfeldtheorie wird in dieser Arbeit die Licht-Licht Streuung in vorwärts Richtung verknüpft mit Integrale der $\gamma^*\gamma$ Fusionswirkungsquerschnitte. Es werden vorerst eine Reihe von superkonvergenz Summenregeln hergeleitet, sowie Summenregeln welche die Niederenergiekonstanten der $\gamma\gamma$ Wechselwirkung verknüpfen mit $\gamma\gamma$ Wirkunsgquerschnitten.

Die hergeleiteten Summenregeln werden in der Arbeit getestet für Baumgraphen sowie Einschleifengraphen in der skalaren und spinor Quantenelektrodynamik (QED), sowie am Beispiel der massiven Spin-1 QED. Im weiteren werden die Summenregeln für die vorwärts Licht-Licht Streuung angewandt im Rahmen der ϕ^4 Quantenfeldtheorie. Innerhalb dieser Theorie leiten wir ein Kausalitätskriterium her und wenden es auf eine nicht-perturbative Resummation von Graphen innerhalb dieser Theorie an. Wir zeigen dass als Folge solcher Resummation nicht-perturbative, gebundene Zustände dynamisch erzeugt werden. Angewandt auf die $\gamma^*\gamma$ Produktion von Mesonen, wird gezeigt dass die Summenregeln zu Beziehungen zwischen $\gamma\gamma$ Zerfallsbreiten und $\gamma^*\gamma$ Formfaktoren für pseudo-skalare, axiale, sowie tensor Mesonen führen. Die phänomenologische Relevanz dieser Resultate wird sowohl im leichten wie auch im Charm Quark Sektor diskutiert.

Im zweiten Teil der Arbeit wird der Formalismus entwickelt für eine verbesserte Abschätzung der hadronischen Licht-Licht Korrektur (HLbL) zum anomalen magnetischen Moment des Myons, a_μ. Wir betrachten dabei den Beitrag von Mesonen, über diesen der führenden pseudoskalare Mesonen hinaus. Dies ist motiviert durch die derzeitige 3σ Diskrepanz zwischen der direkten Messung von a_μ und seinen theoretischen Wert im Standardmodell. Eine neue Messung, die geplant ist am Fermilab um den experimentellen Wert von a_μ um ein Faktor 4 zu verbessern, motiviert auch eine verbesserte theoretische Beschreibung von a_μ, insbesondere der HLbL Korrektur. In den Abschätzungen in dieser Arbeit verwenden wir die verfügbaren Daten, sowie die Einschränkungen der hergeleiteten Summenregeln, um den Beitrag der axialen, skalaren, und tensor Mesonen zu a_μ zu bestimmen. Der hier hergeleitete Formalismus wird es auch erlauben um die Abschätzungen zu verbessern wenn neue Daten für solche Mesonen verfügbar werden. Im letzen Teil der Arbeit wird ein neuer Dispersionformalismus entwickelt für die HLbL Korrektur zu a_μ, und wird getestet am Beispiel der skalaren Feldtheorie. Dieser neue Formalismus öffnet die Möglichkeit um Daten von e^+e^- Beschleunigern konsistent zu benutzen in der Abschätzung der HLbL Korrektur zu a_μ, sowie um die systematische Unsicherheiten in a_μ besser zu kontrollieren, was wesentlich ist in der Suche nach neuer Physik in dieser Präzisionsgrösse.

Contents

Chapter 1

Introduction

With discovery of the electron in the end of the nineteenth century several new phenomenological disciplines, including physics of elementary particles as well as physics of atoms and nuclei were born. Early theoretical studies in these fields gave rise to the establishment of quantum mechanics and general relativity which allowed to successfully explain a vast range of microscopic phenomena within atomic and nuclear physics and laid the foundation of the theory of elementary particles. In the beginning of the twentieth century the known content of the microscopic world was very limited and the prevalent view was that the existing picture of the microscopic physics is complete. In 1930, Max Born, after learning of the Dirac equation, said, "Physics as we know it will be over in six months."

The discovery of new particles in cosmic rays marked the beginning of a new era in particle physics. This revelation unveiled the real complexity of the microscopic world and stimulated the development of particle accelerators. The progress on accelerator technology provided intense and controlled beams of particles with known energy which opened a wide spectrum of possibilities for systematic study of the microscopic physics and led to a plethora of fundamental discoveries and theoretical developments. The quark substructure of hadrons and the gauge nature of fundamental interactions were revealed and with the development of quantum field theory (QFT) in the 70's, the subject was put on a sound quantitative basis. The accumulated experimental information was embodied in the theoretical framework in the first complete phenomenological model of particles and fundamental interactions, the Standard Model (SM). It gave predictions and explanations of many fundamental effects which were successively confirmed in experiments, for a review, see [1] and references therein.

The continuous improvement of the theoretical and experimental tools deepened our understanding of the structure of matter and the laws it obeys at the microscopic level. We reached the scales where we can test very fine predictions of theory and tune its parameters to an unprecedented accuracy. This stimulates further improvement of the experimental techniques and construction of more and more advanced and sophisticated machines, accessing unprecedented scales. More than twenty years of work of over 10,000 scientists and engineers from over 100 countries, as well as hundreds of universities and laboratories, have finally been crowned with the creation of "one of the great engineering milestones of mankind" [2]: the Large Hadron Collider (LHC), a fascinating triumph of the forefront synergy between technology and science of nowadays. Being the highest-energy particle collider ever made, it allows us to get insight into the structure of matter to the depths which were formerly hard to conceive. Already after the first few years of operation, the machine justified the efforts put in its construction. It made possible an experimental discovery [3, 4] of the Higgs boson [5, 6, 7] and confirmation of the mechanisms of mass generation, a crucial constituent of the Standard Model. To make this discovery possible a huge amount of information at all-time high $7-8$ TeV center-of-mass energies equivalent to an integrated luminosity of about 12 fb^{-1} had to be collected and analyzed, which was unrealizable with previous facilities. To compare, the same luminosity was collected by its predecessor – Tevatron – during 26 years of operation. The high statistics reached by LHC is indispensable, as the processes with a direct involvement of the Higgs boson

are extremely rare compared to other background processes which makes it extremely difficult to detect. Remarkably, the first signs of the Higgs boson were observed in the two-photon decay process (Fig. 1.1). This occurrence may be attributed to the fact that though being electromagnetically suppressed compare to other channels, this process can be clearly separated from a large background originating from the strongly interacting particles. Being free from strong interactions, the two-photon channel is therefore of a crucial importance in present searches for new heavy particles, whose main interaction with the visible matter is through electromagnetic interaction (e.g. Dirac's monopoles, heavy leptons etc.). In addition, the energy and momentum of photons can be measured very precisely, giving an accurate reconstruction of the mass of the decaying particle. For these reasons photons perfectly match the role of a clean probe of strongly interacting systems and and hence provide an important tool for studying hadronic effects.

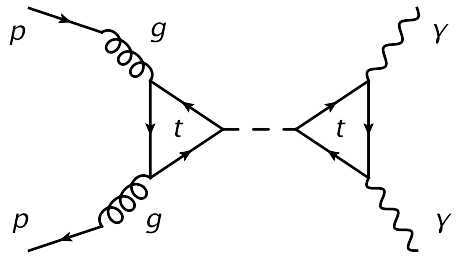

Figure 1.1: Feynman diagrams showing the cleanest channels associated with the low-mass, $\sim$ 125 GeV, Higgs candidate observed by ATLAS and CMS at the LHC. The dominant production mechanism at this mass involves two gluons from each proton fusing to a top-quark loop, which couples strongly to the Higgs field to produce a Higgs boson. It subsequently decays into 2γ ray photons by virtual interaction with a W boson loop or top-quark loop. Experimental analysis of this channel reached a significance of 5σ [3].

An early interest in the two-photon processes had risen after the discovery of the positron by Anderson in 1932 and experiments on fast particle interaction with matter [8]. There appeared to be a necessity to find out the process in which positrons are generated. Studying e^+e^- pair production in the collision of fast particles, Landau and Lifshitz [9] ascertained that, although being suppressed by four orders of the electromagnetic constant $\alpha = 1/137$, the two-photon channel is dominant for the experiments with colliding e^+e^- beams. With a subsequent development of e^+e^- colliders a study of this process gained a tremendous importance. The present interest in the two-photon production is due, first of all, to the study of the reaction $\gamma\gamma \to h$ (hadrons). The electromagnetic interaction provides a clean probe and the two-photon state allows to produce hadrons with nearly all quantum numbers (with $C = +1$, see Fig. 1.2), in contrast to the well studied single-photon scattering or production, which only accesses the vector states. A study of hadron production by photons opens unique ways towards the solutions of a number of fundamental problems in strong interaction physics and also fundamental questions in Quantum Electrodynamics (QED).

As we have already mentioned, another essential advantage of this process is the possibility of studying the reaction dependence on not only energy, but also on the "masses" of both colliding particles (photons). When producing exclusive final states such as in the $\gamma^*\gamma^* \to$ meson process, one accesses meson transition form factors (FFs), which are some of the simplest observables where the approach to the asymptotic limit of Quantum Chromodynamics (QCD) is studied along with the quark content of mesons described by distribution amplitudes (DAs). The non-perturbative dynamics of QCD is also playing a profound role in these FFs at low momentum

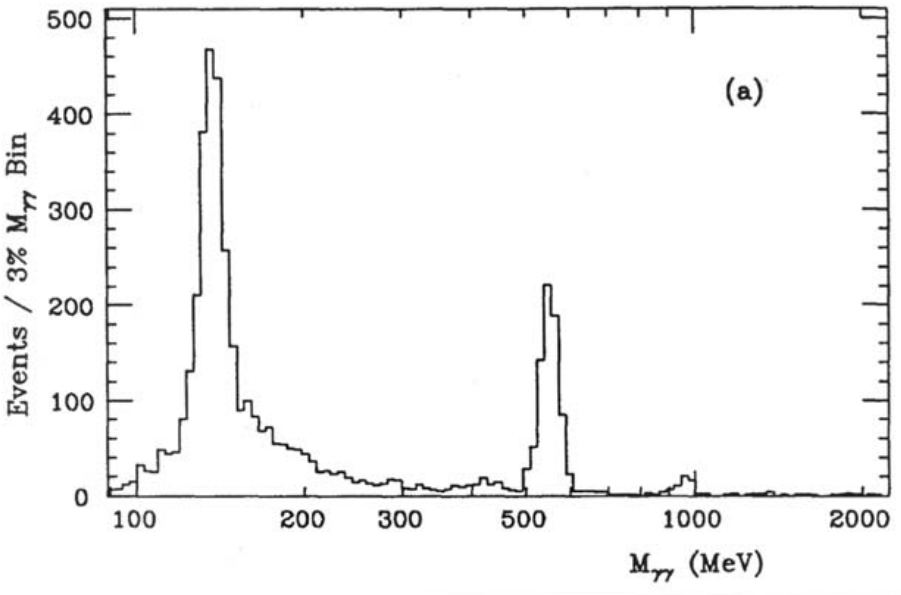

Figure 1.2: Fig. 3.6. The spectrum of invariant $\gamma\gamma$ masses obtained with the Crystal Ball detector [10, 11]. The three rather pronounced spikes seen are the $\gamma\gamma \to \mathcal{P}$ excitations. $\mathcal{P} = \pi^0, \eta, \eta'$

transfers. For example, the transition FFs of the η and η' mesons depend on the interplay of various symmetry breaking mechanisms in QCD, i.e.: $U_A(1)$ symmetry breaking [12], dynamical and explicit chiral symmetry breaking [13].

In recent years, new experiments at high luminosity e^+e^- colliders such as BABAR and Belle have vastly expanded the field of $\gamma\gamma$ physics. The result of a measurement of the $\gamma^*\gamma \to \pi^0$ FF at large momentum transfers by the BABAR Collaboration [14] came as a surprise, as this form factor seems to rise much faster than the perturbative QCD predictions for momentum transfers up to 40 GeV^2. A new $\gamma\gamma$ physics program is being realized now by the BES-III Collaboration [15]. It will yield high-statistics results at intermediate momentum transfers for a multitude of $\gamma^*\gamma^* \to$ hadron observables (see Chapter 2).

Despite the recent development in the two-photon phenomenology, our understanding of the hadronic production is still very limited. On the experimental side, only pseudo-scalar meson production was studied in detail in processes involving two quasi-real photons, or one real and one virtual photon (see [16] and references therein). Besides that, a very few measurements involving the axial-vector mesons were carried out. Finally, no measurements involving two virtual photons have so far been performed. On the theoretical side, a quantitative description of two-photon processes is presently available only in the asymptotic regimes of the process, where perturbative expansions hold. Some well studied approaches include expansions in the coupling constant (pQCD), low momenta (Chiral Perturbation Theory), heavy quark mass (HQFT) or the number of colors N_c. In the non-perturbative regime, very few model-dependent frameworks exist. A big disadvantage of model-dependent approaches is that, they do not allow for a systematic control of uncertainties unlike in perturbative expansions. Of course, lattice QCD provides ab initio calculation of hadron structure formulated within an Euclidian space-time framework. However, a general description of light-by-light processes on the lattice still entails a huge challenge at present. One of the very few model independent frameworks in the non-perturbative regime is provided by dispersion theory, which is based on fundamental principles of analyticity and unitarity.

In this work we use the dispersion theory to relate the two phenomena of the elastic scattering

of photons on photons (or light-by-light scattering (LbL))and $\gamma^*\gamma$ fusion, and express the low-energy LbL scattering as integrals over the $\gamma^*\gamma$-fusion cross sections, where one photon is real while the second may have arbitrary (space-like) virtuality. These integrals, or 'sum rules', lead to interesting constraints on $\gamma\gamma$ decay widths or $\gamma^*\gamma$ transition FFs of $q\bar{q}$ states, and more general meson states. The first sum rule of this type involves the helicity-difference cross-section for real photons and reads as:

$$\int_{s_0}^{\infty} \frac{ds}{s} \Big[\sigma_2(s) - \sigma_0(s)\Big] = 0, \tag{1.1}$$

where s is the total energy squared, s_0 is the first inelastic threshold for the $\gamma\gamma$ fusion process, and the subscripts 0 or 2 for the $\gamma\gamma$ cross sections indicate the total helicity of the state of two circularly polarized photons. This sum rule was originally[1] inferred [18, 19] from the the Gerasimov–Drell–Hearn (GDH) sum rule [20, 21], using the fact that the photon has no anomalous moments.

Parameterizing the lowest energy LbL interaction by means of an effective Lagrangian (which contains operators of dimension eight at lowest order) as

$$\mathcal{L}^{(8)} = c_1(F_{\mu\nu}F^{\mu\nu})^2 + c_2(F_{\mu\nu}\tilde{F}^{\mu\nu})^2, \tag{1.2}$$

with F and $\tilde{F}$ being the electromagnetic field strength and its dual, one finds sum rules for the LbL low-energy constants (LECs) [22]:

$$c_1 = \frac{1}{8\pi}\int_{s_0}^{\infty} \mathrm{d}s\, \frac{\sigma_{\parallel}(s)}{s^2}\,, \qquad c_2 = \frac{1}{8\pi}\int_{s_0}^{\infty} \mathrm{d}s\, \frac{\sigma_{\perp}(s)}{s^2}\,, \tag{1.3}$$

where the subscripts $\parallel$ or $\perp$ indicate if the colliding photons are polarized parallel or perpendicular to each other. While the GDH-type sum rule provides a stringent constraint on the polarized $\gamma\gamma$ fusion, the sum rules for the LECs allow one in principle to fully determine the low-energy LbL interaction through measuring the linearly polarized $\gamma\gamma$ fusion.

In Chapter 2 we will extend the GDH type sum rule to the case where one of the colliding photons is virtual, with an arbitrary (space-like) virtuality. Furthermore, we will find additional sum rules, involving the longitudinally polarized $\gamma^*\gamma$ cross sections. All the derived sum rules will be studied and verified in field theory and applied to the real process of $\gamma^*\gamma^*$ fusion to mesons in Chapter 3. Using the available data, we will quantitatively study the new sum rules for the case of production of light quark mesons as well as mesons containing charm quarks, both by real photons and by virtual photons.

There is another reason to investigate two-photon processes motivated by precision measurements. The idea of the latter approach is, instead of producing heavy particle directly in collisions, to measure a particular SM observable with very high precision. This allows to measure contributions from virtual processes with heavy particles by observing subtle deviations in the measured parameters. Historically, precision experiments provided the first direct tests of QFT and subsequently took their place among the key experimental approaches in particle physics. The simplest observables to study in the precision experiments are the static electromagnetic properties of charged particles. A big advantage of the electromagnetic phenomena

[1] An earlier version of this sum rule had been proposed in Ref. [17], where a contribution from π^0 production appears on the right-hand side (*rhs*) of Eq. (2.58), while integration on the *lhs* starts at the 2π production threshold. That version would be fully compatible with Eq. (2.58), if it were not for the sign of the π^0 contribution obtained in [17].

is that they may be successfully described by perturbation theory in the experimentally accessible region, and thus can be defined to needed accuracy. However, higher-order corrections to electroweak processes become contaminated by hadronic contributions as well. The hadronic corrections originate from the vacuum polarization effects which couple to QED diagrams via photons. In particular, leading two- (propagator of photon) and- four-photon (or light-by-light scattering) correlation functions play a key role in this context.

The most familiar and best studied electromagnetic property of particles is the magnetic dipole moment[2]. The magnetic moment is a quantity which is responsible for the interaction of a charged particle with the magnetic field. This interaction is defined by the Hamiltonian

$$\mathcal{H}_{\mathcal{I}} = -\boldsymbol{\mu} \cdot \mathbf{B}. \tag{1.4}$$

where μ denotes the magnetic moment operator and $\mathbf{B}$ states for the magnetic field strength. The magnetic moment of a particle is related to its spin similarly how the orbiting charge exhibits a magnetic dipole moment proportional to its orbital angular momentum:

$$\mu = g\, Q\, \mu_0\, \frac{\boldsymbol{\sigma}}{2}. \tag{1.5}$$

In the above equation $\boldsymbol{\sigma}$ is the Pauli matrix originating from the spin operator $\mathbf{S} = \hbar\,\boldsymbol{\sigma}/2$, Q is the electric charge in units of e and $\mu_0 = e\hbar/2mc$ is the Bohr magneton and g denotes the so-called gyromagnetic ratio (g-factor). The latter defines the absolute value of the magnetic moment and exhibits important information about the dynamics of leptons. For a free lepton the relativistic theory predicts $g = 2$, as was shown by Dirac in 1928 [25, 26]. However due to quantum fluctuations via virtual photon electron interactions the actual observable value deviates from the Dirac prediction. This deviation is defined as the anomalous magnetic moment

$$a_l = \frac{g-2}{2}. \tag{1.6}$$

In a local renormalizable relativistic quantum field theory $g-2$ vanishes at tree level and thus is not a renormalizable parameter. This implies that $g-2$ can be unambiguously prdicted in the theory and confronted with experiments. At the same time the anomalous magnetic moment is an observable which can be relatively easily observed experimentally from the motion of the lepton in an external magnetic field. These aspects of $g-2$ open a vast field for testing the SM predictions and searches for new physics. For the first time the precision determination was made for the anomalous moment of the electron, a_e. The electron is a stable particle and exists in atoms which opens a possibility to study it by atomic spectroscopy. The original precision measurement for a_e was performed by a study of the hyperfine-structure of atomic spectra in a constant magnetic field in 1948 [27]. This result had a tremendous significance verifying the prediction of the leading quantum correction $\alpha/2\pi$ (see Fig. 1.3) in the framework of newly-developed perturbative QFT made by Schwinger [28]. A continuous development of the experimental techniques over last 50 years resulted in a fascinating 10^6 fold improvement of the precision compared to the first experiments. At the present moment a_e is experimentally known to the accuracy of .66 parts per billion (ppb) supported by a profound theoretical understanding of the phenomenon.

The theoretical framework required to reach such accuracy becomes sensitive to suppressed higher order quantum corrections and requires a deep understanding of the microscopic processes. Despite the remarkable success of the Standard Model in a description of a wide range of phenomena, a number of observed discrepancies still remain unexplained. This arouses suspicion that the microscopic world is going beyond the known content. In light of existing

[2]Other exemples of properties studied in precision experiments are the weak mixing angle [23] and the proton charge radius [24].

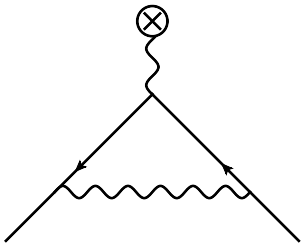

Figure 1.3: The leading one-loop correction to the magnetic moment of a lepton in QED.

experimental information it seems rather plausible that the expected new physics appears at scales sizably higher than what is reachable within the present hadron colliders. Compared to direct measurements, precision experiments allow to access much larger scales indirectly, by studying possible effects of new physics at the level of virtual quantum corrections. A special place in this field is assigned to the anomalous magnetic moment of the muon a_μ which is the main subject of the second part of this dissertation. It is one of the most precisely measured quantities in particle physics and has been playing a vital role in testing the framework of QFT since its development more than half a century ago, as well as in searching for new physics beyond the Standard Model, for a comprehensive review see [29] and references therein. A crucial distinction of the muon compared to the electron is its larger mass. In 1956 it was pointed out by Berestetskii et al. [30, 31] that the sensitivity of a_l to a heavy mass M scales as

$$\frac{\delta a_l}{a_l} \sim \frac{m_l^2}{M^2}, \tag{1.7}$$

where m_l and M are the masses of the lepton and the heavier SM particle or a hypothetical state beyond SM. It means that the effects of higher masses are magnified in a_μ relative to a_e by a factor $(m_\mu/m_e)^2 \sim 4 \times 10^4$, which makes it more suitable for testing of SM at small distances. Contrary to the electron, which is a stable particle on the Universe lifetime scale, the muon lives only 2.197×10^{-6} seconds which complicates its experimental studies. This problem is resolved by using highly relativistic muons in the storage ring which was realized at CERN [32] and BNL [33]. The present experimental world average for a_μ is [34, 33]:

$$a_\mu(\text{exp}) = (116\,592\,089 \pm 63) \times 10^{-11}, \tag{1.8}$$

which corresponds to a relative precision of 0.54 parts per million.

From the theoretical point of view, in the SM a_μ is defined by electromagnetic (QED), electroweak, and hadronic contributions. The dominant QED contribution, which at present has been calculated including all terms up to fifth-order in the fine structure constant [35, 36], is known to an impressive theoretical precision of $\delta a_\mu(\text{QED}) = 8 \times 10^{-13}$. The much smaller electroweak contribution, which has been calculated up to 2-loop order [37, 38, 39, 40], is also known with good accuracy $\delta a_\mu(\text{weak}) = 2 \times 10^{-11}$, which is more than a factor of 30 smaller than the present experimental precision. Within the Standard Model, the largest source of uncertainty is given by the hadronic contribution, which contains two parts: the hadronic vacuum polarization (HVP) and the hadronic light-by-light scattering (HLbL), see Fig. 1.4. The HVP has been estimated based on data for $e^+e^- \to$ hadrons, $e^+e^- \to \gamma +$ hadrons, as well as τ decays, by several groups [41, 42, 43, 44, 45, 46, 47, 48, 49, 50]. A recent evaluation of the leading order HVP has found [50] :

$$a_\mu(\text{l.o. HVP}) = (6886.0 \pm 42.4) \times 10^{-11}. \tag{1.9}$$

The next-to-leading order HVP has been estimated as [48]:

$$a_\mu(\text{n.l.o. HVP}) = (-98.4 \pm 0.7) \times 10^{-11}. \tag{1.10}$$

The HLbL, although much smaller in size than the HVP, has a similar theoretical uncertainty. It has been estimated by different groups as :

$$a_\mu(\text{HLbL}) = (116 \pm 39) \times 10^{-11} \qquad \text{Ref. [29]}, \tag{1.11}$$

$$a_\mu(\text{HLbL}) = (105 \pm 26) \times 10^{-11} \qquad \text{Ref. [51]}. \tag{1.12}$$

When comparing theory with experiment for a_μ, the difference has recently been evaluated as [50]

$$a_\mu(\text{exp}) - a_\mu(\text{theory}) = (312.5 \pm 57.6\,(\text{theory}) \pm 63\,(\text{exp})) \times 10^{-11}, \tag{1.13}$$

which corresponds with a 3.7σ discrepancy. The different analyses for the l.o. HVP and HLbL contributions, give results which all agree within 1σ [52].

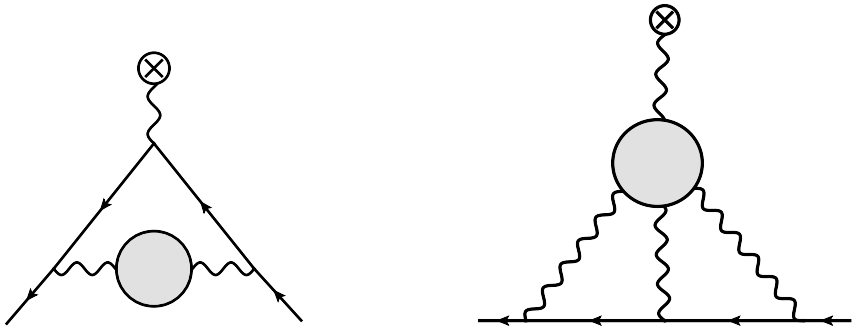

Figure 1.4: The hadronic contributions to the anomalous magnetic moment of the muon. Left panel: hadronic vacuum polarization (HVP). Right panel: hadronic light-by-light contribution (HLbL). The grey blobs denote hadronic intermediate states.

In order to conclude whether this discrepancy is a sign of new physics beyond the standard model, new experiments are planned in the near future both at Fermilab [53] as well as at J-PARC [54] to further improve on the precision. The Fermilab experiment aims to reduce the experimental uncertainty by a factor 4 to $\delta a_\mu \approx 16 \times 10^{-11}$. Such improvement also calls to improve on the theoretical accuracy by at least a factor of 2 in order to obtain a definitive test for the presently observed discrepancy. As the theoretical uncertainty is totally dominated by the knowledge of the HVP, Eq. (1.9), and the HLbL, Eq. (1.11), the main effort on the theoretical side will be to improve on both estimates. For the HVP, new data from ongoing experiments at Novosibirsk and BES-III will provide valuable experimental input to further constrain this contribution. It was estimated in Ref. [52] that such data will allow to reduce the uncertainty in the HVP to $\delta a_\mu(\text{l.o. HVP}) = 26 \times 10^{-11}$. For the HLbL scattering, new data are expected from KLOE-2 for the $\gamma^*\gamma \to \pi^0$ transition form factor at very low photon virtualities, and from BES-III for the reactions $\gamma^*\gamma \to X$, where $X = \pi^0, \eta, \eta', 2\pi$. Such data do require a theoretical analysis in order to further constrain the HLbL evaluation.

In Chapter 4 we provide an improved estimate for the HLbL contribution, by considering single meson contributions beyond the leading pseudo-scalar mesons (π^0, η, η') and incorporating available experimental input as well as constraints from light-by-light scattering sum rules [22, 55]. The framework which will be presented will also allow to further improve on the estimate, once new data, in particular from BES-III, for such meson states will become available. Subsequently in Chapter 5, we will present a new dispersion formalism developed for HLbL contribution to $(g-2)_\mu$. We will discuss the details of this approach and will see how it fundamentally affects the determination of the hadronic contributions to the anomalous magnetic moment of the muon. The new framework opens a possibility for a consistent incorporation of data from e^+e^- colliders and allows to systematically control the hadronic LbL uncertainty in the $(g-2)_\mu$.

Chapter 2

Two-photon physics and sum rules

The processes of $\gamma^*\gamma^*$ fusion (by quasi-real photons γ or virtual photons γ^*) into leptons and hadrons and two-photon decays have been observed at nearly all high-energy colliders. These processes are a rich source of information on strong interaction physics and are crucial for a number of fundamental questions in QED. On the other hand the light-by-light (LbL) elastic scattering which is a prediction of the quantum theory [56, 57] has thus-far not been directly observed, mainly due to smallness of the cross section. The two processes of elastic and inelastic photon-photon scattering can be related by dispersion relations giving a strict non-perturbative constraint on the energy behavior of the fusion cross-sections and the low-energy forward scattering amplitudes. To start with, we will discuss how the two-photon processes can be studied experimentally and review the methods for extracting information on the two-photon transition from experimental data. We will show how the transition amplitudes for single meson production can be phenomenologically described in terms of non-perturbative form factors, while the tensor structure can be fixed by the Lorentz invariance. The sum rules for light-by-light scattering involving the measurable correlation functions will be derived subsequently.

2.1 Experimental approaches in two-photon physics

The experimental studies of the electromagnetic decays of hadrons is complicated by the fact that being of higher orders in QED coupling constant these processes are suppressed. As a consequence, they have relatively low probability compare to the background, requiring very sensitive high-intensity experiments with simultaneous detection of all secondary decay products (both charged particles and γ quanta) for a reliable elimination of numerous background processes. Important information on the electromagnetic decay width and the transition form factors of some mesons has been obtained by studying such subtle effects as the production of particles in the Coulomb field of a nucleus (Primakoff effect) or in $\gamma\gamma$ collisions. In the first case experiments have to be conducted with very high energy primary beams of π and K mesons in order for the Coulomb processes to be reliably singled out. In the second case one needs high-energy high-luminosity e^+e^- colliding-beam storage rings. Another type of experiments which became feasible only relatively recently are hadronic decays to two photons and e^+e^- radiative annihilation production of hadrons. The two-photon radiative transitions to mesons have been widely studied in the past years. The formalism as well as the state-of-the-art of this work and a detailed bibliography are found in a number of review papers and conference talks (e.g., see [58, 16]), so that here we only very briefly touch on the relevant point.

The main object to study in these processes is the matrix element

$$\langle \gamma^*(q_1)\gamma^*(q_2)|X(p_X)\rangle \tag{2.1}$$

with $q_1 + q_2 = p_X$. Experimentally only the information for the on-shell mesons is available. It is not clear how to separate and to define the hadronic resonant states off their mass shell. At

the same time the virtualities of photons q_1^2 and q_2^2 may be varied depending on the set up of the experiment. Physically we can distinguish two regimes of the process depending on whether the photons' virtualities are space-like or time-like. There are several reasons for that. The main distinction between two regimes is that, as the virtuality of a photon q^2 increases in the region of space-like momentum the form factors decrease: if the momentum transfer is large, the virtual photon is sensitive only to the "inner part" of a hadron. Contrary to that in the time-like region we come across another phenomenon: the resonance interaction between photons and hadrons. The time-like domain includes the physical region of a single photon production, e.g. pair production $\gamma^* \to \pi^+\pi^-$. Therefore, the analytical structure of the corresponding matrix element possesses singularities and is substantially different from the space-like domain in this way. The second reason is that the two regimes are accessed experimentally in different processes. The time-like processes appear in a Dalitz decay and inclusive production where for the first case a meson decays to two-photons and in the second case an e^+e^- pair annihilates with emission of a time-like virtual photon which then creates a system of hadrons and a single photon. The processes involving space-like photons are studied in e^+e^- scattering and Primakoff reaction. Here the final state is produced by two virtual photons which are emitted by colliding leptons. Another process involving the two-photon-meson transition amplitude is a very rare direct dilepton decay $\pi^0 \to e^+e^-$. Two photons emitted in this process convert to a dilepton by lepton exchange, see Fig. 2.1 and Ref. [59]. The meson transition amplitude enters the corresponding "QED loop"; see, e.g., Ref. [60].

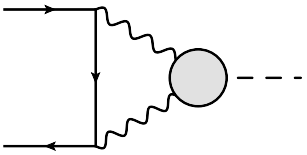

Figure 2.1: Dilepton rare decay of mesons.

As we already mentioned, the main fundamental distinction of the time-like processes is that they involve the physical processes of a single-photon production. In this case the photo-production amplitudes posses singularities in the complex Q^2-plane. In a widely used Vector Meson Dominance (VMD) approach and its modifications, the source of these singularities are intermediate vector states produced by virtual photons which then decay into hadrons, so-called hadronization of photons (Fig. 2.2). This regime is particularly involved in the dispersive analysis of the process, therefore is of a substantial importance, especially for the dispersion determination of $(g-2)_\mu$ where the hadronic light-by-light tensor is related by dispersion relations and unitarity to the meson transition amplitudes.

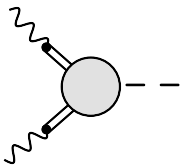

Figure 2.2: Two-photon production in the VMD model. The double lines represent the vector meson states.

In this thesis, we mostly pay attention to the processes involving a single meson which are also the best studied at the moment. The two-photon multi-hadron production has been studied at different facilities for the final states $\pi\pi$, 4π, 6π (for review see [61, 62, 63, 64], and references therein). At BES-III an extensive program underway to access these channels down

to threshold and for one or both virtual photons. These channels are both of importance for understanding non-perturbative regime of QCD and for determination of the hadronic LbL contribution to $(g-2)_\mu$, see [64, 29]. Including the multi-hadron states to the analysis is the logical continuation of the presented in this document work. In the following we discuss the details of the experimental observables and their relation to hadron transition amplitudes.

2.1.1 Electromagnetic decays of mesons.

In the direct detection of electromagnetic decays particles under study are produced either in hadron collisions or in electromagnetic interactions (meson photoproduction, their resonance production in e^+e^- colliding beams, etc.). As a rule to select rare electromagnetic decays it is necessary to detect all decay products – charged particles as well as photons – to measure their momenta and to reconstruct the effective mass of the decay particles. The kinematical constraints in this procedure are very important for the suppression of background processes.

When two real photons are detected, i.e. in process $\pi_0 \to 2\gamma$ one can measure the meson decay width. It is well described by the chiral anomaly encoded in the Wess-Zumino-Witten action, see, e.g., Refs. [65], [66]. The transition amplitudes as functions of the photons' four-momenta squared can be studied in the processes with the detection of the dilepton pair produced by a time-like virtual photon, i.e. in processes $\pi^0 \to \gamma e^+e^-$ and $\pi^0 \to e^+e^-e^+e^-$, as an illustration, see Fig. 2.3.

Figure 2.3: Single and double Dalitz decays. The momenta of the photons are q_1 and q_2

The momenta of the virtual photons q_1^2 and q_2^2 for the conversion (Dalitz) decays in Fig. 2.3, are equal to the invariant mass squared of the lepton-antilepton pair, and $m_M^2 \geqslant q_{1,2}^2 \geqslant 4m_l^2$ (time-like virtual photons). The amplitude of the single conversion decay of a pseudoscalar meson P (which is presently the only studied channel) is given by

$$M(P \to l^+l^-\gamma) = ieF_P(q_1^2, 0)\varepsilon_{\mu\nu\sigma\tau}\epsilon_1^\sigma \epsilon_2^\mu q_2^\nu \frac{1}{q_1^2}[\bar{u}\gamma^\tau u], \tag{2.2}$$

where $1/q_1^2$ is the photon propagator and the last term is the leptonic current. The function $F_P(q_1^2, q_2^2)$ is the form factor of a particle. The form factor characterizes the particle as an extended object. The analysis of the decays of mesons with spin is more complicated, although the pattern remains qualitatively the same. Now there are more configurations of the process allowed by the the angular momentum conservation which can be described by helicity amplitudes and cross sections. Each helicity amplitude has a spatial distribution which is characterized by its own form factor. For instance, a description of the two-photon transition of scalar mesons, which are spin-0 particles, requires two different form factors to be introduced. The form factors of higher spin mesons are currently measured only in two-photon fusion at e^+e^--colliders and will be discussed in detail further on.

Experimentally, the time-like form factor can be extracted from the $q^2 = q_1^2$ distribution given by

$$\mathrm{d}\Gamma(P \to l^+l^-\gamma) = \frac{2\alpha}{3\pi}\frac{1}{q^2}\sqrt{1-\frac{4m_l^2}{q^2}}\left(1+\frac{2m_l^2}{q^2}\right)\left(1-\frac{q^2}{M_P^2}\right)^3 |F_P(q^2,0)|^2 \tag{2.3}$$

It was measured mostly for η mesons at MAMI [67] and VEPP-2M [68] experiments. The example of the distribution for η Dalitz decay is presented in Fig. 2.4. The distributions for

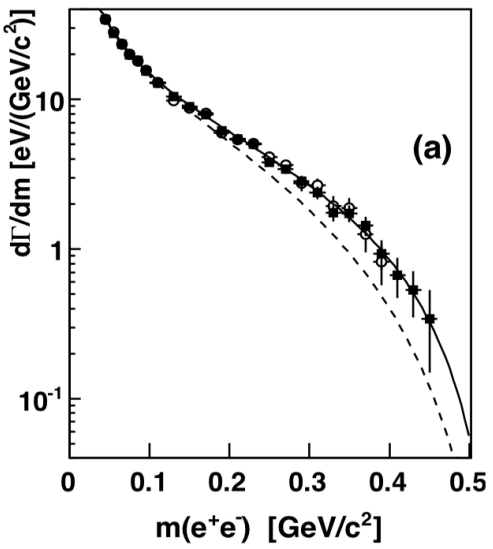

Figure 2.4: $\mathrm{d}\Gamma(\eta \to e^+e^-\gamma)/\mathrm{d}m(e^+e^-)$ distributions for the single Dalitz decays of the η meson (here $m^2 = q^2$) from [67]. The solid line corresponds to $\eta \to e^+e^-\gamma$ with $F_\eta(m^2, 0) = 1$; the dashed line shows the $\eta \to e^+e^-\gamma$ with the VMD form factor with $\Lambda^{-2} = 1.95\ GeV^{-2}$.

the $e^+e^-\gamma$ final states are peaked at $4m_l^2$ due to the $1/q^2$ QED term. The form factor can be obtained by dividing out the QED dependence (see Fig. 2.9 further on). To extract the form factor slope, a dependence on the q^2 variable is often fitted with a VMD inspired single-pole formula, which can be defined as follows:

$$F(q^2, 0) = \frac{\Lambda^2}{\Lambda^2 - q^2 - i\Gamma\Lambda}. \tag{2.4}$$

2.1.2 Two-photon production of mesons

Let us now consider the possibilities of studying the transition form factors of the neutral mesons in e^+e^- colliding beam experiments. These experiments can yield information on the form factors in a wider kinematic region in contrast to those on conversion decays. In addition, since in this case the dominant hadrons' coupling to leptons is via photons, a complicated question about the origin of the produced hadrons does not arise. In particular, while studying resonances no special hypothesis about the production mechanism would be necessary for separating a resonance from background are required as, e.g. in an analysis of πp collisions. The fact that there are no other hadrons but those produced by photons makes the interpretation of results transparent. All this makes electron colliding beams (e^+e^- or e^-e^-) the main instrument for the study of $\gamma\gamma \to h$ processes presently.

When studying two-photon processes at e^+e^--colliders the main research objects are the amplitudes for the $\gamma\gamma \to h$ process, for both space- and time-like off-mass shell as well as for almost real photons. The processes of main interest are the radiative one-photon annihilation

$e^+e^- \to h\gamma$ or $e^+e^- \to he^+e^-$ on Fig. 2.5 and the two-photon particle production $e^+e^- \to he^+e^-$ on Fig. 2.6.

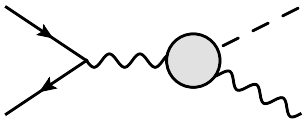

Figure 2.5: e^+e^- radiative one-photon annihilation.

We will firstly discuss the radiative annihilation process. It allows to study the process in the time-like region. In the process of the radiative one-photon annihilation the colliding leptons annihilate to a time-like virtual photon which than decays to a system of hadrons and a single virtual (real) photon. The information on $\gamma\gamma \to h$ reaction in the time-like region may be extracted from the measured cross section by

$$\sigma(e^+e^- \to h\gamma) = 4\pi\alpha\Gamma_{\gamma\gamma}\left(\frac{s-M^2}{sM}\right)^3 |F(q^2=s,0)|^2 \tag{2.5}$$

where all non-perturbative information is contained in the form factor F. The time-like data on the light pseudo-scalar meson transition form factors was measured by SND [68] and CMD-2 [69] collaborations and is summarized in Fig. 2.9.

The main two processes to study the two-photon production in a space-like region are e^+e^- and Primakoff effect Figs. 2.7 and 2.6. The Primakoff effect is the resonant production of neutral pseudoscalar mesons by high-energy photons interacting with an atomic nucleus. In the two-photon production two colliding leptons emit virtual photons which fuse to form a system of hadrons. The colliding photons are space-like and may have both a transverse polarization and a longitudinal one. The experiments can be carried out in the single-tag mode, i.e. by tagging one of the two scattered leptons at large polar angle and by requiring that the second is scattered at small polar angles or the double-tag mode when both leptons are detected. Only the single-tag mode has been realized so far and the double-tag experiments are planned in the nearest future, particularly at BES-III [15].

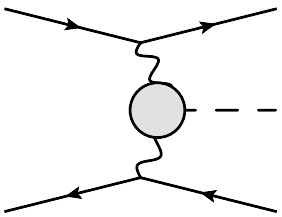

Figure 2.6: Two-photon production of hadrons.

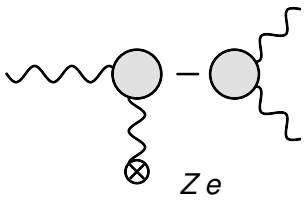

Figure 2.7: Two-photon production of hadrons in the heavy nucleus field (Primakoff effect).

The differential distributions of the process $e^+e^- \to e^+e^-X$ may be written in such a way that the contributions from vertices and transition amplitudes $\gamma\gamma \to h$ are factorized. When using two-photon production processes the main research objects are the amplitudes of the process

$$\gamma^*(\lambda_1, q_1) + \gamma^*(\lambda_2, q_2) \to \mathrm{X}(p_\mathrm{X}), \tag{2.6}$$

for the case of both off-shell photons as well as for almost real photons. Here the colliding photons with momenta q_1 and q_2 are space-like ($q_i^2 < 0$). The produced system X is C-even and its invariant mass is $s = (q_1 + q_2)^2$. The observed $e^+e^- \to e^+e^-X$ differential cross

section is expressed in terms of the off-shell $\gamma^*\gamma^* \to X$ helicity cross sections depending on the virtualities of photons q_1^2 and q_2^2 and a crossing invariant variable $\nu = (s - q_1^2 - q_2^2)/2$:

$$\begin{aligned} d\sigma = & \frac{\alpha^2}{16\pi^4\, Q_1^2\, Q_2^2}\, \frac{2\sqrt{X}}{s(1-4m^2/s)} \cdot \frac{d^3\vec{p}_1'}{E_1'} \cdot \frac{d^3\vec{p}_2'}{E_2'} \\ & \times \left\{ 4\,\rho_1^{++}\,\rho_2^{++}\,\sigma_{TT} + \rho_1^{00}\,\rho_2^{00}\,\sigma_{LL} + 2\,\rho_1^{++}\,\rho_2^{00}\,\sigma_{TL} + 2\,\rho_1^{00}\,\rho_2^{++}\,\sigma_{LT} \right. \\ & + 2\,\left(\rho_1^{++}-1\right)\,\left(\rho_2^{++}-1\right)\,\left(\cos 2\tilde{\phi}\right)\,\tau_{TT} \\ & + 8\,\left[\frac{\left(\rho_1^{00}+1\right)\,\left(\rho_2^{00}+1\right)}{\left(\rho_1^{++}-1\right)\,\left(\rho_2^{++}-1\right)}\right]^{1/2}\,\left(\cos\tilde{\phi}\right)\,\tau_{TL} \\ & + h_1 h_2\, 4\left[\left(\rho_1^{00}+1\right)\,\left(\rho_2^{00}+1\right)\right]^{1/2}\,\tau_{TT}^a \\ & \left. + \; h_1 h_2\, 8\left[\left(\rho_1^{++}-1\right)\,\left(\rho_2^{++}-1\right)\right]^{1/2}\,\left(\cos\tilde{\phi}\right)\,\tau_{TL}^a \right\}, \end{aligned} \tag{2.7}$$

here $h_1 = \pm 1$ and $h_2 = \pm 1$ are both lepton beam helicities and the kinematical factors ρ_i^{ab} are expressed in a known way in terms of the momenta p_i and q_i and are given in the Appendix. The cross sections denoted by $\sigma_0(\sigma_2)$ are the $\gamma^*\gamma^* \to$ X cross sections for total helicity 0 (2) respectively, and $\sigma_\parallel(\sigma_\perp)$ are the cross sections for linear photon polarizations with both photon polarization directions parallel (perpendicular) to each other respectively. The remaining cross sections (positive definite quantities σ) involve either two longitudinal photon polarizations σ_{LL}, or one transverse (T) and one longitudinal (L) photon polarization σ_{LT} and σ_{TL} related as :

$$\sigma_{LT}(\nu, Q_1^2, Q_2^2) = \sigma_{TL}(\nu, Q_2^2, Q_1^2). \tag{2.8}$$

Besides, the result involves four additional interfering terms $\tau_{TT}, \tau_{TT}^a, \tau_{TL}, \tau_{TL}^a$ (which are not sign-definite) with either both photons transverse (TT), or for one transverse and one longitudinal photon (TL), where the superscript a indicates the combinations which are odd in ν. For instance, the quantity τ_{TT} is the difference between cross sections for scattering transverse photons with linear polarizations: $\tau_{TT} = \sigma_\parallel - \sigma_\perp$. Analogously, the quantity τ_{TT}^a is the difference between the cross sections for scattering of transverse photons with circular polarizations $\tau_{TT}^a = \sigma_0 - \sigma_2$.

This quantities can be connected to the absorptive part of the $\gamma^*\gamma^* \to \gamma^*\gamma^*$ forward scattering amplitudes $M_{\lambda_1'\lambda_2',\lambda_1\lambda_2}$ and to the amplitudes $\mathcal{M}_{\lambda_1\lambda_2}$ of the $\gamma^*\gamma^* \to X$ transition. Denoting the absorptive part as

$$W_{\lambda_1'\lambda_2',\lambda_1\lambda_2} \equiv \mathrm{Abs}\, M_{\lambda_1'\lambda_2',\lambda_1\lambda_2}, \tag{2.9}$$

the optical theorem yields:

$$W_{\lambda_1'\lambda_2',\lambda_1\lambda_2} = \frac{1}{2}\int d\Gamma_{\mathrm{X}} (2\pi)^4 \delta^4(q_1 + q_2 - p_{\mathrm{X}})\, \mathcal{M}_{\lambda_1\lambda_2}(q_1, q_2; p_{\mathrm{X}})\, \mathcal{M}^*_{\lambda_1'\lambda_2'}(q_1, q_2; p_{\mathrm{X}}), \tag{2.10}$$

where $\mathcal{M}_{\lambda_1\lambda_2}(q_1, q_2; p_{\mathrm{X}})$ denotes the invariant amplitude for the process

$$\gamma^*(\lambda_1, q_1) + \gamma^*(\lambda_2, q_2) \to \mathrm{X}(p_{\mathrm{X}}). \tag{2.11}$$

As a result, the absorptive parts are related to eight independent $\gamma^*\gamma^* \to$ X cross sections by

the relations (see Ref. [58] for details):

$$W_{++,++} + W_{+-,+-} \equiv 2\sqrt{X}\,(\sigma_0 + \sigma_2) = 2\sqrt{X}\,\left(\sigma_\parallel + \sigma_\perp\right) \equiv 4\sqrt{X}\,\sigma_{TT}, \tag{2.12a}$$

$$W_{++,++} - W_{+-,+-} \equiv 2\sqrt{X}\,(\sigma_0 - \sigma_2) \equiv 4\sqrt{X}\,\tau^a_{TT}, \tag{2.12b}$$

$$W_{++,--} \equiv 2\sqrt{X}\,\left(\sigma_\parallel - \sigma_\perp\right) \equiv 2\sqrt{X}\,\tau_{TT}, \tag{2.12c}$$

$$W_{00,00} \equiv 2\sqrt{X}\,\sigma_{LL}, \tag{2.12d}$$

$$W_{+0,+0} \equiv 2\sqrt{X}\,\sigma_{TL}, \tag{2.12e}$$

$$W_{0+,0+} \equiv 2\sqrt{X}\,\sigma_{LT}, \tag{2.12f}$$

$$W_{++,00} + W_{0+,-0} \equiv 4\sqrt{X}\,\tau_{TL}, \tag{2.12g}$$

$$W_{++,00} - W_{0+,-0} \equiv 4\sqrt{X}\,\tau^a_{TL}, \tag{2.12h}$$

where the virtual photon flux factor is defined through

$$X \equiv (q_1 \cdot q_2)^2 - q_1^2 q_2^2 = \nu^2 - Q_1^2 Q_2^2. \tag{2.13}$$

The response functions extracted from differential distributions (2.3, 2.5, 2.7) allow to study meson transition amplitudes. The Lorentz structure of these amplitudes can in general be constructed on the basis of the relativistic invariance and the non-perturbative information can be isolated in the meson form factors. The general structure of these amplitudes is developed further.

2.2 Two-photon coupling to mesons

In this section we detail the formalism and the available data for the $\gamma^*\gamma^* \to$ meson transition form factors (FFs), and successively discuss the C-even pseudo-scalar ($J^{PC} = 0^{-+}$), scalar ($J^{PC} = 0^{++}$), axial-vector ($J^{PC} = 1^{++}$), and tensor ($J^{PC} = 2^{++}$) mesons.

2.2.1 Pseudo-scalar mesons

The process $\gamma^*(q_1, \lambda_1) + \gamma^*(q_2, \lambda_2) \to \mathcal{P}$, describing the transition from an initial state of two virtual photons, with four-momenta q_1, q_2 and helicities $\lambda_1, \lambda_2 = 0, \pm 1$, to a pseudo-scalar meson $\mathcal{P} = \pi^0, \eta, \eta', \eta_c, ...$ ($J^{PC} = 0^{-+}$) with mass m_P, is described by the matrix element :

$$\mathcal{M}(\lambda_1, \lambda_2) = -i\, e^2\, \varepsilon_{\mu\nu\alpha\beta}\, \varepsilon^\mu(q_1, \lambda_1)\, \varepsilon^\nu(q_2, \lambda_2)\, q_1^\alpha\, q_2^\beta\, F_{\mathcal{P}\gamma^*\gamma^*}(Q_1^2, Q_2^2), \tag{2.14}$$

where $\varepsilon^\alpha(q_1, \lambda_1)$ and $\varepsilon^\beta(q_2, \lambda_2)$ are the polarization vectors of the virtual photons, and where the meson structure information is encoded in the form factor (FF) $F_{\mathcal{P}\gamma^*\gamma^*}$, which is a function of the virtualities of both photons, satisfying $F_{\mathcal{P}\gamma^*\gamma^*}(Q_1^2, Q_2^2) = F_{\mathcal{P}\gamma^*\gamma^*}(Q_2^2, Q_1^2)$. From Eq. (2.14), one can easily deduce that the only non-zero $\gamma^*\gamma^* \to \mathcal{P}$ helicity amplitudes, which we define in the rest frame of the produced meson, are given by :

$$\mathcal{M}(\lambda_1 = +1, \lambda_2 = +1) = -\mathcal{M}(\lambda_1 = -1, \lambda_2 = -1) = -e^2\,\sqrt{X}\,F_{\mathcal{P}\gamma^*\gamma^*}(Q_1^2, Q_2^2)\,. \tag{2.15}$$

The FF at $Q_1^2 = Q_2^2 = 0$, $F_{\mathcal{P}\gamma^*\gamma^*}(0, 0)$, describes the two-photon decay width of the pseudo-scalar meson :

$$\Gamma_{\gamma\gamma}(\mathcal{P}) = \frac{\pi\alpha^2}{4}\, m_P^3\, |F_{\mathcal{P}\gamma^*\gamma^*}(0, 0)|^2, \tag{2.16}$$

with m_P the pseudo-scalar meson mass, and $\alpha = e^2/(4\pi) \simeq 1/137$.

In this document, we study the cross sections for one real photon and one virtual photon. For one real photon ($Q_2^2 = 0$), the only non-vanishing cross sections in Eq. (2.12) are given by :

$$\begin{aligned}[\sigma_0]_{Q_2^2=0} &= [\sigma_\perp]_{Q_2^2=0} = 2\,[\sigma_{TT}]_{Q_2^2=0} = -\,[\tau_{TT}]_{Q_2^2=0} \\ &= \delta(s-m_P^2)\,16\,\pi^2\,\frac{\Gamma_{\gamma\gamma}(\mathcal{P})}{m_P}\,\left(1+\frac{Q_1^2}{m_P^2}\right)\,\left[\frac{F_{\mathcal{P}\gamma^*\gamma^*}(Q_1^2,0)}{F_{\mathcal{P}\gamma^*\gamma^*}(0,0)}\right]^2 .\end{aligned} \tag{2.17}$$

For massless quarks, the divergence of the isovector axial current, $A_3^\mu \equiv \frac{1}{\sqrt{2}}(\bar{u}\gamma^\mu\gamma_5 u - \bar{d}\gamma^\mu\gamma_5 d)$, does not vanish but exhibits an anomaly due to the triangle graphs which allow the π^0 to couple to two vectors currents (Wess-Zumino-Witten anomaly). For the π^0, the chiral (isovector axial) anomaly, predicts that its transition FF at $Q_1^2 = Q_2^2 = 0$ is given by :

$$F_{\pi^0\gamma^*\gamma^*}(0,0) = \frac{1}{4\pi^2 f_\pi}, \tag{2.18}$$

where the pion decay constant f_π is defined through the isovector axial current matrix element :

$$\langle 0|A_3^\mu(0)|\pi^0(p)\rangle = i\,(\sqrt{2}\,f_\pi)\,p^\mu. \tag{2.19}$$

When using the current empirical value of the pion decay constant $f_\pi \simeq 92.4$ MeV to evaluate the chiral anomaly prediction of Eq. (2.18), one obtains the value $F_{\pi^0\gamma\gamma}(0,0) \simeq 0.274$ GeV^{-1}, which yields through Eq. (4.39) a 2γ decay width in very good agreement with the experimental value.

	Λ_P [MeV]
π^0	776 ± 22
η	774 ± 29
η'	859 ± 28
$\eta_c(1S)$	2920 ± 160

Table 2.1: Experimental extraction of the monopole mass parameter in the $\gamma^*\gamma \to \mathcal{P}$ form factors, according to the fit of Eq. (2.20). The measured value of Λ_P for $\mathcal{P} = \pi^0, \eta, \eta'$ is from the CLEO Collaboration [70]. For the $\eta_c(1S)$ state, the measured value is from the BABAR Collaboration [71].

Being the lowest excitations in the $\gamma\gamma$-production spectrum (Fig. 1.2) the three pseudo scalar mesons π, η, η' are the best studied channels in the $\gamma\gamma$ fusion process. The form factors $F_{\mathcal{P}\gamma^*\gamma^*}(Q_1^2,0)$ for one virtual photon and one real photon have been measured for π^0, η, η' by the CELLO [72] , CLEO [70], and BABAR [14, 73] Collaborations, and for $\eta_c(1S)$ by the BABAR Collaboration [71]. Available data on $F_{\pi\gamma^*\gamma^*}(Q_1^2,0)$ for low Q_1^2 values are presented in Fig. 2.8. For theoretical calculations of the pion form factor see, e.g., Refs. [74, 75, 76, 77] and references therein. The models either use strict vector meson dominance Ref. [78] , or, as, e.g., in Ref. [76], include point interactions in addition. For a review on vector mesons and their interactions, see also Ref. [79]. In the Q_1^2 range up to 10 GeV^2, a good parameterization of the data is obtained by the monopole form :

$$\frac{F_{\mathcal{P}\gamma^*\gamma^*}(Q_1^2,0)}{F_{\mathcal{P}\gamma^*\gamma^*}(0,0)} = \frac{1}{1+Q_1^2/\Lambda_P^2}, \tag{2.20}$$

where Λ_P is the monopole mass parameter. In Table 4.2, we show the experimental extraction of Λ_P for the π^0, η, η', and $\eta_c(1S)$ mesons.

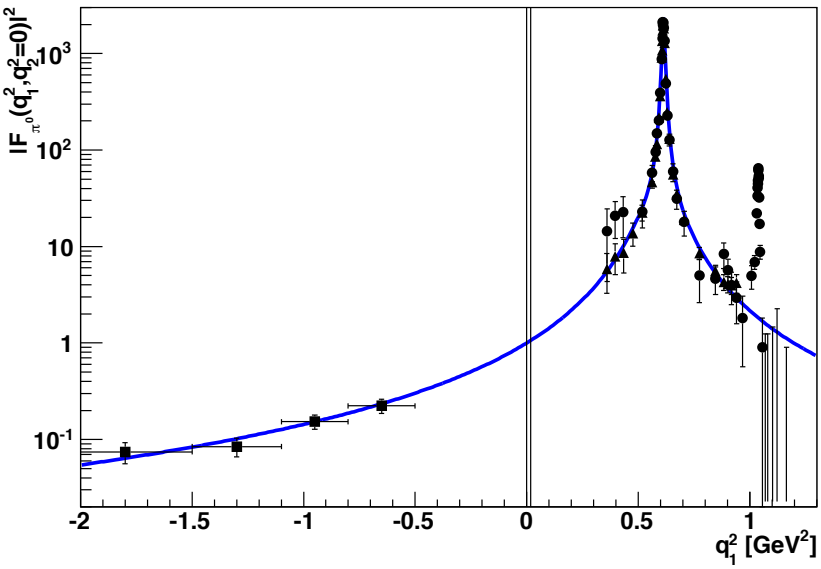

Figure 2.8: Single off-shell π^0 meson transition form factor in the low Q^2 region from SND [68] and CMD-2 [69] data on the reaction $e^+e^- \to \pi^0\gamma$ and CELLO data on the reaction $e^+e^- \to e^+e^-\gamma^*\gamma^* \to e^+e^-\pi^0$ [72]. Figure from Ref. [16].

Due to the approximate SU(3) flavor symmetry, the pion transition form factor is closely related to the corresponding transition form factor of the η meson and, via $\eta - \eta'$ mixing, also to the transition form factor of the η'. In fact, the whole discussion of $\eta - \eta'$ mixing, interesting in its own right, is strongly based on these transition form factors [80, 81, 82]. Both processes $\pi^0 \to \gamma\gamma^*$ and $\eta \to \gamma\gamma^*$ can be described by vector meson dominance [59]. For the η this is illustrated with the available low q^2 data on $F_\eta(q^2, 0)$ in Fig. 2.9. Note that this does not necessarily mean that the double-virtual processes $\pi^0/\eta \to \gamma^*\gamma^*$ would also be well described by vector meson dominance. Indeed, some theories show deviations [76, 83].

2.2.2 Scalar mesons

We next consider the process $\gamma^*(q_1, \lambda_1) + \gamma^*(q_2, \lambda_2) \to \mathcal{S}$, describing the transition from an initial state of two virtual photons, with four-momenta q_1, q_2 and helicities $\lambda_1, \lambda_2 = 0, \pm 1$, to a scalar meson $\mathcal{S}$ ($J^{PC} = 0^{++}$) with mass m_S. Scalar mesons can be produced either by two transverse photons or by two longitudinal photons [85, 86]. Therefore, the $\gamma^*\gamma^* \to \mathcal{S}$ transition can be described by the matrix element :

$$\begin{aligned}\mathcal{M}(\lambda_1, \lambda_2) = e^2\, \varepsilon^\mu(q_1, \lambda_1)\, \varepsilon^\nu(q_2, \lambda_2) \left(\frac{\nu}{m_S}\right) \Big\{ -R^{\mu\nu}(q_1, q_2) F^T_{\mathcal{S}\gamma^*\gamma^*}(Q_1^2, Q_2^2) \\ + \frac{\nu}{X} \left(q_1^\mu + \frac{Q_1^2}{\nu} q_2^\mu\right) \left(q_2^\nu + \frac{Q_2^2}{\nu} q_1^\nu\right) F^L_{\mathcal{S}\gamma^*\gamma^*}(Q_1^2, Q_2^2) \Big\},\end{aligned} \tag{2.21}$$

where we introduced the symmetric transverse tensor $R^{\mu\nu}$:

$$R^{\mu\nu}(q_1, q_2) \equiv -g^{\mu\nu} + \frac{1}{X} \left\{ \nu \left(q_1^\mu\, q_2^\nu + q_2^\mu\, q_1^\nu\right) + Q_1^2\, q_2^\mu\, q_2^\nu + Q_2^2\, q_1^\mu\, q_1^\nu \right\}, \tag{2.22}$$

which projects onto both transverse photons, having the properties :

$$\begin{aligned} q_{1\mu} R^{\mu\nu}(q_1, q_2) = 0, \quad q_{1\nu} R^{\mu\nu}(q_1, q_2) = 0, \\ q_{2\mu} R^{\mu\nu}(q_1, q_2) = 0, \quad q_{2\nu} R^{\mu\nu}(q_1, q_2) = 0. \end{aligned}$$

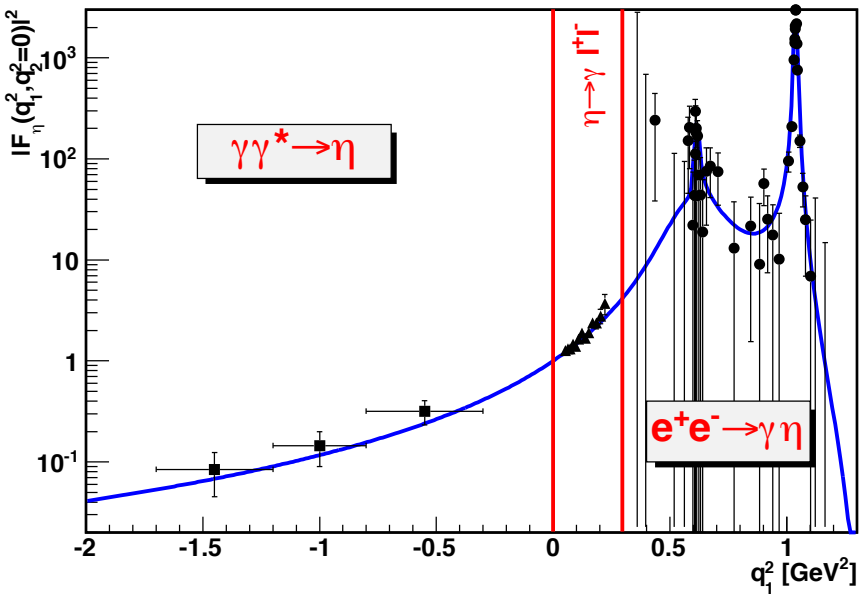

Figure 2.9: Figure 6: Single off-shell η meson transition form factor from NA60 data on $\eta \to \gamma\mu^+\mu^-$ decay [84]; from SND [68] and CMD-2 [69] data on the reaction $e^+e^- \to \eta\gamma$ reaction, and CELLO data on the reaction $e^+e^- \to e^+e^-\gamma^*\gamma^* \to e^+e^-\eta$ [72]. Figure from Ref. [16].

In Eq. (2.21), the scalar meson structure information is encoded in the form factors $F^T_{\mathcal{S}\gamma^*\gamma^*}$ and $F^L_{\mathcal{S}\gamma^*\gamma^*}$, which are a function of the virtualities of both photons, where the superscripts indicate the situation where either both photons are transverse (T) or longitudinal (L). Note that the pre-factor ν/m_S in Eq. (2.21) is chosen such that the FFs are dimensionless. Furthermore, both form factors are symmetric under interchange of both virtualities :

$$F^{T,L}_{\mathcal{S}\gamma^*\gamma^*}(Q_1^2, Q_2^2) \;=\; F^{T,L}_{\mathcal{S}\gamma^*\gamma^*}(Q_2^2, Q_1^2). \tag{2.23}$$

From Eq. (2.21), one can easily deduce that the only non-zero $\gamma^*\gamma^* \to \mathcal{S}$ helicity amplitudes are given by :

$$\begin{aligned} \mathcal{M}(\lambda_1 = +1, \lambda_2 = +1) \;&=\; \mathcal{M}(\lambda_1 = -1, \lambda_2 = -1) = e^2\,\frac{\nu}{m_S}\,F^T_{\mathcal{S}\gamma^*\gamma^*}(Q_1^2, Q_2^2)\,, \\ \mathcal{M}(\lambda_1 = 0, \lambda_2 = 0) \;&=\; -\,e^2\,\frac{Q_1 Q_2}{m_S}\,F^L_{\mathcal{S}\gamma^*\gamma^*}(Q_1^2, Q_2^2)\,. \end{aligned} \tag{2.24}$$

The transverse FF at $Q_1^2 = Q_2^2 = 0$, $F^T_{\mathcal{S}\gamma^*\gamma^*}(0,0)$, describes the two-photon decay width of the scalar meson :

$$\Gamma_{\gamma\gamma}(\mathcal{S}) = \frac{\pi\alpha^2}{4} m_S\,|F^T_{\mathcal{S}\gamma^*\gamma^*}(0,0)|^2. \tag{2.25}$$

In this paper, we study the sum rules involving cross sections for one real photon and one virtual photon. For one real photon ($Q_2^2 = 0$), the only non-vanishing cross sections in Eq. (2.12) are given by :

$$\begin{aligned} [\sigma_0]_{Q_2^2=0} &= \left[\sigma_{\|}\right]_{Q_2^2=0} = 2\,[\sigma_{TT}]_{Q_2^2=0} = [\tau_{TT}]_{Q_2^2=0} \\ &= \delta(s - m_S^2)\,16\,\pi^2\,\frac{\Gamma_{\gamma\gamma}(\mathcal{S})}{m_S}\left(1 + \frac{Q_1^2}{m_S^2}\right)\left[\frac{F^T_{\mathcal{S}\gamma^*\gamma^*}(Q_1^2, 0)}{F^T_{\mathcal{S}\gamma^*\gamma^*}(0,0)}\right]^2. \end{aligned} \tag{2.26}$$

Presently, there is no experimental data on scalar transition amplitudes. It is expected in the nearest future to measure these processes at BES III by an analysis of the $\gamma^*\gamma^* \to \pi\pi$ channels.

2.2.3 Axial-vector mesons

We next discuss the two-photon production of an axial vector meson. Due to the symmetry under rotational invariance, spatial inversion as well as the Bose symmetry of a state of two real photons, the production of a spin-1 resonance by two real photons is forbidden, which is known as the Landau-Yang theorem [87]. However the production of an axial-vector meson by two photons is possible when one or both photons are virtual. The matrix element for the process $\gamma^*(q_1,\lambda_1)+\gamma^*(q_2,\lambda_2) \to \mathcal{A}$, describing the transition from an initial state of two virtual photons, with four-momenta q_1, q_2 and helicities $\lambda_1, \lambda_2 = 0, \pm 1$, to an axial-vector meson $\mathcal{A}$ ($J^{PC} = 1^{++}$) with mass m_A and helicity $\Lambda = \pm 1, 0$ (defined along the direction of $\vec{q_1}$), is described by three structures [85, 86], and can be parameterized as :

$$\begin{aligned}\mathcal{M}(\lambda_1,\lambda_2;\Lambda) &= e^2\,\varepsilon_\mu(q_1,\lambda_1)\,\varepsilon_\nu(q_2,\lambda_2)\,\varepsilon^{\alpha *}(p_f,\Lambda) \\ &\times i\,\varepsilon_{\rho\sigma\tau\alpha}\left\{R^{\mu\rho}(q_1,q_2)R^{\nu\sigma}(q_1,q_2)\,(q_1-q_2)^\tau\,\frac{\nu}{m_A^2}\,F^{(0)}_{\mathcal{A}\gamma^*\gamma^*}(Q_1^2,Q_2^2)\right. \\ &+\,R^{\nu\rho}(q_1,q_2)\left(q_1^\mu+\frac{Q_1^2}{\nu}q_2^\mu\right)q_1^\sigma\,q_2^\tau\,\frac{1}{m_A^2}\,F^{(1)}_{\mathcal{A}\gamma^*\gamma^*}(Q_1^2,Q_2^2) \\ &\left.+\,R^{\mu\rho}(q_1,q_2)\left(q_2^\nu+\frac{Q_2^2}{\nu}q_1^\nu\right)q_2^\sigma\,q_1^\tau\,\frac{1}{m_A^2}\,F^{(1)}_{\mathcal{A}\gamma^*\gamma^*}(Q_2^2,Q_1^2)\right\}. \qquad (2.27)\end{aligned}$$

In Eq. (2.27), the axial-vector meson structure information is encoded in the form factors $F^{(0)}_{\mathcal{A}\gamma^*\gamma^*}$ and $F^{(1)}_{\mathcal{A}\gamma^*\gamma^*}$, where the superscript indicates the helicity state of the axial-vector meson. Note that only transverse photons give a non-zero transition to a state of helicity zero. The form factors are functions of the virtualities of both photons, and $F^{(0)}_{\mathcal{A}\gamma^*\gamma^*}$ is symmetric under the interchange $Q_1^2 \leftrightarrow Q_2^2$. In contrast, $F^{(1)}_{\mathcal{A}\gamma^*\gamma^*}$ does not need to be symmetric under interchange of both virtualities, as can be seen from Eq. (2.27).

From Eq. (2.27), one can easily deduce that the only non-zero $\gamma^*\gamma^* \to \mathcal{A}$ helicity amplitudes are given by :

$$\begin{aligned}\mathcal{M}(\lambda_1=+1,\lambda_2=+1;\Lambda=0) &= -\mathcal{M}(\lambda_1=-1,\lambda_2=-1;\Lambda=0) \qquad (2.28)\\ &= e^2\,(Q_1^2-Q_2^2)\,\frac{\nu}{m_A^3}\,F^{(0,T)}_{\mathcal{A}\gamma^*\gamma^*}(Q_1^2,Q_2^2)\,,\end{aligned}$$

$$\mathcal{M}(\lambda_1=0,\lambda_2=+1;\Lambda=-1) = -\,e^2\,Q_1\left(\frac{X}{\nu m_A^2}\right)F^{(1)}_{\mathcal{A}\gamma^*\gamma^*}(Q_1^2,Q_2^2)\,, \qquad (2.29)$$

$$\mathcal{M}(\lambda_1=-1,\lambda_2=0;\Lambda=-1) = -\,e^2\,Q_2\left(\frac{X}{\nu m_A^2}\right)F^{(1)}_{\mathcal{A}\gamma^*\gamma^*}(Q_2^2,Q_1^2)\,. \qquad (2.30)$$

Note that the helicity amplitude with two transverse photons vanishes when both photons are real, in accordance with the Landau-Yang theorem.

The matrix element $F^{(1)}_{\mathcal{A}\gamma^*\gamma}(0,0)$ allows to define an equivalent two-photon decay width for an axial-vector meson to decay in one quasi-real longitudinal photon and a (transverse) real

photon as [1]:

$$\tilde{\Gamma}_{\gamma\gamma}(\mathcal{A}) \equiv \lim_{Q_1^2\to 0} \frac{m_A^2}{Q_1^2}\frac{1}{2}\Gamma\left(\mathcal{A}\to\gamma_L^*\gamma_T\right) = \frac{\pi\alpha^2}{4}\, m_A\, \frac{1}{3}\left[F^{(1)}_{\mathcal{A}\gamma^*\gamma^*}(0,0)\right]^2, \tag{2.31}$$

where we have introduced the decay width $\Gamma\left(\mathcal{A}\to\gamma_L^*\gamma_T\right)$ for an axial-vector meson to decay in a virtual longitudinal photon, with virtuality Q_1^2, and a real transverse photon ($Q_2^2=0$), as :

$$\Gamma\left(\mathcal{A}\to\gamma_L^*\gamma_T\right) = \frac{\pi\alpha^2}{2}\, m_A\, \frac{1}{3}\,\frac{Q_1^2}{m_A^2}\,\left(1+\frac{Q_1^2}{m_A^2}\right)^3\,\left[F^{(1)}_{\mathcal{A}\gamma^*\gamma^*}(Q_1^2,0)\right]^2. \tag{2.32}$$

In this work, we will study the sum rules involving cross sections for one real photon and one virtual photon. For one quasi-real photon ($Q_2^2\to 0$), we can obtain from the above helicity amplitudes and using Eq. (2.10) the axial-vector meson contributions to the response functions of Eq. (2.12) as :

$$\begin{aligned}[\sigma_0]_{Q_2^2=0} &= [\sigma_\perp]_{Q_2^2=0} = 2\,[\sigma_{TT}]_{Q_2^2=0} = -\,[\tau_{TT}]_{Q_2^2=0} \\ &= \delta(s-m_A^2)\,4\,\pi^3\alpha^2\,\frac{Q_1^4}{m_A^4}\left(1+\frac{Q_1^2}{m_A^2}\right)\left[F^{(0)}_{\mathcal{A}\gamma^*\gamma^*}(Q_1^2,0)\right]^2,\end{aligned} \tag{2.33}$$

$$[\sigma_{LT}]_{Q_2^2=0} = \delta(s-m_A^2)\,16\,\pi^2\,\frac{3\,\tilde{\Gamma}_{\gamma\gamma}(\mathcal{A})}{m_A}\,\frac{Q_1^2}{m_A^2}\left(1+\frac{Q_1^2}{m_A^2}\right)\left[\frac{F^{(1)}_{\mathcal{A}\gamma^*\gamma^*}(Q_1^2,0)}{F^{(1)}_{\mathcal{A}\gamma^*\gamma^*}(0,0)}\right]^2, \tag{2.34}$$

$$\begin{aligned}[\tau_{TL}]_{Q_2^2=0} &= -\,[\tau^a_{TL}]_{Q_2^2=0} = \delta(s-m_A^2)\,8\,\pi^2\,\frac{3\,\tilde{\Gamma}_{\gamma\gamma}(\mathcal{A})}{m_A}\,\frac{Q_1Q_2}{m_A^2} \\ &\times\left(1+\frac{Q_1^2}{m_A^2}\right)\left[\frac{F^{(1)}_{\mathcal{A}\gamma^*\gamma^*}(Q_1^2,0)}{F^{(1)}_{\mathcal{A}\gamma^*\gamma^*}(0,0)}\cdot\frac{F^{(1)}_{\mathcal{A}\gamma^*\gamma^*}(0,Q_1^2)}{F^{(1)}_{\mathcal{A}\gamma^*\gamma^*}(0,0)}\right].\end{aligned} \tag{2.35}$$

Extracting the FFs $F^{(1)}$, and $F^{(0)}$ separately from experiment requires the measurements of σ_{LT} and σ_{TT} respectively. As experiments to date have not achieved this separation, one is so far only sensitive to the quantity $\sigma_{TT}+\varepsilon_1\,\sigma_{LT}$, where ε_1 is a kinematical parameter (so-called virtual photon polarization parameter) defined as $\varepsilon_1\equiv\rho_1^{00}/2\rho_1^{++}$, see Appendix A. Note that in high-energy collider experiments, one typically has $\varepsilon_1\approx 1$. From Eq. (2.35) one then obtains for this experimentally accessible combination :

$$\begin{aligned}\left[\sigma_{LT}\left(1+\frac{1}{\varepsilon_1}\frac{\sigma_{TT}}{\sigma_{LT}}\right)\right]_{Q_2^2=0} &= \delta(s-m_A^2)\,16\,\pi^2\,\frac{3\,\tilde{\Gamma}_{\gamma\gamma}(\mathcal{A})}{m_A}\,\frac{Q_1^2}{m_A^2}\left(1+\frac{Q_1^2}{m_A^2}\right) \\ &\times\left(\left[\frac{F^{(1)}_{\mathcal{A}\gamma^*\gamma^*}(Q_1^2,0)}{F^{(1)}_{\mathcal{A}\gamma^*\gamma^*}(0,0)}\right]^2+\frac{1}{\varepsilon_1}\,\frac{Q_1^2}{2\,m_A^2}\left[\frac{F^{(0)}_{\mathcal{A}\gamma^*\gamma^*}(Q_1^2,0)}{F^{(1)}_{\mathcal{A}\gamma^*\gamma^*}(0,0)}\right]^2\right),\end{aligned} \tag{2.36}$$

We can compare the above general formalism for the two-photon production of an axial-vector meson with the description of Ref. [90], which is commonly used in the literature, and is based on a non-relativistic quark model calculation leading to only one independent amplitude for the $\gamma^*\gamma^*\to\mathcal{A}$ process as :

$$\mathcal{M}(\lambda_1,\lambda_2;\Lambda) = \quad e^2\,\varepsilon^\mu(q_1,\lambda_1)\,\varepsilon^\nu(q_2,\lambda_2)\,\varepsilon^{\alpha *}(p_f,\Lambda)\;i\varepsilon_{\mu\nu\tau\alpha}\,\left(-Q_1^2\,q_2^\tau+Q_2^2\,q_1^\tau\right)\,A(Q_1^2,Q_2^2), \tag{2.37}$$

[1] In defining the equivalent two-photon decay width for an axial-vector meson, we follow the convention of Ref. [86], which is also followed in experimental analyses [88, 89]. Note however that the definition for $\tilde{\Gamma}_{\gamma\gamma}$ adopted here is one half of that used in Ref. [90].

where the independent form factor A satisfies : $A(Q_1^2, Q_2^2) = A(Q_2^2, Q_1^2)$. In such a non-relativistic quark model limit, we can recover Eq. (2.37) from Eq. (2.27) through the identifications :

$$\begin{aligned} F^{(0)}(Q_1^2, Q_2^2) &= m_A^2\, A(Q_1^2, Q_2^2), \\ F^{(1)}(Q_1^2, Q_2^2) &= -\frac{\nu}{X}(\nu + Q_2^2)\, m_A^2\, A(Q_1^2, Q_2^2), \\ F^{(1)}(Q_2^2, Q_1^2) &= -\frac{\nu}{X}(\nu + Q_1^2)\, m_A^2\, A(Q_1^2, Q_2^2), \end{aligned} \tag{2.38}$$

in which $2\nu = m_A^2 + Q_1^2 + Q_2^2$. In such model, the experimentally measured two-photon cross section combination of Eq. (2.36), where $Q_2^2 = 0$, is proportional to :

$$\begin{aligned} \left[\sigma_{LT}\left(1 + \frac{1}{\varepsilon_1}\frac{\sigma_{TT}}{\sigma_{LT}}\right)\right]_{Q_2^2=0} &= \delta(s - m_A^2)\, 16\,\pi^2\, \frac{3\,\tilde{\Gamma}_{\gamma\gamma}(\mathcal{A})}{m_A}\, \frac{Q_1^2}{m_A^2} \\ &\times \left(1 + \frac{Q_1^2}{m_A^2}\right)\left(1 + \frac{1}{\varepsilon_1}\,\frac{Q_1^2}{2\,m_A^2}\right)\left[\frac{A(Q_1^2, 0)}{A(0,0)}\right]^2 . \end{aligned} \tag{2.39}$$

To apply this formula to experimental results where the axial-vector meson has a finite width, one commonly replaces the delta-function in Eq. (2.39) by a Breit-Wigner form, yielding :

$$\begin{aligned} \left[\sigma_{LT}\left(1 + \frac{1}{\varepsilon_1}\frac{\sigma_{TT}}{\sigma_{LT}}\right)\right]_{Q_2^2=0} &= 48\,\pi\, \frac{\tilde{\Gamma}_{\gamma\gamma}(\mathcal{A})\,\Gamma_{total}}{(s - m_A^2)^2 + m_A^2\,\Gamma_{total}^2}\, \frac{Q_1^2}{m_A^2} \\ &\times \left(1 + \frac{Q_1^2}{m_A^2}\right)\left(1 + \frac{1}{\varepsilon_1}\,\frac{Q_1^2}{2\,m_A^2}\right)\left[\frac{A(Q_1^2, 0)}{A(0,0)}\right]^2 , \end{aligned} \tag{2.40}$$

where Γ_{total} is the total decay width of the axial-vector meson.

Phenomenologically, the two-photon production cross sections have been measured for the two lowest lying axial-vector mesons : $f_1(1285)$ and $f_1(1420)$. The most recent measurements were performed by the L3 Collaboration [88, 89] (Fig. 2.10).

In those works, the non-relativistic quark model expression of Eq. (2.40) in terms of a single FF A has been assumed, and the resulting FF has been parameterized by a dipole :

$$\frac{A(Q_1^2, 0)}{A(0,0)} = \frac{1}{\left(1 + Q_1^2/\Lambda_A^2\right)^2}\,, \tag{2.41}$$

where Λ_A is a dipole mass. By fitting the resulting expression of Eq. (2.40) to experiment (for which $\varepsilon_1 \approx 1$, and for a Q_1^2 range which extends up to 6 GeV^2), one can then extract the parameters $\tilde{\Gamma}_{\gamma\gamma}$ and Λ_A. Table 4.3 shows the present experimental status of the equivalent 2γ decay widths of the axial-vector mesons $f_1(1285)$, and $f_1(1420)$, which we use in this work.

2.2.4 Tensor mesons

The process $\gamma^*(q_1, \lambda_1) + \gamma^*(q_2, \lambda_2) \to \mathcal{T}(\Lambda)$, describing the transition from an initial state of two virtual photons to a tensor meson $\mathcal{T}$ ($J^{PC} = 2^{++}$) with mass m_T and helicity $\Lambda = \pm 2, \pm 1, 0$ (defined along the direction of $\vec{q}_1$), is described by five independent structures [85, 86], and can

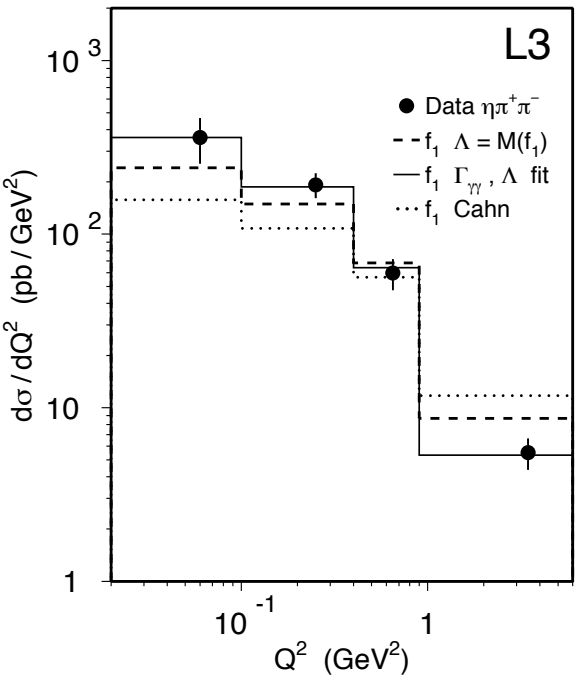

Figure 2.10: Experimental differential cross section $\mathrm{d}\sigma/Q^2$ compared to calculations of the GaGaRes Monte Carlo (dashed line) and to the calculations of [90] and [91] (dotted line). The full line is a fit of the data with the GaGaRes model, with Λ and $\tilde{\Gamma}_{\gamma\gamma}$ as free parameters. Figure from Ref. [88]

be parameterized as :

$$
\begin{aligned}
\mathcal{M}(\lambda_1,\lambda_2;\Lambda) &= e^2\,\varepsilon_\mu(q_1,\lambda_1)\,\varepsilon_\nu(q_2,\lambda_2)\,\varepsilon^*_{\alpha\beta}(p_f,\Lambda) \\
&\times\Bigg\{\Big[R^{\mu\alpha}(q_1,q_2)R^{\nu\beta}(q_1,q_2) \\
&+\frac{s}{8X}\,R^{\mu\nu}(q_1,q_2)(q_1-q_2)^\alpha\,(q_1-q_2)^\beta\Big]\,\frac{\nu}{m_T}\,T^{(2)}(Q_1^2,Q_2^2) \\
&+\;R^{\nu\alpha}(q_1,q_2)(q_1-q_2)^\beta\left(q_1^\mu+\frac{Q_1^2}{\nu}q_2^\mu\right)\,\frac{1}{m_T}\,T^{(1)}(Q_1^2,Q_2^2) \\
&+\,R^{\mu\alpha}(q_1,q_2)(q_2-q_1)^\beta\left(q_2^\nu+\frac{Q_2^2}{\nu}q_1^\nu\right)\,\frac{1}{m_T}\,T^{(1)}(Q_2^2,Q_1^2) \\
&+\;R^{\mu\nu}(q_1,q_2)(q_1-q_2)^\alpha\,(q_1-q_2)^\beta\,\frac{1}{m_T}\,T^{(0,T)}(Q_1^2,Q_2^2) \\
&+\left(q_1^\mu+\frac{Q_1^2}{\nu}q_2^\mu\right)\left(q_2^\nu+\frac{Q_2^2}{\nu}q_1^\nu\right)(q_1-q_2)^\alpha(q_1-q_2)^\beta \\
&\times\frac{1}{m_T^3}\,T^{(0,L)}(Q_1^2,Q_2^2)\Bigg\},
\end{aligned}
\tag{2.42}
$$

where $\varepsilon_{\alpha\beta}(p_f,\Lambda)$ is the polarization tensor for the tensor meson with four-momentum p_f and helicity Λ. Furthermore in Eq. (2.43) $T^{(\Lambda)}$ are the $\gamma^*\gamma^* \to \mathcal{T}$ transition form factors, for tensor meson helicity Λ. For the case of helicity zero, there are two form factors depending on whether both photons are transverse (superscript T) or longitudinal (superscript L).

	m_A [MeV]	$\tilde{\Gamma}_{\gamma\gamma}$ [keV]	Λ_A [MeV]
$f_1(1285)$	1281.8 ± 0.6	3.5 ± 0.8	1040 ± 78
$f_1(1420)$	1426.4 ± 0.9	3.2 ± 0.9	926 ± 78

Table 2.2: Present values [1] of the $f_1(1285)$ meson and $f_1(1420)$ meson masses m_A, their equivalent 2γ decay widths $\tilde{\Gamma}_{\gamma\gamma}$, defined according to Eq. (2.31), as well as their dipole masses Λ_A entering the FF of Eq. (2.41). For $\tilde{\Gamma}_{\gamma\gamma}$, we use the experimental results from the L3 Collaboration : $f_1(1285)$ from Ref. [88], $f_1(1420)$ from Ref. [89]. Note that for the $f_1(1420)$ state, only the branching ratio $\tilde{\Gamma}_{\gamma\gamma} \times \Gamma_{K\bar{K}\pi}/\Gamma_{total}$ is measured so far, which we use as a lower limit on $\tilde{\Gamma}_{\gamma\gamma}$.

From Eq. (2.43), we can easily calculate the different helicity amplitudes as :

$$\begin{aligned}
\mathcal{M}(\lambda_1 = +1, \lambda_2 = -1; \Lambda = +2) &= \mathcal{M}(\lambda_1 = -1, \lambda_2 = +1; \Lambda = -2) \qquad (2.43)\\
&= e^2 \, \frac{\nu}{m_T} \, T^{(2)}(Q_1^2, Q_2^2) \, ,\\
\mathcal{M}(\lambda_1 = 0, \lambda_2 = +1; \Lambda = -1) &= -e^2 \, Q_1 \, \frac{1}{\sqrt{2}} \left(\frac{2X}{\nu m_T^2} \right) T^{(1)}(Q_1^2, Q_2^2) \, , \qquad (2.44)\\
\mathcal{M}(\lambda_1 = -1, \lambda_2 = 0; \Lambda = -1) &= e^2 \, Q_2 \, \frac{1}{\sqrt{2}} \left(\frac{2X}{\nu m_T^2} \right) T^{(1)}(Q_2^2, Q_1^2) \, , \qquad (2.45)\\
\mathcal{M}(\lambda_1 = +1, \lambda_2 = +1; \Lambda = 0) &= \mathcal{M}(\lambda_1 = -1, \lambda_2 = -1; \Lambda = 0) \qquad (2.46)\\
&= -e^2 \sqrt{\frac{2}{3}} \left(\frac{4X}{m_T^3} \right) T^{(0,T)}(Q_1^2, Q_2^2) \, ,\\
\mathcal{M}(\lambda_1 = 0, \lambda_2 = 0; \Lambda = 0) &= -e^2 \, Q_1 Q_2 \sqrt{\frac{2}{3}} \left(\frac{4X^2}{\nu^2 m_T^5} \right) T^{(0,L)}(Q_1^2, Q_2^2) \, . \qquad (2.47)
\end{aligned}$$

The transverse FFs $T^{(2)}$ and $T^{(0,T)}$ at $Q_1^2 = Q_2^2 = 0$ describe the two-photon decay widths of the tensor meson with helicities $\Lambda = 2$ and $\Lambda = 0$ respectively :

$$\begin{aligned}
\Gamma_{\gamma\gamma}\left(\mathcal{T}(\Lambda = 2)\right) &= \frac{\pi\alpha^2}{4} \, m_T \, \frac{1}{5} \, |T^{(2)}(0,0)|^2 \, , \qquad (2.48)\\
\Gamma_{\gamma\gamma}\left(\mathcal{T}(\Lambda = 0)\right) &= \frac{\pi\alpha^2}{4} \, m_T \, \frac{2}{15} \, |T^{(0,T)}(0,0)|^2 \, . \qquad (2.49)
\end{aligned}$$

In this work, we study the sum rules involving cross sections for one real photon and one virtual photon. For one quasi-real photon ($Q_2^2 \to 0$), we can obtain from the above helicity amplitudes and using Eq. (2.10) the tensor meson contributions to the response functions of

Eq. (2.12) as :

$$[\sigma_2]_{Q_2^2=0} = \delta(s-m_T^2)\,16\,\pi^2\frac{5\,\Gamma_{\gamma\gamma}(\mathcal{T}(\Lambda=2))}{m_T}\,\left(1+\frac{Q_1^2}{m_T^2}\right)\,\left[\frac{T^{(2)}(Q_1^2,0)}{T^{(2)}(0,0)}\right]^2\,, \tag{2.50}$$

$$[\sigma_0]_{Q_2^2=0} = \delta(s-m_T^2)\,16\,\pi^2\,\frac{5\,\Gamma_{\gamma\gamma}(\mathcal{T}(\Lambda=0))}{m_T}\,\left(1+\frac{Q_1^2}{m_T^2}\right)^3\,\left[\frac{T^{(0,T)}(Q_1^2,0)}{T^{(0,T)}(0,0)}\right]^2\,, \tag{2.51}$$

$$\left[\sigma_{\parallel}\right]_{Q_2^2=0} = \left[\frac{1}{2}\sigma_2+\sigma_0\right]_{Q_2^2=0}\,, \tag{2.52}$$

$$[\sigma_{\perp}]_{Q_2^2=0} = \left[\frac{1}{2}\sigma_2\right]_{Q_2^2=0}\,, \tag{2.53}$$

$$[\sigma_{LT}]_{Q_2^2=0} = \delta(s-m_T^2)\,8\,\pi^3\alpha^2\,\frac{Q_1^2}{m_T^2}\,\left(1+\frac{Q_1^2}{m_T^2}\right)\,\left[T^{(1)}(Q_1^2,0)\right]^2\,, \tag{2.54}$$

$$\begin{aligned}\left[\frac{1}{Q_1Q_2}\tau_{TL}\right]_{Q_2^2=0} &= \delta(s-m_T^2)\,8\,\pi^3\alpha^2\,\frac{1}{m_T^2}\,\left(1+\frac{Q_1^2}{m_T^2}\right)\\ &\times\left\{\frac{2}{3}\left(1+\frac{Q_1^2}{m_T^2}\right)^2 T^{(0,T)}(Q_1^2,0)\,T^{(0,L)}(Q_1^2,0)-\right.\\ &\left.\frac{1}{2}T^{(1)}(Q_1^2,0)\,T^{(1)}(0,Q_1^2)\right\}\,,\end{aligned} \tag{2.55}$$

$$\begin{aligned}\left[\frac{1}{Q_1Q_2}\tau_{TL}^a\right]_{Q_2^2=0} &= \delta(s-m_T^2)\,8\,\pi^3\alpha^2\,\frac{1}{m_T^2}\,\left(1+\frac{Q_1^2}{m_T^2}\right)\\ &\times\left\{\frac{2}{3}\left(1+\frac{Q_1^2}{m_T^2}\right)^2 T^{(0,T)}(Q_1^2,0)\,T^{(0,L)}(Q_1^2,0)\right.\\ &\left.+\,\frac{1}{2}T^{(1)}(Q_1^2,0)\,T^{(1)}(0,Q_1^2)\right\}\,,\end{aligned} \tag{2.56}$$

$$[\sigma_{LL}]_{Q_2^2=0} = 0\,. \tag{2.57}$$

The experimental information on the Q^2 dependence of the tensor form factor is not available at the moment. As we will see later, one can learn a lot about these form factors using constraints imposed by the sum rules for light-by-light scattering which are the subject of the following sections.

2.3 Sum rules for light-light scattering

We can use the dispersion theory to relate the two phenomena of LbL scattering and $\gamma^*\gamma$ fusion, and express the low-energy LbL scattering as integrals over the $\gamma^*\gamma$-fusion cross sections, where one photon is real while the second may have arbitrary (space-like) virtuality. These integrals, or 'sum rules', lead to interesting constraints on $\gamma\gamma$ decay widths or $\gamma^*\gamma$ transition FFs of $q\bar{q}$ states, and more general meson states. The first sum rule of this type involves the helicity-difference cross-section for real photons and reads as:

$$\int_{s_0}^{\infty}\frac{ds}{s}\left[\sigma_2(s)-\sigma_0(s)\right]=0, \tag{2.58}$$

where s is the total energy squared, s_0 is the first inelastic threshold for the $\gamma\gamma$ fusion process, and the subscripts 0 or 2 for the $\gamma\gamma$ cross sections indicate the total helicity of the state of

two circularly polarized photons. This sum rule was originally[2] inferred [18, 19] from the Gerasimov–Drell–Hearn (GDH) sum rule, using the fact that the photon has no anomalous moments.

Parameterizing the lowest energy LbL interaction by means of an effective Lagrangian (which contains operators of dimension eight at lowest order) as

$$\mathcal{L}^{(8)} = c_1(F_{\mu\nu}F^{\mu\nu})^2 + c_2(F_{\mu\nu}\tilde{F}^{\mu\nu})^2, \tag{2.59}$$

with F and $\tilde{F}$ being the electromagnetic field strength and its dual, one finds sum rules for the LbL low-energy constants (LECs) [22]:

$$c_1 = \frac{1}{8\pi}\int\limits_{s_0}^{\infty} \mathrm{d}s\, \frac{\sigma_{\parallel}(s)}{s^2}\,, \qquad c_2 = \frac{1}{8\pi}\int\limits_{s_0}^{\infty} \mathrm{d}s\, \frac{\sigma_{\perp}(s)}{s^2}\,, \tag{2.60}$$

where the subscripts $\parallel$ or $\perp$ indicate if the colliding photons are polarized parallel or perpendicular to each other. While the GDH-type sum rule provides a stringent constraint on the polarized $\gamma\gamma$ fusion, the sum rules for the LECs allow one in principle to fully determine the low-energy LbL interaction through measuring the linearly polarized $\gamma\gamma$ fusion. In the following we subsequently derive and give a detailed description of already known sum rules for real photons as well as their generalization and a set of new sum rules for the case of one (quasi-)real and one virtual photon.

2.3.1 Forward $\gamma^*\gamma^*$- scattering

We start from a discussion of the elastic forward scattering of photons. In the most general case we consider the forward scattering of virtual photons on virtual photons:

$$\gamma^*(\lambda_1, q_1) + \gamma^*(\lambda_2, q_2) \to \gamma^*(\lambda_1', q_1) + \gamma^*(\lambda_2', q_2), \tag{2.61}$$

where q_1, q_2 are photon four-momenta, and λ_1, λ_2 (λ_1', λ_2') are the helicities of the initial (final) virtual photons, which can take on the values ± 1 (transverse polarizations) and zero (longitudinal). The total helicity in the $\gamma^*\gamma^*$ c.m. system is given by $\Lambda = \lambda_1 - \lambda_2 = \lambda_1' - \lambda_2'$. To define the kinematics, we firstly introduce the photon virtualities $Q_1^2 = -q_1^2$, $Q_2^2 = -q_2^2$, the Mandelstam invariants: $s = (q_1 + q_2)^2$, $u = (q_1 - q_2)^2$, and the following crossing-symmetric variable:

$$\nu \equiv \tfrac{1}{4}(s - u) = q_1 \cdot q_2, \tag{2.62}$$

such that $s = 2\nu - Q_1^2 - Q_2^2$, $u = -2\nu - Q_1^2 - Q_2^2$.

The $\gamma^*\gamma^* \to \gamma^*\gamma^*$ forward scattering amplitudes, denoted as $M_{\lambda_1'\lambda_2',\lambda_1\lambda_2}$, are functions of ν, Q_1^2, Q_2^2. Parity invariance (P) and time-reversal invariance (T) imply the following relations among the matrix elements with different helicities :

$$P: \quad M_{\lambda_1'\lambda_2',\lambda_1\lambda_2} = M_{-\lambda_1'-\lambda_2',-\lambda_1-\lambda_2}, \tag{2.63}$$

$$T: \quad M_{\lambda_1'\lambda_2',\lambda_1\lambda_2} = M_{\lambda_1\lambda_2,\lambda_1'\lambda_2'}, \tag{2.64}$$

which leaves out only eight independent amplitudes [92]:

$$M_{++,++},\, M_{+-,+-},\, M_{++,--},\, M_{00,00},\, M_{+0,+0},\, M_{0+,0+},\, M_{++,00},\, M_{0+,-0}. \tag{2.65}$$

[2] An earlier version of this sum rule had been proposed in Ref. [17], where a contribution from π^0 production appears on the right-hand side (*rhs*) of Eq. (2.58), while integration on the *lhs* starts at the 2π production threshold. That version would be fully compatible with Eq. (2.58), if it were not for the sign of the π^0 contribution obtained in [17].

We next consider the constraint imposed by crossing symmetry, which requires that the amplitudes for the process (2.61) equal the amplitudes for the process where the photons with e.g. label 2 are crossed:

$$\gamma^*(\lambda_1, q_1) + \gamma^*(-\lambda_2', -q_2) \to \gamma^*(\lambda_1', q_1) + \gamma^*(-\lambda_2, -q_2). \tag{2.66}$$

As under photon crossing $\nu \to -\nu$, one obtains

$$M_{\lambda_1'\lambda_2',\lambda_1\lambda_2}(\nu, Q_1^2, Q_2^2) \;=\; M_{\lambda_1'-\lambda_2,\lambda_1-\lambda_2'}(-\nu, Q_1^2, Q_2^2), \tag{2.67}$$

it becomes convenient to introduce amplitudes which are either even or odd in ν (at fixed Q_1^2 and Q_2^2). One easily verifies that the following six amplitudes are *even* in ν :

$$(M_{++,++} + M_{+-,+-})\,, \quad M_{++,--}, \quad M_{00,00}, \tag{2.68}$$

$$M_{+0,+0}, \quad M_{0+,0+}, \quad (M_{++,00} + M_{0+,-0})\,, \tag{2.69}$$

whereas the following two amplitudes are *odd* in ν :

$$(M_{++,++} - M_{+-,+-})\,, \qquad (M_{++,00} - M_{0+,-0})\,. \tag{2.70}$$

2.3.2 Dispersion relations

The principle of (micro-)causality is known to translate into exact statements about analytic properties of the scattering amplitude in the complex energy plane. In our case this principle translates into the statement of analyticity of the forward $\gamma^*\gamma^*$ scattering amplitude in the entire ν plane, except for the real axis where the branch cuts associated with particle production are located. Assuming that the threshold for particle production is $\nu_0 > 0$, one can write down the usual dispersion relations, in which the amplitude is given by integrals over the non-analyticities, which in this case are branch cuts extending from $\pm\nu_0$ to $\pm\infty$. Finally, for amplitudes that are even or odd in ν we can write (for any fixed values of $Q_1^2, Q_2^2 > 0$):

$$f_{even}(\nu) \;=\; \frac{2}{\pi}\int_{\nu_0}^{\infty} d\nu' \frac{\nu'}{\nu'^2 - \nu^2 - i0^+}\,\mathrm{Abs}\, f_{even}(\nu'), \tag{2.71a}$$

$$f_{odd}(\nu) \;=\; \frac{2\nu}{\pi}\int_{\nu_0}^{\infty} d\nu' \frac{1}{\nu'^2 - \nu^2 - i0^+}\,\mathrm{Abs}\, f_{odd}(\nu'), \tag{2.71b}$$

where 0^+ is an infinitesimal positive number.

These dispersion relations are derived with the provision that the integrals converge. If they do not, subtractions must be made; e.g., the once-subtracted dispersion relation for the even amplitudes reads:

$$f_{even}(\nu) \;=\; f_{even}(0) + \frac{2\nu^2}{\pi}\int_{\nu_0}^{\infty} d\nu' \frac{1}{\nu'(\nu'^2 - \nu^2 - i0^+)}\,\mathrm{Abs}\, f_{even}(\nu'). \tag{2.72}$$

We are thus led to examine the high-energy behavior ($\nu \to \infty$ at fixed Q_1^2, Q_2^2) of the absorptive parts given by Eq. (2.12). In Ref. [92], a Regge pole model assumption for the high-energy asymptotics of the light-by-light forward amplitudes yielded:

$$\begin{aligned} (W_{++,++} + W_{+-,+-})\,, \quad W_{+0,+0}, \quad W_{0+,0+}, \quad W_{00,00} \quad &\sim \quad \nu^{\alpha_P(0)}, \\ (W_{++,++} - W_{+-,+-})\,, \quad W_{++,--} \quad &\sim \quad \nu^{\alpha_\pi(0)}, \\ (W_{++,00} + W_{0+,-0})\,, \quad (W_{++,00} - W_{0+,-0}) \quad &\sim \quad \nu^{\alpha_\pi(0)-1}, \end{aligned} \tag{2.73}$$

where $\alpha_P(0) \simeq 1.08$ is the intercept of the Pomeron trajectory, and $\alpha_\pi(0) \simeq -0.014$ is the intercept of the pion trajectory. This means that for all the even amplitudes, except $M_{++,00} + M_{0+,-0}$, one can only use the subtracted dispersion relation Eq. (2.72). We therefore need the information about these amplitudes at zero energy ν. Anticipating the discussion of the low-energy expansion of the LbL scattering, we can state that at $\nu = 0$ these amplitudes vanish when one of the photons is real [cf. Eq. (2.77)]. Using Eq. (2.12) then to substitute the cross sections in place of the absorptive parts, we obtain the following sum rules for the case of one real and one virtual photon (when the virtual photon flux factor becomes $X = \nu^2$):

$$M_{++,++}(\nu) + M_{+-,+-}(\nu) = \frac{4\nu^2}{\pi}\int_{\nu_0}^{\infty} d\nu' \, \frac{\sigma_\parallel(\nu') + \sigma_\perp(\nu')}{\nu'^2 - \nu^2 - i0^+}, \tag{2.74a}$$

$$M_{++,--}(\nu) = \frac{4\nu^2}{\pi}\int_{\nu_0}^{\infty} d\nu' \, \frac{\sigma_\parallel(\nu') - \sigma_\perp(\nu')}{\nu'^2 - \nu^2 - i0^+}, \tag{2.74b}$$

$$M_{0+,0+}(\nu) = \frac{4\nu^2}{\pi}\int_{\nu_0}^{\infty} d\nu' \, \frac{\sigma_{LT}(\nu')}{\nu'^2 - \nu^2 - i0^+}, \tag{2.74c}$$

$$M_{+0,+0}(\nu) = \frac{4\nu^2}{\pi}\int_{\nu_0}^{\infty} d\nu' \, \frac{\sigma_{TL}(\nu')}{\nu'^2 - \nu^2 - i0^+}. \tag{2.74d}$$

We cannot write such a subtracted sum rule for $M_{00,00}$, since it trivially vanishes when one of the photons is real. Instead, considering an unsubtracted dispersion relation, we find the following sum rule:

$$M_{00,00}(\nu) = \frac{4}{\pi}\int_{\nu_0}^{\infty} d\nu' \, \frac{\nu'\sqrt{X'}\,\sigma_{LL}(\nu')}{\nu'^2 - \nu^2 - i0^+}, \tag{2.74e}$$

with $X' = \nu'^2 - Q_1^2 Q_2^2$. At least in perturbative QED calculations (cf. Appendix B), the above integral converges which seems to validate this sum rule in a renormalizable, perturbative field theory. We emphasize however that this observation is in contradiction with the expectation of non-convergence from the Regge pole model shown above. A validation of this sum rule in non-perturbative field theory, particularly in QCD, is therefore an open issue.

For all the remaining amplitudes the asymptotic behavior of Eq. (2.74) justifies the use of unsubtracted dispersion relations which, upon substituting Eq. (2.12), lead to the following sum rules, valid for both photons virtual:

$$M_{++,++}(\nu) - M_{+-,+-}(\nu) = \frac{4\nu}{\pi}\int_{\nu_0}^{\infty} d\nu' \, \frac{\sqrt{X'}\left[\sigma_0(\nu') - \sigma_2(\nu')\right]}{\nu'^2 - \nu^2 - i0^+}, \tag{2.74f}$$

$$M_{++,00}(\nu) - M_{0+,-0}(\nu) = \frac{8\nu}{\pi}\int_{\nu_0}^{\infty} d\nu' \, \frac{\sqrt{X'}\,\tau_{TL}^a(\nu')}{\nu'^2 - \nu^2 - i0^+}, \tag{2.74g}$$

$$M_{++,00}(\nu) + M_{0+,-0}(\nu) = \frac{8}{\pi}\int_{\nu_0}^{\infty} d\nu' \, \frac{\nu'\sqrt{X'}\,\tau_{TL}(\nu')}{\nu'^2 - \nu^2 - i0^+}, \tag{2.74h}$$

where the dependence on virtualities Q_1^2, Q_2^2 is tacitly assumed.

The above sum rules, relating all the forward $\gamma^*\gamma^*$ elastic scattering amplitudes to the energy integrals of the $\gamma^*\gamma^*$ fusion cross sections, should hold for any space-like photon virtualities in the unsubtracted cases, and for one of the virtualities equal to zero in the subtracted cases. In the following we examine the low-energy expansion of these sum rules.

2.3.3 Low-energy expansion via effective Lagrangian

To obtain more specific relations from the sum rules established in Eq. (2.74), we parametrize the low-energy (small ν) behavior of the $\gamma^*\gamma^* \to \gamma^*\gamma^*$ forward scattering amplitudes M,

appearing on the left hand side of Eqs. (2.74) At lowest order in the energy, the self-interactions of the electromagnetic field are described by an effective Lagrangian (of fourth order in the photon energy and/or momentum, and fourth order in the electromagnetic field):

$$\mathcal{L}^{(8)} = c_1(F_{\mu\nu}F^{\mu\nu})^2 + c_2(F_{\mu\nu}\tilde{F}^{\mu\nu})^2, \tag{2.75}$$

where $F_{\mu\nu} = \partial_\mu A_\nu - \partial_\nu A_\mu$, $\tilde{F}^{\mu\nu} = \varepsilon^{\mu\nu\alpha\beta}\partial_\alpha A_\beta$, and where c_1, c_2 are two low-energy constants (LECs) which contain the structure dependent information. It is often referred to as Euler-Heisenberg Lagrangian due to the seminal work [56].

At the next order in energy, one considers the terms involving two derivatives on the field tensors, corresponding with the sixth order in the photon energy and/or momentum. Writing down all such dimension-ten operators and reducing their number using the antisymmetry of the field tensors, the Bianchi identities, as well as adding or removing total derivative terms, we find that there are 6 independent terms at that order, which we choose as :

$$\begin{aligned}
\mathcal{L}^{(10)} &= c_3(\partial_\alpha F_{\mu\nu})(\partial^\alpha F^{\lambda\nu})F_{\lambda\rho}F^{\mu\rho} + c_4(\partial_\alpha F_{\mu\nu})(\partial^\alpha F^{\mu\nu})F_{\lambda\rho}F^{\lambda\rho} \\
&+ c_5(\partial^\alpha F_{\alpha\nu})(\partial_\beta F^{\beta\nu})F_{\lambda\rho}F^{\lambda\rho} + c_6(\partial_\alpha\partial^\alpha F_{\mu\nu})F^{\lambda\nu}F_{\lambda\rho}F^{\mu\rho} \\
&+ c_7(\partial_\alpha\partial^\alpha F_{\mu\nu})F^{\mu\nu}F_{\lambda\rho}F^{\lambda\rho} + c_8(\partial^\alpha F_{\alpha\mu})(\partial_\beta F^{\beta\lambda})F_{\rho\lambda}F^{\rho\mu},
\end{aligned} \tag{2.76}$$

where $c_3, \ldots, c_8$ are the new LECs arising at this order. Only c_3 and c_4 appear in the case of real photons.

We can now specify the low-energy limit of the light-by-light scattering amplitudes in terms of the LECs describing the low-energy self-interactions of the electromagnetic field:

$$\begin{aligned}
M_{++,++} + M_{+-,+-} &= Q_1^2Q_2^2\,[64(c_1 - c_2) \\
&+ 4(Q_1^2 + Q_2^2)(-c_3 - 8c_4 - 4c_5 + 8c_7 - c_8) + \mathcal{O}(Q^4)\big] \\
&+ 8\nu^2\,[8(c_1 + c_2) \\
&+ \left(Q_1^2 + Q_2^2\right)(-c_3 + 3c_6 + 4c_7) + \mathcal{O}(Q^4)\big] + \mathcal{O}(\nu^4), && \text{(2.77a)} \\
M_{++,--} &= Q_1^2Q_2^2\left[64c_2 + 4(Q_1^2 + Q_2^2)(-c_3 + 2c_6 - c_8) + \mathcal{O}(Q^4)\right] \\
&+ 8\nu^2\left[8(c_1 - c_2) + \left(Q_1^2 + Q_2^2\right)(c_6 + 4c_7) + \mathcal{O}(Q^4)\right] + \mathcal{O}(\nu^4), && \text{(2.77b)} \\
M_{0+,0+} &= Q_1^2Q_2^2\left[-32c_1 + 4Q_1^2c_8\right. \\
&+ 4(Q_1^2 + Q_2^2)(c_3 + 4c_4 + 2c_5 - 2c_6 - 4c_7) + \mathcal{O}(Q^4)\big] \\
&+ \nu^2\left[-4Q_1^2c_8 + \mathcal{O}(Q^4)\right] + \mathcal{O}(\nu^4), && \text{(2.77c)} \\
M_{+0,+0} &= Q_1^2Q_2^2\left[-32c_1 + 4Q_2^2c_8\right. \\
&+ 4(Q_1^2 + Q_2^2)(c_3 + 4c_4 + 2c_5 - 2c_6 - 4c_7) + \mathcal{O}(Q^4)\big] \\
&+ \nu^2\left[-4Q_2^2c_8 + \mathcal{O}(Q^4)\right] + \mathcal{O}(\nu^4), && \text{(2.77d)} \\
M_{00,00} &= Q_1^2Q_2^2\,[96c_1 \\
&+ 4(Q_1^2 + Q_2^2)(-2c_3 - 4c_4 - 2c_5 + 6c_6 + 12c_7 - c_8) + \mathcal{O}(Q^4)\big] \\
&+ \mathcal{O}(\nu^2), && \text{(2.77e)} \\
M_{++,++} - M_{+-,+-} &= 8\nu Q_1^2Q_2^2\left[-c_3 - 4c_5 + c_8 + \mathcal{O}(Q^2)\right] \\
&+ \nu^3\left[-64c_4 + \mathcal{O}(Q^2)\right] + \mathcal{O}(\nu^5), && \text{(2.77f)} \\
M_{++,00} - M_{0+,-0} &= \nu Q_1Q_2\left[-64c_1 + \left(Q_1^2 + Q_2^2\right)(4c_3 - 16c_6 - 32c_7 + 4c_8) + \mathcal{O}(Q^4)\right] \\
&+ \mathcal{O}(\nu^3), && \text{(2.77g)} \\
M_{++,00} + M_{0+,-0} &= Q_1^3Q_2^3\left[4c_5 - 12c_8 + \mathcal{O}(Q^2)\right] \\
&+ 4\nu^2Q_1Q_2\left[2c_3 + 16c_4 + 4c_5 + c_8 + \mathcal{O}(Q^2)\right] \\
&+ \mathcal{O}(\nu^4). && \text{(2.77h)}
\end{aligned}$$

These expressions can be treated as a simultaneous expansion in ν and the virtualities Q_i^2 of the *lhs* of the sum rules Eq. (2.74). Concerning the Q dependence, it is important that the leading in ν term, in any of the amplitudes, is proportional to $Q_1 Q_2$ and hence vanishes for at least one real photon. The latter statement is valid for any values of virtualities, not just when they are small. For example, let us show for the amplitude $(M_{++,++} - M_{+-,+-})$ its leading term in ν is proportional to the combination $Q_1^2 Q_2^2$, to all orders in Q_1 and Q_2.

Since all photons are transversely polarized the only non-vanishing structures involving polarization vectors of photons $\varepsilon(\lambda_i)$ are their mutual scalar products $\varepsilon(\lambda_i)\cdot\varepsilon(\lambda_j)$. Due to gauge invariance, the electromagnetic fields enter the Lagrangian through the field tensor $F_{\mu\nu}$, which contributes to the amplitude as $q_\mu \varepsilon_\nu - q_\nu \varepsilon_\mu$. Thus an arbitrary term in the effective Lagrangian contributes to $(M_{++,++} - M_{+-,+-})$ as:

$$M_{++,++} - M_{+-,+-} \sim q_1^\mu q_2^\nu q_1^\lambda q_2^\rho T_{\mu\nu\lambda\rho}, \tag{2.78}$$

where the tensor $T_{\mu\nu\lambda\rho}$ is constructed from four-vectors q_i and the metric tensor. Since this amplitude is odd with respect to ν, it is required to be proportional to at least ν^1. Assuming that one factor ν comes from contraction of two of the q's in Eq. (2.78), we are left with $q_1^\mu q_2^\nu$. Now, if we suppose that q_1 is contracted with q_2 we obtain an extra power of ν, and such an amplitude vanishes when taking the limit $\nu \to 0$. Thus, both q_1 and q_2 must be contracted with another q_1 and q_2 respectively, giving a global factor $Q_1^2 Q_2^2$.

We are now in position to examine the sum rules in Eq. (2.74) order by order in ν. For this we expand the *rhs* of Eq. (2.74) using $1/(\nu'^2 - \nu^2) = 1/\nu'^2 + \nu^2/\nu'^4 + \mathcal{O}(\nu^4)$. As the result we obtain from Eqs. (2.74f,2.74g,2.74h) the following set of super-convergence relations, valid for at least one real photon (e.g., $Q_1 \geq 0$, $Q_2^2 = 0$):

$$0 = \int_{s_0}^{\infty} ds \frac{1}{(s+Q_1^2)}\, \tau_{TT}^a(s, Q_1^2, 0), \tag{2.79a}$$

$$0 = \int_{s_0}^{\infty} ds\, \frac{1}{(s+Q_1^2)^2} \left[\sigma_\parallel + \sigma_{LT} + \frac{(s+Q_1^2)}{Q_1 Q_2} \tau_{TL}^a\right]_{Q_2^2=0}, \tag{2.79b}$$

$$0 = \int_{s_0}^{\infty} ds\, \left[\frac{\tau_{TL}(s, Q_1^2, Q_2^2)}{Q_1 Q_2}\right]_{Q_2^2=0}. \tag{2.79c}$$

and the following set of sum rules for the LECs of the dimension-8 (Euler-Heisenberg) Lagrangian, valid when both photons are quasi-real:

$$c_1 = \frac{1}{8\pi} \int_{s_0}^{\infty} \frac{ds}{s^2}\, \sigma_\parallel(s, 0, 0), \tag{2.80a}$$

$$= -\frac{1}{8\pi} \int_{s_0}^{\infty} \frac{ds}{s}\, \left[\frac{\tau_{TL}^a(s, Q_1^2, Q_2^2)}{Q_1 Q_2}\right]_{Q_1^2=Q_2^2=0}, \tag{2.80b}$$

$$= \frac{1}{8\pi} \int_{s_0}^{\infty} ds\, \left[\frac{\sigma_{LL}(s, Q_1^2, Q_2^2)}{Q_1^2 Q_2^2}\right]_{Q_1^2=Q_2^2=0}, \tag{2.80c}$$

$$c_2 = \frac{1}{8\pi} \int_{s_0}^{\infty} \frac{ds}{s^2}\, \sigma_\perp(s, 0, 0), \tag{2.80d}$$

where $s_0 = 2\nu_0 - Q_1^2 - Q_2^2$. We emphasize again that, unlike the other sum rules, the sum rule of Eq. (2.80c) is only shown to hold in perturbative field theory.

There are as well the sum rules for the LECs of the dimension-10 Lagrangian, most notably:

$$c_4 \;=\; -\frac{1}{4\pi}\int\limits_{s_0}^{\infty}\frac{ds}{s^3}\,\tau_{TT}^{a}(s,0,0), \tag{2.81}$$

but presently they are of far lesser importance and we do not write them out explicitly here.

Let us remark again that the relation of Eq. (2.79a), obtained by combining Eqs. (2.74f) and (2.77f), is essentially a GDH sum rule for the photon target, see [18, 19, 17]. For large virtuality Q_1^2, it leads to the sum rule for the photon structure function g_1^γ [93]: $\int_0^1 dx g_1^\gamma(x,Q^2) = 0$.

The sum rules in Eqs. (2.80a) and (2.80d), first established in [22], are obtained by combining Eqs. (2.74a) with (2.77a) and Eqs. (2.74b) with (2.77b), respectively. All the other relations presented above are new. In the following section we will sequentially discuss applications of these sum rules in field theory and hadronic phenomenology.

Chapter 3

Applications of the sum rules

The sum rules derived in the previous chapter can be rigorously tested in field theory and in consistent model calculations. In this case the sum rules can be interpreted as consistency conditions that constrain low-energy behavior of the theory, i.e. constrain the parameters of an effective action. Conversely, when the low-energy structure is fixed by the gauge invariance, dispersion relations give constraints on the ultraviolet behavior of the theory. Starting from perturbative examples we will subsequently discuss the impact of the sum rules in field theory. When applied perturbatively these sum rules must hold exactly for each order of the perturbation expansion. All of the new relations will be verified exactly at leading and one-loop order in scalar and spinor QED. Subsequently, we will discuss the transition to the non-perturbative regime on the example of applying the sum rules to a study of bound states in a scalar ϕ^4 theory. On the other hand as their derivation is based on general principles they must be satisfied as well for the observable hadronic cross-sections. When applied to the $\gamma^*\gamma$ production of mesons they lead to intricate relations between the $\gamma\gamma$ decay widths or the $\gamma^*\gamma$ transition form factors for (pseudo-) scalar, axial-vector and tensor mesons. We will proceed to the phenomenological applications for the production of hadrons in the last part of this section.

3.1 Sum rules in perturbation theory

We start from two-photon particle production in perturbative field theory. First, we will consider tree-level processes in scalar QED (e.g., Born approximation to $\gamma^*\gamma^* \to \pi^+\pi^-$), spinor QED ($\gamma^*\gamma^* \to q\bar{q}$ where q stands for a charged lepton or a quark) and vector QED ($\gamma^*\gamma^* \to W^+W^-$ with spin-1 point-like particles). After that we discuss a pair-production in a model field theory, the ϕ^4 scalar QED at one-loop level.

3.1.1 Tree-level pair production

Scalar QED. At leading order the process is defined by Feynman graphs in Fig.(3.1) representing the production of a pair. In the Lorentz gauge (i.e. $q_\mu \epsilon^\mu(q) = 0$) the process $\gamma^*\gamma^* \to \phi^*\phi$, describing the transition from an initial state of two virtual photons with four-momenta q_1, q_2 and helicities λ_1, $\lambda_2 = 0, \pm 1$ to a pair of charged scalar particles with four-momenta p_1 and p_2 is described by the matrix element:

$$i\mathcal{M}^{(0)}_{\lambda_1\lambda_2} = 2ie^2\varepsilon^\mu(q_1,\lambda_1)\varepsilon^\nu(q_2,\lambda_2)\left[\frac{2p_{1\mu}p_{2\nu}}{(q_1-p_1)^2-m^2} + \frac{2p_{2\mu}p_{1\nu}}{(q_2-p_1)^2-m^2} + g_{\mu\nu}\right]. \qquad (3.1)$$

From Eq. (3.1) we can easily compute $\gamma^*\gamma^* \to \phi^*\phi$ polarized cross sections involving transverse and longitudinal photons to leading order in α in the limit where one of the photons becomes real ($Q_2^2 = 0$) or quasireal ($Q_2^2 \approx 0$) :

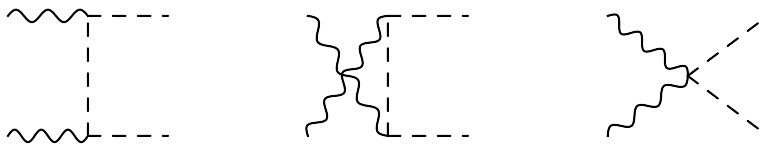

Figure 3.1: Pair production in scalar QED at leading order

$$\left[\sigma_{\parallel}+\sigma_{\perp}\right]_{Q_2^2=0} = \alpha^2 4\pi \frac{s^2}{(s+Q_1^2)^3}\left\{\sqrt{1-\frac{4m^2}{s}}\left(1+\frac{4m^2}{s}+\frac{Q_1^4}{s^2}\right)\right.$$
$$\left.-\frac{8m^2}{s}\left(1-\frac{2m^2}{s}-\frac{Q_1^2}{s}\right)L\right\}, \tag{3.2}$$

$$\left[\sigma_{\parallel}-\sigma_{\perp}\right]_{Q_2^2=0} = \alpha^2 4\pi \frac{s^2}{(s+Q_1^2)^3}\left\{\sqrt{1-\frac{4m^2}{s}}\left(\frac{2m^2}{s}+\frac{Q_1^4}{s^2}\right)\right.$$
$$\left.+\frac{8m^2}{s}\left(\frac{m^2}{s}+\frac{Q_1^2}{s}\right)L\right\}, \tag{3.3}$$

$$\left[\sigma_0-\sigma_2\right]_{Q_2^2=0} = \alpha^2 4\pi \frac{s}{(s+Q_1^2)^2}\left\{-\sqrt{1-\frac{4m^2}{s}}\left(1-\frac{Q_1^2}{s}\right)+\frac{8m^2}{s}L\right\}, \tag{3.4}$$

$$\left[\frac{1}{Q_1^2Q_2^2}\sigma_{LL}\right]_{Q_2^2=0} = \alpha^2 8\pi \frac{s^2}{(s+Q_1^2)^5}\left\{\sqrt{1-\frac{4m^2}{s}}\left(8+\frac{s}{4m^2}\left(1-\frac{Q_1^2}{s}\right)^2\right)\right.$$
$$\left.-\left(7+\frac{Q_1^2}{s}\right)\left(1-\frac{Q_1^2}{s}\right)L\right\}, \tag{3.5}$$

$$\left[\frac{1}{Q_1^2}\sigma_{LT}\right]_{Q_2^2=0} = \alpha^2 4\pi \frac{s}{(s+Q_1^2)^3}\left\{-3\sqrt{1-\frac{4m^2}{s}}+2\left(1+\frac{2m^2}{s}\right)L\right\}, \tag{3.6}$$

$$\left[\frac{1}{Q_1Q_2}\tau_{TL}\right]_{Q_2^2=0} = \alpha^2 4\pi \frac{s}{(s+Q_1^2)^3}\left\{-\sqrt{1-\frac{4m^2}{s}}+\left(1-\frac{Q_1^2}{s}-\frac{4m^2}{s}\right)L\right\}, \tag{3.7}$$

$$\left[\frac{1}{Q_1Q_2}\tau_{TL}^a\right]_{Q_2^2=0} = \alpha^2 8\pi \frac{s^2}{(s+Q_1^2)^4}\left\{\sqrt{1-\frac{4m^2}{s}}\left(1-\frac{2Q_1^2}{s}\right)\right.$$
$$\left.-\left[\frac{1}{2}\left(1-\frac{Q_1^2}{s}\right)^2+\frac{4m^2}{s}\right]L\right\}, \tag{3.8}$$

with

$$[L]_{Q_2^2=0} = \ln\left(\frac{\sqrt{s}}{2m}\left[1+\sqrt{1-\frac{4m^2}{s}}\right]\right), \tag{3.9}$$

We firstly study the three sum rules of Eqs. (2.79a, 2.79b, 2.79c) for the case of one real or quasi-real photon ($Q_2^2 \to 0$) and for arbitrary space-like virtuality ($Q_1^2 \geq 0$) of the other photon. To better see the cancellation which must take place in these sum rules between contributions at low and higher energies, we show the integrands of the three sum rules in Figs. 3.2-3.4 multiplied by s. In this way, when plotted logarithmically, one can clearly see how the low and high energy contributions cancel each other. For the sum rule of Eq. (2.79b), we denote the

integrand as :

$$I = \frac{1}{(s+Q_1^2)^2}\left[\sigma_{\parallel} + \sigma_{LT} + \frac{(s+Q_1^2)}{Q_1 Q_2}\tau_{TL}^a\right]_{Q_2^2=0}. \tag{3.10}$$

All three sum rules of Eqs. (2.79a, 2.79b, 2.79c) are exactly verified in scalar QED for arbitrary space-like values of Q_1^2. One notices from Figs. 3.2, 3.3, 3.4 that for larger values of Q_1^2 the zero crossing of the integrands shifts to larger values of s, requiring higher energy contributions for the cancellation to take place. For the helicity difference sum rule of Eq. (2.79a), one notices that at low energies σ_0 dominates while with increasing energies σ_2 overtakes.

Besides exactly verifying the sum rules which integrate to zero, we can also use the above derived sum rules to study the low-energy coefficients for light-by-light scattering in scalar QED. Using Eqs. (2.80a, 2.80d), we obtain for the tree-level contributions to the lowest order coefficients c_1 and c_2 in scalar QED:

$$c_1 = \frac{\alpha^2}{m^4}\frac{7}{1440}, \qquad c_2 = \frac{\alpha^2}{m^4}\frac{1}{1440}. \tag{3.11}$$

Spinor QED. Analogously to the previous case the response functions in spinor QED to lowest order in the electromagnetic coupling in the limit where one of the virtual photons becomes real ($Q_2^2 = 0$) or quasi-real ($Q_2^2 \approx 0$) are given by :

$$\begin{aligned}
\left[\sigma_{\parallel} + \sigma_{\perp}\right]_{Q_2^2=0} &= \alpha^2 8\pi \frac{s^2}{(s+Q_1^2)^3}\left\{\sqrt{1-\frac{4m^2}{s}}\left[-\left(1-\frac{Q_1^2}{s}\right)^2 - \frac{4m^2}{s}\right]\right. \\
&\quad \left. + 2\left(1 + \frac{4m^2}{s} - \frac{8m^4}{s^2} + \frac{Q_1^4}{s^2}\right)L\right\}, && (3.12)\\
\left[\sigma_{\parallel} - \sigma_{\perp}\right]_{Q_2^2=0} &= -\alpha^2 8\pi \frac{s^2}{(s+Q_1^2)^3}\left\{\sqrt{1-\frac{4m^2}{s}}\left(\frac{2m^2}{s} + \frac{Q_1^4}{s^2}\right)\right. \\
&\quad \left. + \frac{8m^2}{s}\left(\frac{m^2}{s} + \frac{Q_1^2}{s}\right)L\right\}, && (3.13)\\
\left[\sigma_0 - \sigma_2\right]_{Q_2^2=0} &= \alpha^2 8\pi \frac{s}{(s+Q_1^2)^2}\left\{\sqrt{1-\frac{4m^2}{s}}\left(3 - \frac{Q_1^2}{s}\right) - 2\left(1 - \frac{Q_1^2}{s}\right)L\right\}, && (3.14)\\
\left[\frac{1}{Q_1^2 Q_2^2}\sigma_{LL}\right]_{Q_2^2=0} &= \alpha^2 128\pi \frac{s^2}{(s+Q_1^2)^5}\left\{-\sqrt{1-\frac{4m^2}{s}} + L\right\}, && (3.15)\\
\left[\frac{1}{Q_1^2}\sigma_{LT}\right]_{Q_2^2=0} &= \alpha^2 16\pi \frac{s}{(s+Q_1^2)^3}\left\{\sqrt{1-\frac{4m^2}{s}} - \frac{4m^2}{s}L\right\}, && (3.16)\\
\left[\frac{1}{Q_1 Q_2}\tau_{TL}\right]_{Q_2^2=0} &= 0, && (3.17)\\
\left[\frac{1}{Q_1 Q_2}\tau_{TL}^a\right]_{Q_2^2=0} &= \alpha^2 16\pi \frac{s^2}{(s+Q_1^2)^4}\left\{-\sqrt{1-\frac{4m^2}{s}}\left(1 - \frac{2Q_1^2}{s}\right)\right. \\
&\quad \left. + \left(-\frac{2Q_1^2}{s} + \frac{4m^2}{s}\right)L\right\}, && (3.18)
\end{aligned}$$

with

$$[L]_{Q_2^2=0} = \ln\left(\frac{\sqrt{s}}{2m}\left[1 + \sqrt{1-\frac{4m^2}{s}}\right]\right). \tag{3.19}$$

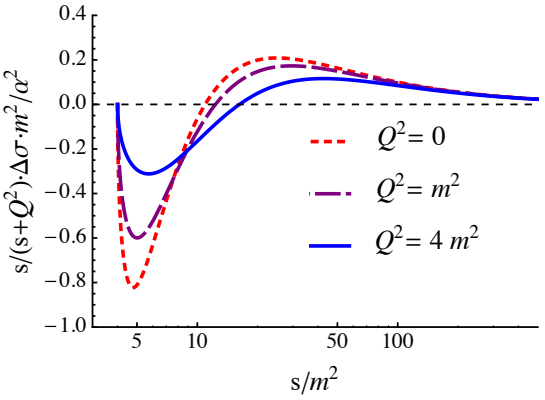

Figure 3.2: The $\gamma^*\gamma \to \pi^+\pi^-$ tree level result (scalar QED) for the integrand in the $\Delta\sigma \equiv \sigma_2 - \sigma_0$ sum rule of Eq. (2.79a), multiplied by s, where one of the photons is real. The definitions of the curves are as in Fig. 3.4.

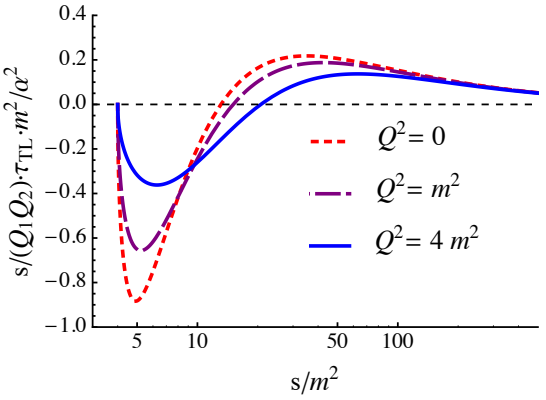

Figure 3.3: The $\gamma^*\gamma \to \pi^+\pi^-$ tree level result (scalar QED) for the integrand in the τ_{TL} sum rule of Eq. (2.79c) multiplied by s, where one of the photons is quasi-real. The definitions of the curves are as in Fig. 3.4.

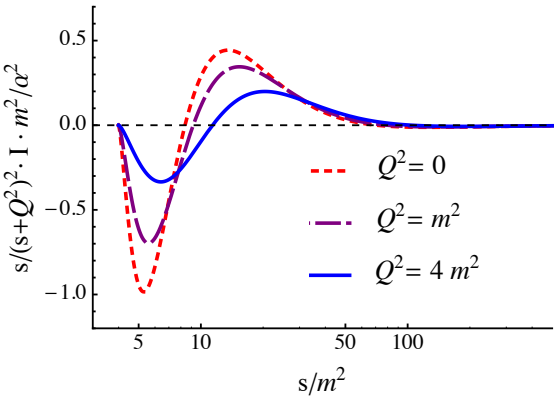

Figure 3.4: The $\gamma^*\gamma \to \pi^+\pi^-$ tree level result (scalar QED) for the integrand I in the sum rule of Eq. (2.79b) multiplied by s, with I given by Eq. (3.10), where one of the photons is quasi-real. The different curves are for different virtualities for the other photon : $Q_1^2 = 0$ (short-dashed red curve), $Q_1^2 = m^2$ (dashed purple curve), $Q_1^2 = 4m^2$ (solid blue curve).

We again study the three sum rules of Eqs. (2.79a, 2.79b, 2.79c) for the case of one real or quasi-real photon ($Q_2^2 \to 0$) for different space-like virtualities of the other photon. As the tree level contribution to τ_{TL} in spinor QED vanishes for one quasi-real photon, one notices that the sum rule of Eq. (2.79c) is trivially satisfied. For the sum rules involving the helicity difference of Eq. (2.79a), and involving the integrand I of Eq. (3.10), we show the corresponding integrands multiplied by s in Figs. 3.5, 3.6 for the case of one real or quasi-real photon and for different virtualities of the other photon. We again verify that the sum rules involve an exact cancellation between low and high energy contributions.

Using Eqs. (2.80a, 2.80d), we obtain for the tree-level contributions to the lowest order coefficients c_1 and c_2 for light-by-light scattering in spinor QED :

$$c_1 = \frac{\alpha^2}{m^4}\frac{1}{90}, \qquad c_2 = \frac{\alpha^2}{m^4}\frac{7}{360}. \tag{3.20}$$

In these case we also are able to verify the sum rule in Eq. (2.81), yielding

$$c_4 = -\frac{\alpha^2}{m^6}\frac{1}{315}, \tag{3.21}$$

in agreement with the result obtained in Ref. [94] for the low-energy photon-photon scattering.

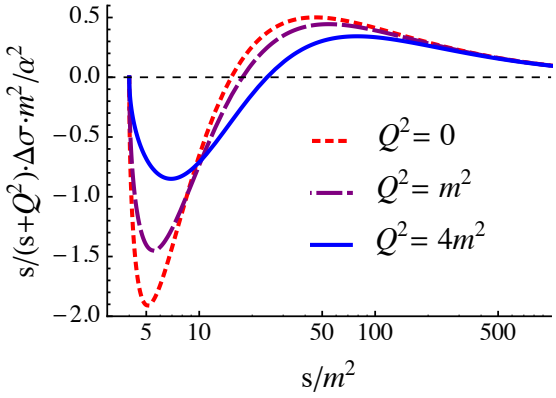

Figure 3.5: The $\gamma^*\gamma \to e^+e^-$ tree level result (spinor QED) for the integrand in the $\Delta\sigma \equiv \sigma_2 - \sigma_0$ sum rule of Eq. (2.79a), multiplied by s, where one of the photons is real. The definitions of the curves are as in Fig. 3.4.

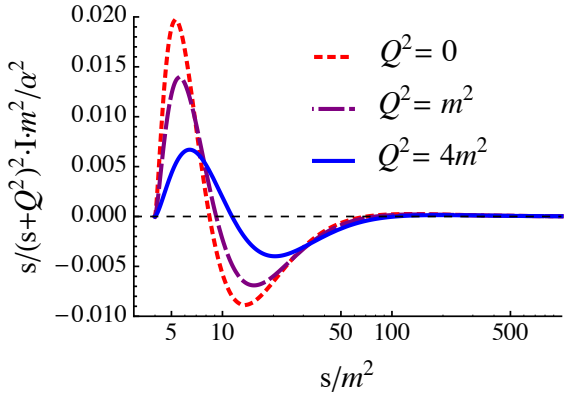

Figure 3.6: The $\gamma^*\gamma \to e^+e^-$ tree level result (spinor QED) for the integrand I in the sum rule of Eq. (2.79b) multiplied by s, with I given by Eq. (3.10), where one of the photons is quasi-real. The definitions of the curves are as in Fig. 3.4.

Vector QED Now we will discuss two-photon production of a spin-1 massive pair described by a complex vector field $W_\mu(x)$. A spin-1 particle with mass M may have an electric charge (e), magnetic dipole (μ), and an electric quadrupole moment (Q), and thus to describe its interaction with the electromagnetic field (A_μ) we ought in general to write the following Lagrangian density :

$$\begin{aligned}\mathcal{L} = &-\frac{1}{4}F_{\mu\nu}F^{\mu\nu} - \frac{1}{2}W^*_{\mu\nu}W^{\mu\nu} - M^2W^*_\mu W^\mu \\ &+ ieW^*_{\mu\nu}A^\mu W^\nu - ieA_\mu W^*_\nu W^{\mu\nu} + e^2A^2W^*_\mu W^\mu \\ &+ iel_1W^*_\mu W_\nu F^{\mu\nu} + el_2\left[(D^*_\mu W^*_\nu)W^\alpha\partial_\alpha F^{\mu\nu} + W^*_\alpha(D_\mu W_\nu)\partial^\alpha F^{\mu\nu}\right]/(2M^2)\end{aligned} \tag{3.22}$$

where $D_\mu = \partial_\mu + ieA_\mu$, $W_{\mu\nu} = \partial_\mu W_\nu - \partial_\nu W_\mu$, and the electromagnetic moments are given in terms of parameters l_i as follows :

$$\begin{aligned}\mu &= (1+l_1)\frac{e}{2M}, \\ Q &= (l_2-l_1)\frac{e}{M^2}.\end{aligned} \tag{3.23}$$

The previous studies show that the feature of the tree-level unitarity[1] is maintained for theories with so-called 'natural' values of electromagnetic moments. In such theories the particles are structureless from electromagnetic point of view and their charge distribution is pointlike. According to previous findings, the natural values for a spin-1 particle electromagnetic moments are: $\mu = e/M$, $Q = -e/M$, and hence we deduce the natural values for our model parameters: $l_1 = 1$ (corresponding with a g-factor $g = 2$), $l_2 = 0$.

For this case we study the helicity-difference sum rule of Eq. (2.79a) with both real or quasi-real photons ($Q_i^2 \to 0$). The $\gamma^*\gamma^* \to W^*W$ cross sections to lowest order in α in the limit where both of the virtual photons become real ($Q_2^2 = 0$) are given by :

$$\Delta\sigma = \frac{4\pi\alpha^2}{s}\left[-19\sqrt{1-\frac{4M^2}{s}} + 8\left(2-\frac{5M^2}{s}\right)\operatorname{arctanh}\sqrt{1-\frac{4M^2}{s}}\right] \tag{3.24}$$

$$\begin{aligned}\sigma_{tot} = \frac{4\pi\alpha^2}{M^2s^3}\Bigg[&s(12M^4+3M^2s+4s^2)\sqrt{1-\frac{4M^2}{s}} \\ &-24M^4(s-2M^2)\operatorname{arctanh}\sqrt{1-\frac{4M^2}{s}}\Bigg]\end{aligned} \tag{3.25}$$

$$\begin{aligned}\sigma_\parallel = \frac{2\pi\alpha^2}{M^2s^3}\Bigg[&s(18M^4+3M^2s+4s^2)\sqrt{1-\frac{4M^2}{s}} \\ &-24M^4(s-3M^2)\operatorname{arctanh}\sqrt{1-\frac{4M^2}{s}}\Bigg]\end{aligned} \tag{3.26}$$

$$\begin{aligned}\sigma_\perp = \frac{2\pi\alpha^2}{M^2s^3}\Bigg[&s(6M^4+3M^2s+4s^2)\sqrt{1-\frac{4M^2}{s}} \\ &-24M^4(s-M^2)\operatorname{arctanh}\sqrt{1-\frac{4M^2}{s}}\Bigg]\end{aligned} \tag{3.27}$$

For the sum rules involving the helicity difference of Eq. (2.79a) we show the corresponding integrand multiplied by s in Fig. 3.7. We observe that the expected cancellation between low and high energy contributions occurs only for natural values of electromagnetic moments. This can be related to the unitarity violation for a theory with non-point like fields. The tree-level contributions to the lowest order coefficients c_1 and c_2 for light-by-light scattering in spin-1 QED are given by

[1] Tree-level unitarity provides a criterion for the renormalizability of a model at a given energy scale. [95]

$$c_1 = \frac{29\alpha^2}{160M^4}, \qquad c_2 = \frac{27\alpha^2}{160M^4} \tag{3.28}$$

When comparing Eqs. (3.11), (3.20) and (3.28) we observe another curious pattern for the values of the difference of low-energy constants $c_2 - c_1$ when considering different spins. From the cases of spin 0, 1/2 and 1, it seems, that this value can be related to a spin by a very simple formula :

$$c_2 - c_1 = (-1)^{(2l+1)} \frac{(2l+1)\alpha^2}{240M^4} \tag{3.29}$$

Again this relation is valid only in the case of natural moments, i.e. point-like particles. One can suppose that such a rule holds for any spins. It would be interesting to check this assumption for the spin-3/2 fields which is the only remaining consistent theory of higher spin fields.

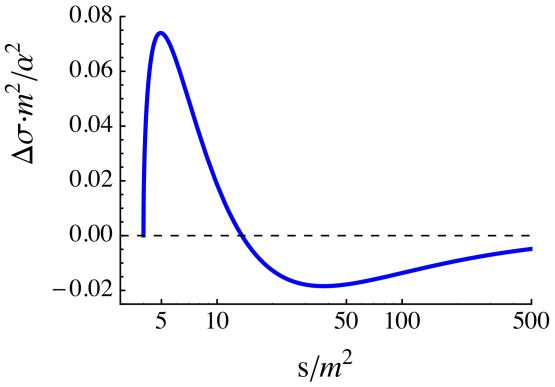

Figure 3.7: The $\gamma\gamma \to W^*W$ tree level result (vector QED) for the integrand in the $\Delta\sigma \equiv \sigma_2 - \sigma_0$ sum rule of Eq. (2.79a), multiplied by s (where both of the photons are real).

3.1.2 Loop corrections in scalar QED

To examine the sum rules at higher orders of perturbation theory we will study the two-photon production process in a specific model quantum field theory. We take one of the simplest examples: a self-interacting scalar field $\phi(x)$ with charge e and mass m as described by the following Lagrangian density,

$$\mathcal{L} = (D^\mu\phi)^* D_\mu\phi - m^2\phi^*\phi - \frac{\lambda_0}{4}(\phi^*\phi)^2 - \frac{1}{4}F^{\mu\nu}F_{\mu\nu}, \tag{3.30}$$

where λ_0 is the self-interaction coupling constant, while the covariant derivatives and electromagnetic field-strength tensor are given as usual by $D_\mu = \partial_\mu + ieA_\mu$ and $F_{\mu\nu} = \partial_\mu A_\nu - \partial_\nu A_\mu$.

We already discussed the two-photon production of a scalar pair at leading order in α. Now we consider $\gamma\gamma$-fusion at the order of $\mathcal{O}(\lambda\alpha)$ which is described by a set of one-loop Feynman graphs in Fig.(3.8). First two diagrams include correction to the propagator giving rise to the ultraviolet divergence, which is absorbed by renormalization of mass. The four diagrams including the vertex correction vanish. In the end the non-vanishing contribution comes from the three graphs in the last row on Fig. 3.8. The explicit expression for the one-loop production

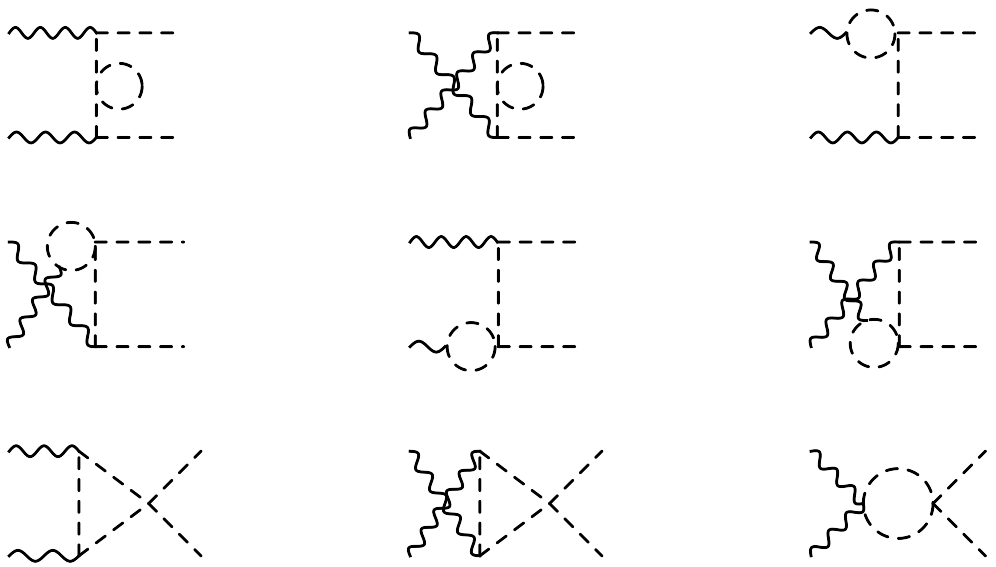

Figure 3.8: Pair production in scalar QED with self-interaction at one-loop order.

process is given by:

$$\begin{aligned} M^{(1-loop)}_{\lambda_1\lambda_2} &= -i\,4\pi\alpha\tilde{\lambda}_0\,2\,\mu^{4-d}\,\varepsilon_\mu(q_1,\lambda_1)\,\varepsilon_\nu(q_2,\lambda_1) \\ &\times\int\frac{d^dl}{(2\pi)^d}\left\{\frac{(2l+q_1)_\mu(2l-q_2)_\nu}{((q_1+l)^2-m^2)((q_2-l)^2-m^2)(l^2-m^2)}\right. \\ &\left.-\frac{g_{\mu\nu}}{(l^2-m^2)((q_1+q_2-l)^2-m^2)}\right\}, \end{aligned} \tag{3.31}$$

where $\varepsilon^\mu(q,\lambda)$ denotes the photon polarization vector, with helicity $\lambda=\pm1$. In Eq. (3.31), the first term describes the contribution of the first and the second diagrams and the second term corresponds to the contribution of the third graph in the last row in Fig. 3.8. Note that all three diagrams contribute only to M_{++} and M_{00}, i.e. helicity-0 amplitudes, because we have only s-wave rescattering. Helicity-2 contributions would necessarily involve the d-waves and higher due to conservation of the angular momentum. For exactly the same reason we have no angular dependence of the loop contribution. The sum of the 3 diagrams is finite because it is proportional to $q_1\,q_2$, i.e, the two external momenta. This happens indeed due to current conservation. In this case the superficial divergence of the result is less then the superficial divergence of each diagram.

For the considered theory the one-loop amplitude for the case when one of photons has zero virtuality has the following covariant decomposition :

$$\begin{aligned} \left[i\mathcal{M}^{(1)}_{\lambda_1\lambda_2}\right]_{Q_2^2=0} =& ie^2\varepsilon^\mu(q_1,\lambda_1)\varepsilon^\nu(q_2,\lambda_2)\left[F_T(s,Q_1^2,Q_2^2)\,(q_1\cdot q_2 g_{\mu\nu}-q_{2\mu}q_{1\nu})+\right. \\ &\left.+\frac{Q_1^2Q_2^2}{X}\left[F_L(s,Q_1^2,Q_2^2)-F_T(s,Q_1^2,Q_2^2)\right]q_{2\mu}q_{1\nu}\right]_{Q_2^2=0}, \end{aligned} \tag{3.32}$$

$F(s)$ denotes the (dimensionless) form factor describing the transition of photons to a scalar pair at one-loop order and the subscripts T and L stand for transverse and longitudinal photons respectively.

The explicit expressions for form factors are given by :

$$F^T(s,Q_1^2,0) = \frac{1}{(2\pi)^2(s+Q_1^2)^2}\left\{s+Q_1^2+4m^2\text{arctanh}^2\frac{1}{\beta}+ \right. \\ \left. +2Q_1^2\beta\text{arctanh}\frac{1}{\beta} - m^2\ln^2\frac{\kappa+1}{\kappa-1} - Q_1^2\kappa\ln\frac{\kappa+1}{\kappa-1}\right\}, \tag{3.33}$$

$$F^L(s,Q_1^2,0) = \frac{1}{4(2\pi)^2(s+Q_1^2)^2}\left\{8(s+Q_1^2)+4\,\text{arctanh}\frac{1}{\beta}\left[-4s\beta+(s-Q_1^2)\text{arctanh}\frac{1}{\beta}\right]- \right. \\ \left. -(s-Q_1^2)\ln^2\frac{\kappa+1}{\kappa-1}+4(s-Q_1^2)\kappa\ln\frac{\kappa+1}{\kappa-1}\right\}, \tag{3.34}$$

with $\kappa = \sqrt{1+4m^2/Q_1^2}$.

Next-to-leading order corrections to the cross-sections are given by an interference of the tree-level amplitudes with the one-loop :

$$W^{(1)}_{\lambda_1'\lambda_2'\lambda_1\lambda_2} = \frac{\beta}{32\pi}\int_0^\pi \mathrm{d}\cos\theta\left(\mathcal{M}^{(1)}_{\lambda_1\lambda_2}\mathcal{M}^{(0)*}_{\lambda_1'\lambda_2'}+\mathcal{M}^{(0)}_{\lambda_1\lambda_2}\mathcal{M}^{(1)*}_{\lambda_1'\lambda_2'}\right), \tag{3.35}$$

which can be related to cross sections using Eqs. (2.12). The cross sections σ_2, $\sigma_\perp$, σ_{TL} vanish at this order according to previous discussion. The non-vanishing response functions for the case when one photon is (quasi-)real are given by

$$\left[\sigma_0^{(1)}\right]_{Q_2^2=0} = \left[\sigma_\parallel^{(1)}\right]_{Q_2^2=0} = \alpha^2\lambda\pi\beta\xi_T\text{Re}\,F_T(s,Q_1^2,0), \\ \left[\frac{\tau_{TL}^{(1)}}{Q_1Q_2}\right]_{Q_2^2=0} = \alpha^2\lambda\pi\frac{\beta}{2(s+Q_1^2)}\left[\xi_L F_T(s,Q_1^2,0)-\xi_T F_L(s,Q_1^2,0)^*\right], \tag{3.36}$$

where we used the notation:

$$\xi_T = \frac{2}{\beta(s+Q_1^2)}\left[\beta Q_1^2+4m^2\text{arctanh}\beta\right], \\ \xi_L = \frac{2}{\beta(s+Q_1^2)}\left[-2\beta s+(s-Q_1^2)\text{arctanh}\beta\right]. \tag{3.37}$$

We firstly study the sum rules Eqs. (2.79a), (2.79b) and (2.79c) for the case of one real or quasi-real photon $Q_2^2 \to 0$ and for arbitrary space-like virtuality of the other photon. As the one-loop contribution to τ_{TL} vanishes for one quasi-real photon, one notices that the sum rule of Eq. (2.79b) is trivially satisfied. For the sum rules of Eqs. (2.79a) and (2.79c) the corresponding integrands multiplied by s for the case of one real or quasi-real photon and for different virtualities of the other photon are shown on Fig. 3.9 and Fig. 3.10. One can clearly see how the low and high-energy contributions cancel each other. Thus all three sum rules of Eqs. (2.79a), (2.79b) and (2.79c) are exactly verified for arbitrary space-like values of Q_1^2. One notices from Figs. 3.9 and 3.10 that for larger values of Q_1^2 the zero crossing of the integrands shifts to larger values of s, requiring higher energy contributions for cancellation to take place. For the helicity difference sum rule of Eq. (2.79a) one notices that analogously to the leading order result, σ_0 dominates at low energies while with increasing energies σ_2 overtakes. For the one-loop contribution, it was verified both analytically and numerically that the sum rule is obeyed at the one-loop level.

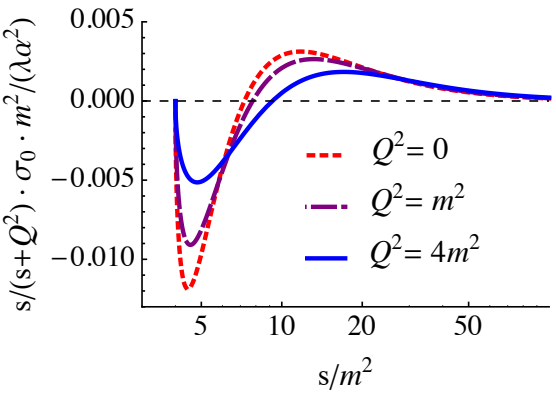

Figure 3.9: The integrand of the SR (2.79a) in one-loop approximation in the scalar QED. The definitions of the curves are as in Fig. 3.4.

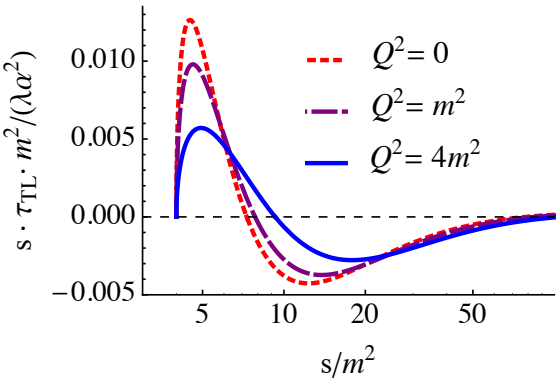

Figure 3.10: The integrand of the SR (2.79c) for the scalar QED in one-loop approximation. The definitions of the curves are as in Fig. 3.4.

Finally using Eqs. (2.80a, 2.80d), we obtain for the $\mathcal{O}(\alpha^2\lambda)$ contributions to the lowest order coefficients c_1 and c_2 :

$$c_1 = \frac{1}{8\pi}\int_{4m^2}^{\infty} \mathrm{d}s \frac{\sigma_{\parallel}(s,0,0)}{s^2} = -\frac{\alpha^2\lambda}{4608\pi^2 m^4}, \qquad c_2 = \frac{1}{8\pi}\int_{4m^2}^{\infty} \mathrm{d}s \frac{\sigma_{\perp}(s,0,0)}{s^2} = 0,$$
$$c_4 = -\frac{1}{4\pi}\int_{4m^2}^{\infty} \mathrm{d}s \frac{\sigma_0(s,0,0)}{s^3} = \frac{\alpha^2\lambda}{8640\pi^2 m^6}. \tag{3.38}$$

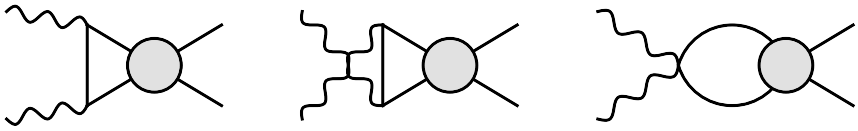

Figure 3.11: The contribution to the $\gamma\gamma$-fusion process within the ϕ^4 field theory considered in this work. The solid lines denote the charged scalar fields.

3.2 Sum rules in non-perturbative field theory

We already demonstrated how the sum rules are realized in a perturbation theory for the tree level amplitudes as well as for the one-loop corrections. Now we are going to examine the sum rules at higher orders of perturbation theory and study how they apply in the non-perturbative regime.

Being based on general assumptions about analytic structure of the amplitude and unitarity, sum rules apply also outside the regime where perturbative expansions hold. As sum rules are consequences of such general principles as analyticity and unitarity, they allow to establish rigorous relations between physical observables, even when the underlying theory is non-perturbative in nature and cannot be solved exactly at the moment.

Studies of causality constraints on the basis of different sum rules were carried out in the past in a number of different contexts. Especially the realization of the well-known GDH sum rule within perturbative field theory was analyzed for spin-1/2 targets at the lowest nontrivial order [96] as well as at higher orders in QED [97]. In Refs. [98, 99] consequences of the sum rules within asymptotically free theories were considered. In more recent years, they have also been discussed within the context of quantum gravity [100, 101].

In the following, we will use light-by-light scattering sum rules as a tool to study causality constraints within a model field theory, the ϕ^4 scalar theory. We will consider a bubble-chain resummation and demonstrate it to be consistent with causality to all orders of perturbation theory. Furthermore, it is shown that the sum rule strictly defines the non-perturbative structure of the solutions which arise dynamically within this approximation. In a particular regime of the coupling constant the spectrum of solutions contains a dynamically generated bound state and a K-matrix pole. For another domain the solution possesses an unphysical pole with negative invariant mass being a direct sign of the inconsistency of the approximation.

3.2.1 Bubble-chain sum

A class of diagrams naturally arises when one analyzes how the sum rules are realized at higher orders in perturbation theory, and in fact beyond perturbation theory. In the following, we discuss the contribution of the bubble-chain type diagrams to the $\gamma\gamma$-fusion process as shown on Fig. 3.11, where the shaded blob now denotes a bubble-chain contribution to the four-particle vertex, as shown in Fig. 3.12. The bubble-chain approximation arises in many contexts, but most notably as the leading large-N result of the $\mathcal{O}(N)$ models. The interest in such an approximation is due to the fact that it preserves much of the non-linear structure of the exact theory [102, 103].

The bubble-chain only contributes to the helicity-0 amplitude M_{++}, with the n-bubble contribution being given by

$$M_{++}^{(n+1)}(s) = 4\pi\alpha\,\tilde{\lambda}_0\,[-\tilde{\lambda}_0 B(s)]^n\,2F(s). \tag{3.39}$$

In the dimensional regularization scheme the one-loop corrections to the four-particle vertex,

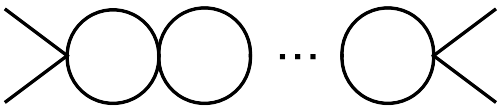

Figure 3.12: The bubble chain corection to the four-point vertex function arising in the scalar ϕ^4 theory.

corresponding with a single bubble in Fig.C.16, can be expressed through the scalar integral:

$$B(s) \equiv -i\,(4\pi)^2\mu^{4-d}\int \frac{d^dl}{(2\pi)^d}\frac{1}{[(q_1+q_2+l)^2-m^2+i\varepsilon]\,[l^2-m^2+i\varepsilon]}. \tag{3.40}$$

This integral has the explicit form:

$$B(s) = -L_d(\mu^2) + 2 - \beta\,\ln\frac{1+\beta}{1-\beta} + i\pi\beta\theta(s-4m^2). \tag{3.41}$$

Here $L_d = -2/(4-d) + \gamma_E + \log(m^2/4\pi\mu^2)$ is the dimensional regularization factor and μ is the corresponding dimensional regularization scale, $\gamma_E = -\Gamma'(1) \simeq 0.5772$ is Euler constant. We define a renormalized coupling constant $\tilde{\lambda}$ by the equation

$$\tilde{\lambda}^{-1}(\mu^2) = \tilde{\lambda}_0^{-1} - L_d(\mu^2) + 2. \tag{3.42}$$

This gap equation allows to renormalize the calculated contribution to each order perturbatively. Using such renormalization, leads to the renormalized (subtracted) one-loop four-point function:

$$\tilde{B}(s) \equiv B(s) - B(4m^2) = -\beta\,\ln\frac{1+\beta}{1-\beta} + i\pi\beta\theta(s-4m^2). \tag{3.43}$$

We notice that our renormalization procedure is conveniently chosen so as to make a subtraction at threshold: $\tilde{B}(4m^2) = 0$. We show the real and imaginary parts of the renormalized function $\tilde{B}(s)$ versus s in Fig. 3.13.

The interference of two chain diagrams with total number of $(n-1)$ bubble loops gives rise to a cross-section correction of the order $\mathcal{O}(\tilde{\lambda}^n)$. For the helicity-difference cross-section, which in the given case is equal to the helicity-0 cross section, we obtain as correction beyond the tree-level:

$$\Delta\sigma^{(n)}(s) = \alpha^2(-\tilde{\lambda})^n\frac{4\pi}{s}\beta\left\{\xi\,\mathrm{Re}\left[F(s)\tilde{B}^{n-1}(s)\right] - |F(s)|^2\sum_{i=0}^{n-2}\tilde{B}^i(s)\left[\tilde{B}^{n-2-i}(s)\right]^*\right\}. \tag{3.44}$$

We note that the renormalized mass m, which enters the cross-section of Eq. (3.44) is also μ dependent such that the full result is not. A very nice discussion of the renormalization scale dependence in this model can be found in Section II of Ref. [103].

We checked explicitly that the expression of Eq. (3.44) satisfies the helicity-difference sum rule exactly in each order of perturbation theory, i.e.

$$\mathrm{I}^{(n)}(\tilde{\lambda}) \equiv \int\limits_{4m^2}^{\infty}\mathrm{d}s\,\frac{\Delta\sigma^{(n)}(s)}{s} = 0. \tag{3.45}$$

In Fig. 3.14, we plot the integrands of the sum rule at different orders of perturbation theory. One sees that in all cases the low- and high-energy contributions cancel.

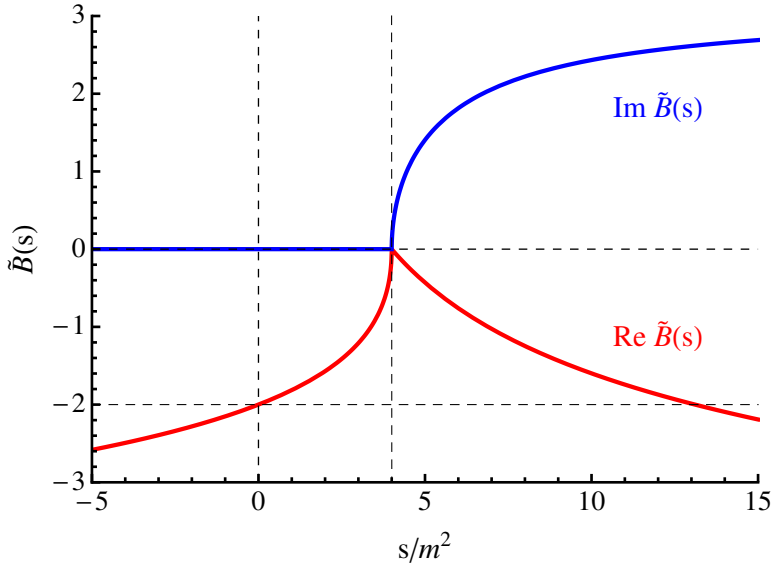

Figure 3.13: Real and imaginary part of the renormalized one-loop correction to the four-point function of Eq. (3.43), as function of s.

It is well-known in quantum field theory that when trying to sum the different orders of perturbation theory, the resulting series is mostly divergent and has at best a meaning as an asymptotic series, a notable exception being the case of theories which have the property of asymptotic freedom [104, 105, 106]. As a result, the perturbation theory often can not determine the solution uniquely. If we are only interested in perturbative phenomena, it is not a problem to deal with it in the region of small coupling constants. However if we are interested in non-perturbative phenomena then we are faced with the problem to give a meaning to a divergent series.

For example, the photon propagator calculated in the leading logarithmic approximation possesses an unphysical pole associated with negative invariant mass and negative probability, usually called the "Landau ghost" [107, 108]. In QED, however, due to the smallness of the coupling constant the ghost appears at an extremely high energy scale, and the results at the energy scales accessible in experiment are not influenced by it. However, in contrast to the QED case, in the theory under consideration the coupling constant is not constrained to small values, and we are faced with the need to regularize our solution. The appearance of the Landau singularity is usually attributed to non-Borel-summability of the considered series, where some individual Feynman amplitudes are positive and grow like the factorial of the number of vertices producing a singularity on the real positive axis of the Borel transform of the perturbative series [109]. A similar situation arises also in the context of our model. We can easily see how non-Borel-summability manifests itself in the context of sum rules, by analyzing the contribution from the high-energy region to the sum rule integral. In the example under study, the cross section Eq. (3.44) in the n-bubble approximation behaves at large s as:

$$\Delta\sigma^{(n)}(s) \sim \tilde{\lambda}^n \frac{(\ln s/m^2)^{n-2}}{s} \,. \tag{3.46}$$

The contribution of the high-energy region to the sum rule integral can then be approximated

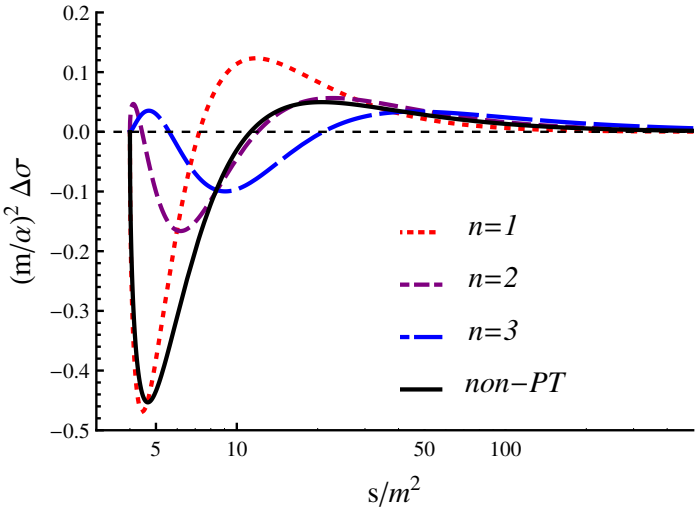

Figure 3.14: The integrand of the sum rule Eq. (3.45) for the scalar QED with four-particle self-interaction. The (red) fine-dashed line corresponds with the one-loop approximation, the (purple and blue) medium- and large-dashed lines correspond with two- and three-loop approximations respectively, the (black) solid line corresponds with the non-perturbative sum of loop diagrams. The integrands are shown for $\tilde{\lambda}^{-1} = -4$.

by:

$$\int\limits_{\Lambda^2}^{\infty} \frac{\Delta\sigma^{(n)}(s)}{s} \mathrm{d}s \sim \int\limits_{\Lambda^2}^{\infty} \tilde{\lambda}^n \frac{(\ln s/m^2)^{n-2}}{s^2} \mathrm{d}s = \tilde{\lambda}^n (n-2)! \frac{1}{\Lambda^2} \left(1 + \ln\frac{\Lambda^2}{m^2} + \mathcal{O}(1/n)\right), \qquad (3.47)$$

where $\Lambda^2 \gg m^2$. As we see for positive $\tilde{\lambda}$ the high-energy contribution to the sum rule integral is positive definite and grows factorially with the order of perturbation theory, which amounts to the non-Borel summability of the series

$$\mathrm{I}(\tilde{\lambda}) \equiv \sum_{n=0}^{\infty} \mathrm{I}^{(n)}(\tilde{\lambda}) = \sum_{n=0}^{\infty} \int\limits_{s_0}^{\infty} \frac{\Delta\sigma^{(n)}(s)}{s} \mathrm{d}s\,. \qquad (3.48)$$

As a result we can consider $\sum_{n=0}^{\infty} \Delta\sigma^{(n)}(s)$ only in the sense of an asymptotic series. According to Poincaré [110], a divergent series is an asymptotic expansion of a function $f(\lambda)$ if

$$\lim_{|\lambda|\to 0} \left[\frac{1}{\lambda^n} \left| f(\lambda) - \sum_{k=0}^{n} f_k \lambda^k \right|\right] = 0, \qquad \text{for } n \geqslant 0. \qquad (3.49)$$

This definition implies that an asymptotic series does not define a function uniquely. The expansion coefficients of a function of the type $e^{-1/\lambda} \sum_{k=0}^{n} f_k \lambda^k$ being identically zero, such a function can be added to $f(\lambda)$ without changing Eq. (3.49)[111].

Thus it is natural to expect that in order to obtain the correct behavior of $I(\tilde{\lambda})$ for positive $\tilde{\lambda}$, one has to modify a formal resummation of the geometric series of renormalized bubble-chain corrections to the cross section in Eq. (3.44), which is given by:

$$\Delta\sigma(s) = \sum_{n=0}^{\infty} \Delta\sigma^{(n)}(s) = \Delta\sigma^{(\mathrm{tree})} - \alpha^2 \frac{4\pi}{s} \beta \left\{ \xi\, \mathrm{Re}\left[\frac{F(s)}{\tilde{\lambda}^{-1} + \tilde{B}(s)}\right] + \left|\frac{F(s)}{\tilde{\lambda}^{-1} + \tilde{B}(s)}\right|^2 \right\}, \qquad (3.50)$$

where the tree-level cross section satisfies the sum rule by itself. As was discussed above, due to the non-Borel-summability of the series of Eq. (3.48), we do not have any reasons to expect that the sum rule integral will vanish for the resummed theory. In Fig. 3.15 we show the dependence of the sum rule integral for the cross section of Eq. (3.50) on the value of $\tilde{\lambda}$. We indeed notice from Fig. 3.15 that the sum rule is only valid for negative values of $\tilde{\lambda}$ (denoted by region I), but is violated for positive values of $\tilde{\lambda}$ (regions II and III on Fig. 3.15), showing that the naive procedure of the resummation is not applicable. In order to preserve validity of the sum rules beyond the region I, we need to find a way to evaluate the cross section correctly. We will discuss the physical situation for the three regions of $\tilde{\lambda}$ in the following.

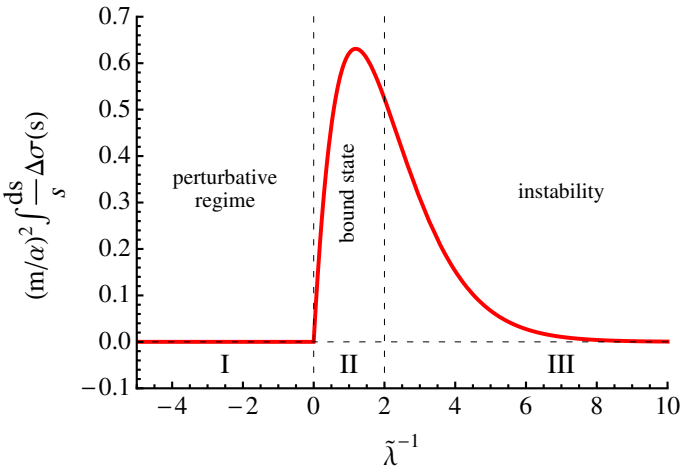

Figure 3.15: The dependence of the sum rule integral for the helicity difference cross section of the $\gamma\gamma \to X$ process on the inverse coupling $\tilde{\lambda}^{-1}$.

3.2.2 Discussion of the results

Region I : convergent perturbative expansion

Though the sum of Eq. (3.48) is formally undetermined, we can still use a naive resummation at least in the region of negative $\tilde{\lambda}$, as one can see from Fig. 3.15. For $\tilde{\lambda}^{-1} < 0$ (region I) the series is alternating-sign, since $\mathrm{Re}\tilde{B}(s) < 0$, and one can expect the series to be resummable. Alternatively we can interpret such a resummation at the level of photon-photon-fusion amplitudes by summing up contributions of bubble-chain diagrams at different orders, which yields the amplitude :

$$M_{++}(s,\theta) = M_{++}^{(tree)}(s,\theta) + 4\pi\alpha \, \frac{2F(s)}{\tilde{\lambda}^{-1} + \tilde{B}(s)} \,, \tag{3.51}$$

with tree-level amplitude given as in Eq. (3.1). Squaring the amplitude of Eq. (3.51) then yields the cross section of Eq. (3.50). In the region I, the amplitude (3.51) has no poles for all complex values of s, and the series is conventionally convergent for all values of s. Thus the formal resummation of Eq. (3.50) satisfies the sum rule.

Region II : Bound state and K-matrix pole

Now we proceed to the discussion of the second domain, denoted by region II on Fig. 3.15. In the range of $0 < \tilde{\lambda}^{-1} < 2$ the sum rule is not valid for the naive cross section, given by Eq. (3.50). It is easy to see that the amplitude of Eq. (3.51) acquires additional singularities below the two-particle production threshold. Indeed from Fig. 3.13 we can see that the imaginary part

of $\tilde{B}(s)$ vanishes for $s < 4m^2$ and monotonically increases for $s > 4m^2$. The real part satisfies the inequality

$$-\infty < \mathrm{Re}\tilde{B}(s) \leqslant 0, \tag{3.52}$$

for $0 \leqslant s < \infty$, with the upper limit attained for $s = 4m^2$. Thus we see that for $\tilde{\lambda}^{-1} > 0$ there is always a S-matrix pole for $s < 4m^2$. Above the two-particle threshold, there is a value of s where $\tilde{\lambda}^{-1} = -\mathrm{Re}\tilde{B}(s)$, corresponding with a K-matrix pole as will be discussed below.

We firstly discuss the S-matrix pole below the threshold. Such a pole is usually interpreted in a relativistic field theory as s bound state with a propagator given by :

$$P_B(s) = \frac{1}{s - M_B^2}. \tag{3.53}$$

One notices from Fig. 3.13 that the mass of the bound state varies continuously from $M_B^2 = 4m^2$ for $\tilde{\lambda}^{-1} = 0$ to $M_B^2 = 0$ for $\tilde{\lambda}^{-1} = 2$ as we sweep over the bound state region on Fig. 3.15. In general, the position of the bound state pole is defined by the equation :

$$\tilde{\lambda}^{-1} = -\tilde{B}(M_B^2). \tag{3.54}$$

It is important to note that the bound state singularity is not described by perturbation theory being essentially of non-perturbative nature. The (effective) coupling of the $\phi\phi^*$ to the bound state is defined by the residue of the pole as :

$$g_{\mathrm{eff}}^2 = \frac{1}{|\tilde{B}'(M_B^2)|}, \qquad \tilde{B}'(M_B^2) = \frac{d}{ds}\tilde{B}(s)\Big|_{s=M_B^2}, \tag{3.55}$$

and the coupling of the bound state to two photons is given by $e^2 2F(s)$. Then the second term in Eq. (3.51) corresponds to a Feynman graph on Fig. 3.16 where the dashed line denotes the propagation of the bound state and the bubble loops define the mass correction.

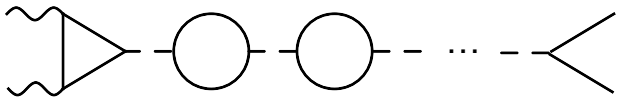

Figure 3.16: The $\gamma\gamma$-fusion amplitude corresponding with the dynamical generation of a bound state.

The agreement with the sum rule can now be remedied by treating the bound state as a new asymptotic state of the theory and thus including the channel of its production in $\gamma\gamma$ collisions, see Fig. 3.17. The total helicity cross-section for the case of the single particle final state can be defined as follows:

$$\Delta\sigma(s) = \frac{1}{2s}\int \frac{d^4p}{(2\pi)^3}\delta^4(p - q_1 - q_2)(2\pi)^4\delta(s - M_B^2)|M|^2. \tag{3.56}$$

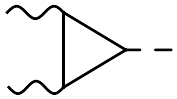

Figure 3.17: The amplitude of the bound state production in the $\gamma\gamma$-fusion process.

The contribution of the bound state production to the helicity-0 cross section is:

$$\sigma_0^{(\gamma\gamma\to B)}(s) = 4\pi\alpha^2\frac{g_{\mathrm{eff}}^2}{M_B^2}|F(M_B^2)|^2\,\delta(s - M_B^2). \tag{3.57}$$

It is not difficult to see now that its contribution to the sum rule integral:

$$\int_0^\infty \frac{ds}{s}\,\sigma_0^{(\gamma\gamma\to B)}(s) = 4\pi\alpha^2\,\frac{g_{\rm eff}^2}{M_B^4}\,|F(M_B^2)|^2, \tag{3.58}$$

exactly counter-balances the contribution of the $\gamma\gamma \to \phi\phi^*$ channel shown in Fig. 3.15. Thus the causality is restored in this region of $\tilde{\lambda}$.

We now turn to the position of the singularity above the two-particle threshold. To describe the elastic $\phi\phi$ scattering in the bubble-chain approximation in the ϕ^4 theory, we only need to consider S-wave scattering. The (dimensionless) elastic forward scattering amplitude $f(s)$ is expressed through a real phase shift $\delta(s)$ as:

$$f(s) = e^{i\delta(s)}\sin\delta(s), \tag{3.59}$$

or through the K-matrix amplitude $K(s) \equiv \tan\delta(s)$ as:

$$f(s) = \frac{1}{K^{-1}(s) - i}. \tag{3.60}$$

Since the imaginary part of the loop function is

$$\mathrm{Im}\,B(s) = \pi\beta\,\theta\left(s - 4m^2\right), \tag{3.61}$$

for $s \geq 4m^2$ we can define the elastic amplitude as :

$$f(s) = \pi\beta\frac{1}{-\tilde{\lambda}^{-1} - \tilde{B}(s)} = \left(-\frac{1}{\tilde{\lambda}\pi\beta} + \frac{\beta}{\pi}\ln\frac{1+\beta}{1-\beta} - i\right)^{-1}, \tag{3.62}$$

and hence

$$K^{-1}(s) = -\frac{1}{\tilde{\lambda}\pi\beta} + \frac{\beta}{\pi}\ln\frac{1+\beta}{1-\beta}. \tag{3.63}$$

In Fig. 3.18 we show plots of the phase shift for different values of the coupling constant. Note that for positive $\tilde{\lambda}$ the phase-shift starts from π which indicates the presence of one bound state. Also for positive $\tilde{\lambda}$ the phase shift crosses $\pi/2$ at $s > 4m^2$ satisfying the following equation:

$$\tilde{\lambda}^{-1} = -\mathrm{Re}\,\tilde{B}(M_K^2). \tag{3.64}$$

This is the location of the K-matrix pole, corresponding with a scattering amplitude which becomes purely imaginary. Usually this behaviour is attributed to a resonance. However, above the threshold, the imaginary part of $B(s)$ is not zero for all complex s and $\tilde{\lambda}$ is real, the amplitude (3.51) does not possess a S-matrix pole for $s > 4m^2$. Hence there is no resonance associated with this K-matrix pole. Note that on the left side of region II on Fig. 3.15, corresponding with $\tilde{\lambda}^{-1} = 0$, the K-matrix pole merges with the bound state and is defined by the position $M_K^2 = 4m^2$. When reaching the right side of region II on Fig. 3.15, corresponding with $\tilde{\lambda}^{-1} = 2$, the mass is obtained from $\mathrm{Re}B(M_K^2) = 0$, which implies $M_K^2 \approx 13.1m^2$.

Region III : Ground state instability and tachyonic solution

If $\tilde{\lambda}^{-1}$ becomes larger than $+2$ (corresponding with region III on Fig. 3.15), the binding energy of the bound state exceeds $2m$, and the pole crosses the point $s = 0$, moving into the unphysical region $s < 0$, and producing a tachyonic solution (a pole with negative invariant mass). The occurrence of a pole for negative values of s signals that the ground state of the theory is unstable [102, 103]. We could formally still include this pole in the $\gamma\gamma$-production channel as

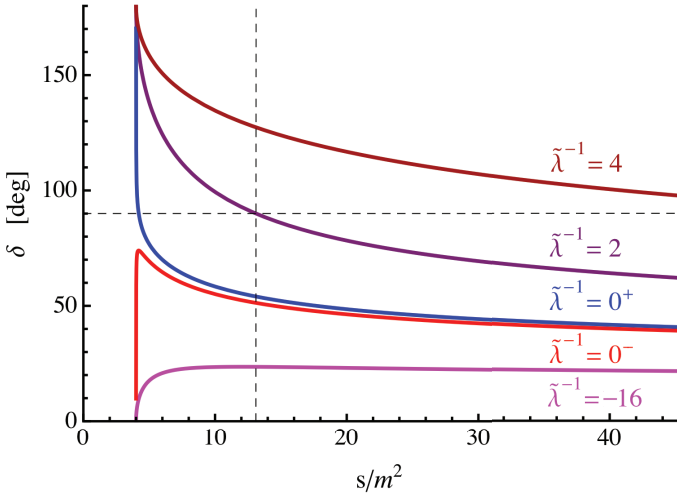

Figure 3.18: Phase shift for different values of $\tilde{\lambda}$.

an asymptotic state and add its contribution to the total cross section in the same way as we did for the bound state, which restores the validity of the sum rule. For small positive values of $\tilde{\lambda}$, i.e. $\tilde{\lambda}^{-1} \to +\infty$, corresponding with the right asymptotic edge of the region III in Fig. 3.15, the contribution of the tachyon pole is vanishingly small and the sum rule is satisfied approximately. This is consistent with the observations in other models, for example, in the leading logarithmic approximation in QED, where the position of the Landau pole appears at very large scales due to the smallness of the fine structure constant. The position of the tachyon pole in this limit is defined by

$$M^2 \sim -e^{1/\tilde{\lambda}}, \tag{3.65}$$

which shows explicitly the non-perturbative structure of this contribution. The contribution of this pole in this sum rule is asymptotically defined as

$$\Delta\sigma(s) \sim 1/M^2 \sim -e^{-1/\tilde{\lambda}} \tag{3.66}$$

and vanishes when $\tilde{\lambda}^{-1} \to +\infty$. However such a procedure has a number of inconsistencies. Being required by the sum rule such extra contribution spoils the general principles of field theory. The cross section of Eq. (3.66) is negative, thus indicating that the appearance of a tachyon ghost state contradicts the usual quantum mechanical probabilistic interpretation and spoils unitarity. Moreover, the delta function is located at a space-like squared four momentum $-M^2$ indicating the occurrence of a tachyonic instability and spoiling the analyticity principle. All these facts show that the bubble-chain approximation is essentially inconsistent in region III of the coupling constant. For the full theory, such unphysical state will not appear among the exact eigenstates.

3.3 Meson production in $\gamma\gamma$ collision

In the previous section, the sum rules of Eqs. (2.79a, 2.79b, 2.79c) integrating to zero have been shown to hold exactly in perturbative calculations (e.g., in QED or QCD in the perturbative regime) and in the non-perturbative regime. As their derivation is general, their realization in QCD, in its non-perturbative regime, allows to gain insight in the $\gamma^*\gamma \to$ hadrons cross-sections. This was illustrated in Ref. [22] for the sum rule of Eq. (2.79a). In the following, we will elaborate on the discussion of Ref. [22] and extend it to the other sum rules presented above. The required non-perturbative input for the absorptive parts of the sum rules are the $\gamma^*\gamma \to$ hadrons response functions. We will perform an analysis by estimating the hadronic contributions to these response functions by the corresponding $\gamma^*\gamma^* \to M$ (with M a meson) production processes, which are described in terms of the $\gamma^*\gamma^* \to M$ transition form factors.

3.3.1 Real photons

We first consider the helicity sum rule of Eq. (2.79a) with two real photons producing a meson, as well as the sum rules of Eq. (2.80d) for the mesonic contributions to the low-energy constants c_1 and c_2 describing the forward light-by-light scattering amplitude. When producing mesons, the sum rules will hold separately for states of given intrinsic quantum numbers. Therefore, we will separately study the sum rule contributions for light quark isovector mesons (Table 3.1), for light quark isoscalar mesons (Table 3.2), as well as $c\bar{c}$ mesons (Table 3.3). For the isoscalar mesons, one could in principle separate the contributions according to singlet or octet states (or alternatively according to $(u\bar{u} + d\bar{d})/\sqrt{2}$ or $s\bar{s}$ states). The corresponding mesons involve mixings however which complicate such separation, as this mixing is not known well enough for some of the states. We will postpone such a separation for a future work and add all isoscalar meson contributions in the present work.

The pseudo-scalar mesons contribute to the helicity-0 cross section only, given by Eq. (2.17). The corresponding contributions to the helicity sum rule of Eq. (2.79a) as well as the c_1 and c_2 sum rules are shown for the π^0 in Table 3.1, for the η, η' in Table 3.2, and for the $\eta_c(1S)$ state in Table 3.3.

Besides the pseudo-scalar mesons, also scalar mesons can only contribute to σ_0. We show the contributions of the $a_0(980)$ in Table 3.1, for the $f_0(980)$ and $f_0'(1370)$ in Table 3.2, and for the $\chi_{c0}(1P)$ state in Table 3.3. For the scalar mesons, mainly the $f_0'(1370)$ state gives a sizable contribution due to its large 2γ decay width. An analogous analysis for the contribution of the $f_0(500)$ may yield a sizable although largely uncertain contribution. The uncertainty mainly comes from the relatively large range in the extracted values for the 2γ decay width $\Gamma_{\gamma\gamma}$ as well as the mass of the $f_0(500)$, as listed by the PDG [1]. Furthermore, given the large width of the $f_0(500)$, a strong interference with the $\gamma\gamma \to \pi\pi$ non-resonant background contribution is expected here. Estimating such contribution goes beyond the narrow resonance analysis performed in this work, and will require to perform the sum rule analysis directly for multi-meson channels ($\pi\pi$, $K\bar{K}$, ...). Such an analysis is certainly an interesting topic for future studies.

For the helicity sum rule, one notices that in order to compensate the large negative contribution from the pseudo-scalar mesons, and to lesser extent from the scalar meson states, an equal strength is required in the helicity-2 cross section, σ_2. For light quark mesons, the dominant feature of the helicity-2 cross section in the resonance region arises from the multiplet of tensor mesons $f_2(1270)$, $a_2(1320)$, and $f_2'(1525)$. For $c\bar{c}$ tensor mesons, the dominant tensor contribution is given by the $\chi_{c2}(1P)$ state.

Measurements at various e^+e^- colliders, notably the recent high statistics measurements by the BELLE Collaboration of the $\gamma\gamma$ cross sections to $\pi^+\pi^-$, $\pi^0\pi^0$, $\eta\pi^0$, and K^+K^- chan-

nels [112, 113, 114] have allowed to accurately establish their parameters. For the light quark mesons, the experimental analyses of decay angular distributions have found [115] that the tensor mesons are produced predominantly (around 95% or more) in a state of helicity $\Lambda = 2$. We will therefore assume in all of the following analyses that $\Gamma_{\gamma\gamma}(\mathcal{T}(\Lambda = 0)) \approx 0$, and that $\Gamma_{\gamma\gamma}(\mathcal{T}(\Lambda = 2)) \approx \Gamma_{\gamma\gamma}(\mathcal{T})$ in Tables 3.1, 3.2, 3.3. We show all tensor meson contributions to the helicity difference sum rule as well as the c_1, c_2 sum rules for which the 2γ decay widths are known.

For the isovector meson contributions to the helicity sum rule, shown in Table 3.1, we conclude that the lowest isovector tensor meson composed of light quarks, $a_2(1320)$, compensates to around 70% the contribution of the π^0, which is entirely governed by the chiral anomaly. Including the $a_0(980)$ and $a_2(1700)$ meson contributions, one notices from Table 3.1 that the deviation from zero for the helicity sum rule is at the 3 σ level. This is most likely due to additional, yet unmeasured, two-photon strength at higher energies in the tensor channel, contributing to σ_2. The perturbative calculation for the $\gamma\gamma \to q\bar{q}$ cross sections indeed shows that at higher energies σ_2 dominates over σ_0, see Fig. 3.5. Using a duality argument, one can then expect additional strength from tensor mesons at higher energies.

For the isoscalar states composed of light quarks, the cancellation is even more remarkable: the sum of $f_2(1270)$ and $f_2'(1525)$, within the experimental accuracy, nearly entirely compensates the combined contribution of the η and η' mesons. Also here, one may expect the remaining strength to arise from tensor mesons at higher energies.

	m_M [MeV]	$\Gamma_{\gamma\gamma}$ [keV]	$\int \frac{ds}{s}\,\Delta\sigma$ [nb]	c_1 [10^{-4} GeV^{-4}]	c_2 [10^{-4} GeV^{-4}]
π^0	134.9766 ± 0.0006	$(7.8 \pm 0.5)\ 10^{-3}$	-195 ± 13	0	10.94 ± 0.70
$a_0(980)$	980 ± 20	0.3 ± 0.1	-20 ± 8	0.021 ± 0.007	0
$a_2(1320)$	1318.3 ± 0.6	1.00 ± 0.06	134 ± 8	0.039 ± 0.002	0.039 ± 0.002
$a_2(1700)$	1732 ± 16	0.30 ± 0.05	18 ± 3	0.003 ± 0.001	0.003 ± 0.001
Sum			-63 ± 17	0.06 ± 0.01	10.98 ± 0.70

Table 3.1: $\gamma\gamma$ sum rule contributions of the light quark isovector mesons based on the present PDG values [1] of the meson masses (m_M) and their 2γ decay widths $\Gamma_{\gamma\gamma}$. Fourth column: $\sigma_2 - \sigma_0$ sum rule of Eq. (2.79a). Fifth, sixth columns: c_1, c_2 sum rules of Eqs. (2.80a, 2.80d) respectively.

For the $c\bar{c}$ states, one notices that the known strength in the tensor channel from the $\chi_{c2}(1P)$ state only compensates about 20% of the strength arising from the $\eta_c(1S)$ and $\chi_{c0}(1P)$ states. We can however expect a sizable contribution to this sum rule from states above the nearby $D\bar{D}$ threshold, which we denote by $s_D = 4m_D^2 \approx 14$ GeV^2, using the D-meson mass $m_D \approx 1.87$ GeV. So far, the helicity cross sections have not been measured above $D\bar{D}$ threshold. To estimate this continuum contribution to the helicity sum rule, which we denote by I_{cont}, we use a quark-hadron duality argument [116] , which amounts to replacing the integral of the helicity difference cross section for the $\gamma\gamma \to X$ process (with X any hadronic final state containing charm quarks) by the corresponding integral of the helicity difference cross section for the perturbative $\gamma\gamma \to c\bar{c}$ process :

$$I_{cont} \equiv \int_{s_D}^{\infty} ds\, \frac{1}{s}\,[\sigma_2 - \sigma_0]\,(\gamma\gamma \to X) \approx \int_{s_D}^{\infty} ds\, \frac{1}{s}\,[\sigma_2 - \sigma_0]\,(\gamma\gamma \to c\bar{c}), \tag{3.67}$$

where the perturbative cross section is given in Appendix B.2. The duality expressed by the approximate equality in Eq. (3.67) is meant to hold in a global sense, i.e. after integration over

	m_M [MeV]	$\Gamma_{\gamma\gamma}$ [keV]	$\int \frac{ds}{s}\,\Delta\sigma$ [nb]	c_1 [10^{-4}GeV^{-4}]	c_2 [10^{-4}GeV^{-4}]
η	547.853 ± 0.024	0.510 ± 0.026	-191 ± 10	0	0.65 ± 0.03
η'	957.78 ± 0.06	4.29 ± 0.14	-300 ± 10	0	0.33 ± 0.01
$f_0(980)$	980 ± 10	0.29 ± 0.07	-19 ± 5	0.020 ± 0.005	0
$f_0'(1370)$	$1200 - 1500$	3.8 ± 1.5	-91 ± 36	0.049 ± 0.019	0
$f_2(1270)$	1275.1 ± 1.2	3.03 ± 0.35	449 ± 52	0.141 ± 0.016	0.141 ± 0.016
$f_2'(1525)$	1525 ± 5	0.081 ± 0.009	7 ± 1	0.002 ± 0.000	0.002 ± 0.000
$f_2(1565)$	1562 ± 13	0.70 ± 0.14	56 ± 11	0.012 ± 0.002	0.012 ± 0.002
Sum			-89 ± 66	0.22 ± 0.03	1.14 ± 0.04

Table 3.2: $\gamma\gamma$ sum rule contributions of the light quark isoscalar mesons based on the present PDG values [1] of the meson masses (m_M) and their 2γ decay widths $\Gamma_{\gamma\gamma}$. Fourth column: $\sigma_2 - \sigma_0$ sum rule of Eq. (2.79a). Fifth, sixth columns: c_1, c_2 sum rules of Eqs. (2.80a, 2.80d) respectively.

	m_M [MeV]	$\Gamma_{\gamma\gamma}$ [keV]	$\int \frac{ds}{s}\,\Delta\sigma$ [nb]	c_1 [10^{-7}GeV^{-4}]	c_2 [10^{-7}GeV^{-4}]
$\eta_c(1S)$	2980.3 ± 1.2	6.7 ± 0.9	-15.6 ± 2.1	0	1.79 ± 0.24
$\chi_{c0}(1P)$	3414.75 ± 0.31	2.32 ± 0.13	-3.6 ± 0.2	0.31 ± 0.02	0
$\chi_{c2}(1P)$	3556.2 ± 0.09	0.50 ± 0.06	3.4 ± 0.4	0.14 ± 0.02	0.14 ± 0.02
Sum resonances			-15.8 ± 2.1	0.49 ± 0.03	1.97 ± 0.24
continuum			15.1		
resonances + continuum			-0.7 ± 2.1		

Table 3.3: $\gamma\gamma$ sum rule contributions of the lowest $c\bar{c}$ mesons based on the present PDG values [1] of the meson masses (m_M) and their 2γ decay widths $\Gamma_{\gamma\gamma}$. Fourth column: the $\sigma_2 - \sigma_0$ sum rule of Eq. (2.79a), for which we also show the duality estimate of Eq. (3.70) for the continuum contribution above $D\bar{D}$ threshold ($\sqrt{s} \geq 2m_D$), as well as the sum of resonances and continuum contributions. Fifth, sixth columns: c_1, c_2 sum rules of Eqs. (2.80a, 2.80d) respectively.

the energy of the helicity difference cross section above the threshold s_D. As we have verified in Section 3.1 that the perturbative cross section satisfies the helicity sum rule exactly, i.e.

$$0 = \int\limits_{4m_c^2}^{\infty} ds\, \frac{1}{s}\, [\sigma_2 - \sigma_0]\, (\gamma\gamma \to c\bar{c}), \tag{3.68}$$

with m_c the charm quark mass, we can re-express Eq. (3.67) as:

$$I_{cont} \approx - \int\limits_{4m_c^2}^{s_D} ds\, \frac{1}{s}\, [\sigma_2 - \sigma_0]\, (\gamma\gamma \to c\bar{c}). \tag{3.69}$$

Using Eq. (3.14) for the $\gamma\gamma \to c\bar{c}$ helicity difference cross section, we finally obtain:

$$I_{cont} \approx -8\pi\,\alpha^2 \int\limits_{4m_c^2}^{s_D} ds\, \frac{1}{s^2} \left\{ -3\sqrt{1 - \frac{4m_c^2}{s}} + 2\,\ln\left(\frac{\sqrt{s}}{2m_c} \left[1 + \sqrt{1 - \frac{4m_c^2}{s}} \right] \right) \right\}. \tag{3.70}$$

Using the PDG value $m_c \approx 1.27$ GeV [1], we show the duality estimate for $-I_{cont}$ in Fig. 3.19, as function of the integration limit s_D (solid red curve). Using the physical value of the $D\bar{D}$ threshold, $s_D \approx 14$ GeV^2, we obtain: $I_{cont} \approx 15.1$ nb. We notice that within the experimental uncertainty, this fully cancels the sum of the $\eta_c(1S), \chi_{c0}(1P)$, and $\chi_{c2}(1P)$ resonance contributions to the $\sigma_2 - \sigma_0$ sum rule, as is shown in Table 3.3. This cancellation quantitatively illustrates the interplay between resonances with hidden charm ($c\bar{c}$ states) and production of charmed mesons in order to satisfy the sum rule. It will be interesting to further test this experimentally by measuring the $\gamma\gamma$ production cross sections above $D\bar{D}$ threshold, where a plethora of new states (so-called XYZ states) have been found in recent years, see e.g. Ref. [117] for a review.

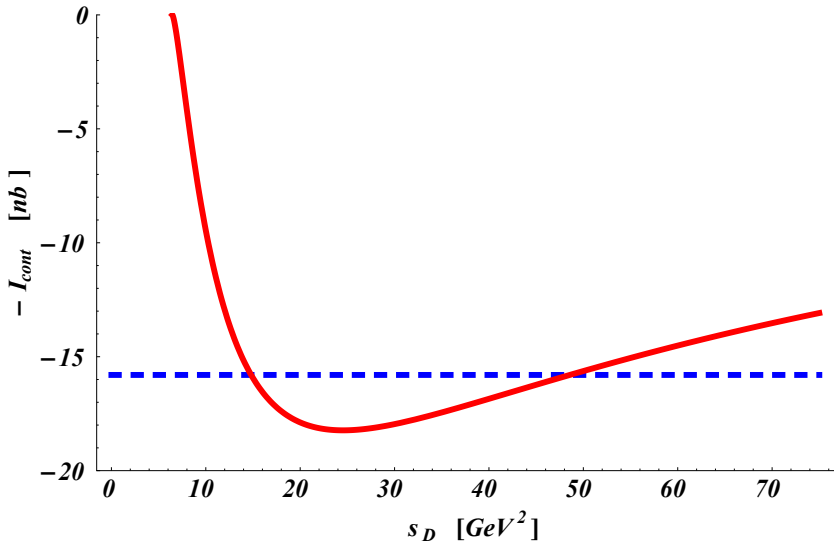

Figure 3.19: Solid (red) curve: duality estimate for the negative of the continuum contribution of Eq. (3.70) to the helicity difference sum rule for charm quarks as function of the integration limit s_D, which represents the threshold for charmed meson production ($D\bar{D}$ threshold). For reference, the dashed (blue) horizontal curve indicates the sum of the $\eta_c(1S), \chi_{c0}(1P)$, and $\chi_{c2}(1P)$ resonance contributions to the $\sigma_2 - \sigma_0$ sum rule, as listed in Table 3.3. The intersection between both curves near the physical $D\bar{D}$ threshold, $s_D \approx 14$ GeV^2 indicates a perfect cancellation between these resonance contributions and the duality estimate for the continuum contribution.

We have also computed the meson contributions to the forward light-by-light scattering coefficients c_1 and c_2 (fifth and sixth columns respectively in Tables 3.1, 3.2, 3.3). The dimensionality of these coefficients requires them to scale with the meson mass m_M as $1/m_M^4$. Therefore, the higher mass mesons contribute very insignificantly to these coefficients. One notes that the coefficient c_1, which involves the cross section $\sigma_\parallel$, does not receive any contributions from pseudo-scalar mesons, and is dominated by the tensor mesons $a_2(1320)$ and $f_2(1270)$, with smaller contributions from the scalar states around 1 GeV. On the other hand, the coefficient c_2, which involves the cross section $\sigma_\perp$, is totally dominated by the contributions from pseudo-scalar mesons, especially the light π^0, with contributions of η and η' at the 10% level of the π^0 contribution.

3.3.2 Virtual photons

We next discuss the sum rule of Eq. (2.79b) when both photons are quasi-real. One immediately observes that pseudo-scalar mesons do not contribute to this sum rule. However scalar, axial-vector and tensor mesons will contribute to this sum rule. The sum rule will therefore require a cancellation mechanisms between scalar, axial-vector and tensor mesons, which we will study subsequently. According to Eq. (2.26), scalar mesons (with mass m_S) can only contribute to the $\sigma_\parallel$ term in the sum rule, and their contribution is given by:

$$\int ds \, \frac{1}{s^2} \left[\sigma_\parallel\right]_{Q_1^2=Q_2^2=0} = 16\pi^2 \, \frac{\Gamma_{\gamma\gamma}(\mathcal{S})}{m_S^5}. \tag{3.71}$$

In contrast, Eq. (2.35) shows that axial-vector mesons (with mass m_A) can only contribute to the τ_{TL}^a term in the sum rule as:

$$\int ds \, \frac{1}{s} \left[\frac{\tau_{TL}^a}{Q_1 Q_2}\right]_{Q_1^2=Q_2^2=0} = -8\pi^2 \, \frac{3\,\tilde{\Gamma}_{\gamma\gamma}(\mathcal{A})}{m_A^5}, \tag{3.72}$$

where we introduced the equivalent 2γ decay width $\tilde{\Gamma}_{\gamma\gamma}(\mathcal{A})$ of Eq. (2.31).

The tensor mesons in general contribute to both terms of the sum rule of Eq. (2.79b). For the $\sigma_\parallel$ contribution, we will use the experimental observation that light tensor mesons are produced predominantly (around 95 % or more) in a state of helicity $\Lambda = 2$, as discussed above. Neglecting therefore the much smaller σ_0 term, we obtain from Eq. (2.57):

$$\int ds \, \frac{1}{s^2} \left[\sigma_\parallel\right]_{Q_1^2=Q_2^2=0} = \int ds \, \frac{1}{s^2} \frac{1}{2} \left[\sigma_2\right]_{Q_1^2=Q_2^2=0} = 8\pi^2 \, \frac{5\,\Gamma_{\gamma\gamma}(\mathcal{T})}{m_T^5}, \tag{3.73}$$

with tensor meson mass m_T. For the τ_{TL}^a contribution to the sum rule of Eq. (2.79b), one sees from Eq. (2.57) that it involves a helicity-1 amplitude for tensor meson production by quasi-real photons, which unfortunately is not known experimentally for any tensor meson. It is reasonable to assume that for quasi-real photons this amplitude is much smaller than the helicity-2 amplitude which is known to dominate in the real photon limit. We will therefore neglect the helicity-1 contribution in the following analysis.

One notes from Eqs. (3.71, 3.72, 3.73) that only axial-vector mesons give a negative contribution to the sum rule of Eq. (2.79b), whereas scalar and tensor mesons contribute positively. As the sum rule has to integrate to zero, one therefore obtains a cancellation mechanism between axial-vector mesons on one hand, and scalar and tensor mesons on the other. In Table 3.4, we show the contributions of the lowest lying scalar, axial-vector and tensor mesons, for which the 2γ widths are known experimentally. One sees from Table 3.4 that the two lowest lying axial-vector mesons $f_1(1285)$ and $f_1(1420)$ are entirely cancelled, within error bars, by the contribution of the dominant tensor meson $f_2(1270)$. Using the experimentally known 2γ widths, the deviation of the (zero) sum rule value is at the 2σ level, which hints at a moderate contribution of either another higher mass axial-vector meson state or a non-resonant contribution with axial-vector quantum numbers.

At finite Q_1^2, for $Q_2^2 = 0$, the three sum rules of Eqs. (2.79a, 2.79b, 2.79c) imply relations between the transition form factors for the contributing mesons. To date, experimental results for the $\gamma^*\gamma \to$ meson FFs only exist for the pseudo-scalar mesons π^0, η, η', and $\eta_c(1S)$, as well as for the axial-vector mesons $f_1(1285)$, and $f_1(1420)$. For other mesons, in particular the tensor mesons, the corresponding form factors still wait to be extracted. We have seen from Table 3.2 that for real photons the dominant contributions to the helicity sum rule of Eq. (2.79a) come from η, η', and $f_2(1270)$ mesons, where the $f_2(1270)$ contribution cancels

	m_M [MeV]	$\Gamma_{\gamma\gamma}$ [keV]	$\int \frac{ds}{s^2}\,\sigma_\parallel(s)$ [nb / GeV^2]	$\int ds\,\left[\frac{1}{s}\frac{\tau^a_{TL}}{Q_1Q_2}\right]_{Q_i^2=0}$ [nb / GeV^2]	$\int ds\,[I]_{Q_i^2=0}$ [nb / GeV^2]
$f_1(1285)$	1281.8 ± 0.6	3.5 ± 0.8	0	-93 ± 21	-93 ± 21
$f_1(1420)$	1426.4 ± 0.9	3.2 ± 0.9	0	-50 ± 14	-50 ± 14
$f_0(980)$	980 ± 10	0.29 ± 0.07	20 ± 5	0	20 ± 5
$f_0'(1370)$	$1200 - 1500$	3.8 ± 1.5	48 ± 19	0	48 ± 19
$f_2(1270)$	1275.1 ± 1.2	3.03 ± 0.35	138 ± 16	$\gtrsim 0$	138 ± 16
$f_2'(1525)$	1525 ± 5	0.081 ± 0.009	1.5 ± 0.2	$\gtrsim 0$	1.5 ± 0.2
$f_2(1565)$	1562 ± 13	0.70 ± 0.14	12 ± 2	$\gtrsim 0$	12 ± 2
Sum					76 ± 36

Table 3.4: Light isoscalar meson contributions to the sum rule of Eq. (2.79b) based on the present PDG values [1] of the meson masses (m_M) and their 2γ decay widths $\Gamma_{\gamma\gamma}$. For the axial-vector mesons, we quote the equivalent 2γ decay width $\tilde{\Gamma}_{\gamma\gamma}$ of Table 4.3. Fourth column: $\sigma_\parallel$ contribution, fifth column: τ^a_{TL} contribution, sixth column: total contribution to the sum rule of Eq. (2.79b).

to 90% the contribution from the η and η' mesons. We will therefore use the corresponding sum rule of Eq. (2.79a) at finite Q_1^2 to estimate the $\gamma^*\gamma \to f_2(1270)$ helicity-2 FF from the measured η and η' FFs, given by Eq. (2.20). Assuming that the helicity sum rule of Eq. (2.79a) is saturated by the η, η', and $f_2(1270)$ mesons, we then obtain:

$$\frac{5\,\Gamma_{\gamma\gamma}(f_2)}{m_{f_2}^3}\left[\frac{T_{f_2}^{(2)}(Q_1^2,0)}{T_{f_2}^{(2)}(0,0)}\right]^2 \simeq c_\eta\,\frac{1}{\left(1+Q_1^2/\Lambda_\eta^2\right)^2} + c_{\eta'}\,\frac{1}{\left(1+Q_1^2/\Lambda_{\eta'}^2\right)^2}, \tag{3.74}$$

where we have introduced the shorthand notation:

$$c_P \equiv \frac{\Gamma_{\gamma\gamma}(\mathcal{P})}{m_P^3}. \tag{3.75}$$

For $Q_1^2 = 0$, the $f_2(1270)$ meson contribution cancels to 90% the $\eta + \eta'$ contributions to the helicity sum rule. We can therefore use

$$\frac{5\,\Gamma_{\gamma\gamma}(f_2)}{m_{f_2}^3} \simeq c_\eta + c'_\eta, \tag{3.76}$$

which allows us to express Eq. (3.74) as:

$$\frac{T_{f_2}^{(2)}(Q_1^2,0)}{T_{f_2}^{(2)}(0,0)} \simeq \left[\frac{c_\eta}{c_\eta + c_{\eta'}}\,\frac{1}{\left(1+Q_1^2/\Lambda_\eta^2\right)^2} + \frac{c_{\eta'}}{c_\eta + c_{\eta'}}\,\frac{1}{\left(1+Q_1^2/\Lambda_{\eta'}^2\right)^2}\right]^{1/2}. \tag{3.77}$$

We can obtain a second estimate for the $T^{(2)}$ FF for the $f_2(1270)$ meson from the sum rule of Eq. (2.79b). We have seen from Table 3.4 that for quasi-real photons the dominant contributions to this sum rule come from $f_1(1285)$, $f_1(1420)$, and $f_2(1270)$ mesons, where the $f_2(1270)$ contribution cancels to 95 % the contribution from the $f_1(1285)$ and $f_1(1420)$ mesons. We can then also use the corresponding sum rule of Eq. (2.79b) at finite Q_1^2 to estimate the $\gamma^*\gamma \to f_2(1270)$ helicity-2 FF from the measured $f_1(1285)$ and $f_1(1420)$ FFs, using Eqs. (2.38, 2.41). Assuming that the helicity sum rule of Eq. (2.79b) is saturated by the $f_1(1285)$, $f_1(1420)$,

and $f_2(1270)$ mesons, which we denote by f_1, f_1', and f_2 respectively, and retaining only the supposedly dominant $\Lambda = 2$ FF for the tensor mesons, we obtain:

$$\frac{5\,\Gamma_{\gamma\gamma}(f_2)}{m_{f_2}^5}\,\frac{1}{\left(1+\frac{Q_1^2}{m_{f_2}^2}\right)}\left[\frac{T_{f_2}^{(2)}(Q_1^2,0)}{T_{f_2}^{(2)}(0,0)}\right]^2 \simeq c_{f_1}\,\frac{1}{\left(1+Q_1^2/\Lambda_{f_1}^2\right)^4}+c_{f_1'}\,\frac{1}{\left(1+Q_1^2/\Lambda_{f_1'}^2\right)^4}, \quad (3.78)$$

where

$$c_A \equiv \frac{3\,\tilde{\Gamma}_{\gamma\gamma}(\mathcal{A})}{m_A^5}. \quad (3.79)$$

For $Q_1^2 = 0$, the $f_2(1270)$ meson contribution cancels to 95% the $f_1(1285) + f_1(1420)$ contributions to the sum rule of Eq. (2.79b), which implies:

$$\frac{5\,\Gamma_{\gamma\gamma}(f_2)}{m_{f_2}^5} \simeq c_{f_1} + c_{f_1'}. \quad (3.80)$$

This allows to obtain a second estimate for the $T^{(2)}$ FF for the $f_2(1270)$ meson as:

$$\frac{T_{f_2}^{(2)}(Q_1^2,0)}{T_{f_2}^{(2)}(0,0)} \simeq \left(1+\frac{Q_1^2}{m_{f_2}^2}\right)^{1/2}\left[\frac{c_{f_1}}{c_{f_1}+c_{f_1'}}\,\frac{1}{\left(1+Q_1^2/\Lambda_{f_1}^2\right)^4}+\frac{c_{f_1'}}{c_{f_1}+c_{f_1'}}\,\frac{1}{\left(1+Q_1^2/\Lambda_{f_1'}^2\right)^4}\right]^{1/2} \quad (3.81)$$

In Fig. 3.20 we show the two sum rule estimates of Eqs. (3.77) and (3.81) for the FF $T^{(2)}$ for the tensor meson $f_2(1270)$ using the known experimental information for either η, η' in Eq. (3.77), or $f_1(1285), f_1(1420)$ in Eq. (3.81). When taking the ratio of both estimates, one sees that it is larger than 80% below 1 GeV^2 and around 65% around $Q^2 = 2$ GeV^2. It will be interesting to confront these estimates with a direct measurement of the $T^{(2)}$ FF for the $f_2(1270)$ tensor meson.

In an analogous way, we can provide an estimate for the $a_2(1320)$ FF from the π^0 FF. We have seen from Table 3.1 that π^0 and $a_2(1320)$ provide the dominant isovector contributions to the helicity sum rule of Eq. (2.79a), where the $a_2(1320)$ contribution cancels to 70% the contribution from the π^0. We can therefore use the sum rule of Eq. (2.79a) for one virtual photon to estimate the helicity-two FF $T^{(2)}$ for the $a_2(1320)$ meson in terms of the π^0 FF, given by Eq. (2.20), as:

$$\frac{T_{a_2}^{(2)}(Q_1^2,0)}{T_{a_2}^{(2)}(0,0)} \simeq \frac{1}{\left(1+Q_1^2/\Lambda_\pi^2\right)}. \quad (3.82)$$

As empirically the $\gamma^*\gamma \to \pi^0$ FF is the best known meson transition FF, it will be interesting to test the above prediction for the $a_2(1320)$ FF experimentally.

3.4 Conclusions

We have studied the forward light-by-light scattering sum rules which involve energy weighted integrals of $\gamma^*\gamma$ fusion cross sections, measurable at e^+e^- colliders, which integrate to zero

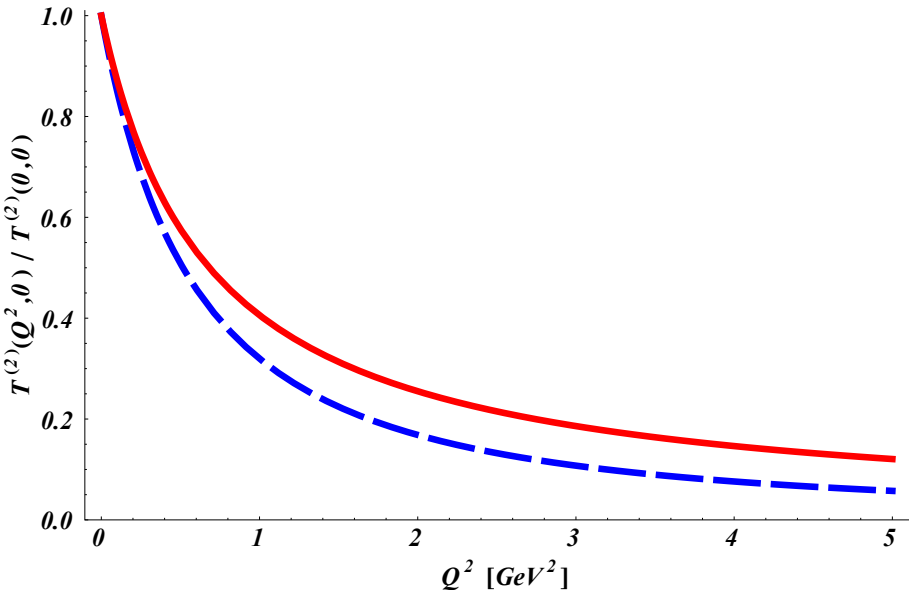

Figure 3.20: Sum rule estimates for the form factor $T^{(2)}(Q^2,0)/T^{(2)}(0,0)$ with helicity $\Lambda = 2$ for the tensor meson $f_2(1270)$. Red solid curve: sum rule estimate from Eq. (3.77), using the experimental input from the η and η' FFs. Blue dashed curve: sum rule estimate from Eq. (3.81), using the experimental input from the $f_1(1285)$ and $f_1(1420)$ FFs.

(super-convergence relations):

$$
\begin{aligned}
0 &= \int\limits_{s_0}^{\infty} ds \frac{1}{(s+Q_1^2)} \left[\sigma_0 - \sigma_2\right]_{Q_2^2=0}, \\
0 &= \int\limits_{s_0}^{\infty} ds \, \frac{1}{(s+Q_1^2)^2} \left[\sigma_{\parallel} + \sigma_{LT} + \frac{(s+Q_1^2)}{Q_1 Q_2} \tau_{TL}^a \right]_{Q_2^2=0}, \\
0 &= \int\limits_{s_0}^{\infty} ds \, \left[\frac{\tau_{TL}}{Q_1 Q_2}\right]_{Q_2^2=0}.
\end{aligned}
$$

In these sum rules the $\gamma^*\gamma$ fusion cross sections are for one (quasi-) real photon and a second virtual photon which can have arbitrary (space-like) virtuality. The first of the sum rules generalizes the GDH sum rule for the helicity-difference $\gamma\gamma$ fusion cross section to the case of one real and one virtual photon. The two further sum rules are for $\gamma^*\gamma$ fusion cross sections which involve longitudinal photon amplitudes.

These sum rules were tested and verified exactly at tree and one-loop level in scalar and spinor QED for the case of two (quasi-)real and one virtual and one (quasi-)real photons. We have observed that for larger values of the photon's virtuality the higher energy contributions are required for cancellations to take place. Another observation is that for the helicity difference sum rule of Eq. (2.79a) the σ_0 cross section dominates at lower energies while with increasing energies σ_2 overtakes. Similar pattern is observed in the production of the hadronic states showing deep relation between perturbative production of $q\bar{q}$ pairs and hadronic resonances. Furthermore, we have tested the criterium of the tree-level unitarity imposed by the sum rules on the example of the massive spin-1 QED. We have observed that when applied to the

processes of higher spin particles production the sum rules hold for the natural values of the corresponding electromagnetic moments only.

Next, we have studied consequences of causality constraints imposed by the helicity-difference sum rule for the forward light-by-light scattering process within the ϕ^4 scalar quantum field theory. Within this theory, we have performed a non-perturbative resummation of bubble graphs. We have demonstrated that depending on the value of the renormalized self-interaction coupling of the ϕ^4 theory, three different regimes emerge. In a first regime, the perturbative series is convergent and the sum rule as calculated from the continuum states in the theory holds exactly. In a second regime for the renormalized coupling, the resummed amplitude acquires additional singularities: a dynamically generated bound state below the two-particle production threshold and a K-matrix pole above the two-particle production. Is was shown that when evaluating the light-by-light sum rule, the bound state contribution exactly cancels the continuum contribution, so as to verify the sum rule. Furthermore, we found a third regime of the renormalized coupling where a tachyonic solution with negative invariant mass appears, signaling that in this regime the vacuum is unstable and that the considered non-perturbative resummation is essentially inconsistent.

The results within the considered model relativistic quantum field theory have demonstrated that such sum rules provide a very powerful tool to quantitatively connect dynamically generated bound states with the continuum region of the theory. As such this can be a first step, to apply such a tool e.g. to the study meson bound states produced in the $\gamma\gamma$-fusion process presently under study at different e^+e^- collider facilities.

Finally, we have performed a detailed quantitative study of the new sum rules for the case of the production of light quark mesons as well as for the production of mesons in the charm quark sector. Using the empirical information in evaluating the sum rules, we have found that the helicity-difference sum rule requires cancellations between different mesons, implying non-perturbative relations. For the light quark isovector mesons, the π^0 contribution was found to be compensated to around 70% by the contribution of the lowest lying isovector tensor meson $a_2(1320)$. For the isoscalar light quark mesons, the η and η' contributions were found to be entirely compensated within the experimental accuracy by the two lowest-lying tensor mesons $f_2(1270)$ and $f_2'(1525)$. In the charm quark sector, the situation is different as it involves the narrow resonance contributions below $D\bar{D}$ threshold, and the continuum contribution above $D\bar{D}$ threshold. For the narrow resonances, the η_c was found to give by far the dominant contribution. When using a duality estimate for the continuum contribution, we found that it entirely cancels the narrow resonance contributions, verifying the sum rule, and pointing to large tensor strength (helicity 2) in the cross sections above $D\bar{D}$ threshold. It will be interesting to test this property experimentally.

The helicity difference sum rule has also been applied for the case of one real and one virtual photon. In this case the $\gamma^*\gamma$ fusion cross sections depend on the meson transition form factors (FFs). We have reviewed the general formalism and parameterization for the $\gamma^*\gamma \to$ meson transition FFs for (pseudo-) scalar, axial-vector, and tensor mesons. Because for scalar and tensor mesons the $\gamma^*\gamma$ transition FFs have not yet been measured, a direct test of the sum rules for finite virtuality is not possible at present. However, we were able to show that the helicity-difference sum rule allows to provide an estimate for the $f_2(1270)$ tensor FF in terms of the η, and η' FFs, and for the $a_2(1320)$ tensor FF in terms of the π^0 FF. Since empirical information on pseudo-scalar meson FFs is available, these relations provide predictions for tensor meson FFs which will be interesting to confront with experiment.

The sum rules involving the $\sigma_\parallel, \sigma_{LT}$, and τ^a_{TL} $\gamma^*\gamma$ response functions, have also been tested for the case of quasi-real photons. As pseudo-scalar mesons cannot contribute to this sum rule, a cancellation between scalar and tensor mesons on one hand and axial-vector mesons on the other hand is at work. Using the existing empirical information for quasi-real photons,

the contribution of the two lowest lying axial-vector mesons $f_1(1285)$ and $f_1(1420)$ was found to be entirely cancelled, within error bars, by the contribution of the dominant tensor meson $f_2(1270)$. When applying this sum rule to the case of one virtual photon, it again allows one to relate the $f_2(1270)$ tensor FF, this time to the transition FFs for the $f_1(1285)$ and $f_1(1420)$ mesons, which have both been measured. The predictions from the two different sum rules for the $f_2(1270)$ FF were found to agree within 20% for a virtuality below 1 GeV^2, and within 35% up to about 2 GeV^2. The sum rules which express the coefficients in a low-energy expansion of the forward light-by-light scattering amplitude in terms of $\gamma^*\gamma \to X$ cross sections may be used as a cross-check for models of the non-forward light-by-light scattering which are applied to evaluate the hadronic LbL contribution to $(g-2)_\mu$.

On the experimental side, the ongoing $\gamma\gamma$ physics programs by the BABAR, Belle and BES-III Collaborations, will allow to further improve the data situation significantly. In particular, the extraction of the $\gamma^*\gamma$ response functions through their different azimuthal angular dependencies, and the measurements of multi-meson final states ($\pi\pi$, $\pi\eta, \ldots$) promise to access besides the pseudo-scalar meson FFs also the scalar, axial-vector and tensor meson FFs, thus allowing direct tests of the sum rule predictions presented in this work.

Chapter 4

Hadronic light-by-light contribution to the anomalous magnetic moment of the muon

In previous chapters we discussed in detail the process of light-by-light scattering and in particular, the hadronic contribution to this process. The subject of the second part of this work is related to the contribution of the hadronic light-by-light scattering to the anomalous magnetic moment of the muon. The following chapter is devoted to the hadronic light-by-light correction to $(g-2)_\mu$ via the single meson exchange. To carry out our computation we will use a phenomenological description of the meson transition amplitudes. The two-loop integrals appearing in the calculation are treated by first performing the angular integration analytically, followed by a numerical evaluation of the remaining integrals. The values obtained, are the first estimates for the contributions of the scalar, axial-vector and tensor mesons based on the phenomenological information on the form factors and significantly disagree with other recent calculations. Our result completes a list of relevant single meson contributions to the hadronic light-by-light part of the muon's anomalous magnetic moment.

4.1 Introduction

Similarly to polarization effects in a dielectric medium, a charge in vacuum is continually emitting and reabsorbing virtual particles producing a shielding effect, the so-called vacuum polarization. As a result, due to virtual corrections the effective strength of interactions is substantially dependent on the interaction distance. This feature of the relativistic quantum field theory plays a fundamental role for an understanding and description of interaction processes. When the force is weak, or in other words, when the coupling is small the processes may be well described by the perturbation theory. While electromagnetic and weak interactions allow to apply perturbation expansions in a wide range of energy scales up to a Landau pole [107, 108], strong interaction coupling becomes small only at high energies as inferred by the property of asymptotic freedom. In particular, quantum chromodynamics (QCD) acquires the form of a perturbation theory (pQCD) only at energies above about 2 GeV, which as we will see, does not apply in the regime of interest to us. As we approach lower energies the strength of the strong coupling constant increases dramatically and the low-energy QCD becomes non-perturbative in character. This is the reason why the processes involving hadrons are usually hard to describe from first principles. To handle the phenomena of the non-perturbative nature one is compelled to resort to different approximations and model descriptions, which result is a substantial increase of the uncertainties. As a consequence, it is not surprising that the dominant part of the Standard Model (SM) uncertainty in the calculation of the anomalous magnetic moment of the muon originates from hadronic effects.

The strong interaction effects in the $(g-2)_\mu$ show up by virtue of the hadronic vacuum polarization in the photon propagator $\langle 0|TA^\mu(x_1)A^\nu(x_2)|0\rangle$ and in the light-by-light scattering four-point Green function $\big\langle 0|TA^\mu(x_1)A^\nu(x_2)A^\lambda(x_3)A^\rho(x_4)|0\big\rangle$. Being the leading in the electromagnetic coupling constant hadronic correction (i.e. starting at $\mathcal{O}(\alpha^2)$), the photon polarization

type diagrams (hereinafter vacuum polarization) shown in Fig. 4.1 are covering a major part of the hadronic contribution. The non-perturbative effects appearing in the hadronic vacuum polarization (VP) may be reliably described by exploiting causality (analyticity) and unitarity (optical theorem) in terms of experimental low energy data on electron-positron annihilation to hadrons. In particular, the VP has been estimated based on data for $e^+e^- \to$ hadrons, $e^+e^- \to \gamma+$hadrons, as well as τ decays, by several groups [41, 42, 43, 44, 45, 46, 47, 48, 49, 50]. It is expected, that the new data from ongoing experiments at Novosibirsk and BES-III will provide valuable experimental input to further constrain this contribution. It was estimated in Ref. [52] that such data will allow to reduce the uncertainty in the HVP to $\delta a_\mu(\text{l.o. HVP}) = 26 \times 10^{-11}$, compared to the most recent evaluation of the leading order VP [50] which sets it to the accuracy $\delta a_\mu(\text{HVP}) = 42.4 \times 10^{-11}$.

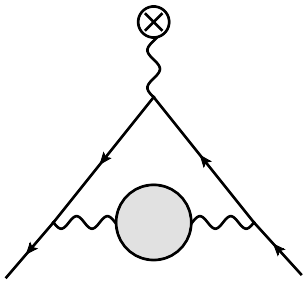

Figure 4.1: The hadronic vacuum polarization contribution to the anomalous magnetic moment of the muon

A much more problematic type of hadronic corrections are those related to hadronic Light-by-Light scattering (LbL). Though it sets in at order $\mathcal{O}(\alpha^3)$ only, experience shows that this contribution can be dramatically enhanced as happens in the leptonic counterpart [118]. Being a constituent of a loop diagram as shown in Fig. 4.2 it implies that three of the four photons[1] have off-shell momenta to be integrated over full four-momentum phase space. Obviously, perturbation theory can not give a satisfactory description of the strong interactions in such conditions, especially in the low-energy region, where the spectrum of the two-photon production shows sharp spikes of π^0, η and η' mesons while pQCD predicts a smooth continuum (Fig. 1.2). Moreover, it is believed that the process is even dominated by the low-energy region which makes a consistent calculation from the first principles unrealizable at the moment. Unfortunately, the direct experimental input for the non-perturbative dressed four-photon matrix element available at present is also very limited and the lattice QCD is still far away from the calculation of such objects with the required precision.

The early calculations were based on the assumption that the process is entirely dominated by the region around the muon mass. Within such an assumption it is suitable to apply Chiral Perturbation Theory (ChPT), which is limited to the low energy tail only. As would be expected, the applicability of the effective field theories (EFT) possesses the traditional limitations. The first kind of problem we face when dealing with the EFTs is their non-renormalizability. It means that the effective expansions are well-defined at low energies, however possess unphysical ultra-violet behavior in contrast to the underlying QCD, which is renormalizable at high energies, but has not well-defined infra-red behavior. Such an inconsistency in the cut-off dependence of two frameworks results in the fact that the predictions we obtain when trying to match low- and high-energy pieces acquire dependence on the cut-off scale. In the EFTs such dependence is usually absorbed in model parameters, which are then tuned to fit the appro-

[1] One of the photons is external in the considered diagram. Moreover the evaluation of the $(g-2)_\mu$ as we will see further implies setting the limit $k \to 0$

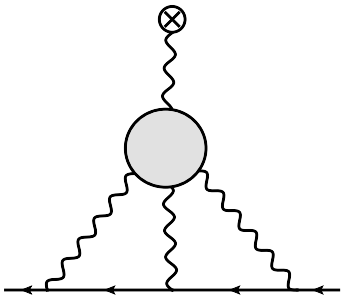

Figure 4.2: The hadronic light-by-light scattering contribution to the anomalous magnetic moment of the muon

priate short distance behavior. However, an estimate of the real model dependence is very difficult in the considered case as long as the exact solution of the problem is not known.

Another kind of complication we face when applying the EFTs to estimate the hadronic light-by-light correction is related to the absence of a clear distinction between different asymptotic regimes. As was mentioned before the loop integration implies the dependence of the integrand on three photon virtualities which run over the entire range of values. In the case of the hadronic vacuum polarization the two-point correlator is a function of a single variable, which allows to make a clear separation between low- and high- energy regions and accordingly to apply the low-energy effective theory and perturbative QCD consistently. In contrast, in multi-scale problems it is not possible to carry out such a separation to the full extent. We can still safely use the effective field theory and perturbative QCD in the soft and hard regions (where all the scales are either small or large), respectively. However, in the mixed soft-hard regions the effective and perturbative expansions are not valid any more. The approaches agreed as a framework for the evaluation of the hadronic light-by-light effects in such regions are for instance, operator product expansions and soft/hard factorization theorems [119].

At long last, all the attempts to apply the low-energy effective description of strong interactions in its pure form hardly meet with success. In such a situation one may naturally resort to phenomenological facts to ascertain some empirical patterns and constraints. First of all, although it was originally assumed that the process under study is low-energy in character, it was later observed that this assumption does not hold in general and the contributions from higher momentum region, around $0.5 \sim 1$ GeV are relevant as well. It means that the hadron resonances beyond the Goldstone bosons of ChPT may also play an important role in this process and have to be taken into account. Note that in photon-hadron interactions the photon mixes with hadronic vector-mesons like the ρ^0. From the hadronic VP, we know that the ρ meson is indeed expected to play an important role in the game. It thus looks natural to apply a vector-meson dominance (VMD) like model. The naive VMD model attempts to take into account this hadronic dressing by replacing the photon propagator as

$$\frac{ig^{\mu\nu}}{q^2} + \ldots \to \frac{ig^{\mu\nu}}{q^2}\frac{m_\rho^2}{m_\rho^2 - q^2} + \ldots \tag{4.1}$$

Of course real photons $q^2 \to 0$ in any case remain undressed and the dressing would go away for $m^2 \to \infty$. The main effect is that it provides a damping at high energies with the ρ mass as an effective cut-off (physical version of a Pauli-Villars cut-off). However, the naive VMD model does not respect chiral symmetry properties. The combination of correct low-energy structure of QCD with the vector-meson dominance (VMD) principles was realized in a consistent way in the resonance lagrangian approach [120, 121], as an extension of ChPT. Other effective theories which may be to some extent successfully used for the estimates of the hadronic light-by-light

effects are the Extended Nambu-Jona-Lasinio (ENJL) model [122] or the very similar hidden local symmetry (HLS) [123, 124, 125] and massive Yang-Mills models [79, 126].

An alternative approach commonly used for an effective description of QCD is the one based on the large-N_c limit. In this approach QCD is considered as $SU(N_c)$ for $N_c \to \infty$ and a true theory is approximated by an expansion in $1/N_c$ [127, 128, 129, 130, 81]. It turns out that the loop corrections appearing in the perturbative expansion are suppressed by powers of $1/N_c$ when the number of colors becomes large. In the context of chiral perturbation theory it means that the leading order contributions are covered by the tree-level effective Lagrangian assuming the scalar QED for the interaction of the photon with the charged pseudoscalars.

Based on EFT models, two major estimates of the full a_μ^{LbL} contribution exist. The BPP estimate [131, 132] is based on an extended Nambu-Jona-Lasinio model in which both a $1/N_c$ and chiral counting was used. The HKS estimate [133, 134, 135] was based on a hidden local gauge symmetry model. It is remarkable that despite considerable differences (which results in a different splitting of long and short distance physics), the results of two approaches are in a good agreement. It provided to be essentially dominated by the π^0-meson exchange, which was taken with the wrong sign, however. In order to eliminate the cut-off dependence in separating long distance and short distance physics when modeling the hadronic amplitudes, the arguments based on a quark-hadron duality, which holds exactly in the large-N_c limit of QCD [136, 137, 138], may be used successively. The spectrum of the large-N_c which amounts to an infinite series of narrow vector states may be fairly well approximated by a suitable lowest meson dominance (LMD+V) ansatz [139]. In this approximation the hadronic amplitudes assumed to be saturated by known low lying physical states of appropriate quantum numbers. This approach was adopted in a reanalysis of [140] in 2001, in which a sign mistake was discovered in the previous estimates of the dominant π^0, η, η' exchange contribution. This correction changed the central value of a_μ by $+167 \times 10^{-11}$, a 2.8σ shift, and reduced a larger discrepancy between theory and experiment. More recently [141] additional problems were found in previous calculations, this time in the short distance constraints (QCD/OPE) used in matching the high energy behavior of the effective models used for the π^0, η, η' exchange contribution. In addition, most of the evaluations do not take into account the dependence of the $\pi^0\gamma\gamma$ vertex on the pion virtuality. Such an assumption may be interpreted as a pole approximation of the hadronic production amplitude. In this case, however, to calculate the pole contribution consistently one has to respect the energy-momentum conservation in the external vertex, which is violated when trying to evaluate the on-shell pion contribution in the approaches used before. We will discuss this issue in more detail further on and present a new approach based on dispersion techniques which allows to avoid such inconsistencies in the next chapter. Nevertheless, experience shows that the corrections arising when taking into account the off-shell effects are suppressed and despite the defects of such approach adopted in the past it may still be considered as a first approximation and give us an idea about the order of the dominant effects.

Though the contributions of the pseudo-scalar mesons are expected to be dominating in the hadronic light-by-light scattering, there are signs that the corrections from other meson states may also be relevant in this context. As we saw from the sum rules there is a sizable contribution to the low-energy light-by-light effective constants originating from a sequence of scalar, axial and tensor states. At finite virtualities of the photons the contributions of these states may be even enhanced as compared to the real-photon scattering (e.g. the axial vector meson, which due to Landau-Yang theorem gives a vanishing contribution to the real-photon scattering, but is non-zero when the photons are virtual), giving a sizable corrections to the $(g-2)_\mu$ which were not yet taken into account consistently. The increasing accuracy of the experiments and the substantial reduction of the uncertainty of other hadronic contributions spurs us to include other hadronic states in such evaluation.

There were a number of attempts to make model estimates for the single meson corrections. Their predictions for axial-vector mesons differ quite a lot. The before mentioned BPP estimate [131, 132] and the HKS estimates [133, 134, 135] for axial-vector meson give results concordant within the uncertainty. It has been argued by PdRV [51] that the errors in the BPP and HKS calculations were underestimated, and an intermediate estimate with larger error has been suggested. The MV estimate [142], which was also adopted in JN [29] and uses a constant Wess-Zumino-Witten form factor is an order of magnitude larger than the BPP and HKS estimates.

For the scalar mesons, BPP has performed an estimate, which was adopted by N/JN and PdRV (by increasing the error bar to 100 %). The contribution of the tensor mesons has never been estimated before and will be presented in this work for the first time.

	axial-vectors	scalars	tensors
BPP [131, 132]	2.5 ± 1.0	-7 ± 2	-
HKS [133, 134, 135]	1.7 ± 1.7	-	-
MV [142]	22 ± 5	-	-
PdRV [51]	15 ± 10	-7 ± 7	-
N/JN [29]	22 ± 5	-7 ± 2	-

Table 4.1: HLbL contribution to a_μ (in units 10^{-11}) due to axial-vector, scalar, and tensor mesons obtained in this work, compared with various previous estimates.

We can see that except for the pseudo scalar exchange these results vary considerably from one group to another. This is not a surprise as all these estimates are strongly dependent on model assumptions and, as a result have a large not well controlled uncertainty. Our aim is to provide an improved estimate for the HLbL contribution, by considering single meson contributions beyond the leading pseudo-scalar mesons (π^0, η, η'), which have been evaluated in the pioneering work of [140]. We will incorporate available experimental input as well as constraints from light-by-light scattering sum rules [22, 55] to estimate the effects of axial-vector, scalar, and tensor mesons to the HLbL contribution. The framework which will be presented will also allow to further improve on the estimate, once new data, in particular from BES-III, for such meson states will become available.

4.1.1 General formalism and definitions

In quantum field theory a_μ may be calculated perturbatively by considering a scattering of a muon in a static electromagnetic field. In momentum space this process is described by a vertex matrix element of the electromagnetic current between an incoming $\mu^-(p)$ and an outgoing $\mu^-(p')$ states:

$$\left\langle \mu^-(p') \left| j^\mu_{em}(0) \right| \mu^-(p) \right\rangle = (-ie)\bar{u}(p')\Gamma^\mu(p',p)u(p). \tag{4.2}$$

The vertex $\Gamma^\mu(p',p)$ has a relativistically covariant decomposition of the form

$$\Gamma^\mu(p',p) = \gamma^\mu F_1(k^2) + i\frac{\sigma^{\mu\nu}k_\nu}{2m} F_2(k^2), \tag{4.3}$$

where $k = p' - p$ is the photon momentum, $u(p)$ denote the Dirac spinors and the matrix $\sigma_{\mu\nu} = \frac{i}{2}[\gamma_\mu, \gamma_\nu]$ represents the spin 1/2 angular momentum tensor. $F_1(k^2)$ is the Dirac form factor and in the static (classical) limit corresponding to zero momentum transfer $(p' - p \equiv k \to 0)$ defines the charge renormalization:

$$F_1(0) = 1, \tag{4.4}$$

in units of the physical positron charge e. $F_2(k^2)$ is the Pauli form factor and at $k \to 0$

$$F_2(0) = a_\mu, \tag{4.5}$$

giving the finite prediction for the anomalous magnetic moment of the muon. Experience shows that the straightforward calculation of the electromagnetic form factors turns out to be quite tedious at the one-loop level already. In particular, it happens due to the occurrence of higher order tensor integrals. Alternatively, one may project out the form factors directly from the vertex function using a projection operator technique which appears to be a much more clever set up for such calculations. In particular, the desired Pauli form factor may be extracted by using relation

$$F_2(k^2) = \mathrm{Tr}\left[(\not{p} + m)\Lambda_\mu(p', p)(\not{p}' + m)\Gamma^\mu(p', p)\right], \tag{4.6}$$

with the help of projector

$$\Lambda_\mu(p', p) = \frac{m^2}{k^2(4m^2 - k^2)}\left[\gamma_\mu + \frac{k^2 + 2m^2}{m(k^2 - 4m^2)}(p' + p)_\mu\right]. \tag{4.7}$$

To obtain the muon anomaly we need to work out the classical limit of the form factor $F_2(k^2)$:

$$a_\mu = \lim_{k^2 \to 0} F_2(k^2). \tag{4.8}$$

It is important to briefly remark some peculiarities of the limiting procedure in Eq. (4.8). One has two ways to proceed. One way is to perform angular integration in the loop integrals assuming finite k and then, when all the angular dependence in the remaining expression is eliminated to take the limit $k^2 \to 0$ directly.

Alternatively, one can use the fact that the trace under consideration projects to a scalar, which allows to average the k dependence over all spacial directions without changing the result:

$$\int \frac{\mathrm{d}\Omega(\hat{\mathbf{k}})}{4\pi}\, a_\mu(\mathbf{k}) = a_\mu \tag{4.9}$$

As a result now the limit may be taken even before the loop integration. In some cases when the integrand has a simple polynomial expansion in k a simplified limiting procedure may be implemented. Such a method was adopted in previous calculations [140] and will be pursued in details further in the next section by applying to the case of pseudo scalar and axial vector exchanges. However, for most of the simplified procedure can be applied only after carrying out the loop integration explicitly. Such a technique is described later on the example of a scalar and tensor meson exchange contribution.

4.1.2 Hadronic light-by-light correction to the $(g-2)_\mu$

The hadronic light-by-light contribution to the electromagnetic vertex $\Gamma^\mu(p', p)$ arises from a diagram in Fig.4.3. According to this diagram, the vertex matrix element is given by

$$\begin{aligned}(-ie)\bar{u}(p')\Gamma_\rho(p', p)u(p) = &\int \frac{\mathrm{d}^4q_1}{(2\pi)^4}\int \frac{\mathrm{d}^4q_2}{(2\pi)^4}\frac{(-i)^3}{q_1^2 q_2^2 (k - q_1 - q_2)^2}\\ &\times \frac{i}{(p + q_1)^2 - m^2}\frac{i}{(p + k - q_2)^2 - m^2}\times\\ &\times(-ie)^3\bar{u}(p')\gamma^\lambda(\not{p}' - \not{q}_2 + m)\gamma^\nu(\not{p} + \not{q}_1 + m)\gamma^\mu u(p)\times\\ &\times(ie)^4\Pi_{\mu\nu\lambda\rho}(q_1, k - q_1 - q_2, q_2),\end{aligned} \tag{4.10}$$

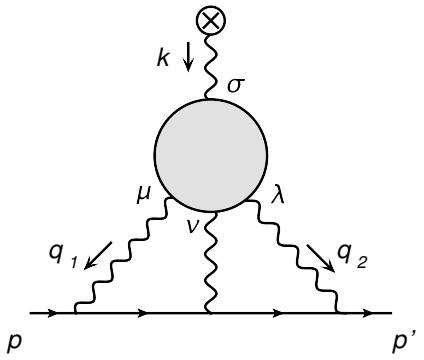

Figure 4.3: The LbL scattering contribution to the anomalous magnetic moment of the muon

where

$$\Pi_{\mu\nu\lambda\rho}(q_1,q_2,q_3) = \int \mathrm{d}^4x_1 \int \mathrm{d}^4x_2 \int \mathrm{d}^4x_3\, e^{i(q_1\cdot x_1+q_2\cdot x_2+q_3\cdot x_3)} \times \langle \Omega \,|\mathrm{T}\{j_\mu(x_1)j_\nu(x_2)j_\lambda(x_3)j_\rho(0)\}|\,\Omega\rangle \tag{4.11}$$

is the fourth-rank quark hadronic vacuum polarization tensor with $|\Omega\rangle$ denoting the QCD vacuum. The external momentum k is incoming and momenta of the virtual photons are outgoing from the hadronic "blob". The $j_\mu(x) \equiv (\bar\psi\hat Q\gamma_\mu\psi)(x)$ (with $\bar\psi = (\bar u, \bar d, \bar s)$ and the charge matrix $\hat Q = \mathrm{diag}(2/3, -1/3, -1/3)$) denotes the light quark part of the electromagnetic current.

By virtue of electromagnetic current conservation, the tensor $\Pi^{\mu\nu\lambda\sigma}$ satisfies the Ward identities

$$\{q_1^\mu; q_2^\nu; q_3^\lambda; (q_1+q_2+q_3)^\rho\}\Pi_{\mu\nu\lambda\rho}(q_1,q_2,q_3) = 0, \tag{4.12}$$

which entail that

$$k_\sigma \frac{\partial}{\partial k_\rho}\Pi^{\mu\nu\lambda\sigma}(q_1, k-q_1-q_2, q_2) = -\Pi^{\mu\nu\lambda\rho}(q_1, k-q_1-q_2, q_2). \tag{4.13}$$

Inserting the definition of the vertex correction from Eq. (4.10) into Eq. (5.2) we obtain a master formula for the hadronic light-by-light contribution to the anomalous magnetic moment

$$a_\mu^{LbL} = \lim_{k\to 0} ie^6 \int \frac{\mathrm{d}^4q_1}{(2\pi)^4} \int \frac{\mathrm{d}^4q_2}{(2\pi)^4} \frac{1}{q_1^2 q_2^2 (k-q_1-q_2)^2} \frac{1}{(p+q_1)^2-m^2} \frac{1}{(p'-q_2)^2-m^2} \times T^{\mu\nu\lambda\sigma}(q_1, k-q_1-q_2, q_2)\Pi_{\mu\nu\lambda\sigma}(q_1, k-q_1-q_2, q_2) \tag{4.14}$$

with

$$T^{\mu\nu\lambda\sigma}(q_1, k-q_1-q_2, q_2) = \mathrm{Tr}\left[(\not p + m)\Lambda^\sigma(p',p)(\not p' + m) \times\gamma^\lambda(\not p' - \not q_2 + m)\gamma^\nu(\not p + \not q_1 + m)\gamma^\mu\right]. \tag{4.15}$$

As mentioned before, the hadronic tensor $\Pi_{\mu\nu\lambda\sigma}(q_1, k-q_1-q_2, q_2)$ we have to deal with, has a very complicated structure and no general approach which allows to define it in a consistent way exists. Fortunately, as we saw there are a number of considerations which indicate that this matrix element is dominated by the long distance interaction, in other words the process is dominated by the exchanges of light quark single mesons and meson pairs. The subsequent discussion is devoted to a survey of the single meson contribution to the anomalous magnetic moment of the muon.

4.1.3 Single meson contributions to the hadronic light-by-light scattering

In this work, we will consider the contributions of a single meson with an arbitrary spin to Π, which have the general form:

$$\begin{aligned}(ie)^4\Pi_{\mu\nu\lambda\sigma}(q_1,k-q_1-q_2,q_2) &= \mathcal{M}_{\mu\nu,\{\alpha\}}(q_1,k-q_1-q_2)\frac{iP^{\{\alpha\},\{\beta\}}(k-q_2)}{(k-q_2)^2-M^2}\mathcal{M}_{\lambda\sigma,\{\beta\}}(q_2,-k)\\ &+\mathcal{M}_{\mu\sigma,\{\alpha\}}(q_1,-k)\frac{iP^{\{\alpha\},\{\beta\}}(k-q_1)}{(k-q_1)^2-M^2}\mathcal{M}_{\nu\lambda,\{\beta\}}(k-q_1-q_2,q_2)\\ &+\mathcal{M}_{\mu\lambda,\{\alpha\}}(q_1,q_2)\frac{iP^{\{\alpha\},\{\beta\}}(q_1+q_2)}{(q_1+q_2)^2-M^2}\mathcal{M}_{\nu\sigma,\{\beta\}}(k-q_1-q_2,-k).\end{aligned} \tag{4.16}$$

where the three terms correspond with the three topologies shown in Fig. 4.4.

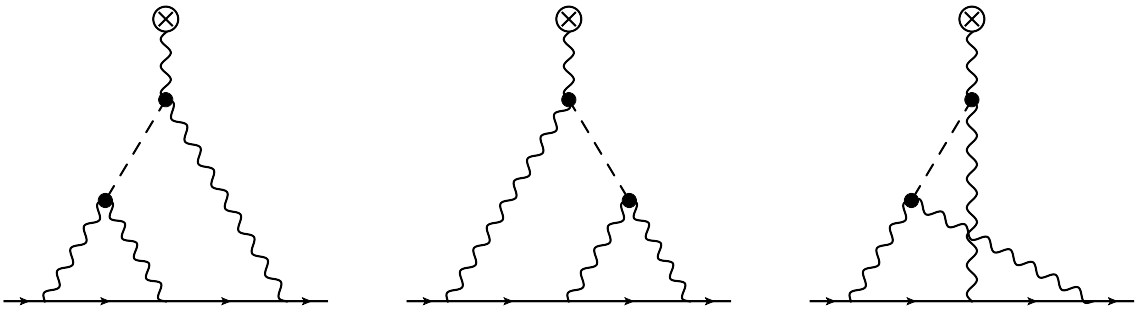

Figure 4.4: The single meson contributions to the hadronic light-by-light scattering.

In Eq. (5.11), the Lorentz amplitude $\mathcal{M}_{\mu\nu,\{\alpha\}}(q_1,q_2)$ describes the transition from the initial state of two virtual photons with momenta q_1 and q_2 to a C-even (J^{P+}) meson with mass M. Depending on the spin J of the meson, the amplitude $\mathcal{M}_{\mu\nu,\{\alpha\}}$ has different Lorentz structures: for the case of a pseudoscalar ($J^{PC}=0^{-+}$) and a scalar ($J^{PC}=0^{++}$) meson the amplitude is a rank two tensor, for the case of an axial-vector ($J^{PC}=1^{++}$) and a tensor ($J^{PC}=2^{++}$) meson it is a rank three tensor and a rank four tensor respectively. The projector P for spin J entering the meson propagator is defined by the spin sum

$$P^{\{\alpha\},\{\beta\}}(p)=\sum_{\sigma=-J}^{J}\varepsilon_\sigma^{\{\alpha\}}(p)\varepsilon_\sigma^{\{\beta\}*}(p), \tag{4.17}$$

where the $\varepsilon_\sigma^{\{\alpha\}}$ denote the corresponding polarization tensors.

The transition amplitudes are defined in such a way that the non-perturbative physics is contained in the meson transition Form Factors (FFs). It is important to note that these FFs depend on three invariants in the general case [29, 143]. However, mainly due to the absence of reliable information about the off-shell dependence on the virtuality of the exchanged meson we will assume, for the following estimates, the pole-dominance approximation for the FFs:

$$F(q_1^2,q_2^2,(q_1+q_2)^2)=F(q_1^2,q_2^2,M^2)\equiv F_{\mathcal{M}\gamma^*\gamma^*}(q_1^2,q_2^2), \tag{4.18}$$

where q_1^2,q_2^2 denote the two photon virtualities, and $(q_1+q_2)^2$ denotes the meson virtuality.

Given a particular parametrization of the FFs, the loop integrals may be partially performed analytically. In this work, we will use simple VMD-inspired monopole (mon) and dipole (dip)

parameterizations of the form :

$$\frac{F^{\rm mon}_{\mathcal{M}\gamma^*\gamma^*}\left(q_1^2,q_2^2\right)}{F_{\mathcal{M}\gamma^*\gamma^*}\left(0,0\right)} = \frac{1}{\left(1-q_1^2/\Lambda^2_{\rm mon}\right)}\frac{1}{\left(1-q_2^2/\Lambda^2_{\rm mon}\right)}\,, \tag{4.19}$$

$$\frac{F^{\rm dip}_{\mathcal{M}\gamma^*\gamma^*}\left(q_1^2,q_2^2\right)}{F_{\mathcal{M}\gamma^*\gamma^*}\left(0,0\right)} = \frac{1}{\left(1-q_1^2/\Lambda^2_{\rm dip}\right)^2}\frac{1}{\left(1-q_2^2/\Lambda^2_{\rm dip}\right)^2}\,, \tag{4.20}$$

where $\Lambda_{\rm mon}$ ($\Lambda_{\rm dip}$) are the monopole (dipole) mass parameters respectively, which are to be determined from phenomenology. It should be noticed that the behavior of fitting functions for the form factors at large and small momenta ensures ultraviolet and infrared convergence to the loop integrals.

In the following section we shall proceed to work out in details the particular cases of scalar, pseudo scalar, axial vector and tensor meson exchanges.

4.2 Four-dimensional angular integration approach

We now begin our first calculation of a single meson contribution to the anomalous magnetic moment of the muon, the pseudo scalar and axial vector exchanges. These two cases are traditionally considered to be a dominant source of the single meson light-by-light correction. As we saw this assumption is supported by low-energy effective models and quark-hadron duality arguments.

In contrast to the case of a scalar and a tensor meson the pseudo scalar and the axial vector transition amplitudes can be constructed as local operators (i.e. without involving the projectors of Eq. (2.22)). This allows to implement the simplified $k \to 0$ limiting procedure. In the subsequent computation we will follow the traditional approach adopted in [144].

The classical limit $k \to 0$ of Eq. (5.2) may be worked out in the following way. Because of the singular factor $1/k^2$ in the projector Λ_μ we are required to expand the amplitude $\Gamma_\mu(p,k)$ to first order for small k,

$$\Gamma_\mu(p',p) \simeq \Gamma_\mu(p',p)|_{k=0} + k^\nu \frac{\partial}{\partial k^\nu}\Gamma_\mu(p',p)|_{k=0} \equiv \Gamma^c_\mu(p) + k^\nu \Gamma_{\nu\mu}(p), \tag{4.21}$$

Other factors of k come from expanding the trace by setting $p' = p+k$ explicitly. We note that due to the on-shell condition $p^2 = (p+k)^2 = m^2$ we have $(p\cdot k) = -k^2/2$. The only relevant k_μ dependence left are the terms linear and quadratic in k, proportional to k_μ and $k_\mu k_\nu$. Since the trace under consideration projects to a scalar, we may average the residual k dependence over all spatial directions without changing the result. Since p and k are two independent and in the limit $k \to 0$ orthogonal vectors, the averaging is relative to the direction of p. For the linear term we have

$$\overline{k^\mu} \equiv \int \frac{{\rm d}\Omega(p,k)}{4\pi} k^\mu = 0, \tag{4.22}$$

since the integrand is an odd function, while

$$\overline{k^\mu k^\nu} \equiv \int \frac{{\rm d}\Omega(p,k)}{4\pi} k^\mu k^\nu = \alpha g^{\mu\nu} + \beta \frac{p^\mu p^\nu}{p^2} \tag{4.23}$$

must be a second rank tensor in p. Since $(p\cdot k) = \mathcal{O}(k^2)$, the contraction with p_μ is vanishing, which requires

$$\beta = -\alpha. \tag{4.24}$$

The other possible contraction with $g_{\mu\nu}$ yields k^2:

$$\int \frac{\mathrm{d}\Omega(p,k)}{4\pi} k^2 = k^2 \int \frac{\mathrm{d}\Omega(p,k)}{4\pi} = k^2 = 4\alpha + \beta = 3\alpha \tag{4.25}$$

and hence

$$\alpha = \frac{k^2}{3} \tag{4.26}$$

therefore

$$\overline{k^\mu k^\nu} = \frac{k^2}{3}\left(g^{\mu\nu} - \frac{p^\mu p^\nu}{p^2}\right). \tag{4.27}$$

Using these averages we may work out the limit explicitly, which yields

$$\begin{aligned} a_\mu =& \frac{1}{48m}\mathrm{Tr}\{(\not{p}+m)[\gamma^\mu,\gamma^\nu](\not{p}+m)\Gamma_{\nu\mu}(p)\} \\ &+\frac{1}{12m^2}\mathrm{Tr}\{\left[m^2\gamma^\mu - 3mp^\mu - 4\not{p}p^\mu\right]\Gamma^c_\mu(p)\}_{p^2=m^2} \end{aligned} \tag{4.28}$$

as a master formula for the calculation of a_μ [144, 145]. The form of the first term is obtained upon anti-symmetrization in the indices $[\mu\nu]$. The amplitudes $\Gamma^c_\mu(p)$ and $\Gamma_{\nu\mu}(p)$ depend on one on-shell momentum p, only.

We now exploit the electromagnetic current conservation and write the Ward-Takahashi identity for the derivative vertex: $k^\rho k^\sigma \bar{u}(p')\Gamma_{\rho\sigma}(p',p)u(p) = 0$, which implies that the light-by-light contribution to the Dirac form factor vanishes or $\Gamma_\rho(p',p)|_{k=0} \equiv \Gamma^c(p) = 0$. Recalling Eq. (4.14) and Eq. (4.13) the hadronic light-by-light contribution to the muon anomalous magnetic moment for the considered case reads

$$\begin{aligned} a_\mu^{LbL} = F_2(0) =& \frac{-ie^6}{48m}\int\frac{\mathrm{d}^4q_1}{(2\pi)^4}\int\frac{\mathrm{d}^4q_2}{(2\pi)^4}\frac{1}{q_1^2q_2^2(k-q_1-q_2)^2}\frac{1}{(p+q_1)^2-m^2}\frac{1}{(p-q_2)^2-m^2} \\ &\times\mathrm{Tr}\left[(\not{p}+m)\left[\gamma^\rho,\gamma^\sigma\right](\not{p}'+m)\gamma^\lambda(\not{p}-\not{q}_2+m)\gamma^\nu(\not{p}+\not{q}_1+m)\gamma^\mu\right] \\ &\times\frac{\partial}{\partial k^\rho}\Pi_{\mu\nu\lambda\sigma}(q_1,k-q_1-q_2,q_2)\Big|_{k\to 0} \end{aligned} \tag{4.29}$$

4.2.1 Pseudo scalar meson exchange.

According to Eq. (2.14) the amplitude of the two-photon production of the pseudoscalar meson (P) is taken as

$$\mathcal{M}^{(P)}_{\mu\nu}(q_1,q_2) = -ie^2\varepsilon_{\mu\nu\alpha\beta}q_1^\alpha q_2^\beta F_P(q_1^2,q_2^2;(q_1+q_2)^2). \tag{4.30}$$

The spin projection operator for $J=0$ has a trivial form

$$P(p) = 1. \tag{4.31}$$

The contribution of the pseudo-scalar meson to the light-by-light scattering may then be written in terms of the meson form factors, as

$$\begin{aligned} &\Pi^{(P)}_{\mu\nu\lambda\sigma}(q_1,k-q_1-q_2,q_2) = \\ &\quad i\frac{F_{P\gamma^*\gamma^*}\left(q_1^2,(k-q_1-q_2)^2\right)F_{P\gamma^*\gamma^*}\left(q_2^2,k^2\right)}{(q_2-k)^2-M_P^2}\varepsilon_{\mu\nu\alpha\beta}q_1^\alpha(k-q_1-q_2)^\beta\varepsilon_{\lambda\sigma\gamma\delta}q_2^\gamma k^\delta \\ &+i\frac{F_{P\gamma^*\gamma^*}\left(q_1^2,k^2\right)F_{P\gamma^*\gamma^*}\left((q_1+q_2-k)^2,q_2^2\right)}{(q_1-k)^2-M_P^2}\varepsilon_{\mu\sigma\alpha\beta}q_1^\alpha k^\beta\varepsilon_{\lambda\nu\gamma\delta}q_2^\gamma(k-q_1-q_2)^\delta \\ &+i\frac{F_{P\gamma^*\gamma^*}\left(q_1^2,q_2^2\right)F_{P\gamma^*\gamma^*}\left((q_1+q_2-k)^2,k^2\right)}{(q_1+q_2)^2-M_P^2}\varepsilon_{\mu\lambda\alpha\beta}q_1^\alpha q_2^\beta\varepsilon_{\nu\sigma\gamma\delta}(k-q_1-q_2)^\gamma k^\delta. \end{aligned} \tag{4.32}$$

For the calculation we need

$$\begin{aligned}\frac{\partial}{\partial k^\rho}\Pi^{(P)}_{\mu\nu\lambda\sigma}(q_1,k-q_1-q_2,q_2) = &-i\frac{F_{P\gamma^*\gamma^*}\left(q_1^2,(q_1+q_2)^2\right)F_{P\gamma^*\gamma^*}\left(q_2^2,0\right)}{q_2^2-M_P^2}\varepsilon_{\mu\nu\alpha\beta}q_1^\alpha(q_1+q_2)^\beta\varepsilon_{\lambda\sigma\gamma\rho}q_2^\gamma\\ &-i\frac{F_{P\gamma^*\gamma^*}\left(q_1^2,0\right)F_{P\gamma^*\gamma^*}\left((q_1+q_2)^2,q_2^2\right)}{q_1^2-M_P^2}\varepsilon_{\mu\sigma\alpha\rho}q_1^\alpha\varepsilon_{\lambda\nu\gamma\delta}q_2^\gamma(q_1+q_2)^\delta\\ &-i\frac{F_{P\gamma^*\gamma^*}\left(q_1^2,q_2^2\right)F_{P\gamma^*\gamma^*}\left((q_1+q_2)^2,0\right)}{(q_1+q_2)^2-M_P^2}\varepsilon_{\mu\lambda\alpha\beta}q_1^\alpha q_2^\beta\varepsilon_{\nu\sigma\gamma\rho}(q_1+q_2)^\gamma\\ &+\mathcal{O}(k).\end{aligned} \tag{4.33}$$

Inserting the last expression into Eq. (4.29) and computing corresponding Dirac traces, we obtain

$$\begin{aligned}a_\mu^{LbL} = &\frac{-e^6}{48m}\int\frac{\mathrm{d}^4q_1}{(2\pi)^4}\int\frac{\mathrm{d}^4q_2}{(2\pi)^4}\frac{1}{q_1^2q_2^2(q_1+q_2)^2}\frac{1}{(p+q_1)^2-m^2}\frac{1}{(p-q_2)^2-m^2}\\ &\times\left[\frac{F_{P\gamma^*\gamma^*}\left(q_1^2,(q_1+q_2)^2\right)F_{P\gamma^*\gamma^*}\left(q_2^2,0\right)}{q_2^2-M_P^2}T_1(q_1,q_2,p)\right.\\ &\left.+\frac{F_{P\gamma^*\gamma^*}\left(q_1^2,q_2^2\right)F_{P\gamma^*\gamma^*}\left((q_1+q_2)^2,0\right)}{(q_1+q_2)^2-M_P^2}T_2(q_1,q_2,p)\right]\end{aligned} \tag{4.34}$$

with

$$\begin{aligned}\frac{1}{48m}T_1(q_1,q_2,p) = &\frac{16}{3}(p\cdot q_1)(p\cdot q_2)(q_1\cdot q_2)-\frac{16}{3}(p\cdot q_2)^2q_1^2\\ &-\frac{8}{3}(p\cdot q_1)(q_1\cdot q_2)q_2^2+8(p\cdot q_2)q_1^2q_2^2-\frac{16}{3}(p\cdot q_2)(q_1\cdot q_2)^2\\ &+\frac{16}{3}m^2q_1^2q_2^2-\frac{16}{3}m^2(q_1\cdot q_2)^2,\end{aligned} \tag{4.35}$$

$$\begin{aligned}\frac{1}{48m}T_2(q_1,q_2,p) = &\frac{16}{3}(p\cdot q_1)(p\cdot q_2)(q_1\cdot q_2)-\frac{16}{3}(p\cdot q_1)^2q_2^2\\ &+\frac{8}{3}(p\cdot q_1)(q_1\cdot q_2)q_2^2+\frac{8}{3}(p\cdot q_1)q_1^2q_2^2\\ &+\frac{8}{3}m^2q_1^2q_2^2-\frac{8}{3}m^2(q_1\cdot q_2)^2.\end{aligned} \tag{4.36}$$

In deriving Eq. (4.34), we have used the fact that, upon a trivial change of variables in the two-loop integral (4.29), the two first terms of Eq. (4.33) lead to identical contributions. Furthermore, in writing $T_2(q_1,q_2,p)$ we have taken into account the invariance of the remaining factors of the corresponding integrand under the exchange $q_1\leftrightarrow -q_2$.

According to mentioned before (we take the on-shell form factor) the form factors $F_{P\gamma^*\gamma^*}(q_1^2,0)$ for one virtual photon and one real photon are well known experimentally and a good parameterization of the data is obtained by the monopole form:

$$F(q_1^2,q_2^2,(q_1+q_2)^2) = F(q_1^2,q_2^2,M_P^2)\equiv F(q_1^2,q_2^2) \tag{4.37}$$

$$\frac{F_{P\gamma^*\gamma^*}(q_1^2,q_2^2)}{F_{P\gamma^*\gamma^*}(0,0)} = \frac{1}{1-q_1^2/\Lambda_P^2}\frac{1}{1-q_2^2/\Lambda_P^2}, \tag{4.38}$$

where Λ_P is the monopole mass parameter. The normalization of the form factor at $q_1^2 = q_2^2 = 0$ is fixed by

$$\Gamma_{\gamma\gamma}(P) = \frac{\pi\alpha^2}{4} M_P^3 \, |F_{P\gamma^*\gamma^*}(0,0)|^2, \tag{4.39}$$

Within the introduced parametrization Eq. (4.34) becomes

$$\begin{aligned} a_\mu^{LbL,PS} = \frac{\alpha(4\pi)^2\Lambda_P^6\tilde{\Gamma}_{\gamma\gamma}(P)}{3m\,M_P^3} \int \frac{\mathrm{d}^4q_1}{(2\pi)^4} \int \frac{\mathrm{d}^4q_2}{(2\pi)^4} \frac{1}{q_1^2 q_2^2 (q_1^2-\Lambda_P^2)(q_2^2-\Lambda_P^2)} \\ \times \frac{1}{(q_1+q_2)^2\left[(q_1+q_2)^2-\Lambda_P^2\right]} \\ \times \frac{1}{(p+q_1)^2-m^2} \frac{1}{(p-q_2)^2-m^2} \\ \times \left[\frac{1}{q_2^2-M_P^2} T_1(q_1,q_2,p) + \frac{1}{(q_1+q_2)^2-M_P^2} T_2(q_1,q_2,p)\right]. \end{aligned} \tag{4.40}$$

4.2.2 Axial-vector meson exchange.

We next proceed to compute the contribution of the axial vector meson. Although the production of an *axial-vector meson* (A) by two real photons is forbidden by the Landau-Yang theorem [87], an axial-vector meson can be produced in two-photon processes when one or both photons are virtual. Existing phenomenological analyses have used an expression for the transition amplitude derived from a non-relativistic quark model calculation [90, 88, 89]:

$$\mathcal{M}^{(A)}_{\mu\nu\alpha}(q_1,q_2) = ie^2\varepsilon_{\rho\nu\tau\alpha}\left[(q_1^2 g_\mu^\rho - q_1^\rho q_{1\mu})\, q_2^\tau - (q_2^2 g_\mu^\rho - q_2^\rho q_{2\mu})\, q_1^\tau\right] \frac{1}{M^2} F_{\mathcal{A}\gamma^*\gamma^*}(q_1^2,q_2^2). \tag{4.41}$$

Note that a general discussion of the $\mathcal{A}\gamma^*\gamma^*$ vertex, has to allow for three independent Lorentz structures [85, 86]. However, as no phenomenological information is available at present to disentangle the three helicity structures, we will use the simplified vertex of Eq. (2.37) in the present work. The form factor $F_{A\gamma^*\gamma^*}$ is Bose symmetric $F_{A\gamma^*\gamma^*}(q_1^2,q_2^2) = F_{A\gamma^*\gamma^*}(q_2^2,q_1^2)$ of course, as the two photons are indistinguishable. According to the definition of Eq. (4.17) the projection operator for spin $J = 1$ is

$$P^{\alpha\beta}(p) = \sum_{\sigma=-1}^{1} \varepsilon_\sigma^\alpha(p)\varepsilon_\sigma^{\beta*}(p) = g^{\alpha\beta} - \frac{p^\alpha p^\beta}{M_A^2}. \tag{4.42}$$

The the axial vector-exchange contribution to the light-by-light scattering in three diagrams of Fig. (4.4) reads

$$\begin{aligned} \Pi^{A(1)}_{\mu\nu\lambda\sigma}(q_1,k-q_1-q_2,q_2) = &- i\left\{\varepsilon_{\upsilon\nu\tau\alpha}(q_1^2 g_\mu^\upsilon - q_{1\mu}q_1^\upsilon)(q_1+q_2-k)^\tau \right. \\ &\left. + \varepsilon_{\mu\upsilon\tau\alpha}\left[(q_1+q_2-k)^2 g_\nu^\upsilon - (q_1+q_2-k)_\nu (q_1+q_2-k)^\upsilon\right] q_1^\tau\right\} \\ &\times \left\{\varepsilon_{\eta\sigma\chi\beta}(q_2^2 g_\lambda^\eta - q_{2\lambda}q_2^\eta)k^\chi + \varepsilon_{\lambda\eta\chi\beta}\left(k^2 g_\sigma^\eta - k_\sigma k^\eta\right) q_2^\chi\right\} \\ &\times F_{A\gamma^*\gamma^*}(q_1^2,(q_1+q_2-k)^2) F_{A\gamma^*\gamma^*}\left(q_2^2,k^2\right) \\ &\times \frac{g^{\alpha\beta} - (q_2-k)^\alpha (q_2-k)^\beta/M_A^2}{(q_2-k)^2 - M_A^2}, \end{aligned} \tag{4.43}$$

$$\begin{aligned}\Pi^{A(2)}_{\mu\nu\lambda\sigma}(q_1,k-q_1-q_2,q_2) =& -i\left\{\varepsilon_{\upsilon\sigma\tau\alpha}(q_1^2 g_\mu^\upsilon - q_{1\mu}q_1^\upsilon)k^\tau + \varepsilon_{\mu\upsilon\tau\alpha}\left(k^2 g_\sigma^\upsilon - k_\sigma k^\upsilon\right)q_1^\tau\right\}\\ &\times\left\{\varepsilon_{\eta\nu\chi\beta}(q_2^2 g_\lambda^\eta - q_{2\lambda}q_2^\eta)(q_1+q_2-k)^\chi\right.\\ &\left.+\,\varepsilon_{\lambda\eta\chi\beta}\left((q_1+q_2-k)^2 g_\nu^\eta - (q_1+q_2-k)_\nu(q_1+q_2-k)^\eta\right)q_2^\chi\right\}\\ &\times F_{A\gamma^*\gamma^*}(q_1^2,k^2)F_{A\gamma^*\gamma^*}\left(q_2^2,(q_1+q_2-k)^2\right)\\ &\times\frac{g^{\alpha\beta}-(q_1-k)^\alpha(q_1-k)^\beta/M_A^2}{(q_1-k)^2-M_A^2},\end{aligned} \tag{4.44}$$

$$\begin{aligned}\Pi^{A(3)}_{\mu\nu\lambda\sigma}(q_1,k-q_1-q_2,q_2) =& -i\left[\varepsilon_{\upsilon\lambda\tau\beta}(q_1^2 g_\mu^\upsilon - q_{1\mu}q_1^\upsilon)q_2^\tau - \varepsilon_{\mu\upsilon\tau\beta}(q_2^2 g_\lambda^\upsilon - q_{2\lambda}q_2^\upsilon)q_1^\tau\right]\\ &\times\left[-\varepsilon_{\eta\sigma\chi\alpha}((q_1+q_2-k)^2 g_\nu^\eta - (q_1+q_2-k)_\nu(q_1+q_2-k)^\eta)k^\chi\right.\\ &\left.+\,\varepsilon_{\nu\eta\chi\alpha}(k^2 g_\sigma^\eta - k_\sigma k^\eta)(q_1+q_2-k)^\chi\right]\\ &\times F_{A\gamma^*\gamma^*}(q_1^2,q_2^2)F_{A\gamma^*\gamma^*}((q_1+q_2-k)^2,k^2)\\ &\times\frac{g^{\alpha\beta}-(q_1+q_2)^\alpha(q_1+q_2)^\beta/M_A^2}{(q_1+q_2)^2-M_A^2}.\end{aligned} \tag{4.45}$$

and the full light-by-light scattering tensor is given by the sum of three terms:

$$\Pi^A_{\mu\nu\lambda\sigma} = \Pi^{A(1)}_{\mu\nu\lambda\sigma} + \Pi^{A(2)}_{\mu\nu\lambda\sigma} + \Pi^{A(3)}_{\mu\nu\lambda\sigma}. \tag{4.46}$$

To compute a_μ we need

$$\begin{aligned}\frac{\partial}{\partial k^\rho}\Pi^{A(1)}_{\mu\nu\lambda\sigma}(q_1,k-q_1-q_2,q_2) =& -i\left\{\varepsilon_{\upsilon\nu\tau\alpha}(q_1^2 g_\mu^\upsilon - q_{1\mu}q_1^\upsilon)(q_1+q_2)^\tau + \right.\\ &\left.+\,\varepsilon_{\mu\upsilon\tau\alpha}\left[(q_1+q_2)^2 g_\nu^\upsilon - (q_1+q_2)_\nu(q_1+q_2)^\upsilon\right]q_1^\tau\right\}\\ &\times\varepsilon_{\eta\sigma\rho\beta}(q_2^2 g_\lambda^\eta - q_{2\lambda}q_2^\eta)\times\\ &\times F_{A\gamma^*\gamma^*}(q_1^2,(q_1+q_2)^2)F_{A\gamma^*\gamma^*}\left(q_2^2,0\right)\frac{g^{\alpha\beta}-q_2^\alpha q_2^\beta/M_A^2}{q_2^2-M_A^2}\\ &+\mathcal{O}(k)\end{aligned} \tag{4.47}$$

$$\begin{aligned}\frac{\partial}{\partial k^\rho}\Pi^{A(2)}_{\mu\nu\lambda\sigma}(q_1,k-q_1-q_2,q_2) =& -i\varepsilon_{\upsilon\sigma\rho\alpha}(q_1^2 g_\mu^\upsilon - q_{1\mu}q_1^\upsilon)\\ &\times\left\{\varepsilon_{\eta\nu\chi\beta}(q_2^2 g_\lambda^\eta - q_{2\lambda}q_2^\eta)(q_1+q_2)^\chi + \right.\\ &\left.+\,\varepsilon_{\lambda\eta\chi\beta}\left((q_1+q_2)^2 g_\nu^\eta - (q_1+q_2)_\nu(q_1+q_2)^\eta\right)q_2^\chi\right\}\\ &\times F_{A\gamma^*\gamma^*}(q_1^2,0)F_{A\gamma^*\gamma^*}\left(q_2^2,(q_1+q_2)^2\right)\frac{g^{\alpha\beta}-q_1^\alpha q_1^\beta/M_A^2}{q_1^2-M_A^2}\\ &+\mathcal{O}(k)\end{aligned} \tag{4.48}$$

$$\begin{aligned}\frac{\partial}{\partial k^\rho}\Pi^{A(3)}_{\mu\nu\lambda\sigma}(q_1,k-q_1-q_2,q_2) =& -i\left[-\varepsilon_{\upsilon\lambda\tau\beta}(q_1^2 g_\mu^\upsilon - q_{1\mu}q_1^\upsilon)q_2^\tau + \varepsilon_{\mu\upsilon\tau\beta}(q_2^2 g_\lambda^\upsilon - q_{2\lambda}q_2^\upsilon)q_1^\tau\right]\\ &\times\varepsilon_{\eta\sigma\rho\alpha}\left[(q_1+q_2)^2 g_\nu^\eta - (q_1+q_2)_\nu(q_1+q_2)^\eta\right]\times\\ &\times F_{A\gamma^*\gamma^*}(q_1^2,q_2^2)F_{A\gamma^*\gamma^*}((q_1+q_2)^2,0)\\ &\times\frac{g^{\alpha\beta}-(q_1+q_2)^\alpha(q_1+q_2)^\beta/M_A^2}{(q_1+q_2)^2-M_A^2}\\ &+\mathcal{O}(k)\end{aligned} \tag{4.49}$$

Similarly to the pseudo scalar exchange considered before the contributions of (4.47) and (4.48) are equal. Now it only remains to insert Eqs. (4.47-4.49) into Eq. (4.29) which then results in

$$\begin{aligned} a_\mu^{LbL,A} = \frac{-e^6}{48m}\int\frac{\mathrm{d}^4q_1}{(2\pi)^4}\int\frac{\mathrm{d}^4q_2}{(2\pi)^4}\frac{1}{q_1^2q_2^2(q_1+q_2)^2}\frac{1}{(p+q_1)^2-m^2}\frac{1}{(p-q_2)^2-m^2} \\ \times\left[\frac{F_{A\gamma^*\gamma^*}\left(q_1^2,(q_1+q_2)^2\right)F_{A\gamma^*\gamma^*}\left(q_2^2,0\right)}{q_2^2-M_A^2}T_1(q_1,q_2,p)+\right. \\ \left.+\frac{F_{A\gamma^*\gamma^*}\left(q_1^2,q_2^2\right)F_{A\gamma^*\gamma^*}\left((q_1+q_2)^2,0\right)}{(q_1+q_2)^2-M_A^2}T_2(q_1,q_2,p)\right], \end{aligned} \tag{4.50}$$

with

$$\begin{aligned} T_1(q_1,q_2,p) =& -2\,\mathrm{Tr}\left[(\not p+m)\left[\gamma^\rho,\gamma^\sigma\right](\not p+m)\gamma^\lambda(\not p-\not q_2+m)\gamma^\nu(\not p+\not q_1+m)\gamma^\mu\right] \\ &\times\left\{\varepsilon_{\upsilon\nu\tau\alpha}(q_1^2g_\mu^\upsilon-q_{1\mu}q_1^\upsilon)(q_1+q_2)^\tau\right. \\ &\left.+\,\varepsilon_{\mu\upsilon\tau\alpha}\left[(q_1+q_2)^2g_\nu^\upsilon-(q_1+q_2)_\nu(q_1+q_2)^\upsilon\right]q_1^\tau\right\} \\ &\times\varepsilon_{\eta\sigma\rho\beta}(q_2^2g_\lambda^\eta-q_{2\lambda}q_2^\eta) \\ &\times\left(g^{\alpha\beta}-q_2^\alpha q_2^\beta/M_A^2\right) \end{aligned} \tag{4.51}$$

$$\begin{aligned} T_2(q_1,q_2,p) =& -\,\mathrm{Tr}\left[(\not p+m)\left[\gamma^\rho,\gamma^\sigma\right](\not p+m)\gamma^\lambda(\not p-\not q_2+m)\gamma^\nu(\not p+\not q_1+m)\gamma^\mu\right]\times \\ &\times\left[-\varepsilon_{\upsilon\lambda\tau\beta}(q_1^2g_\mu^\upsilon-q_{1\mu}q_1^\upsilon)q_2^\tau+\varepsilon_{\mu\upsilon\tau\beta}(q_2^2g_\lambda^\upsilon-q_{2\lambda}q_2^\upsilon)q_1^\tau\right] \\ &\times\varepsilon_{\eta\sigma\rho\alpha}\left[(q_1+q_2)^2g_\nu^\eta-(q_1+q_2)_\nu(q_1+q_2)^\eta\right]\times \\ &\times\left(g^{\alpha\beta}-(q_1+q_2)^\alpha(q_1+q_2)^\beta/M_A^2\right) \end{aligned} \tag{4.52}$$

For the form factor with both virtual photons we use the double pole parametrization:

$$\frac{F_{A\gamma^*\gamma^*}\left(q_1^2,q_2^2\right)}{F_{A\gamma^*\gamma^*}\left(0,0\right)}=\frac{1}{\left(1-q_1^2/\Lambda_{A1}^2\right)\left(1-q_1^2/\Lambda_{A2}^2\right)}\frac{1}{\left(1-q_2^2/\Lambda_{A1}^2\right)\left(1-q_2^2/\Lambda_{A2}^2\right)} \tag{4.53}$$

with the normalization fixed by

$$\left[F_{A\gamma^*\gamma^*}\left(0,0\right)\right]^2=\frac{12}{\pi\alpha^2}\frac{1}{M_A^5}\tilde{\Gamma}_{\gamma\gamma}(A) \tag{4.54}$$

With the account of the introduced parametrization Eq. (4.50) becomes

$$\begin{aligned} a_\mu^{LbL,A} =& -\frac{(4\pi)^2\,\alpha}{m\,M_A^5}\left(\Lambda_{A1}^2\Lambda_{A2}^2\right)^3\tilde{\Gamma}_{\gamma\gamma}(A)\int\frac{\mathrm{d}^4q_1}{(2\pi)^4}\int\frac{\mathrm{d}^4q_2}{(2\pi)^4} \\ &\times\frac{1}{q_1^2q_2^2\left(\Lambda_{A1}^2-q_1^2\right)\left(\Lambda_{A2}^2-q_1^2\right)\left(\Lambda_{A1}^2-q_2^2\right)\left(\Lambda_{A2}^2-q_2^2\right)} \\ &\times\frac{1}{(p+q_1)^2-m^2}\frac{1}{(p-q_2)^2-m^2} \\ &\times\frac{1}{(q_1+q_2)^2\left[\Lambda_{A1}^2-(q_1+q_2)^2\right]\left[\Lambda_{A2}^2-(q_1+q_2)^2\right]} \\ &\times\left[\frac{1}{(q_2^2-M_A^2)}T_1(q_1,q_2,p)+\frac{1}{(q_1+q_2)^2-M_A^2}T_2(q_1,q_2,p)\right] \end{aligned} \tag{4.55}$$

4.2.3 Angular integration

To evaluate Eqs. (4.40) and (4.55) the basic approach is to perform the integrations directly in momentum space, without introducing Feynman parameters. To do this, we analytically continue the loop momenta to the Euclidean region, and then introduce four-dimensional spherical (hyperspherical) coordinates. After that we perform the resulting angular integrations analytically. As we shall show in this section, for form factors that have a form of a rational function, it is possible to perform all angular integrations in the two-loop integral of Eqs. (4.40, 4.55) using the technique of Gegenbauer polynomials (hyperspherical approach); see [146, 147]. In order to do so we temporarily discard the constant $p^2 = m^2$ and perform the Wick rotation with p spacelike: $p^2 = -P^2$. It is easily accomplished by letting the energy associated with each external line acquire the same phase ϕ, which is then varied from 0 to $\pi/2$ and making change of variable $p_0 = -iP_0$. We either implement the Wick rotation of the loop momenta q_1 and q_2 and denote corresponding Euclidean momenta by capital letters, with $Q_i^2 = -q_i^2$. We may set $P^2 = -m^2$ in the explicit expressions after angular integration. Since the external momentum P flows only through the massive fermion propagators, we will not need to deform the integration contour for the radial integrals over Q_1^2 and Q_2^2 (see the discussion in [147, 148]).

For a start, we briefly summarize some basic properties of the Gegenbauer polynomials; see also [149, 150]. We introduce the measure of the four-dimensional sphere as follows

$$\mathrm{d}^4Q = Q^3\,\mathrm{d}Q\,\mathrm{d}\Omega(\hat{Q}), \quad \int \mathrm{d}\Omega(\hat{Q}) = 2\pi^2. \tag{4.56}$$

With the account of Wick rotation expressions for the pseudo scalar and axial vector contributions in Eqs. (4.40, 4.55) modify as follows

$$\begin{aligned} a_\mu^{LbL,P} = {} & \frac{\alpha}{(2\pi)^2}\frac{\Lambda_P^6\tilde{\Gamma}_{\gamma\gamma}(P)}{3m\,M_P^3}\int \mathrm{d}Q_1 \int \mathrm{d}Q_2 \int \frac{\mathrm{d}\Omega(\hat{Q}_1)}{2\pi^2}\int \frac{\mathrm{d}\Omega(\hat{Q}_2)}{2\pi^2} \\ & \times \frac{|Q_1||Q_2|}{\left(\Lambda_P^2+Q_1^2\right)\left(\Lambda_P^2+Q_2^2\right)(Q_1+Q_2)^2\left[\Lambda_P^2+(Q_1+Q_2)^2\right]} \\ & \times \frac{1}{(P+Q_1)^2+m^2}\frac{1}{(P-Q_2)^2+m^2} \\ & \left[\frac{1}{(Q_2^2+M_P^2)}T_1(Q_1,Q_2,P)+\frac{1}{(Q_1+Q_2)^2+M_P^2}T_2(Q_1,Q_2,P)\right] \end{aligned} \tag{4.57}$$

for the pseudo scalar exchange, and

$$\begin{aligned} a_\mu^{LbL,A} = {} & \frac{\alpha}{(2\pi)^2}\frac{\Lambda_{A1}^6\Lambda_{A2}^6\tilde{\Gamma}_{\gamma\gamma}(A)}{m\,M_A^5}\int \mathrm{d}Q_1 \int \mathrm{d}Q_2 \int \frac{\mathrm{d}\Omega(\hat{Q}_1)}{2\pi^2}\int \frac{\mathrm{d}\Omega(\hat{Q}_2)}{2\pi^2} \\ & \times \frac{|Q_1||Q_2|}{\left(\Lambda_{A1}^2+Q_1^2\right)\left(\Lambda_{A2}^2+Q_1^2\right)\left(\Lambda_{A1}^2+Q_2^2\right)\left(\Lambda_{A2}^2+Q_2^2\right)} \\ & \times \frac{1}{(Q_1+Q_2)^2\left[\Lambda_{A1}^2+(Q_1+Q_2)^2\right]\left[\Lambda_{A2}^2+(Q_1+Q_2)^2\right]} \\ & \times \frac{1}{(P+Q_1)^2+m^2}\frac{1}{(P-Q_2)^2+m^2} \\ & \left[\frac{1}{(Q_2^2+M_A^2)}T_1(Q_1,Q_2,P)+\frac{1}{(Q_1+Q_2)^2+M_A^2}T_2(Q_1,Q_2,P)\right] \end{aligned} \tag{4.58}$$

for the axial vector exchange. The generating function of the Gegenbauer polynomials $C_n^{(1)}(x)$

(hereinafter we use notation $C_n^{(1)}(x) \equiv C_n(x)$) is given by

$$\frac{1}{z^2 - 2xz + 1} = \sum_{n=0}^{\infty} z^n \, C_n(x), \quad -1 \leq x \leq 1, \; |z| < 1. \tag{4.59}$$

From Eq. (D.1) we immediately obtain the following property under parity transformations $C_n(-x) = (-1)^n C_n(x)$. Furthermore we get $C_n(1) = n+1$. The Gegenbauer polynomials obey the orthogonality conditions

$$\int \mathrm{d}\Omega(\hat{K}) C_n(\hat{Q}_1 \cdot \hat{K}) C_m(\hat{K} \cdot \hat{Q}_2) = 2\pi^2 \frac{\delta_{nm}}{n+1} C_n(\hat{Q}_1 \cdot \hat{Q}_2) \tag{4.60}$$

$$\int \mathrm{d}\Omega(\hat{K}) C_n(\hat{Q} \cdot \hat{K}) C_m(\hat{K} \cdot \hat{Q}) = 2\pi^2 \delta_{nm}, \tag{4.61}$$

where, for instance, $(\hat{Q}_1 \cdot \hat{K})$ is the cosine of the angle between the four-dimensional vectors Q_1 and K.

From the generating function, we obtain the following representation of the propagators in Euclidean space:

$$\frac{1}{(K-L)^2 + M^2} = \frac{Z_{KL}^M}{|K||L|} \sum_{n=0}^{\infty} \left(Z_{KL}^M\right)^n C_n(\hat{K} \cdot \hat{L}) \tag{4.62}$$

$$\frac{1}{(K+L)^2 + M^2} = \frac{Z_{KL}^M}{|K||L|} \sum_{n=0}^{\infty} \left(-Z_{KL}^M\right)^n C_n(\hat{K} \cdot \hat{L}) \tag{4.63}$$

$$Z_{KL}^M = \frac{K^2 + L^2 + M^2 - \sqrt{(K^2 + L^2 + M^2)^2 - 4K^2L^2}}{2|K||L|} \tag{4.64}$$

Note that we have to choose the negative sign in front of the square root in Z_{KL}^M in order that $|Z_{KL}^M| < 1$. For a massless propagator these expressions simplify as follows:

$$\frac{1}{(K-L)^2} = \frac{1}{K^2} \sum_{n=0}^{\infty} \left(\frac{|L|}{|K|}\right)^n C_n(\hat{K} \cdot \hat{L}), \text{ for } |K| > |L| \tag{4.65}$$

Let us introduce the following abbreviations for the propagators in the loop integral in Eqs. (4.57, 4.58):

$$\begin{aligned} &D_1 = Q_1^2, \qquad D_2 = Q_2^2, \qquad D_3 = (Q_1 + Q_2)^2, \qquad D_4 = (P + Q_1)^2 + m^2 \\ &D_5 = (P - Q_2)^2 + m^2, \qquad D_M = (Q_1 + Q_2)^2 + M^2 \end{aligned} \tag{4.66}$$

By rewriting the scalar products $P \cdot Q_1$, $P \cdot Q_2$ and $Q_1 \cdot Q_2$ in terms of the propagators D_4, D_5 and D_3, respectively we can remove some of the terms in the numerator of $T_n/(D_1 D_2 D_3 D_4 D_5)$, n = 1, 2, in Eqs. (4.57, 4.58). If we multiply by the form factors, taking into account their general form from Eqs. (4.8) and (4.9), and using a partial fraction decomposition, we finally obtain the following basic angular integrals. Apart from the trivial one $\int \mathrm{d}\Omega(\hat{Q}_1)\mathrm{d}\Omega(\hat{Q}_2) = 4\pi^2$, they can all be performed using the method of Gegenbauer polynomials (from now on, we write Q_1 instead of $|Q_1|$, etc.). For the sake of demonstration of the technique we will work out explicitly one example and list the remaining integrals in the Appendix.

Let's consider integral:

$$I = \int \frac{\mathrm{d}\Omega(\hat{Q}_1)}{2\pi^2} \int \frac{\mathrm{d}\Omega(\hat{Q}_2)}{2\pi^2} \frac{1}{[(P + Q_1)^2 + m^2]\,[(Q_1 + Q_2)^2 + \Lambda^2]}. \tag{4.67}$$

First, we express the integrand in terms of the polynomial series using expansion (D.14):

$$\frac{1}{(P+Q_1)^2+m^2}\frac{1}{(Q_1+Q_2)^2+\Lambda^2} = \frac{Z^m_{PQ_1}}{PQ_1}\frac{Z^\Lambda_{Q_1Q_2}}{Q_1Q_2}\sum_{n=0}^{\infty}\sum_{k=0}^{\infty}\left(Z^m_{PQ_1}\right)^n\left(Z^m_{Q_1Q_2}\right)^k \times C_n(\hat{P}\cdot\hat{Q}_1)C_k(\hat{Q}_1\cdot\hat{Q}_2) \tag{4.68}$$

We can see that the angular dependence is now contained in the Gegenbauer polynomials. Now we can apply the orthogonality relation (D.2) with the result that

$$\int\frac{\mathrm{d}\Omega(\hat{Q}_1)}{2\pi^2}\int\frac{\mathrm{d}\Omega(\hat{Q}_2)}{2\pi^2}C_n(\hat{P}\cdot\hat{Q}_1)C_k(\hat{Q}_1\cdot\hat{Q}_2) = \delta_{n0}\delta_{m0} \tag{4.69}$$

Applied to Eq. (4.68), it gives

$$I = \frac{Z^m_{PQ_1}Z^\Lambda_{Q_1Q_2}}{PQ_1^2Q_2}. \tag{4.70}$$

4.3 Three-dimensional angular integration approach

As we saw in Chapter 2 the general Lorentz covariant decomposition of the meson transition amplitudes for higher spins involve the projectors of Eq. (2.22). Unlike the case of the axial vector where thanks to a model approximation we could combine the Lorentz structures in such a way that the projectors are eliminated[2], for the scalars and tensors such a parametrization is not known. As a result, the simplified averaging scheme used in the previous section can not be applied in this case. To overcome this complication we may however apply the averaging formula Eq. (4.9) directly to the Eq. (4.29) without expanding the vertex function. The second peculiarity of the case under consideration is that the particular form of the projectors of Eq. (2.22) does not allow simple Gegenbauer polynomial expansion of the integrand after the averaging as was done in the previously. Thus, the analytical integration by means presented in the previous section is not possible as well. However, the situation is not hopeless. It turns out that the integrals over the spatial directions of the loop momenta can still be performed analytically using properties of Legendre polynomials.

4.3.1 Scalar meson exchange

As was mentioned before, A scalar meson ($\mathcal{S}$) may be produced either by two transverse or by two longitudinal photons [85, 86]. As the main contribution to the magnetic moment comes from the region of small photon virtualities, the contribution of the transverse amplitude is dominating. Furthermore, there is no empirical information on the structure of the longitudinal FFs at present. Thus in this work, we will only consider the transverse part of the scalar meson production amplitude which is described by:

$$\mathcal{M}^{(S)}_{\mu\nu}(q_1,q_2) = -e^2\frac{(q_1\cdot q_2)}{M_S}F_{S\gamma^*\gamma^*}(q_1^2,q_2^2)R_{\mu\nu}(q_1,q_2). \tag{4.71}$$

As there is no phenomenological information on the scalar FFs available at the moment, for simplicity, we assume a simple monopole behavior of the form factor with the pole mass Λ_S being a free parameter :

$$\frac{F_{S\gamma^*\gamma^*}(q_1^2,0)}{F_{S\gamma^*\gamma^*}(0,0)} = \frac{1}{1-q_1^2/\Lambda_S^2}, \tag{4.72}$$

[2]It should be noticed that the case of the full transition amplitude for the axial vector involving three independent structures may be treated similarly, using the framework presented in this section.

The normalization of the transverse form factor at $q_1^2 = q_2^2 = 0$ is defined by Eq. (2.25).

According to Eq. (4.14) a scalar meson contribution to the anomalous magnetic moment may be written as :

$$a_\mu^{LbL} = \lim_{k\to 0} -e^6 \int \frac{\mathrm{d}^4q_1}{(2\pi)^4} \int \frac{\mathrm{d}^4q_2}{(2\pi)^4} \frac{1}{q_1^2 q_2^2 (k-q_1-q_2)^2 \left[(p+q_1)^2 - m^2\right] \left[(p+k-q_2)^2 - m^2\right]} \times \left[\frac{F_{S\gamma^*\gamma^*}(q_1^2, (k-q_1-q_2)^2) F_{S\gamma^*\gamma^*}(k^2, q_2^2)}{(k-q_2)^2 - M_S^2} T_1(q_1, k-q_1-q_2, q_2) + \frac{F_{S\gamma^*\gamma^*}(q_1^2, q_2^2) F_{S\gamma^*\gamma^*}((k-q_1-q_2)^2, k^2)}{(q_1+q_2)^2 - M_S^2} T_2(q_1, k-q_1-q_2, q_2) \right] \tag{4.73}$$

with

$$T_1(q_1, k-q_1-q_2, q_2) = -2\, T^{\mu\nu\lambda\sigma}(q_1, k-q_1-q_2, q_2) \times \frac{(q_1 \cdot (k-q_1-q_2))}{M_S} R_{\mu\nu}(q_1, k-q_1-q_2) \frac{(q_2 \cdot k)}{M_S} R_{\lambda\sigma}(q_2, k) \tag{4.74}$$

$$T_2(q_1, k-q_1-q_2, q_2) = -T^{\mu\nu\lambda\sigma}(q_1, k-q_1-q_2, q_2) \times \frac{(q_1 \cdot q_2)}{M_S} R_{\mu\lambda}(q_1, q_2) \frac{((k-q_1-q_2) \cdot k)}{M_S} R_{\nu\sigma}(k-q_1-q_2, k). \tag{4.75}$$

We again used the fact that the first two topologies give equal contributions.

The next step in our calculation is to perform the angular averaging over the spatial directions of k. Firstly, we simplify the expression by keeping the leading terms in k. We omit all the terms of first order in k in the trace and expand the denominators of the propagators by using relation

$$\frac{1}{(k+q)^2 - m^2} = \frac{1}{q^2 - m^2} \left(1 - \frac{2(k \cdot q)}{q^2 - m^2} + \mathcal{O}(k^2) \right). \tag{4.76}$$

Next, we make a change of variables in the two-loop integral. We replace $q_1 \leftrightarrow q_2$ and $p \leftrightarrow -p-k$ in the second and $q_2 \leftrightarrow k-q_1-q_2$ in the third term. After such change of variables the hadronic matrix element has the same form for all three diagrams. As we will see further it significantly simplifies the calculation especially for diagram (c). In addition, we again notice that the first and the second terms give equal contributions. As a result, the two-loop integral for the anomalous moment modifies as follows:

$$a_\mu^{LbL} = \lim_{k\to 0} -\frac{(16\pi)^2 \alpha \Gamma_{\gamma\gamma} \Lambda^6}{M_S} \int \frac{\mathrm{d}^4q_1}{(2\pi)^4} \int \frac{\mathrm{d}^4q_2}{(2\pi)^4} \frac{1}{q_1^2 q_2^2 (q_1^2 - \Lambda_S^2)(q_2^2 - \Lambda_S^2)(q_2^2 - M_S^2)} \times \frac{1}{(q_1+q_2)^2 \left[(q_1+q_2)^2 - \Lambda_S^2\right] \left[(p+q_1)^2 - m^2\right]} \times \left[2\, \frac{T_1(q_1, k-q_1-q_2, q_2)}{\left[(p-q_2)^2 - m^2\right]} + \frac{T_2(q_1, q_2, k-q_1-q_2)}{\left[(p+q_1+q_2)^2 - m^2\right]} \right] \tag{4.77}$$

Computing the Dirac traces (for which we used the computer algebraic system FORM [151]), we find that T_1 and T_2 contain a set of structures of three types :

$$(q_1 \cdot k)^i (q_2 \cdot k)^j, \quad \frac{(q_1 \cdot k)^i (q_2 \cdot k)^j}{(q_2 \cdot k)^2 - q_2^2 k^2}, \quad \frac{(q_1 \cdot k)^i (q_2 \cdot k)^j}{\left[(q_2 \cdot k)^2 - q_2^2 k^2\right]^2}. \tag{4.78}$$

Before proceeding to further steps we will discuss the remaining case of the tensor mesons (T) exchange.

4.3.2 Tensor meson exchange

For the light quark tensor mesons, the experimental analyses of decay angular distributions for $\gamma\gamma$ cross sections to $\pi^+\pi^-$, $\pi^0\pi^0$, $\eta\pi^0$, and K^+K^- channels have shown [115] that the $J = 2$ mesons are produced predominantly (around 95% or more) in a state of helicity $\Lambda = 2$. We will therefore assume in all of the following analyses that the hadronic light-by-light amplitude for tensor states is dominated by the helicity $\Lambda = 2$ exchange. Therefore, the two-photon decay rate is $\Gamma_{\gamma\gamma}\left(T(\Lambda = 2)\right) \approx \Gamma_{\gamma\gamma}(T)$, and we will safely neglect the contribution of the remaining four helicity amplitudes. The relevant part of the Lorentz amplitude for the dominant process $\gamma^*(q_1) + \gamma^*(q_2) \to T(\Lambda = 2)$, can be parameterized as [55]

$$\begin{aligned}\mathcal{M}^{(T)}_{\mu\nu\alpha\beta}(q_1, q_2) = e^2 \frac{(q_1 \cdot q_2)}{m_T} F_{T\gamma^*\gamma^*}(q_1^2, q_2^2)\times \\ \times \{R_{\mu\alpha}(q_1, q_2) R_{\nu\beta}(q_1, q_2)+ \\ + \frac{1}{8(q_1+q_2)^2\left[(q_1\cdot q_2)^2 - q_1^2 q_2^2\right]} R_{\mu\nu}(q_1, q_2)\times \\ \times \left[(q_1+q_2)^2(q_1-q_2)_\alpha - (q_1^2-q_2^2)(q_1+q_2)_\alpha\right]\times \\ \times \left[(q_1+q_2)^2(q_1-q_2)_\beta - (q_1^2-q_2^2)(q_1+q_2)_\beta\right]\} \equiv \\ \equiv \frac{(q_1\cdot q_2)}{m_T} T^{(2)}(q_1^2, q_2^2) M_{\mu\nu\alpha\beta}(q_1, q_2).\end{aligned} \tag{4.79}$$

We consider a dipole parametrization for the form factor and use our estimates for the mass parameters described in the previous chapter. The projector operator for $J = 2$ has the form

$$P_{\alpha\beta,\gamma\delta} = \frac{1}{2}\left(K_{\alpha\gamma}K_{\beta\delta} + K_{\alpha\delta}K_{\beta\gamma}\right) - \frac{1}{3}K_{\alpha\beta}K_{\gamma\delta}, \tag{4.80}$$

with

$$K_{\alpha\beta} = -g_{a\beta} + \frac{p_\alpha p_\beta}{p^2}. \tag{4.81}$$

In the remaining the calculation completely parallels the scalar case. The difference is in the additional structures appearing in the tensor exchange and a large number of terms in the expressions as compared to the scalar case. The intermediate expression become rather lengthy and we use the computer algebraic system FORM to carry out algebraic manipulations, contractions and to calculate the traces.

4.3.3 Angular integration

In the following we will discuss the averaging procedure in details. The only dependence on the direction of k is incorporated in three structures in Eq. (4.78).

First we briefly summarize the main properties of the Legendre polynomials (see [149, 150]). The Legendre polynomial expansion of the propagators is based on series

$$\frac{1}{\Delta - (\hat{\mathbf{K}}\cdot\hat{\mathbf{L}})} = \sum_{n=0}^{\infty}(2n+1)Q_n(\Delta)P_n(\hat{\mathbf{K}}\cdot\hat{\mathbf{L}}), \tag{4.82}$$

The second crucial property we will intensively exploit in our calculations is an orthogonality which reads

$$\int \frac{\mathrm{d}\Omega(\hat{\mathbf{K}})}{4\pi} P_n(\hat{\mathbf{Q}}_1\cdot\hat{\mathbf{K}})P_m(\hat{\mathbf{K}}\cdot\hat{\mathbf{Q}}_2) = \delta_{nm}\frac{P_n(\hat{\mathbf{Q}}_1\cdot\hat{\mathbf{Q}}_2)}{2n+1} \tag{4.83}$$

and

$$\int \frac{\mathrm{d}\Omega(\hat{Q}_i)}{4\pi} P_n(\hat{\mathbf{Q}}_1\cdot\hat{\mathbf{Q}}_2)P_m(\hat{\mathbf{Q}}_1\cdot\hat{\mathbf{Q}}_2) = \frac{\delta_{nm}}{2n+1} \tag{4.84}$$

where, for instance, $(\hat{Q}_1 \cdot \hat{K})$ is the cosine of the angle between the four-dimensional vectors Q_1 and K.

It is convenient to perform the calculation in the muon's rest reference frame: $p = (m, 0, 0, 0)$. We assume that the external photon has a finite space-like virtuality so $k^2 = -K^2$ which is due to a scattering nature of the process. Using mass-shell conditions for the muon $p^2 = m^2$ and $(p+k)^2 = m^2$ the components of four-vector $k = (k^0, \mathbf{k})$ can be defined in the muon's rest frame as :

$$k^0 = \frac{K^2}{2m} \quad \text{and} \quad |\mathbf{k}| = K\sqrt{1 + \frac{K^2}{4m^2}}. \tag{4.85}$$

Using these relations one can expand the scalar products $(q_i \cdot k)$ in the vicinity of a small K:

$$(q_i \cdot k) = q_i^0 k^0 - \mathbf{q}_i \cdot \mathbf{k} = -\mathbf{q}_i \cdot \mathbf{k} + \mathcal{O}(K^2). \tag{4.86}$$

Thus, in the following we always keep only the leading terms in K.

At this point it is convenient to continue the two-loop integral to the Euclidean region. After deforming the contour we make the change of variables $q_i^0 = -iQ_i^0$, where Q_i^0 are the Euclidean zero components of the corresponding four-momenta and denote the modulus of the Euclidean loop momenta by capital letters $q_1^2 = -Q_1^2$ and $q_2^2 = -Q_2^2$. This allows to change to the angular coordinates with the result that the loop integration domain becomes finite. Experience shows, that this is a big advantage for a numerical evaluation. In addition, by doing this analytical continuation we limit the integration to space-like values of the photons' virtualities which keeps us away from production thresholds of the form factors (in the case of monopole form factor, these correspond with vector meson poles).

Now we proceed to work out the averaging integrals explicitly. First, by rewriting the scalar products in terms of the propagators we can remove some of the terms involving $Q_1 \cdot Q_2$ in the numerator. The scalar products $p \cdot Q_1$ and $p \cdot Q_2$ which occur in the fermion propagators don't imply angular dependence in the muon's rest reference frame. The denominators can be simplified using a partial fraction decomposition and we finally obtain a set of angular integrals, which can all be performed using properties of the Legendre polynomials.

As a demonstration of the angular averaging procedure let's consider the integral

$$I = \int \frac{\mathrm{d}\Omega(\hat{\mathbf{k}})}{4\pi} \frac{k^2}{(q_2 \cdot k)^2 - k^2 q_2^2}. \tag{4.87}$$

After rotating the momenta and expanding the scalar products we simplify the integrand by using a rational fraction decomposition, which yields :

$$I = \frac{K}{2Q_2} \int \frac{\mathrm{d}\Omega(\hat{\mathbf{k}})}{4\pi} \left[\frac{1}{-(\mathbf{Q_2} \cdot \mathbf{k}) + KQ_2} - \frac{1}{-(\mathbf{Q_2} \cdot \mathbf{k}) - KQ_2} \right]. \tag{4.88}$$

Using the Legendre polynomial expansion for propagators (4.82) and the orthogonality relation (D.40) we obtain

$$I = \frac{1}{2Q_2|\mathbf{Q_2}|} \left[Q_0\left(\frac{|Q_2|}{|\mathbf{Q_2}|}\right) - Q_0\left(-\frac{|Q_2|}{|\mathbf{Q_2}|}\right) \right] = \frac{1}{2Q_2|\mathbf{Q_2}|} \ln\left(\frac{Q_2 + |\mathbf{Q_2}|}{Q_2 - |\mathbf{Q_2}|}\right). \tag{4.89}$$

Now we can judge the benefit from the change of variables we did before. In the case of direct averaging without the change of variables the expression for the third diagram would involve the sum of two momenta $Q_1 + Q_2$ instead of Q_2 in the argument of logarithm and the following analytical integration would be significantly complicated. The full list of the integrals appearing in the calculation is given in Appendix.

The next step is the integration over loop momenta. The loop integration can be partially done analytically and the remaining integrals can be evaluated using numerical algorithms. The integration technique based on the properties of Gegenbauer polynomials widely used in two-loop calculations does not lead to analytical results in a general case. Due to the structure appearing after angular averaging the three-dimensional angular integral can not be performed analytically for all appearing structures [152]. However, it is possible to perform analytical integration over two-dimensional spherical angles $\Omega(\mathbf{Q}_1)$ and $\Omega(\mathbf{Q}_1)$ with subsequent numerical evaluation of the remaining four-dimensional integral. We notice that the only dependence on the relative angle between vectors $\mathbf{Q}_1$ and $\mathbf{Q}_2$ in the resulting expression is in the Legendre polynomials. It allows us to integrate it out analytically in a similar way to how we did the averaging over k. The details of the integration are given in Appendix D.

Due to the reasons mentioned before, it is convenient to carry out the numerical integration in polar coordinates. In particular, we make the change of variables :

$$Q_i^0 = Q_i \cos\psi_i, \qquad |\mathbf{Q}_i| = Q_i \sin\psi_i. \tag{4.90}$$

The resulting four-dimensional integral for the case of a scalar meson with a monopole FF takes the form :

$$\begin{aligned} a_\mu^{LbL,S} = &- \frac{16\alpha\Gamma_{\gamma\gamma}\Lambda^6}{\pi^4 M_S} \int\limits_0^\infty \mathrm{d}Q_1 \int\limits_0^\pi \mathrm{d}\psi_1 \int\limits_0^\infty \mathrm{d}Q_2 \int\limits_0^\pi \mathrm{d}\psi_2 \\ &\frac{\sin^2\psi_1 \sin^2\psi_2}{Q_1 + 2im\cos\psi_1} \frac{1}{Q_1^2+\Lambda_S^2} \frac{1}{Q_2^2+\Lambda_S^2} \frac{1}{Q_2^2+M_S^2} \\ &\times \left[2\,\frac{\tilde{T}_1(Q_1,Q_2,\psi_1,\psi_2)}{Q_2 - 2im\cos\psi_2} + Q_2 \tilde{T}_2(Q_1,Q_2,\psi_1,\psi_2) \right], \end{aligned} \tag{4.91}$$

where in the third diagram we have absorbed a factor $\left[(Q_1+Q_2)^2 + 2im(\cos\psi_1 + \cos{+}\psi_2)\right]^{-1}$ in the expression for $\tilde{T}_2(Q_1,Q_2,\psi_1,\psi_2)$. Reproducing again all the steps as was done for the scalar exchange we arrive to a similar four-dimensional integral representation for the tensor meson contribution to the muon's anomalous moment,

$$\begin{aligned} a_\mu^{LbL,T} = &- \frac{80\alpha\Gamma_{\gamma\gamma}\Lambda_{T1}^6\Lambda_{T2}^6}{\pi^4 M_T} \int\limits_0^\infty \mathrm{d}Q_1 \int\limits_0^\pi \mathrm{d}\psi_1 \int\limits_0^\infty \mathrm{d}Q_2 \int\limits_0^\pi \mathrm{d}\psi_2 \\ &\frac{\sin^2\psi_1 \sin^2\psi_2}{Q_1 + 2im\cos\psi_1} \frac{1}{Q_1^2+\Lambda_{T1}^2} \frac{1}{Q_2^2+\Lambda_{T1}^2} \frac{1}{Q_1^2+\Lambda_{T2}^2} \frac{1}{Q_2^2+\Lambda_{T2}^2} \frac{1}{Q_2^2+M_T^2} \\ &\times \left[2\,\frac{\tilde{T}_1(Q_1,Q_2,\psi_1,\psi_2)}{Q_2 - 2im\cos\psi_2} + Q_2 \tilde{T}_2(Q_1,Q_2,\psi_1,\psi_2) \right]. \end{aligned} \tag{4.92}$$

The remaining integrals in Eqs. (4.91, 4.92) can not be performed analytically. To accomplish the integration we use numerical algorithms.

4.4 Results and discussion

The integrands in four-dimensional representations of Eqs. (4.91, 4.92) as well as in two-dimensional integrals of Eqs. (4.57, 4.58) are composed of rational functions, square roots and logarithms. The numerical evaluation of the two- and four-dimensional integral representations therefore possesses no real problems. We have used the following input values for the physical constants: $\alpha = 1/137.03599976$ and the mass of the muon $m = m_\mu = 105.66$ MeV. The remaining values of meson masses and their decay constants as well as the form factor parameters are given further in tables. Where it is possible, we will use the available experimental information to define the mass parameters of the form factor fitting functions. Otherwise, we will exploit the constraints obtained from the sum rules to set the mass parameters or vary their values in a certain range. In the end we will compare our predictions with the previous calculations.

4.4.1 Pseudo-scalar mesons

To test the formalism based on three-dimensional angular integration, we have firstly applied it to the case of pseudo-scalar meson poles. This case had been worked out analytically in Ref. [140] and reproduced previously in this work using the Gegenbauer polynomial technique, where for monopole parametrizations of the FFs the HLbL contribution to a_μ had been given by a two-dimensional numerical integral over Q_1 and Q_2. We can alternatively obtain this two-dimensional representation by using the three-dimensional angular integration technique with subsequent two-dimensional numerical integration over ψ_1 and ψ_2. We checked that using e.g. a monopole FF, the result obtained from the analogous to Eq. (4.91) representation for the pseudo scalar mesons is in exact agreement with the result of Ref. [140]. It is shown in Table 4.2. The errors from the numerical integration are much smaller than the last digits given in the table below and the total errors are dominated by the phenomenological uncertainties.

	M [MeV]	$\tilde{\Gamma}_{\gamma\gamma}$ [keV]	$\Lambda_{\rm dip}$ [MeV]	a_μ [10^{-11}]
π^0	134.9766 ± 0.0006	$(7.8 \pm 0.5) \times 10^{-3}$	1040 ± 78	58 ± 10
η	547.853 ± 0.024	0.510 ± 0.026	774 ± 29	13 ± 1
η'	957.78 ± 0.06	4.29 ± 0.14	859 ± 28	12 ± 1
Sum				83 ± 12

Table 4.2: Present values [62] of the π^0. η and η' meson masses M, their equivalent 2γ decay widths $\tilde{\Gamma}_{\gamma\gamma}$, defined according to Eq. (4.39), as well as their monopole masses $\Lambda_{\rm mon}$ entering the FF of Eq. (4.38).

In order to have a better understanding which region of virtualities in the axial-vector meson FFs is contributing mostly to this result, it is instructive to define a density function ρ as :

$$a_\mu = \int_0^\infty dQ_1 \int_0^\infty dQ_2 \, \rho_1^{(P)}(Q_1, Q_2) + \int_0^\infty dQ_1 \int_0^\infty dQ_2 \, \rho_2^{(P)}(Q_1, Q_2). \tag{4.93}$$

For the four-dimensional integral representation the density function may be obtained by two-dimensional integration over polar angles ψ_1 and ψ_2. We show the dependence of $\rho_{1,2}^{(P)}$ on the photon virtualities Q_1 and Q_2, which enter the HLbL scattering diagram, for the π^0 meson in Fig. 4.5.

First of all, we can see that for the pseudo scalar mesons the second distribution function is highly suppressed compare to the first one. It turns out that the corresponding integral converges even for a constant form factor as in the WZW model [140]. It means that it is

less sensitive to the short-distance physics and the contribution is defined by the region of low momenta. As a result the magnitude of this contribution is very stable with respect to the various form factors [140]. Finally, one notices that the dominant contribution arises from the region around $Q_1 \approx Q_2 \approx 0.5$ GeV.

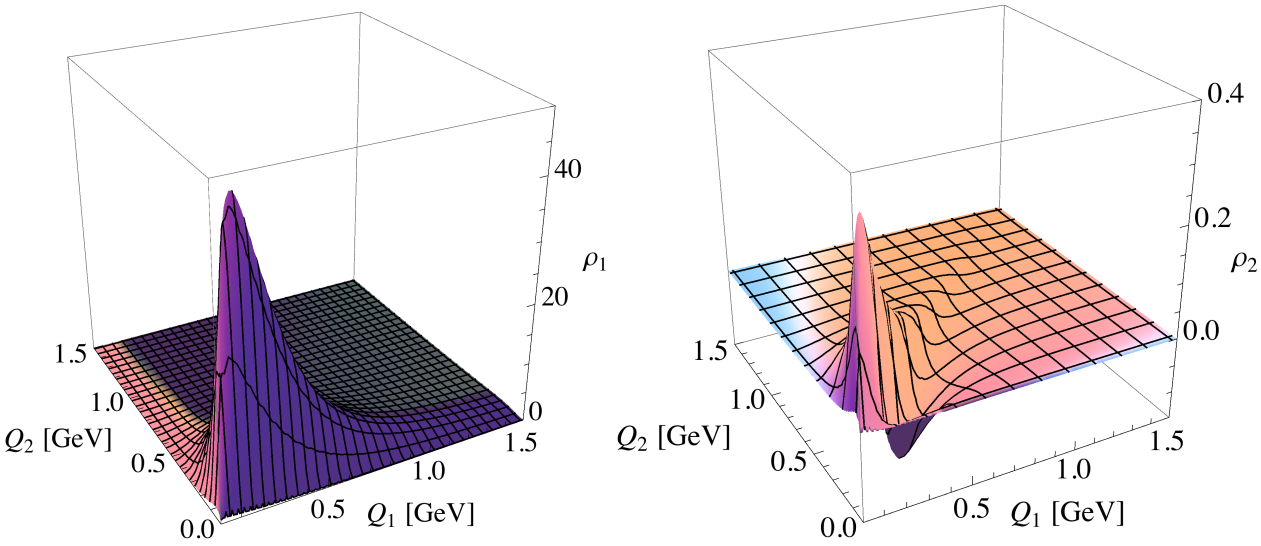

Figure 4.5: The densities $\rho_{1,2}^{(P)}$ as defined in Eq. (4.93), in units 10^{-10} GeV^{-2}, for the π^0 meson. Left panel corresponds with left two diagrams of Fig. 4.4, right panel corresponds with right diagram of Fig. 4.4.

As we discussed due to the more complicated vertex structure for scalar and tensor mesons, the Gegenbauer polynomial technique cannot be easily extended, which is why we resort to the four-dimensional expression of Eq. (4.91). Using this formalism, we subsequently discuss our estimates for the HLbL contribution to a_μ due to axial-vector, scalar and tensor mesons.

4.4.2 Axial-vector mesons

Phenomenologically, the two-photon production cross sections have been measured for the two lowest lying axial-vector mesons : $f_1(1285)$ and $f_1(1420)$. The most recent measurements were performed by the L3 Collaboration [88, 89]. In those works, the non-relativistic quark model expression of Eq. (2.37) in terms of a single FF $F_{\mathcal{A}\gamma^*\gamma^*}$ has been assumed, and the resulting FF has been parameterized by a dipole form as in Eq. (4.20). Table 4.3 shows the present experimental status of the equivalent 2γ decay widths for $f_1(1285)$, and $f_1(1420)$, as well as the phenomenological values for the dipole mass parameters $\Lambda_{\rm dip}$.

Using these values, we can calculate the HLbL contributions of $f_1(1285)$ and $f_1(1420)$ to a_μ, which are shown in Table 4.3. Both contributions sum up to a value of 6.4×10^{-11}, which is roughly one order of magnitude smaller than the dominant HLbL contribution to a_μ due to the π^0 [140]. We like to emphasize that our estimate for the two dominant axial-vector meson contributions is based on available experimental information. In this way, we are also able to provide an error estimate, which derives from the experimental uncertainties in the equivalent 2γ decay widths and from the FF parameterization.

We show the dependence of distribution functions $\rho_{1,2}^{(A)}$ on the photon virtualities Q_1 and Q_2, which enter the HLbL scattering diagram, for the axial-vector meson $f_1(1285)$ in Fig. 4.6. One notices that the dominant contribution arises from the region around $Q_1 \approx Q_2 \approx 0.5$ GeV. One also sees that the contribution beyond $Q_{1,2} \geq 1.5$ GeV becomes negligible.

	M [MeV]	$\tilde{\Gamma}_{\gamma\gamma}$ [keV]	$\Lambda_{\rm dip}$ [MeV]	a_μ $[10^{-11}]$
$f_1(1285)$	1281.8 ± 0.6	3.5 ± 0.8	1040 ± 78	5.0 ± 2.0
$f_1(1420)$	1426.4 ± 0.9	3.2 ± 0.9	926 ± 78	1.4 ± 0.7
Sum				6.4 ± 2.0

Table 4.3: Present values [62] of the $f_1(1285)$ meson and $f_1(1420)$ meson masses M, their equivalent 2γ decay widths $\tilde{\Gamma}_{\gamma\gamma}$, defined according to Eq. (2.31), as well as their dipole masses $\Lambda_{\rm dip}$ entering the FF of Eq. (2.37). For $\tilde{\Gamma}_{\gamma\gamma}$, we use the experimental results from the L3 Collaboration : $f_1(1285)$ from [88], $f_1(1420)$ from [89].

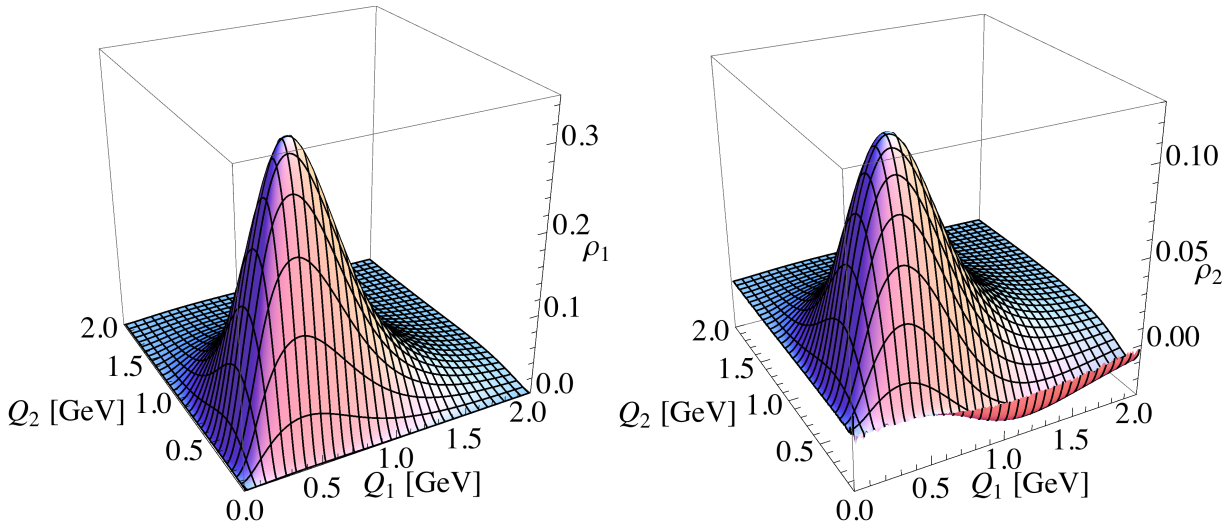

Figure 4.6: The densities $\rho^{(A)}_{1,2}$, in units 10^{-10} GeV^{-2}, for the axial-vector meson $f_1(1285)$. Left panel corresponds with left two diagrams of Fig. 4.4, right panel corresponds with right diagram of Fig. 4.4.

4.4.3 Scalar mesons

When going to virtual photons, unfortunately no empirical information is available at present for the $S\gamma^*\gamma^*$ transition FFs. We will assume a simple monopole behavior of the FF. The monopole mass $\Lambda_{\rm mon}$ is considered as a free parameter, which we will vary in the expected hadronic range $\Lambda_{\rm mon} = 1 - 2$ GeV, in order to obtain the numerical estimates for a_μ. We show our results for the HLbL contribution to a_μ due to the leading scalar mesons f_0, f_0', and a_0 in Table 4.4. We find a negative contribution of the scalar mesons to a_μ which is in the range -1 to -3 (in units 10^{-11}), when varying $\Lambda_{\rm mon}$ in the range 1 to 2 GeV. The opposite to the other contributions sign can clearly seen from the density plots on Fig. 4.7

4.4.4 Tensor mesons

In this work, we also estimate the HLbL contribution to a_μ due to tensor mesons. The dominant tensor mesons produced in two-photon fusion processes are given by : $f_2(1270)$, $a_2(1320)$, $f_2(1565)$, and $a_2(1700)$, see Table 4.5. At the present moment there is unfortunately no direct experimental information about the Q^2 dependence of the tensor meson transition FFs. One can however resort to other phenomenological information based on exact forward sum rules for the light-by-light scattering. For $\gamma^*\gamma \to X$ fusion cross sections, with one real photon (γ) and one virtual photon (γ^*), three super convergence sum rules were derived in Refs. [22, 55].

	M [MeV]	$\Gamma_{\gamma\gamma}$ [keV]	a_μ ($\Lambda_{\rm mon} = 1$ GeV) [10^{-11}]	a_μ ($\Lambda_{\rm mon} = 2$ GeV) [10^{-11}]
$f_0(980)$	980 ± 10	0.29 ± 0.07	-0.19 ± 0.05	-0.61 ± 0.15
$f_0'(1370)$	$1200 - 1500$	3.8 ± 1.5	-0.54 ± 0.21	-1.84 ± 0.73
$a_0(980)$	980 ± 20	0.3 ± 0.1	-0.20 ± 0.07	-0.63 ± 0.21
Sum			-0.9 ± 0.2	-3.1 ± 0.8

Table 4.4: Scalar meson pole contribution to a_μ based on the present PDG values [62] of the scalar meson masses M and their 2γ decay widths $\Gamma_{\gamma\gamma}$.

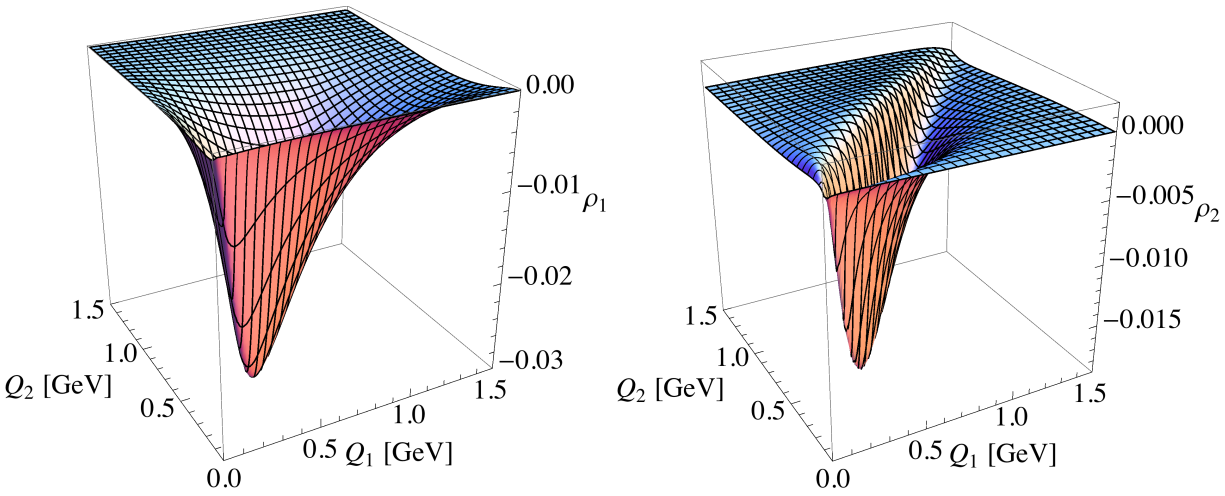

Figure 4.7: The densities $\rho_{1,2}^{(S)}$, in units 10^{-10} GeV^{-2}, for the scalar meson for monopole mass $\Lambda = 1$ GeVx. Left panel corresponds with left two diagrams of Fig. 4.4, right panel corresponds with right diagram of Fig. 4.4.

Applied to the $\gamma^*\gamma$ production of mesons, this leads to intricate relations between transition FFs of pseudo-scalar, axial and tensor mesons. In order to saturate these sum rules, one obtains approximate expressions for the dominant tensor meson transition FFs, given the knowledge of the transition FFs for the pseudo-scalar mesons. In particular, it was shown in Ref. [55] that the η, and η' transition FFs constrain the transition FF for $f_2(1270)$ and the π^0 transition FF constrains the corresponding transition FF for the $a_2(1320)$ state. We found that in the relevant range of virtualities these relations can approximately be expressed by choosing a dipole form for the tensor meson transition FF with dipole mass parameter $\Lambda_{\rm dip} = 1.5$ GeV. We use this estimate in calculating the HLbL contribution to a_μ due to tensor mesons, which is shown in Table 4.5. We see that the four dominant tensor meson contributions add up to a contribution to a_μ of around 1 (in units 10^{-11}). The density plots for the case of ... meson are shown on Fig. 4.8. A curious fact emerges here, the contribution of the tensor meson is cancelled by the contribution of a scalar meson. Similar cancellation we already observed when analyzing of the meson production in the sum rules.

4.4.5 Comparison with previous works

Our results can be compared with previous estimates for axial-vector and scalar mesons, which are shown in Table 4.6 and were mentioned previously. For tensor mesons, our results are the first estimates.

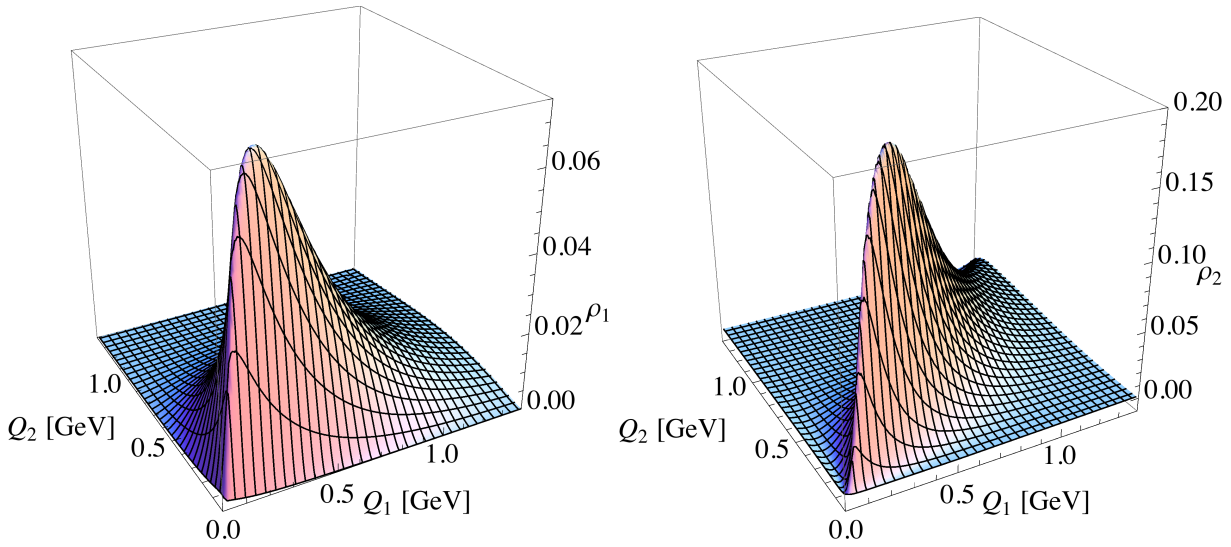

Figure 4.8: The densities $\rho_{1,2}^{(S)}$, in units 10^{-10} GeV^{-2}, for the scalar meson. Left panel corresponds with left two diagrams of Fig. 4.4, right panel corresponds with right diagram of Fig. 4.4.

	M [MeV]	$\Gamma_{\gamma\gamma}$ [keV]	a_μ ($\Lambda_{\rm dip} = 1.5$ GeV) [10^{-11}]
$f_2(1270)$	1275.1 ± 1.2	3.03 ± 0.35	0.79 ± 0.09
$f_2(1565)$	1562 ± 13	0.70 ± 0.14	0.07 ± 0.01
$a_2(1320)$	1318.3 ± 0.6	1.00 ± 0.06	0.22 ± 0.01
$a_2(1700)$	1732 ± 16	0.30 ± 0.05	0.02 ± 0.003
Sum			1.1 ± 0.1

Table 4.5: Tensor meson pole contribution to a_μ based on the present PDG values [62] of the tensor meson masses M and their 2γ decay widths $\Gamma_{\gamma\gamma}$.

The MV [142] and JN [29] estimates are an order of magnitude larger than our estimate, while the BPP [131, 132], HKS [133, 134, 135] and PdRV [51] estimates are enhanced by around a factor 3. The large value of Ref. [142] was obtained because a constant FF was used at the external vertex to reproduce the QCD short-distance constraints. Although such short-distance constraints are surely important for the large Q^2 behavior of the FFs, one can see from Fig. 4.6 that using the empirical information for the $f_1(1285)$ transition FF, the region which dominates the HLbL contribution to a_μ is for virtualities around and below 1 GeV^2. An intermediate estimate of PdRV [51] is in agreement within 1σ with our estimate.

For the scalar mesons, BPP has performed an estimate, which was adopted by N/JN and PdRV (by increasing the error bar to 100 %). Compared with the result of BPP, our result also has the negative sign, but is around a factor of 2 smaller in magnitude. Given that there is no empirical information at all on the scalar meson transition FFs, future data from BES-III would be mostly welcome here to better constrain this contribution.

	axial-vectors	scalars	tensors
BPP [131, 132]	2.5 ± 1.0	-7 ± 2	-
HKS [133, 134, 135]	1.7 ± 1.7	-	-
MV [142]	22 ± 5	-	-
PdRV [51]	15 ± 10	-7 ± 7	-
N/JN [29]	22 ± 5	-7 ± 2	-
this work	6.4 ± 2.0	-3.1 ± 0.8	1.1 ± 0.1

Table 4.6: HLbL contribution to a_μ (in units 10^{-11}) due to axial-vector, scalar, and tensor mesons obtained in this work, compared with various previous estimates. For our scalar meson estimate, we have quoted the value corresponding with $\Lambda_{\rm mon} = 2$ GeV.

4.5 Conclusions

In this chapter we have presented the formalism to calculate the HLbL contribution to the muon's anomalous magnetic moment a_μ due to axial-vector, scalar and tensor meson poles. In this way, we have extended the framework of Ref. [140], where the leading HLbL contribution due to pseudo-scalar mesons was evaluated. To allow for the different Lorentz structures of the $\gamma^*\gamma^* \to$ meson vertex, we have performed a combined analytical and numerical technique, where the angular integrals over the virtual photon momenta were performed analytically using the Legendre polynomial technique, and where the resulting four-dimensional integral for a_μ was performed numerically. We validated our method by reproducing the known result for pseudo-scalar mesons. To estimate the HLbL contribution to a_μ from axial-vector, scalar and tensor mesons, we incorporated available experimental input as well as constraints from light-by-light scattering sum rules. For those mesons which have the largest known couplings to two virtual photons, we obtained as estimates :

$$\begin{aligned} a_\mu(f_1, f_1') &= (6.4 \pm 2.0) \times 10^{-11}, \\ a_\mu(f_0, f_0', a_0) &= [(-0.9 \pm 0.2) \text{ to } (-3.1 \pm 0.8)] \times 10^{-11}, \\ a_\mu(f_2, f_2', a_2, a_2') &= (1.1 \pm 0.1) \times 10^{-11}. \end{aligned}$$

The size of such contributions is about an order of magnitude smaller than the dominant π^0 HLbL contribution. Given a new muon $g-2$ experiment at Fermilab, which aims to reduce the experimental uncertainty to $\delta a_\mu \approx 16 \times 10^{-11}$, it is however crucial to further constrain the theoretical uncertainty due to the HLbL contribution. In this respect, it would be particularly helpful to have $\gamma^*\gamma^* \to$ meson transition form factor measurements with one and two virtual photons for axial-vector, scalar and tensor states. As such information will become available, in particular from future measurements from BES-III, the here developed formalism can be used to further improve on the estimate of the HLbL contribution to a_μ.

The estimates worked out in this chapter shed the light on the hadronic contributions to the $(g-2)_\mu$ giving an important information about the relevance of different intermediate states. However, as we already mentioned there is one issue which should not be dismissed. In order to avoid the inconsistency related to the momentum conservation and due to the absence of the phenomenological information we had to assume constant form factors in the meson mass. This, of course, might be a source of a larger uncertainty of our estimates compare to errors given above. In order to overcome this complication and to define hadronic contributions rigorously we refer to the analytical structure of the hadronic vacuum polarization tensor and develop a novel dispersion technique for the evaluation of the HLbL contribution to the $(g-2)_\mu$

Chapter 5

Hadronic light-by-light contribution to $(g-2)_\mu$ in a dispersion approach

In the previous chapter we have estimated the single meson LbL contributions to the anomalous magnetic moment of the muon by the direct computation of loop integrals in Feynman diagrams. However, our results possess significant limitations. A weak point of the used approach is the on-shell approximation for the meson form factors, while in the loop integral the exchanged meson is significantly off-shell. To overcome this inconsistency we develop a dispersion representation for the two-loop HLbL contribution to $(g-2)_\mu$. The aim is to express the HLbL correction to the anomalous magnetic moment in terms of on-shell hadronic amplitudes which in this case can be directly determined from the experimental data. The integrals appearing in $(g-2)_\mu$ can be generally decomposed in a sum of scalar integrals. As a first step we will develop the formalism for a dispersive representation of the scalar two-loop functions. The general dispersive framework for the muon's anomalous magnetic moment will be discussed subsequently.

5.1 Introduction

When dealing with the strong interactions especially in the non-perturbative regime it is often prohibitive to find a consistent theoretical solution. The background processes involving strong forces are usually a source of large uncertainty which in many situations defies their systematic theoretical control. In such a situation to constrain the hadronic uncertainties one can refer to experimental data. To make such an implementation one needs to express the quantity in terms of on-shell hadronic matrix elements as outside of the mass shell they are highly suppressed and can not be measured experimentally.

The rigorous incorporation of the data into a theoretical analysis can be carried out by means of the dispersion framework. We already showed how, by analyticity and unitarity, the elastic scattering amplitude at low energy may be related to the two-photon fusion cross-sections by sum rules. Similarly, one can apply such an idea for the calculation of loop corrections where the non-perturbative hadronic correlators may be related to measurable cross sections or other observables. An example of such an approach is the determination of the VP correction to $(g-2)_\mu$. The energy scale for the virtual hadrons in this process is of order $m_\mu c^2$, well below the perturbative region of QCD. Using the dispersion representation for the photon polarization, the VP contribution is expressed in terms of measurable $e^+e^- \to h$ cross sections, shown pictorially in Fig. 5.1,

$$a_\mu^{VP} = \left(\frac{\alpha m_\mu}{3\pi}\right)^2 \int\limits_{m_\pi^2}^{\infty} \frac{\mathrm{d}s}{s^2} K(s) R(s), \quad \text{where} \quad R = \frac{\sigma_{tot}(e^+e^- \to \text{hadrons})}{\sigma(e^+e^- \to \mu^+\mu^-)}, \tag{5.1}$$

where $K(s)$ is a kinematic factor ranging from 0.4 at $s = m_\pi^2$ to 0 at $s = \infty$ (see Ref. [153]). Because the integrand contains a factor of s^{-2}, the values of $R(s)$ at low energies (the ρ

resonance) dominate the determination of a_μ^{VP}, however at the level of precision needed, the data up to 2 GeV are very important. Using this approach, the HVP which is the dominating hadronic contribution in $(g-2)_\mu$, is presently determined to a much higher relative precision than the HLbL contribution.

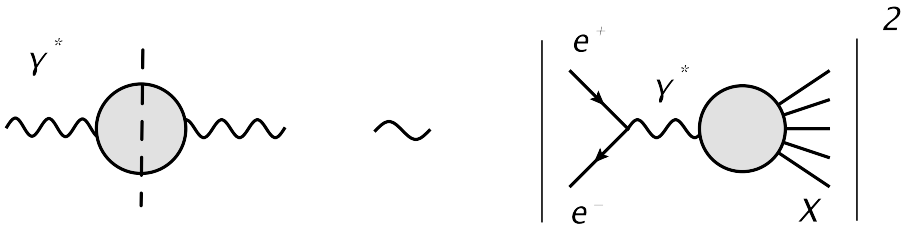

Figure 5.1: The HVP contribution to the anomalous magnetic moment of the muon: cuts in a vertical projection

Up to a present moment, a commonly accepted belief was that the HLbL contribution to $(g-2)_\mu$ cannot be defined in a dispersive framework. Attempts to define the dispersion representation for the HLbL matrix element directly in the loop integral fail due to the kinematical constraints. It may be explained by the following arguments. In a general case, a four-point function may be defined in terms of six invariant variables, e.g. squared masses of the external particles q_1^2, q_2^2, q_3^2, q_4^2 and Mandelstam variables $s = (q_1 + q_2)^2$ and $t = (q_1 - q_3)^2$. The fact that all six variables can be varied independently allows to perform the analytical continuation of the amplitude in each of these parameters for given values of the remaining invariants. However, when considering the loop integral in the limit of the classical external field, i.e. $q_1 \to 0$ (see Fig. 5.2), the hadron invariant mass s and the photon virtuality q_2^2 are not independent any more: $s = (q_1 + q_2)^2 \to q_2^2$, and the dispersion integral can not be written independently. However, it turns out, that it is not the only possible way of the calculation. In the following we present the novel dispersive approach developed specifically for the calculation of the HLbL correction to $(g-2)_\mu$ which allows to overcome this inconsistency.

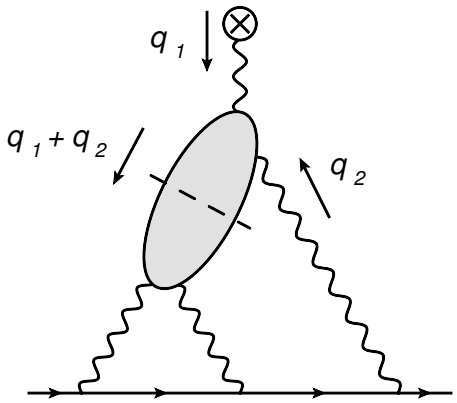

Figure 5.2: The LbL scattering contribution to the anomalous magnetic moment of the muon: cuts in a vertical projection

In the previous section we defined the anomalous magnetic moment as a classical limit of the Pauli form factor $F_2(k^2)$, which in general may be calculated using the projection operator as

$$F_2(k^2) = \mathrm{Tr}\left[(\not{p}' + m)\Lambda_\nu(p', p)(\not{p} + m)\Gamma^\nu(p', p)\right], \tag{5.2}$$

with the projector Λ_μ defined by

$$\Lambda_\nu(p',p) = \frac{m^2}{k^2(4m^2-k^2)}\left[\gamma_\nu + \frac{k^2+2m^2}{m(k^2-4m^2)}(p'+p)_\nu\right]. \tag{5.3}$$

If one knows the vertex $\Gamma^\nu(k^2)$, the a_μ can be defined straightforwardly by the limit $k \to 0$. Alternatively, using the dispersion relation in the virtuality of the external photon $k^2 \equiv t$ we can relate $F_2(0)$ to the absorptive part of the form factor for the time-like process of $\gamma^* \to \mu^+\mu^-$:

$$F_2(0) = \frac{1}{2\pi i}\oint\limits_{\text{Disc}} \frac{\mathrm{d}t}{t}\text{Abs}\, F_2(k^2). \tag{5.4}$$

The absorptive part of the form factor is directly related to the absorptive part of the QED vertex function[1]:

$$\text{Abs}\, F_2(t) = \text{Tr}\left[(\not{p}'+m)\Lambda_\mu(p',p)(\not{p}+m)\text{Abs}\,\Gamma^\mu(p',p)\right] \tag{5.5}$$

Subsequently, using analytical continuation and unitarity relations the absorptive part of the vertex function Γ^μ can be expressed in terms of measurable on-shell hadron production matrix elements. In practice, the unitarity method is realized by means of Cutkosky rules. They can be graphically represented as a cut of a Feynman diagram which crosses all intermediate states allowed in the considered channel by quantum numbers and kinematics. When the cut crosses the propagator it means that the corresponding virtual intermediate state is put on its mass shell. This can be done by a simple substitution of the crossed propagators by delta-functions:

$$\frac{1}{q^2-m^2+i\varepsilon} \to -2\pi i\delta(q^2-m^2). \tag{5.6}$$

When the non-perturbative matrix element is crossed by the cut, the discontinuity in the corresponding invariant energy flowing through the cut is implied

$$M(m_i^2,s_j) \to \text{Disc}_s M(m_i^2,s_j). \tag{5.7}$$

where m_i and s_j are the masses of external legs and energy invariants of the matrix element and s is the squared c.m. energy flowing through the discontinuity.

For better visualization it is convenient to depict the cut diagrams for the HLbL contribution in a 3D image which can be considered as a three-dimensional projection of the four-dimensional momentum phase-space. In this representation each intermediate state appearing in the unitarity relation is represented by an on-shell slice of a phase-space. For example, one of the cuts appearing in Γ^μ is shown in Fig. 5.3. The cut plane is represented by a grey box in the illustration. It crosses the HLbL blob and two virtual muon lines. The absorptive part corresponding to this diagram is defined as a product of $\mu^+\mu^- \to \mu^+\mu^- X$ (below the cut plane) and $\gamma^* \to \mu^+\mu^- X$ (above the cut plane) amplitudes.

To systematize all possible cuts appearing in the considered case it is convenient to use the vertical projection of the 3D Feynman diagrams (see Fig. 5.4). The red curve defines the projection of a cut, thus all the intermediate states which cross this line are on-shell. The black spot depicts the incoming external photon. In terms of Fig. 5.3 the part of the diagram inside the red circle lies above the plane and the outside part lies below. One can notice that the 3D diagram in Fig. 5.3 corresponds with the third graph in the first row of Fig.(5.4).

[1] A seeming kinematical singularity $t = 4m^2$ form the projector does not contribute to the discontinuity. It is cancelled against the numerator after performing all the phase space integrals in the unitarity relation.

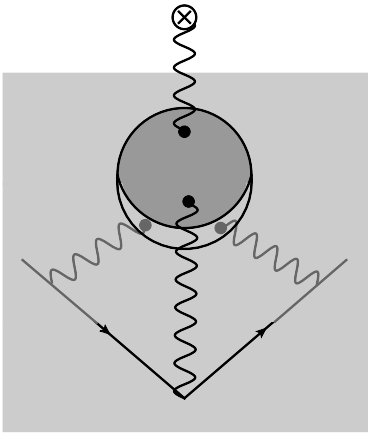

Figure 5.3: The 3D projection of a cut diagram in LbL scattering contribution to the anomalous magnetic moment of the muon.

In a general case (in the absence of the before mentioned kinematical constraints) the HLbL matrix element may be defined via dispersion representation through its discontinuities. The analytical structure of this matrix element is very complicated and has not been widely studied in the past. The intermediate states which contribute to the discontinuities of the HLbL tensor (grey blob in Fig. 5.4) can be separated in two types, the C-positive and C-negative states. They correspond to two types of cuts of the HLbL four-point function. The C-positive intermediate hadronic states contribute to the $\gamma^*\gamma^*$ production channels and appear as poles and branching points in the complex plane of the squared total energy of initial photons. They include a series of single meson intermediate states, i.e. pseudo scalar mesons π^0, η and η' and heavier scalar, axial vector and tensor mesons. Furthermore, they include multi-particle states with the dominant channel $\gamma^*\gamma^* \to \pi^+\pi^-$. These intermediate states explicitly contribute to unitarity diagrams 2, 3, 4, 5 and 6 in Fig. 5.4. The C-negative states contribute to the 'corner' cuts and are originating from the 'hadronization' of the photon. These discontinuities result in poles and branching points in the complex plane of the virtualities of the corresponding photons. A prominent contribution of this kind originates from the fluctuation of a photon to a vector meson, such as ρ^0 or ω. They explicitly contribute to the three diagrams in the last row in Fig. 5.4.

One notices that in the dispersion relation of Eq.(5.4) the contribution of the discontinuities with the branch points located at higher scales are suppressed due to expansion of the phase space. In view of this argument and the fact that the HLbL tensor is weighted by the QED propagators it makes sense to start constraining the uncertainty by systemizing the contributions of the lowest lying singularities. The general idea is to incorporate the experimentally observed behavior in the non-analyticities of the amplitude. For instance, the resonant behavior (a single particle, a resonance or a bound state exchange) corresponds to poles in a complex plane, the logarithmic behavior which originates from multi-particle production channels is related to the branch points located at the production threshold, etc. The parameters (i.e. position of poles and branch points, the residues, etc.) of the introduced singularities are obtained by a fit of the data. This procedure can be formally called 'the analytical parametrization'[2].

The dominant contributions to the two-photon production discontinuity are originating from the intermediate states related to the lightest hadronic state, a single neutral pion ($X = \pi^0$). This C-positive intermediate state can contribute to the $\gamma\gamma$ decay (or $\gamma\gamma \to \gamma\gamma$) channel which

[2]In principle, one can involve the experimental data directly. This can be done by using partial wave decomposition and analytical continuation of the partial wave amplitudes.

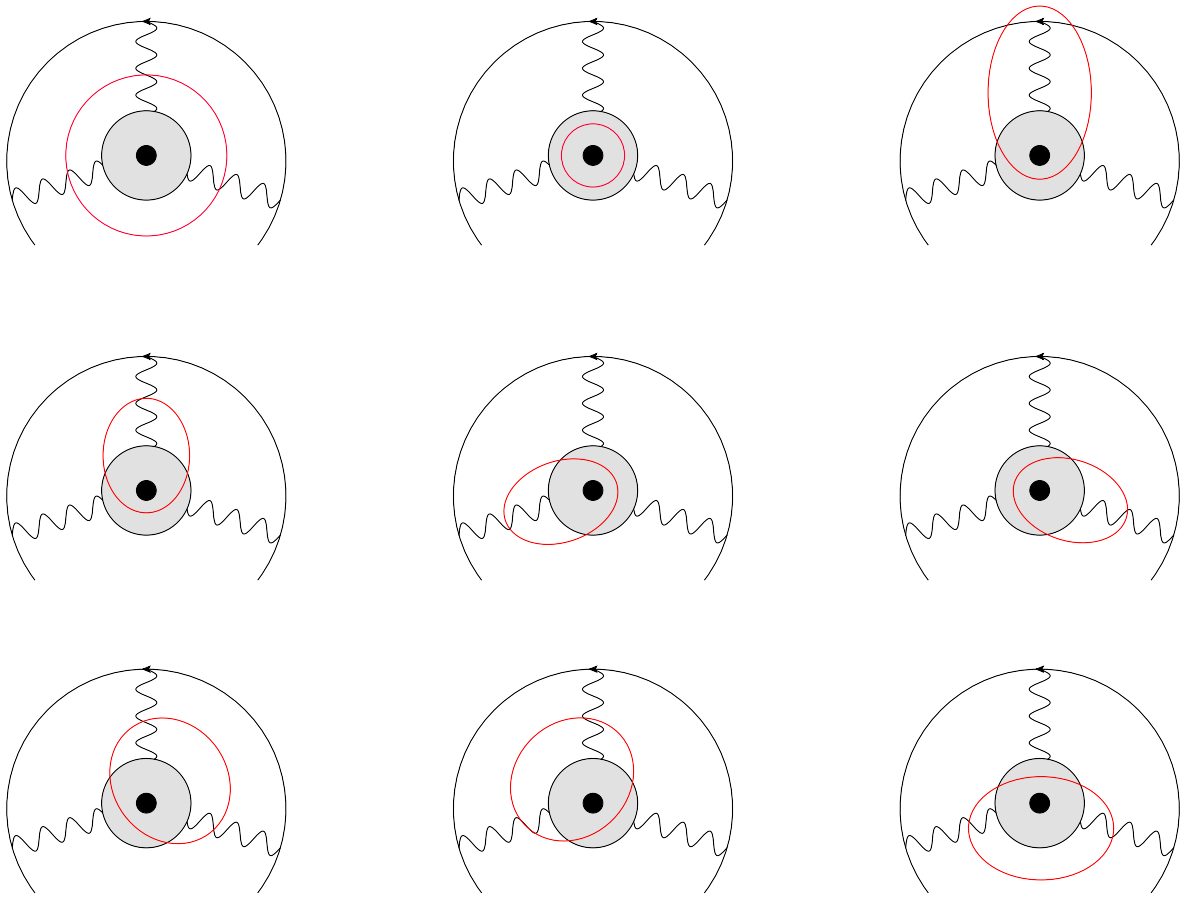

Figure 5.4: The LbL scattering contribution to the anomalous magnetic moment of the muon: cuts in a vertical projection

explicitly appears in unitarity diagrams 2, 3, 4, 5 and 6 in Fig. 5.4[3]. Defining the Mandelstam variables

$$s_1 = (q_1 + q_2)^2, \quad s_2 = (q_1 - q_3)^2, \quad s_3 = (q_1 - q_4)^2, \tag{5.8}$$

the contribution of the meson pole to the light-by-light scattering amplitude discontinuity is given by

$$\begin{aligned} &\mathrm{Disc}_{\pi^0}\Pi_{\lambda_1\lambda_2\lambda_3\lambda_4}(q_1^2,q_2^2,q_3^2,q_4^2,s_1,s_2,s_3) \\ &\qquad = \mathcal{M}_{\lambda_1\lambda_2}(q_1^2,q_2^2,s_1)2\pi\delta\left(s_1 - M^2\right)\mathcal{M}_{\lambda_3\lambda_4}(q_3^2,q_4^2,s_1) \\ &\qquad + \mathcal{M}_{\lambda_1-\lambda_3}(q_1^2,q_3^2,s_2)2\pi\delta\left(s_2 - M^2\right)\mathcal{M}_{\lambda_2-\lambda_4}(q_2^2,q_4^2,s_2) \\ &\qquad + \mathcal{M}_{\lambda_1-\lambda_4}(q_1^2,q_4^2,s_3)2\pi\delta\left(s_3 - M^2\right)\mathcal{M}_{\lambda_2-\lambda_3}(q_2^2,q_3^2,s_3) \end{aligned} \tag{5.9}$$

where for a pseudo-scalar state the $\gamma^*\gamma^* \to M$ helicity amplitude is given by:

$$\mathcal{M}_{\lambda_1\lambda_2}(q_1^2,q_2^2,(q_1+q_2)^2) = -i\epsilon^\mu(q_1,\lambda_1)\epsilon^\nu(q_2,\lambda_2)\varepsilon_{\mu\nu\alpha\beta}q_1^\alpha q_2^\beta F_{P\gamma^*\gamma^*}(q_1^2,q_2^2,(q_1+q_2)^2). \tag{5.10}$$

In the last equations $\epsilon(q_i,\lambda_i)$ stands for the polarization vectors of photon, subscripts λ_i denote their helicities and M is a meson mass. The analytical continuation from the scattering to the

[3]We do not discuss the QED corrections, e.g. processes $\gamma^* \to \gamma^*\pi \to 3\gamma$ as they are suppressed by electromagnetic coupling constant α.

decay channel is trivial in this case[4]. Hence, the pole contribution to the light-by-light scattering amplitude is

$$\begin{aligned}
&\Pi^{\pi^0}_{\lambda_1\lambda_2\lambda_3\lambda_4}(q_1^2,q_2^2,q_3^2,q_4^2,s_1,s_2,s_3)\\
&\qquad=\int \mathrm{d}s_1\,\frac{\mathcal{M}_{\lambda_1\lambda_2}(q_1^2,q_2^2,s_1')\mathcal{M}_{\lambda_3\lambda_4}(q_3^2,q_4^2,s_1')}{s_1-s_1'}\delta\left(s_1'-M^2\right)\\
&\qquad+\int \mathrm{d}s_2\,\frac{\mathcal{M}_{\lambda_1-\lambda_3}(q_1^2,q_3^2,s_2')\mathcal{M}_{\lambda_2-\lambda_4}(q_2^2,q_4^2,s_2')}{s_2-s_2'}\delta\left(s_2'-M^2\right)\\
&\qquad+\int \mathrm{d}s_3\,\frac{\mathcal{M}_{\lambda_1-\lambda_4}(q_1^2,q_4^2,s_3')\mathcal{M}_{\lambda_2-\lambda_3}(q_2^2,q_3^2,s_3')}{s_3-s_3'}\delta\left(s_3'-M^2\right)
\end{aligned}\tag{5.11}$$

As a result of the latter transformation the non-perturbative part of the pion-pole contribution to the HLbL tensor is defined through the on-shell pion transition form factors:

$$\begin{aligned}
\Pi^{\pi^0}_{\lambda_1\lambda_2\lambda_3\lambda_4}(q_1^2,q_2^2,q_3^2,q_4^2,s_1,s_2,s_3)=&\Pi^{\pi^0(1)}_{\lambda_1\lambda_2\lambda_3\lambda_4}(q_1^2,q_2^2,q_3^2,q_4^2,s_1)\\
&+\Pi^{\pi^0(2)}_{\lambda_1\lambda_2\lambda_3\lambda_4}(q_1^2,q_2^2,q_3^2,q_4^2,s_2)\\
&+\Pi^{\pi^0(3)}_{\lambda_1\lambda_2\lambda_3\lambda_4}(q_1^2,q_2^2,q_3^2,q_4^2,s_3)
\end{aligned}\tag{5.12}$$

where we introduced notation

$$\begin{aligned}
\Pi^{\pi^0(1)}_{\lambda_1\lambda_2\lambda_3\lambda_4}(q_1^2,q_2^2,q_3^2,q_4^2,s_1)&=\frac{\mathcal{M}_{\lambda_1\lambda_2}(q_1^2,q_2^2,M^2)\mathcal{M}_{\lambda_3\lambda_4}(q_3^2,q_4^2,M^2)}{s_1-M^2}\\
&=\frac{\tilde{\Pi}^{\pi^0(1)}_{\lambda_1\lambda_2\lambda_3\lambda_4}(q_1^2,q_2^2,q_3^2,q_4^2,s_1)}{s_1-M^2},\\
\Pi^{\pi^0(2)}_{\lambda_1\lambda_2\lambda_3\lambda_4}(q_1^2,q_2^2,q_3^2,q_4^2,s_2)&=\frac{\mathcal{M}_{\lambda_1-\lambda_3}(q_1^2,q_3^2,M^2)\mathcal{M}_{\lambda_2-\lambda_4}(q_2^2,q_4^2,M^2)}{s_2-M^2}\\
&=\frac{\tilde{\Pi}^{\pi^0(2)}_{\lambda_1\lambda_2\lambda_3\lambda_4}(q_1^2,q_2^2,q_3^2,q_4^2,s_2)}{s_2-M^2},\\
\Pi^{\pi^0(3)}_{\lambda_1\lambda_2\lambda_3\lambda_4}(q_1^2,q_2^2,q_3^2,q_4^2,s_3)&=\frac{\mathcal{M}_{\lambda_1-\lambda_4}(q_1^2,q_4^2,M^2)\mathcal{M}_{\lambda_2-\lambda_3}(q_2^2,q_3^2,M^2)}{s_3-M^2}\\
&=\frac{\tilde{\Pi}^{\pi^0(3)}_{\lambda_1\lambda_2\lambda_3\lambda_4}(q_1^2,q_2^2,q_3^2,q_4^2,s_3)}{s_3-M^2}.
\end{aligned}\tag{5.13}$$

Subsequently, the structure of the form factors is defined by the C-odd intermediate hadronic states which contribute to the corner (single-photon) discontinuities. Although the lowest threshold in the C-odd channel corresponds to two-pion production we will consider a simplified picture for this channel where we take into account only the lowest resonant part of the vector-isovector spectrum. Moreover, we assume it to be an exchange of a stable isovector state. This can be conformed with a single pole of the on-shell meson form factor in the complex planes of photons' virtualities q_1^2 and q_2^2 located at Λ^2 (the monopole mass parameter). Physically, it corresponds to the effect of photon hadronization, or conversion of the photon to a vector (e.g. ρ meson) state. The chosen structure of the form factor is motivated by the presently available phenomenological description. Furthermore, it is closely connected to the VMD model for meson form factors widely used in previous calculations and allows direct comparison with the

[4]For the cases of higher-spin meson exchanges or multi-meson intermediate states it can be done separately for each partial wave.

latter. Similarly to the case of the C-even channel the isovector-pole contribution to the meson form factor gives rise to

$$F_{P\gamma^*\gamma^*}\left(q_1^2, q_2^2, M^2\right) = F_{P\gamma^*\gamma^*}\left(0, 0, M^2\right) \frac{1}{1 - q_1^2/\Lambda^2} \frac{1}{1 - q_2^2/\Lambda^2} \tag{5.14}$$

with the residue defined by the normalization in the limit of quasi-real photons

$$|F_{P\gamma^*\gamma^*}(0, 0, M^2)|^2 = \frac{4\Gamma_{\gamma\gamma}}{\pi\alpha^2 M^3}. \tag{5.15}$$

The generalization to include the non-resonant part of the $\gamma^* \to X$ spectrum is also possible in our approach and in fact, is the next step together with including of the C-even $\gamma\gamma \to \pi^+\pi^-$ channel. In practice, the account of multi-particle inelastic thresholds is rather involved technically, due to the multi-particle phase space integration and a complicated structure of the LbL scattering matrix element. The contribution of two-pion intermediate states to the LbL matrix element has been recently discussed in detail in [154].

Among the C-odd singularities, there is also the isovector pole in the external photon virtuality $k^2 = \Lambda^2$. To minimize the efforts we will calculate the vertex multiplied by $k^2/\Lambda^2 - 1$, which rids us from the before mentioned singularity. In other words we re-define the vertex as

$$\Gamma_\mu \to (k^2/\Lambda^2 - 1)\Gamma_\mu. \tag{5.16}$$

From one side, calculations shows that the discontinuity of the vertex Γ decreases faster than $1/t$. Thus, the before mentioned modification does not threaten the convergence of the dispersion integral, where it is additionally suppressed by another factor $1/t$. From the other side, in the limit of $k \to 0$ the modified vertex coincides with Γ and gives the same value of the projection on $F_2(0)$.

The discussed analytical structure may be graphically represented by diagrams in Fig. 5.5 where the dashed line represents the exchanged meson pole and the double solid line stands for the resonant part of the isovector spectrum (i.e. exchange of a ρ-meson pole). The three diagrams originate from the contributions of the three terms $\Pi^{\pi^0(i)}$ in Eq. (5.12). The discontinuities of the corresponding amplitudes can now be easily computed by exploiting Eq. (5.6). Due to symmetry the first two diagrams in Fig. 5.5 give identical contributions. Hence, we will explicitly compute the contributions of the second and the third graphs.

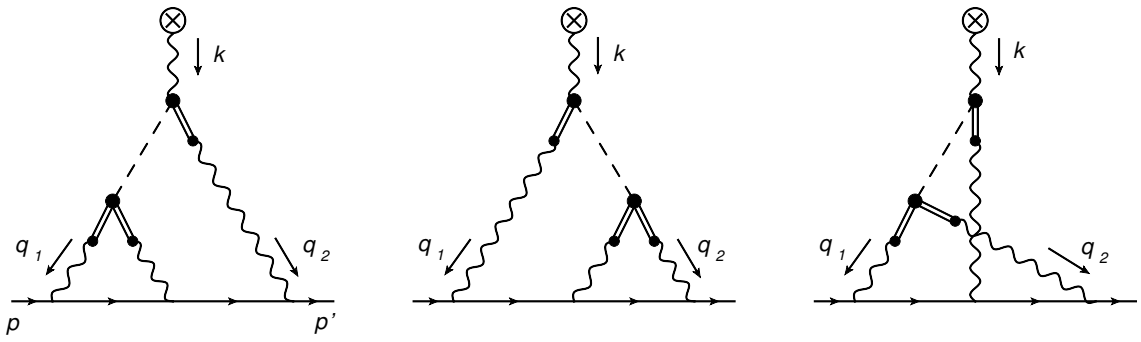

Figure 5.5: The meson-pole contributions to the hadronic light-by-light scattering in $(g-2)_\mu$.

The contribution to the vertex function in Eq. (5.2) corresponding with the second diagram

in Fig. 5.5 may be defined as

$$\begin{aligned}\Gamma_{1\rho}(k^2) = -e^6|F_{P\gamma^*\gamma^*}(0,0,M^2)|^2 \int \frac{\mathrm{d}^4q_1}{(2\pi)^4}\int \frac{\mathrm{d}^4q_2}{(2\pi)^4}\frac{1}{q_1^2}\frac{1}{q_2^2}\frac{1}{(k-q_1-q_2)^2}\frac{1}{(k-q_1)^2-M^2}\\ \times \gamma^\lambda(\not p+\not k-\not q_2+m)\gamma^\nu(\not p+\not q_1+m)\gamma^\mu\frac{1}{(p+q_1)^2-m^2}\frac{1}{(p+k-q_2)^2-m^2}\\ \times \varepsilon_{\mu\rho\alpha\beta}q_1^\alpha k^\beta\varepsilon_{\nu\lambda\gamma\delta}(k-q_1-q_2)^\gamma q_2^\delta\frac{1}{q_1^2/\Lambda^2-1}\frac{1}{q_2^2/\Lambda^2-1}\frac{1}{(k-q_1-q_2)^2/\Lambda^2-1}\end{aligned} \tag{5.17}$$

whereas the third diagram gives rise to

$$\begin{aligned}\Gamma_{2\rho}(k^2) = -e^6|F_{P\gamma^*\gamma^*}(0,0,M^2)|^2 \int \frac{\mathrm{d}^4q_1}{(2\pi)^4}\int \frac{\mathrm{d}^4q_2}{(2\pi)^4}\frac{1}{q_1^2}\frac{1}{q_2^2}\frac{1}{(k-q_1-q_2)^2}\frac{1}{(q_1+q_2)^2-M^2}\\ \times \gamma^\lambda(\not p+\not k-\not q_2+m)\gamma^\nu(\not p+\not q_1+m)\gamma^\mu\frac{1}{(p+q_1)^2-m^2}\frac{1}{(p+k-q_2)^2-m^2}\\ \times \varepsilon_{\mu\rho\alpha\beta}(k-q_1-q_2)^\alpha k^\beta\varepsilon_{\nu\lambda\gamma\delta}q_1^\gamma q_2^\delta\frac{1}{(k-q_1-q_2)^2/\Lambda^2-1}\frac{1}{q_1^2/\Lambda^2-1}\frac{1}{q_2^2/\Lambda^2-1}\end{aligned} \tag{5.18}$$

Exploiting Eq. (5.2) we can define the corresponding contributions to the Pauli form factor as

$$\begin{aligned}F_2^{(1)}(t) = e^6\Lambda^6 F_{P\gamma^*\gamma^*}(0,0,M^2)\int \frac{\mathrm{d}^4q_1}{(2\pi)^4}\int \frac{\mathrm{d}^4q_2}{(2\pi)^4}\\ \times \frac{1}{q_1^2}\frac{1}{q_1^2-\Lambda^2}\frac{1}{q_2^2}\frac{1}{q_2^2-\Lambda^2}\frac{1}{(k-q_1-q_2)^2}\frac{1}{(k-q_1-q_2)^2}\frac{1}{(k-q_1-q_2)^2-\Lambda^2}\\ \times \frac{1}{(p+q_1)^2-m^2}\frac{1}{(p+k-q_2)^2-m^2}\frac{1}{(k-q_1)^2-M^2}T_1(q_1,q_2,p,k),\end{aligned} \tag{5.19}$$

for the first topology and

$$\begin{aligned}F_2^{(2)}(t) = e^6\Lambda^6 F_{P\gamma^*\gamma^*}(0,0,M^2)\int \frac{\mathrm{d}^4q_1}{(2\pi)^4}\int \frac{\mathrm{d}^4q_2}{(2\pi)^4}\\ \times \frac{1}{q_1^2}\frac{1}{q_1^2-\Lambda^2}\frac{1}{q_2^2}\frac{1}{q_2^2-\Lambda^2}\frac{1}{(k-q_1-q_2)^2}\frac{1}{(k-q_1-q_2)^2}\frac{1}{(k-q_1-q_2)^2-\Lambda^2}\\ \times \frac{1}{(p+q_1)^2-m^2}\frac{1}{(p+k-q_2)^2-m^2}\frac{1}{(q_1+q_2)^2-M^2}T_2(q_1,q_2,p,k),\end{aligned} \tag{5.20}$$

for the second topology. Here we introduce notation

$$\begin{aligned}T_1(q_1,q_2,p,k) = \mathrm{Tr}\left[(\not p+\not k+m)\Lambda_\rho(p+k,p)(\not p+m)\gamma^\lambda(\not p+\not k-\not q_2+m)\gamma^\nu(\not p+\not q_1+m)\gamma^\mu\right]\\ \times \varepsilon_{\mu\rho\alpha\beta}q_1^\alpha(-k)^\beta\varepsilon_{\nu\lambda\gamma\delta}(k-q_1-q_2)^\gamma q_2^\delta.\end{aligned} \tag{5.21}$$

and

$$\begin{aligned}T_2(q_1,q_2,p,k) = \mathrm{Tr}\left[(\not p+\not k+m)\Lambda_\rho(p+k,p)(\not p+m)\gamma^\lambda(\not p+\not k-\not q_2+m)\gamma^\nu(\not p+\not q_1+m)\gamma^\mu\right]\\ \times \varepsilon_{\mu\rho\alpha\beta}(k-q_1-q_2)^\alpha(-k)^\beta\varepsilon_{\nu\lambda\gamma\delta}q_1^\gamma q_2^\delta.\end{aligned} \tag{5.22}$$

Applying Cutkosky rules to the vertex functions in Eqs. (5.17, 5.18) we can compute their discontinuities and with the help of Eq. (5.4) evaluate the corresponding contribution to the

anomalous magnetic moment. From Fig. 5.5 as well as Eqs. (5.17, 5.18) we can see that in this case the discontinuity originates from two- and three-body cuts. The two-particle cuts include the ones with $\pi^0\gamma$ and $\pi^0\rho$ intermediate states. In total there are four cut diagrams, two for each topology. They are depicted in Fig. 5.6. The full two-particle discontinuity is obtained by the sum of contributions from two cuts:

$$\text{Disc}^{(2)}\Gamma_i^\rho(t) = \text{Disc}_{\pi^0\gamma}\Gamma_i^\rho(t) + \text{Disc}_{\pi^0\rho}\Gamma_i^\rho(t) \tag{5.23}$$

The three-particle cuts include one of each 3γ and 3ρ and two of each $2\gamma\rho$ and $2\rho\gamma$, in total 8 different cut diagrams for each topology. They may be explicitly represented as shown in Figs. 5.7, 5.8. In addition, there is one cut diagram corresponding with the $2\mu\pi$ discontinuity for the second topology, see Fig. 5.9.

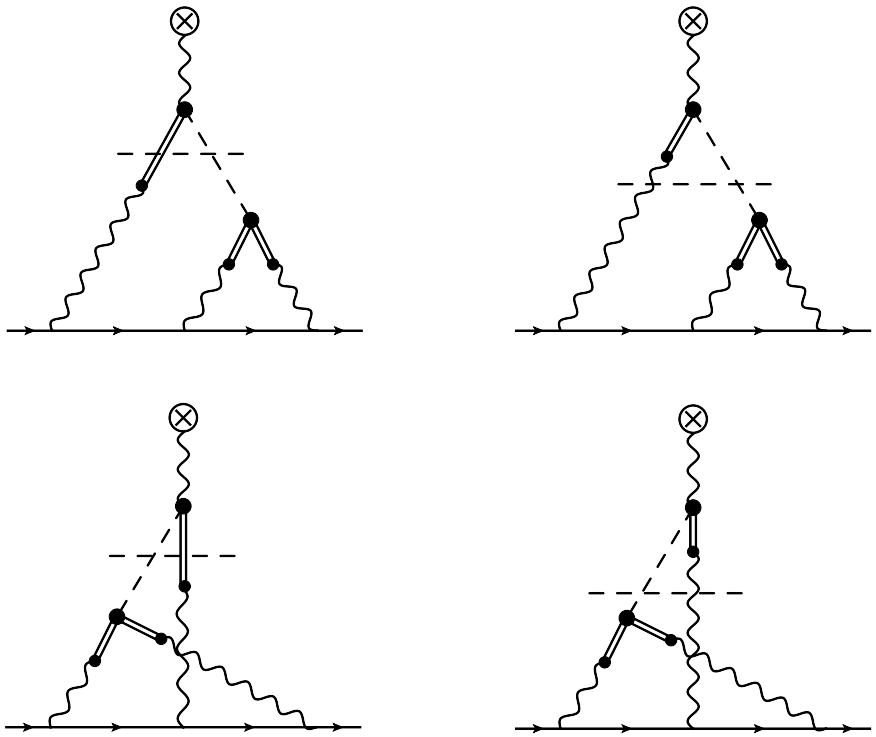

Figure 5.6: The two-body cuts of the second and the third diagrams in Fig. 4.4.

Similarly to the two-particle cut, the full three-particle discontinuity is obtained by the sum of contributions from all cuts. For the first diagram it is

$$\begin{aligned}\text{Disc}^{(3)}\Gamma_1^\rho(t) = \text{Disc}_{\gamma\gamma\gamma}\Gamma_1^\rho(t) + \text{Disc}_{\gamma\gamma\rho}\Gamma_1^\rho(t) + \text{Disc}_{\gamma\rho\gamma}\Gamma_1^\rho(t)\\ +\text{Disc}_{\rho\gamma\gamma}\Gamma_1^\rho(t) + \text{Disc}_{\gamma\rho\rho}\Gamma_1^\rho(t) + \text{Disc}_{\rho\gamma\rho}\Gamma_1^\rho(t)\\ + \text{Disc}_{\rho\rho\gamma}\Gamma_1^\rho(t) + \text{Disc}_{\rho\rho\rho}\Gamma_1^\rho(t).\end{aligned} \tag{5.24}$$

and for the second topology

$$\begin{aligned}\text{Disc}^{(3)}\Gamma_2^\rho(t) = \text{Disc}_{\gamma\gamma\gamma}\Gamma_2^\rho(t) + \text{Disc}_{\gamma\gamma\rho}\Gamma_2^\rho(t) + \text{Disc}_{\gamma\rho\gamma}\Gamma_2^\rho(t)\\ +\text{Disc}_{\rho\gamma\gamma}\Gamma_2^\rho(t) + \text{Disc}_{\gamma\rho\rho}\Gamma_2^\rho(t) + \text{Disc}_{\rho\gamma\rho}\Gamma_2^\rho(t)\\ +\text{Disc}_{\rho\rho\gamma}\Gamma_2^\rho(t) + \text{Disc}_{\rho\rho\rho}\Gamma_2^\rho(t) + \text{Disc}_{\mu\mu\pi}\Gamma_2^\rho(t).\end{aligned} \tag{5.25}$$

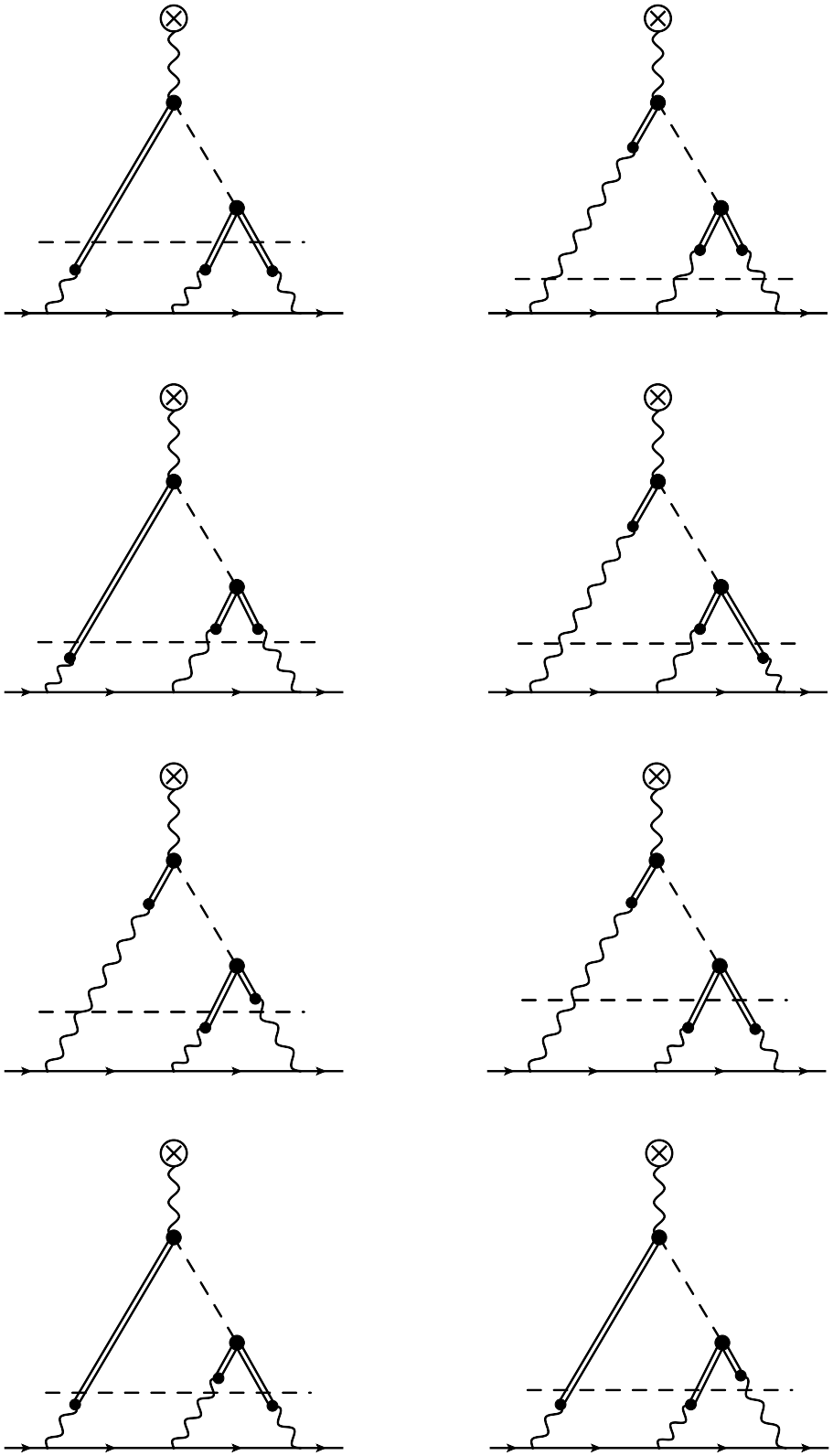

Figure 5.7: The three-body cuts of the second diagram in Fig. 4.4.

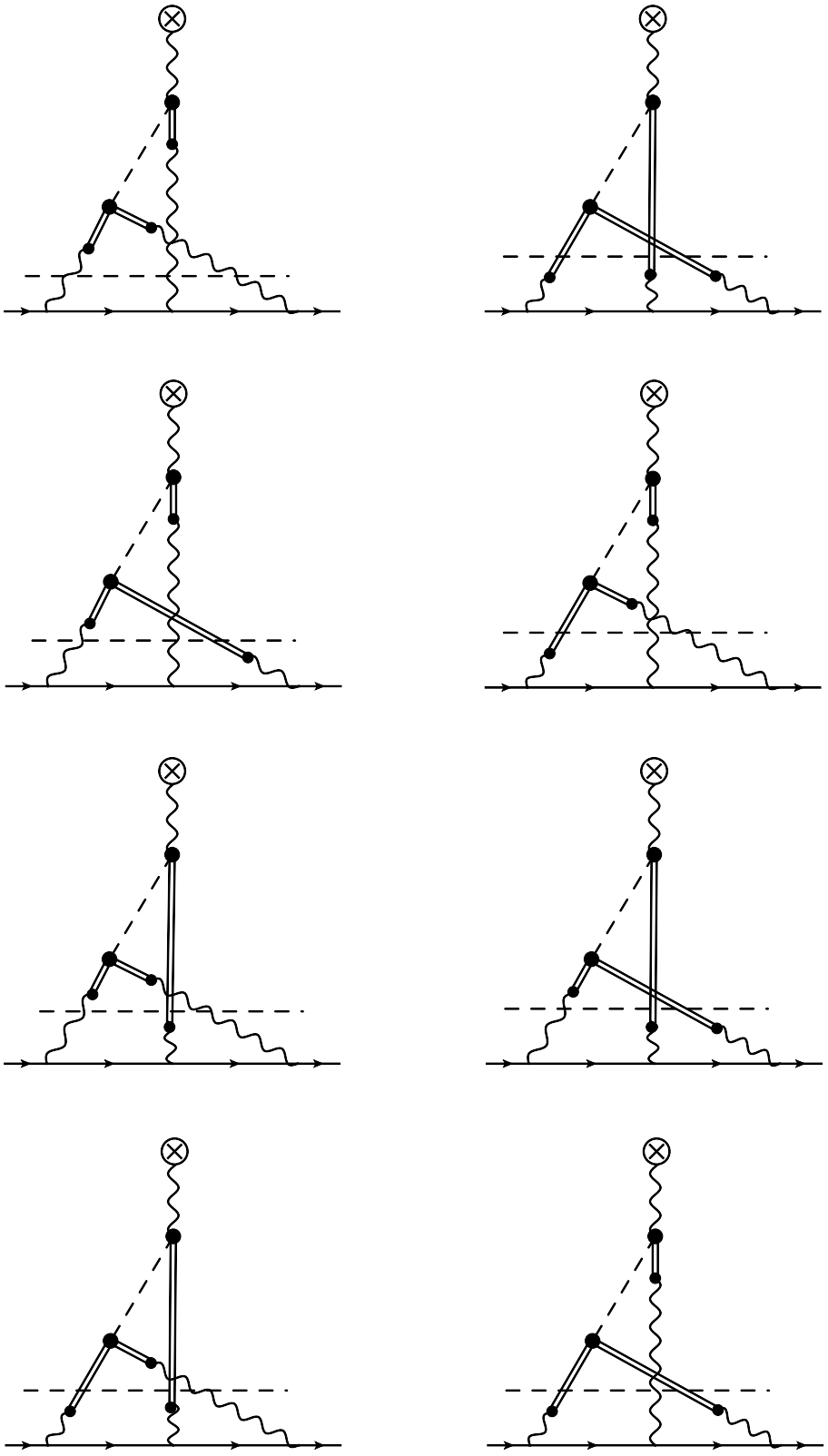

Figure 5.8: The three-body cuts of the third diagram in Fig. 4.4.

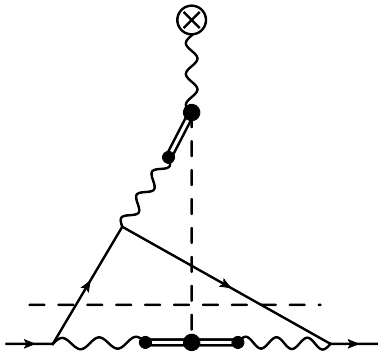

Figure 5.9: The muonic three-body cut of the third diagram in Fig. 4.4.

Using the projection technique and Eq. (5.6) one can explicitly define the corresponding contributions to the discontinuity of the Pauli form factor. For instance, the $\pi^0\gamma$ cut for the first topology contributes to the discontinuity as

$$\begin{aligned}\mathrm{Disc}_{\pi^0\gamma}F_2^{(1)}(t) = e^6\Lambda^6 F_{P\gamma^*\gamma^*}(0,0,M^2)\int\frac{\mathrm{d}^4q_1}{(2\pi)^4}\int\frac{\mathrm{d}^4q_2}{(2\pi)^4}\delta((k-q_1)^2-M^2)\delta(q_1^2)\\ \times\frac{1}{q_1^2-\Lambda^2}\frac{1}{q_2^2}\frac{1}{q_2^2-\Lambda^2}\frac{1}{(k-q_1-q_2)^2}\frac{1}{(k-q_1-q_2)^2-\Lambda^2}\\ \times\frac{1}{(p+q_1)^2-m^2}\frac{1}{(p+k-q_2)^2-m^2}T_1(q_1,q_2,p,k).\end{aligned} \tag{5.26}$$

In practice, it turns out that it is more convenient to perform the calculation in a slightly different way. One can notice that the used parametrization of the form factors allows to simplify the integrand using rational fraction decomposition, e.g.

$$\frac{1}{q_1^2}\frac{1}{q_1^2-\Lambda^2} = \frac{1}{\Lambda^2}\left(\frac{1}{q_1^2-\Lambda^2}-\frac{1}{q_1^2}\right)$$

As a result, the expression for the Pauli form factor in Eqs. (5.19, 5.20) may be transformed into a simpler form. For the contribution of the first topology:

$$\begin{aligned}F_2^{(1)}(t) = e^6\Lambda^6|F(0,0,M^2)|^2\int\frac{\mathrm{d}^4q_1}{(2\pi)^4}\frac{1}{(p+q_1)^2-m^2}\frac{1}{(k-q_1)^2-M^2}\\ \times\left(\frac{1}{q_1^2-\Lambda^2}-\frac{1}{q_1^2}\right)\left(S_3^{\Lambda\Lambda}-S_3^{\Lambda 0}-S_3^{0\Lambda}+S_3^{00}\right),\end{aligned} \tag{5.27}$$

Regarding the second topology it is convenient to make a change of variables for the momenta $q_1 \leftrightarrow k-q_1-q_2$. As a result, we can write

$$\begin{aligned}F_2^{(2)}(t) = e^6\Lambda^6|F(0,0,M^2)|^2\int\frac{\mathrm{d}^4q_1}{(2\pi)^4}\frac{1}{(k-q_1)^2-M^2}\\ \times\left(\frac{1}{q_1^2-\Lambda^2}-\frac{1}{q_1^2}\right)\left(S_4^{\Lambda\Lambda}-S_4^{\Lambda 0}-S_4^{0\Lambda}+S_4^{00}\right).\end{aligned} \tag{5.28}$$

In the latter equations we explicitly isolated the one-loop integrals

$$iS_3^{\Lambda_2\Lambda_3}((p+q_1)^2,p^2,(k-q_1)^2) = \int\frac{\mathrm{d}^4q_2}{(2\pi)^4}\frac{T_1(q_1,q_2,p,k)}{\left[q_2^2-\Lambda_3^2\right]\left[(k-q_1-q_2)^2-\Lambda_2^2\right]\left[(p-q_2+k)^2-m^2\right]} \tag{5.29}$$

and

$$iS_4^{\Lambda_1\Lambda_2}\left((p+q_1)^2,k^2,q_1^2,(k-q_1)^2,p^2,(p+k)^2\right)=\int\frac{\mathrm{d}^4q_2}{(2\pi)^4}\frac{1}{\left[(k-q_1-q_2)^2-\Lambda_1^2\right]\left[q_2^2-\Lambda_2^2\right]}\times\frac{T_2(k-q_1-q_2,q_2,p,k)}{\left[(p+k-q_1-q_2)^2-m_1^2\right]\left[(p+k-q_2)^2-m_2^2\right]}. \tag{5.30}$$

Finally, we can write

$$F_2^{(i)}(t)=F_i^{\Lambda\Lambda\Lambda}(t)-F_i^{\Lambda\Lambda 0}(t)-F_i^{\Lambda 0\Lambda}(t)+F_i^{\Lambda 00}(t)-F_i^{0\Lambda\Lambda}(t)+F_i^{0\Lambda 0}(t)+F_i^{00\Lambda}(t)-F_i^{000}(t) \tag{5.31}$$

where

$$F_1^{\Lambda_1\Lambda_2\Lambda_3}(t)=e^6|F(0,0,M^2)|^2\int\frac{\mathrm{d}^4q_1}{(2\pi)^4}\frac{1}{(p+q_1)^2-m^2}\frac{1}{(k-q_1)^2-M^2}\frac{1}{q_1^2-\Lambda_1^2}S_3^{\Lambda_2\Lambda_3} \tag{5.32}$$

and

$$F_2^{\Lambda_1\Lambda_2\Lambda_3}(t)=e^6|F(0,0,M^2)|^2\int\frac{\mathrm{d}^4q_1}{(2\pi)^4}\frac{1}{(k-q_1)^2-M^2}\frac{1}{q_1^2-\Lambda_1^2}S_4^{\Lambda_2\Lambda_3}. \tag{5.33}$$

For each of Eqs. (5.32, 5.33) the dispersion integral is divergent by itself as it would be in the case with constant form factors, for instance. However the sum of all eight terms is convergent as the divergent terms in each of the dispersion integrals are not dependent on masses Λ_i. One can do the evaluation regularizing the integral over t by a cutoff and keeping in mind that the integrals over infinite contour for both terms are the same and cancel each other, thus the resulting sum is finite and definite.

The dispersive computation of the two-loop integrals in Eqs. (5.32, 5.33) can be illustratively demonstrated on the example of the evaluation of two-loop scalar functions. In fact, the latter possess the same analytical structure and can be straightforwardly generalized to the case of interest.

5.2 Two-loop scalar vertex functions

In this section we will calculate the two-loop scalar graphs depicted in Fig. 5.10. This calculation is relevant for the computation of the single meson contribution to the HLbL correction in $(g-2)_\mu$ as the diagrams appearing there are topologically similar to the ones considered in this section. In the latter the tensor loop integrals can be decomposed in a sum of scalar integrals among which also those appear which correspond to a scalar ϕ^3 theory. Since in the above decomposition the considered type of integrals have the maximum number of propagators (here six) they are the most difficult ones to compute and therefore we present their calculation here. The remaining integrals which contain less propagators than those given by the diagrams in Fig. 5.10 are easier to compute and can be calculated in the analogous way. We will discuss the general case where the scalars corresponding to photons have all different masses (motivated by the integrals which appear when using monopole form factors for the $M\gamma^*\gamma^*$ vertex in the HLbL contribution $(g-2)_\mu$).

The scalar two-loop amplitude corresponding with the first diagram in Fig. 5.10 can be written as

$$\Gamma_1(t)=\int\frac{\mathrm{d}^4q_1}{(2\pi)^4}\int\frac{\mathrm{d}^4q_2}{(2\pi)^4}\frac{1}{(k-q_1-q_2)^2-\Lambda_3^2}\frac{1}{q_1^2-\Lambda_1^2}\frac{1}{q_2^2-\Lambda_2^2}\frac{1}{(k-q_1)^2-M^2}\times\frac{1}{(p+q_1)^2-m_1^2}\frac{1}{(p+k-q_2)^2-m_2^2}. \tag{5.34}$$

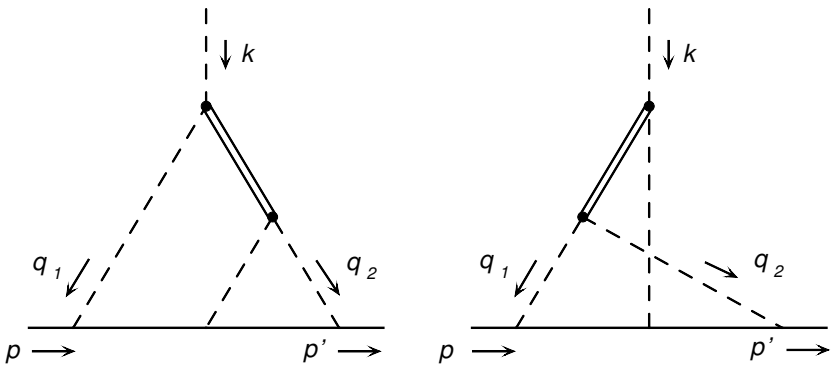

Figure 5.10: Two-loop vertex corrections in a scalar theory. Here the following code for the masses of the scalar propagators is used: the double line denotes the (meson) propagator with mass M, the solid lines denote (lepton) propagators with masses m_1 and m_2 and the dashed lines denote (photon) propagators with masses Λ_1, Λ_2 and Λ_3 (from left to right).

The second diagram corresponds to amplitude

$$\Gamma_2(t) = \int \frac{\mathrm{d}^4 q_1}{(2\pi)^4} \int \frac{\mathrm{d}^4 q_2}{(2\pi)^4} \frac{1}{(k-q_1-q_2)^2-\Lambda_3^2} \frac{1}{q_1^2-\Lambda_1^2} \frac{1}{q_2^2-\Lambda_2^2} \frac{1}{(q_1+q_2)^2-M^2} \times \frac{1}{(p+q_1)^2-m_1^2} \frac{1}{(p+k-q_2)^2-m_2^2}. \tag{5.35}$$

5.2.1 Angular parametrization and integration of the phase space

The scalar two-loop integrals can be represented in a convenient way using a special set of variables. The choice of variables is based on the initial form of the integrand: the non-perturbative vacuum polarization part is dependent only on invariants and the angular integral is reduced to the integration over one polar and azimuthal angle. The same type of the angular integral we meet when integrating the three-particle phase space. It can be evaluated analytically and expressed in a closed form. In this section we discuss the technical details of the angular integration.

The most important ingredient of the dispersion method is the calculation of the angular part of the two- and three-particle phase-space integrals. The loop and external momenta can be defined in terms of the angular coordinates and a set of invariant energy parameters t, t_1, t_2, t_{12} and the invariant masses of virtual photons q_1^2 and q_2^2. In the k-rest frame we define the momenta as

$$\begin{aligned}
k &= \left(\sqrt{t}, 0, 0, 0\right), \\
p &= \frac{\sqrt{t}}{2}\left(-1, 0, 0, \beta\right), \\
q_1 &= \frac{\sqrt{t}}{2}\beta_1 \left(\frac{t-t_1+q_1^2}{t\beta_1}, \sin\theta_1, 0, \cos\theta_1\right), \\
q_2 &= \frac{\sqrt{t}}{2}\beta_2 \left(\frac{t-t_2+q_2^2}{t\beta_2}, -\cos\theta_1\cos\theta_2\sin\theta + \sin\theta_1\cos\theta, \right. \\
&\qquad \left. \sin\theta\sin\theta_2, \sin\theta_1\cos\theta_2\sin\theta + \cos\theta_1\cos\theta\right), \\
\cos\theta &= \frac{2t(q_1^2+q_2^2-t_{12}) + (t-t_1+q_1^2)(t-t_2+q_2^2)}{t^2\beta_1\beta_2}.
\end{aligned} \tag{5.36}$$

with

$$\beta_i = \sqrt{\left(1 + \frac{q_i^2 - t_i}{t}\right)^2 - \frac{4q_i^2}{t}} \quad \text{and} \quad \beta = \sqrt{1 - \frac{4m^2}{t}}. \tag{5.37}$$

This angular parametrization is explained by Fig.(5.11). The space direction of the momentum q_2 is defined with respect to q_1, by a polar angle θ between $\vec{q}_1$ and $\vec{q}_2$ and azimuthal angle θ_2. Such a definition allows to factorize the two-loop expression and to express the angular integral in a closed form.

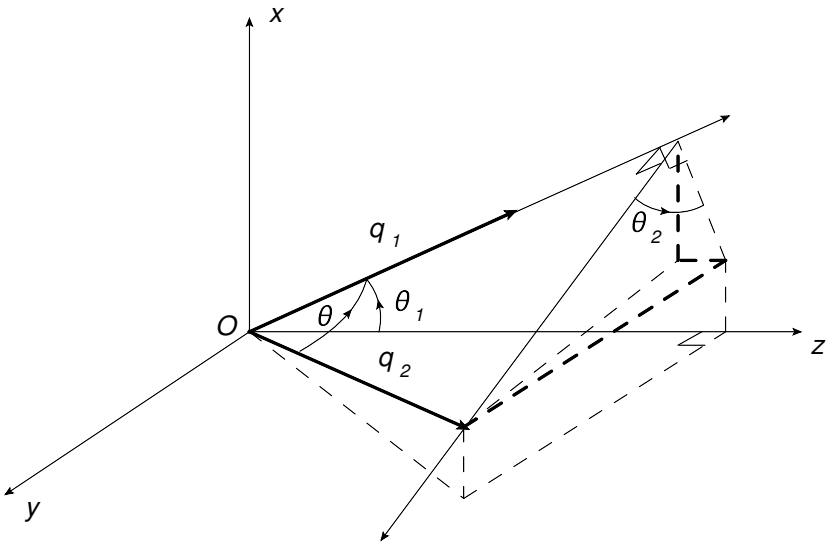

Figure 5.11: The angular coordinates in the one- and two-loop phase space integral.

The invariants which appear in the calculation are related to the introduced parameters as

$$\begin{aligned}
p^2 = p'^2 &= m^2, \\
(k - q_1)^2 &= t_1, \\
(k - q_2)^2 &= t_2, \\
(q_1 + q_2)^2 &= t_{12}, \\
(p + q_1)^2 &= \frac{1}{2}\left[2m^2 + q_1^2 + t_1 - t - t\beta_1\beta\cos\theta_1\right], \\
(p + k - q_1)^2 &= \frac{1}{2}\left[2m^2 + q_1^2 + t_1 - t + t\beta_1\beta\cos\theta_1\right], \\
(p + k - q_2)^2 &= \frac{1}{2}\left[2m^2 + q_2^2 - t + t_2 + t\beta_2\beta(\sin\theta_1\cos\theta_2\sin\theta + \cos\theta_1\cos\theta)\right], \\
(k - q_1 - q_2)^2 &= t_{12} + t_1 + t_2 - t - q_1^2 - q_2^2,
\end{aligned} \tag{5.38}$$

Using the above definitions the transformation of the phase-space integration measure is given by

$$\int \mathrm{d}^4 q_1 = \int \mathrm{d}q_1^2 \int \mathrm{d}t_1 \int_0^\pi \mathrm{d}\cos\theta_1 \int \mathrm{d}\phi \, \frac{\beta_1}{8}, \tag{5.39}$$

$$\int \mathrm{d}^4 q_2 = \int \mathrm{d}q_2^2 \int \mathrm{d}t_2 \int \mathrm{d}t_{12} \int \mathrm{d}\theta_2 \, \frac{1}{4\beta_1 t} \tag{5.40}$$

where the integration domains are explicitly defined by kinematic constraints for each of two- and three-particle cuts separately. Using the introduced parametrization the loop integrals in Eqs. (5.62, 5.35) can be represented as

$$\begin{aligned}\Gamma_1(t) =& \frac{4}{(4\pi)^7 t}\int \mathrm{d}q_1^2 \int \mathrm{d}q_2^2 \int \mathrm{d}t_1 \int \mathrm{d}t_2 \int \mathrm{d}t_{12} \frac{1}{t_{12}+t_1+t_2-t-q_1^2-q_2^2-\Lambda_3^2} \\ &\times \frac{1}{q_1^2-\Lambda_1^2}\frac{1}{q_2^2-\Lambda_2^2}\frac{1}{t_1-M^2}\Omega(t_1,t_2,t_{12},q_1^2,q_2^2,m_1^2,m_2^2),\end{aligned} \tag{5.41}$$

and

$$\begin{aligned}\Gamma_2(t) =& \frac{4}{(4\pi)^7 t}\int \mathrm{d}q_1^2 \int \mathrm{d}q_2^2 \int \mathrm{d}t_1 \int \mathrm{d}t_2 \int \mathrm{d}t_{12} \frac{1}{t_{12}+t_1+t_2-t-q_1^2-q_2^2-\Lambda_3^2} \\ &\times \frac{1}{q_1^2-\Lambda_1^2}\frac{1}{q_2^2-\Lambda_2^2}\frac{1}{t_{12}-M^2}\Omega(t_1,t_2,t_{12},q_1^2,q_2^2,m_1^2,m_2^2)\end{aligned} \tag{5.42}$$

where $\Omega(t_1,t_2,t_{12},q_1^2,q_2^2,m_1^2,m_2^2)$ is the angular integral defined by

$$\begin{aligned}\Omega(t_1,t_2,t_{12},q_1^2,q_2^2,m_1^2,m_2^2) =& \int_0^\pi \mathrm{d}\cos\theta_1 \int_0^{2\pi}\mathrm{d}\theta_2 \, \frac{2}{2m^2-2m_1^2+q_1^2+t_1-t-t\beta_1\beta\cos\theta_1} \\ &\times \frac{2}{2m^2-2m_2^2+q_2^2-t+t_2+t\beta_2\beta(\sin\theta_1\cos\theta_2\sin\theta+\cos\theta_1\cos\theta)}\end{aligned} \tag{5.43}$$

The angular integral Ω can be carried out analytically which yields to

$$\begin{aligned}\Omega(t_1,t_2,t_{12},q_1^2,q_2^2,m_1^2,m_2^2) =& -\frac{4}{\beta_1\beta_2\beta^2t^2}\frac{2\pi}{\sqrt{(a+b)^2-2ab(1+\cos\theta)-\sin^2\theta}} \\ &\times\left[\log\frac{a-1}{a+1}+\log\frac{(a+b)(1-b)-b(1+\cos\theta)+ab(1+\cos\theta)+\sin^2\theta+(\cos\theta+b)c}{-(a+b)(1+b)+b(1+\cos\theta)+ab(1+\cos\theta)+\sin^2\theta-(\cos\theta-b)c}\right]\end{aligned} \tag{5.44}$$

with

$$\begin{aligned}a &= -\frac{2m^2-2m_1^2+q_1^2-t+t_1}{t\beta_1\beta}, \\ b &= \frac{2m^2-2m_2^2+q_2^2-t+t_2}{t\beta_2\beta}, \\ c &= \sqrt{(a+b)^2-2ab(1+\cos\theta)-\sin^2\theta}.\end{aligned} \tag{5.45}$$

The details of the computation are given in the Appendix F.

5.2.2 Discontinuity of the vertex function

Applying the Cutkosky rules to the graphs in Fig. 5.10 we can now calculate the absorptive parts which are represented by the cut diagrams in Figs. 5.12, 5.14. The diagrams can be divided into two-particle and three-particle cut graphs.

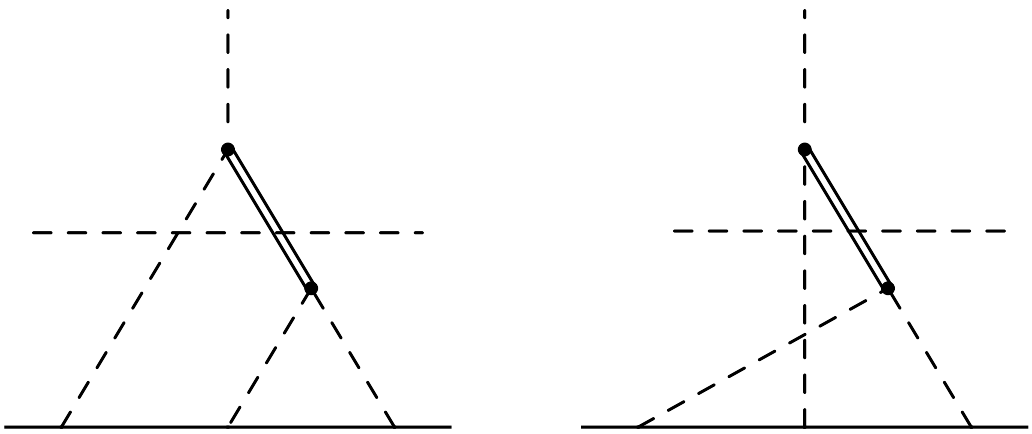

Figure 5.12: The two-particle cuts belonging to the corner vertex three-point functions presented by diagrams in Fig. 5.10.

Two-particle cuts.

The first set contains the one-loop virtual diagram insertions which are represented by the vertex and crossed-box graphs given in Fig. 5.13.

With the right choice of the loop momenta the triangle correction in the first diagram and the crossed-box correction in the second diagram can be isolated as closed integrals. The absorptive part corresponding to the left two-particle cut graph in Fig. 5.12 can be expressed in the form:

$$\begin{aligned}\mathrm{Disc}_{\mathrm{t}}^2\Gamma_1(t) = \int \frac{\mathrm{d}^4q_1}{(2\pi)^4}(2\pi i)^2\delta(q_1^2-\Lambda_1^2)\delta((k-q_1)^2-M^2) \\ \times \frac{1}{(p+q_1)^2-m_1^2}M_3\left((k-q_1^2),(p+q_1)^2,m^2\right).\end{aligned} \tag{5.46}$$

To isolate the one-loop function in a closed form in the right two-particle cut diagram in Fig. 5.12 we relabel momenta as $q_1 \leftrightarrow k-q_1-q_2$. Hence, the discontinuity has form

$$\begin{aligned}\mathrm{Disc}_{\mathrm{t}}^2\Gamma_2(t) = \int \frac{\mathrm{d}^4q_1}{(2\pi)^4}(2\pi i)^2\delta((q_1^2-\Lambda_3^2)\delta((k-q_1)^2-M^2) \\ \times M_4\left((k-q_2)^2,(p+q_1)^2,(k-q_1)^2,q_1^2,m^2,m^2\right).\end{aligned} \tag{5.47}$$

Using the above definitions the two- and three-particle cuts may be reformulated in a compact form. For the two-particle cuts we have

$$\mathrm{Disc}_t^2\Gamma_1(t) = \frac{1}{8\pi}\int \mathrm{d}\cos\theta_1 \frac{\beta_1 M_3(M^2, m^2+q_1^2/2+t_1/2-t/2-t/2\beta_1\beta\cos\theta_1, m^2)}{2m^2-2m_1^2+q_1^2+t_1-t-t\beta_1\beta\cos\theta_1} \tag{5.48}$$

and

$$\mathrm{Disc}_t^2\Gamma_2(t) = \frac{1}{16\pi}\int \mathrm{d}\cos\theta_1\ \beta_1 M_4\left(m^2+q_1^2/2+t_1/2-t/2-t/2\beta_1\beta\cos\theta_1, t, \Lambda_3^2, M^2, m^2, m^2\right). \tag{5.49}$$

where in Eq. 5.49 $q_1^2=\Lambda_3^3$ and $t_1=M^2$. The one-loop three- and four-point functions M_3 and M_4 (see Fig. 5.13) which enter the expressions for the above loop integrals can be thus presented as

$$M_3\left((k-q_1^2),(p+q_1)^2,m^2\right)=\int\frac{\mathrm{d}^4q_2}{(2\pi)^4}\frac{1}{q_2^2-\Lambda_2^2}\frac{1}{(k-q_1-q_2)^2-\Lambda_3^2}\frac{1}{(p+k-q_2)^2-m_2^2}, \tag{5.50}$$

$$\begin{aligned}M_4\left((p+q_1)^2,k^2,q_1^2,(k-q_1)^2,m^2,m^2\right)=&\int\frac{\mathrm{d}^4q_2}{(2\pi)^4}\frac{1}{(k-q_1-q_2)^2-\Lambda_1^2}\frac{1}{q_2^2-\Lambda_2^2}\\&\times\frac{1}{(p+k-q_1-q_2)^2-m_1^2}\frac{1}{(p+k-q_2)^2-m_2^2}.\end{aligned} \tag{5.51}$$

The above integrals belong to a class of one-loop integrals which were studied in quite detail starting with the original work of Ref. [155] (see also Ref. [156] for a review). The original approach is based on the Feynman parametrization which allows to regroup the propagators in a spherically symmetric form and to perform the momentum integral in the Euclidian space directly. The subsequent integration over Feynman parameters can be performed with the account of the analytical structure of the amplitudes. In regions of momentum space where no cuts occur the integrals are rather simple to perform. In principle, the rest can be obtained by analytical continuation, however in practice it is hard to realize. Therefore, it is more efficient to define the integral independently for different kinematical regions. The details of this approach are described in detail in Ref. [155].

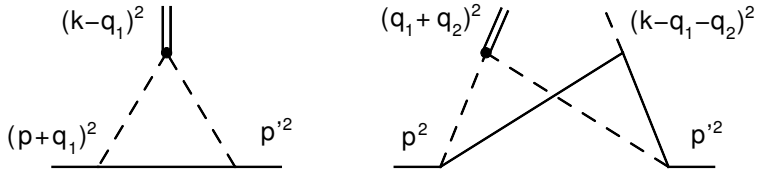

Figure 5.13: One-loop three- and four-point functions in a scalar theory.

A big disadvantage of this approach is a very narrow type of the parametrizations for the nPT functions which allow its application, basically limited to a pole and power parametrizations. It turns out that in this case the dispersion technique is very powerful because the absorptive parts from the two-particle cut can be expressed in a very simple form and is similar to the three-particle cut contribution. Furthermore, it turns out that the dispersion integral representation of the loop integral becomes extremely useful when considering the $(g-2)_\mu$ since it's application is not limited to the simplest pole parametrizations of the $\gamma\gamma\to X$ form factors.

Three-particle cuts.

The three-particle cut diagrams originating from the two diagrams in Fig. 5.10 are depicted in Fig. 5.10 below.

For the first three-particle cut in Fig. 5.14 we have:

$$\begin{aligned}\mathrm{Disc}_{\mathrm{t}}^3\Gamma_1(t)=\int\frac{\mathrm{d}^4q_1}{(2\pi)^4}\int\frac{\mathrm{d}^4q_2}{(2\pi)^4}(2\pi i)^3\delta(q_1^2-\Lambda_1^2)\delta(q_2^2-\Lambda_2^2)\delta((k-q_1-q_2)^2-\Lambda_3^2)\\\times\frac{1}{(k-q_1)^2-M^2}\frac{1}{(p+q_1)^2-m_1^2}\frac{1}{(p+k-q_2)^2-m_2^2}.\end{aligned} \tag{5.52}$$

It occurs that for the second diagram in Fig. 5.10, there are two three-particle cut diagrams which contribute to the discontinuity (see second row in Fig. 5.14). The first (three-photon)

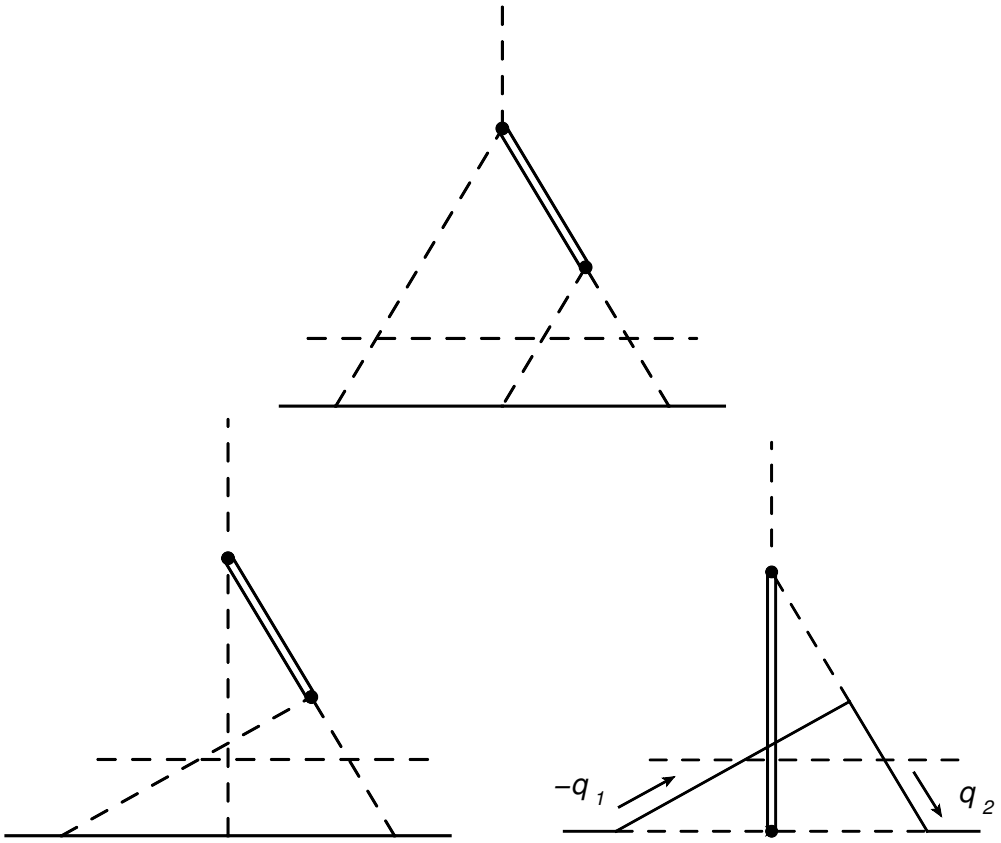

Figure 5.14: The three-particle cuts belonging to the corner vertex three-point functions presented by diagrams in Fig. 5.10. For the third diagram the momenta are relabeled as shown in figure.

cut contribution (left panel in the second row of Fig. 5.14) is given by

$$\begin{aligned}\mathrm{Disc}_{\mathrm{t}}^{3,1}\Gamma_2(t) = \int \frac{\mathrm{d}^4q_1}{(2\pi)^4}\int \frac{\mathrm{d}^4q_2}{(2\pi)^4}(2\pi i)^3\delta(q_1^2-\Lambda_1^2)\delta(q_2^2-\Lambda_2^2)\delta((k-q_1-q_2)^2-\Lambda_3^2)\\ \times \frac{1}{(q_1+q_2)^2-M^2}\frac{1}{(p+q_1)^2-m_1^2}\frac{1}{(p+k-q_2)^2-m_2^2},\end{aligned} \tag{5.53}$$

whereas the second (meson-lepton-lepton) cut contribution (right panel in the second row of Fig. 5.14) is given by

$$\begin{aligned}\mathrm{Disc}_{\mathrm{t}}^{3,2}\Gamma_2(t) = \int \frac{\mathrm{d}^4q_1}{(2\pi)^4}\int \frac{\mathrm{d}^4q_2}{(2\pi)^4}(2\pi i)^3\delta(q_1^2-m_1^2)\delta(q_2^2-m_2^2)\delta((k-q_1-q_2)^2-M^2)\\ \times \frac{1}{(q_1+q_2)^2-\Lambda_3^2}\frac{1}{(p+q_1)^2-\Lambda_1^2}\frac{1}{(p+k-q_2)^2-\Lambda_2^2}.\end{aligned} \tag{5.54}$$

The phase-space integrals in the discontinuities of Eqs. (5.46-5.54) may be partly performed analytically by introducing the angular parametrization. For the three-particle discontinuity in the first diagram defined by Eq. (5.52) we have

$$\begin{aligned}\mathrm{Disc}_{\mathrm{t}}\Gamma_1^{(3)}(t) =& \frac{4}{(4\pi)^3 t}\int \mathrm{d}t_1\int \mathrm{d}t_2\frac{1}{t_1-M^2}\\ &\times \Omega(t_1,t_2,t+\Lambda_1^2+\Lambda_2^2+\Lambda_3^2-t_1-t_2,\Lambda_1^2,\Lambda_2^2,m_1^2,m_2^2).\end{aligned} \tag{5.55}$$

For the discontinuities coming from the left three-particle cut diagram in the second row of Fig. 5.14 defined by Eq. (5.53) we can write

$$\begin{aligned}\mathrm{Disc_t}\Gamma_2^{(3,1)}(t) =& \frac{4}{(4\pi)^3 t}\int \mathrm{d}t_1 \int \mathrm{d}t_2 \frac{1}{t+\Lambda_1^2+\Lambda_2^2+\Lambda_3^2-t_1-t_2-M^2} \\ &\times \Omega(t_1,t_2,t+\Lambda_1^2+\Lambda_2^2+\Lambda_3^2-t_1-t_2,\Lambda_1^2,\Lambda_2^2,m_1^2,m_2^2).\end{aligned} \tag{5.56}$$

The integral over energy variables is performed over two-dimensional region defined by a two-dimensional diagram in Fig. 5.15. It is defined by inequalities

$$q_1^0 \geqslant \Lambda_1 \quad \Rightarrow \quad t_1 \leqslant (\sqrt{t}-\Lambda_1)^2, \tag{5.57}$$

$$q_2^0 \geqslant \Lambda_2 \quad \Rightarrow \quad t_2 \leqslant (\sqrt{t}-\Lambda_2)^2, \tag{5.58}$$

$$k^0 - q_1^0 - q_2^0 \geqslant \Lambda_3 \quad \Rightarrow \quad t_1+t_2 \geqslant 2\sqrt{t}\Lambda_3+\Lambda_1^2+\Lambda_2^2 \tag{5.59}$$

and

$$t_1 \geqslant (\Lambda_3+\Lambda_2)^2, \qquad t_2 \geqslant (\Lambda_1+\Lambda_3)^2. \tag{5.60}$$

An additional constrain is imposed by condition $-1 \leqslant \cos\theta \leqslant 1$ which results in

$$-1 \leqslant \frac{2t(q_1^2+q_2^2-t_{12})+(t-t_1+q_1^2)(t-t_2+q_2^2)}{t^2\beta_1\beta_2} \leqslant 1. \tag{5.61}$$

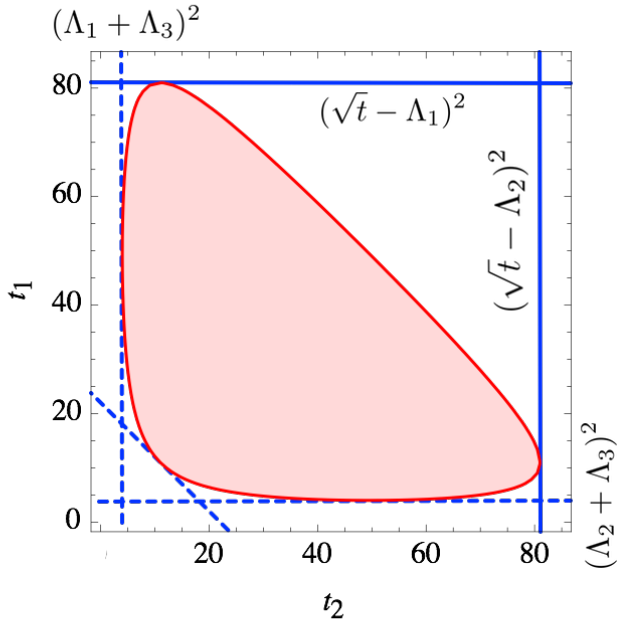

Figure 5.15: The integration domain for the three-particle cut. The blue dashed lines correspond to the conditions in Eq. (5.60); the solid blue line correspond to Eqs. (5.57, 5.58); the red curve represent condition $-1 \leqslant \cos\theta \leqslant 1$.

For the discontinuities coming from the right three-particle cut diagram in the second row of Fig. 5.14 the analogous expressions may be easily obtained by substitutions $m_1 \leftrightarrow \Lambda_1$, $m_2 \leftrightarrow \Lambda_2$, $M \leftrightarrow \Lambda_3$. As a result we obtain expression for the cut in Eq. (5.54):

$$\begin{aligned}\mathrm{Disc_t}\Gamma_2^{(3,2)}(t) =& \frac{4}{(4\pi)^3 t}\int \mathrm{d}t_1 \int \mathrm{d}t_2 \frac{1}{t+m_1^2+m_2^2+M^2-t_1-t_2-\Lambda_3^2} \\ &\times \Omega(t_1,t_2,t+m_1^2+m_2^2+M^2-t_1-t_2,m_1^2,m_2^2,\Lambda_1^2,\Lambda_2^2).\end{aligned} \tag{5.62}$$

5.2.3 Numerical results

We will start from a discussion of the imaginary parts of the two- and three-particle discontinuities. The sum of both should vanish as the full discontinuity has to be a purely imaginary function. The imaginary parts may be easily obtained by re-applying Cutkosky rules to the cut diagrams in Figs. 5.12 and 5.14. For the first diagram the imaginary part of the three-particle discontinuity is originating from the propagator $(t_1 - M^2 + i\varepsilon)^{-1}$; for the second diagram from propagators $(t_1 - M^2 + i\varepsilon)^{-1}$ and $(t_1 - \Lambda_2^2 + i\varepsilon)^{-1}$ for the first and the second cut respectively. The imaginary part of the two-particle discontinuity is coming from the two-particle cut of the triangle and box diagrams in Fig. 5.13. For the case of demonstration we will consider the mass configuration $\Lambda_1 = m$, $\Lambda_2 = 0$, $\Lambda_3 = 3m$ and $M = 3m$. The imaginary parts of the discontinuities are shown in Figs 5.16. We can see that the imaginary part starts exactly at the two-particle (meson-photon) thresholds $(\Lambda_1 + M)^2$ for the first diagram and $(\Lambda_3 + M)^2$ for the second. As is expected, for both topologies the imaginary parts of the two- and three-particle cuts are identical and have opposite signs.

The real parts of the discontinuities are shown on the plots in Figs. 5.17. We can clearly see that the real parts start at the corresponding two- and three-particle thresholds. In the case of the first diagram, it is $(\Lambda_1 + M)^2$ for the two-particle cut and $(\Lambda_1 + \Lambda_2 + \Lambda_3)^2$ for the three-particle cut. Regarding the second diagram, the two-particle cut starts at $(\Lambda_3 + M)^2$ and the three-particle cut start at $(\Lambda_1 + \Lambda_2 + \Lambda_3)^2$ and $(M + 2m)^2$ for the first (three-photon) and the second (meson-lepton-lepton) cuts respectively. We can observe clear spikes in the three-particle cuts exactly at the position where the two-particle cut starts. It corresponds to the opening of a new, two-particle (meson-photon) channel and is correlated with the threshold shown in Fig. 5.16.

Similarly to Eq. (5.4) the $F(0)$ can now be obtained directly by performing the dispersion integral

$$\Gamma(0) = \frac{1}{2\pi i}\int\limits_{(\Lambda_1+M)^2}^{\infty}\frac{\mathrm{d}t}{t}\,\mathrm{Disc}_{\mathrm{t}}^{(2)}\Gamma_1(t) + \frac{1}{2\pi i}\int\limits_{(\Lambda_3+M)^2}^{\infty}\frac{\mathrm{d}t}{t}\,\mathrm{Disc}_{\mathrm{t}}^{(2)}\Gamma_2(t) \tag{5.63}$$
$$+ \frac{1}{2\pi i}\int\limits_{(\Lambda_1+\Lambda_2+\Lambda_3)^2}^{\infty}\frac{\mathrm{d}t}{t}\,\Big[\mathrm{Disc}_{\mathrm{t}}^{(3)}\Gamma_1(t) + \mathrm{Disc}_{\mathrm{t}}^{(3,1)}\Gamma_2(t)\Big] + \frac{1}{2\pi i}\int\limits_{(2m+M)^2}^{\infty}\frac{\mathrm{d}t}{t}\,\mathrm{Disc}_{\mathrm{t}}^{(3,2)}\Gamma_2(t).$$

The dependence of the form factor on (meson) mass M is shown in Fig. 5.18. We can observe spikes in both two- and three-particle cuts located at $M = \Lambda_1 + \Lambda_3$ for the first diagram and $M = \Lambda_1 + \Lambda_2$ for the second. This kink can be attributed to the opening of the two-particle threshold when considering the one-loop diagrams depending on the virtuality t_1. Since in the dispersion evaluation we put the meson on its mass shell, i.e. $t_1 = M^2$ this effect is reflected in the dependencies of the contribution of two- and three-particle discontinuities on M. When performing the loop integral directly, the meson is not an external particle but rather virtual and this effect does not emerge. Practically, when applied to the anomalous moment calculation it means that for light hadronic states or for the states with mass $M \sim \Lambda,\ 2\Lambda$, with Λ a monopole mass parameter of the form factor parametrization, we need additional precision in the data input. We notice from Fig. 5.18 that the sum of two contributions exactly reproduces the dependence obtained by the direct evaluation of the loop integrals using the hyperspherical approach (see Appendix E).

We thus conclude that the developed dispersion technique can be applied to the calculation of the HLbL correction to $(g-2)_\mu$. In the subsequent section we will establish the general formalism and discuss particular features of the calculation.

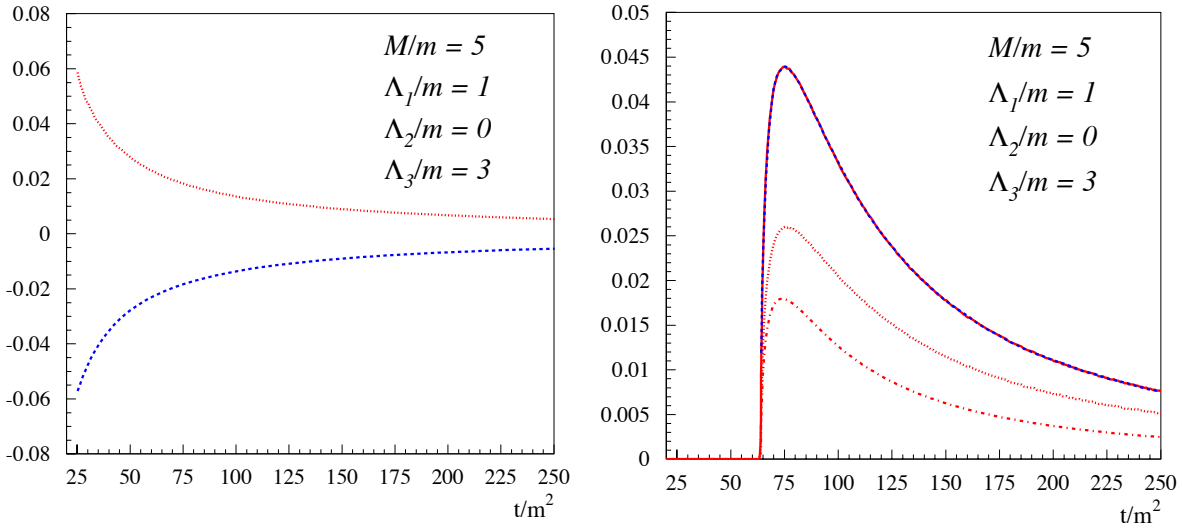

Figure 5.16: The imaginary parts of the vertex function discontinuities. Left panel: the imaginary parts of the two- and three-particle discontinuities of the first diagram. The red dotted (blue dashed) line denotes the imaginary part of the three-particle discontinuity (two-particle discontinuity taken with the opposite sign). Right panel: the imaginary parts of the two- and three-particle discontinuities of the second diagram. The dotted and dash-dotted red lines denote the imaginary part of the three-particle discontinuities (3γ cut and $2\mu\pi^0$ cut respectively), and the solid red line denotes the sum of two. The blue dashed line stands for the imaginary part of the two-particle discontinuity taken with the opposite sign.

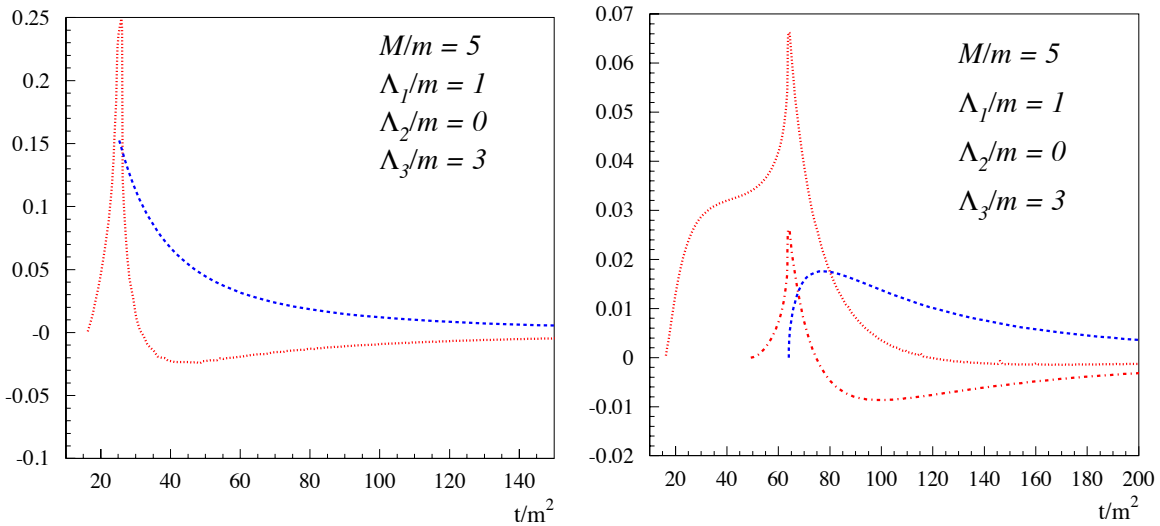

Figure 5.17: The real parts of the vertex function discontinuities: Im $\Gamma_i(t)/t$. Left panel: the real parts of the two- and three-particle discontinuities of the first diagram. The red dotted (blue dashed) line denotes the real part of the three-particle (two-particle) discontinuity. Right panel: the real parts of the two- and three-particle discontinuities of the second diagram. The red dotted and dash-dotted lines denote the real part of the three-particle discontinuities originating from the 3γ and $2\mu\pi^0$ cuts respectively. The blue dashed line stands for the real part of the two-particle discontinuity.

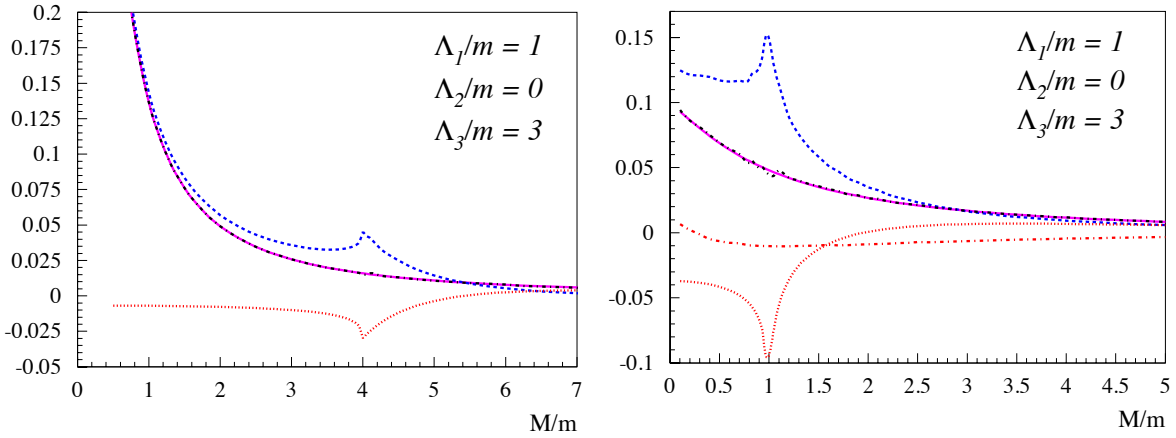

Figure 5.18: The vertex function in the limit of the vanishing external momentum $k \to 0$ depending on (meson) mass M: $\Gamma_i(0)$. Left panel: the contributions which originate from the two- and three-particle discontinuities of the first diagram. The red dotted (blue dashed) line denotes the contribution of the three-particle (two-particle) discontinuity. The black dashed-dotted line denotes the sum of two contributions. The pink solid line is obtained by the direct evaluation of two-loop integrals. Right panel: the contributions of the two- and three-particle discontinuities of the second diagram. The dotted and dash-dotted red lines denote the contributions of the three-particle discontinuities (3γ cut and $2\mu\pi^0$ cut respectively). The blue dashed line stands for the contribution of the two-particle discontinuity. The sum of three contributions is given by black dashed-dotted line. The pink line is obtained by the direct evaluation of two-loop integrals.

5.3 The pion-pole contribution to $(g-2)_\mu$

The subsequent calculation of the meson-pole contribution to $(g-2)_\mu$ generically parallels the computation of the scalar amplitudes. The two-loop functions $F_i^{\Lambda_1\Lambda_2\Lambda_3}$ have the same analytical structure as the scalar integrals and can be represented by the same diagrams. First, we will compute the discontinuity of the two-loop function $F_i^{\Lambda_1\Lambda_2\Lambda_3}$ by introducing the angular parametrization similarly to the case of scalar amplitude. After that the eight terms in Eq. (5.31) can be combined and the dispersion integral can be evaluated numerically.

5.3.1 Two-particle cuts.

The two-particle discontinuities of two-loop functions $F_i^{\Lambda_1\Lambda_2\Lambda_3}$ of Eqs. (5.32, 5.32) corresponding with the diagrams in Fig. (5.12) are given by

$$\begin{aligned}\mathrm{Disc}_t^2 F_1^{\Lambda_1\Lambda_2\Lambda_3}(t) = e^6|F(0,0,M^2)|^2 \int \frac{\mathrm{d}^4 q_1}{(2\pi)^4}(2\pi i)^2 \delta\left((k-q_1)^2-M^2\right)\delta\left(q_1^2-\Lambda_1^2\right)\\ \times \frac{S_3^{\Lambda_2\Lambda_3}}{(p+q_1)^2-m^2}\end{aligned} \tag{5.64}$$

and

$$\mathrm{Disc}_t^2 F_2^{\Lambda_1\Lambda_2\Lambda_3}(t) = e^6|F(0,0,M^2)|^2 \int \frac{\mathrm{d}^4 q_1}{(2\pi)^4}(2\pi i)^2 \delta\left((k-q_1)^2-M^2\right)\delta\left(q_1^2-\Lambda_1^2\right) S_4^{\Lambda_2\Lambda_3}. \tag{5.65}$$

where the one-loop integrals $S_3^{\Lambda_2\Lambda_3}$ and $S_4^{\Lambda_2\Lambda_3}$ are given by Eqs. (5.29, 5.30). To calculate these one-loop integrals we use the Passarino-Veltman reduction scheme and express the result in terms of scalar one-loop integrals including four- and three-point functions $M_3^{\Lambda_2\Lambda_3}$ and $M_4^{\Lambda_2\Lambda_3}$ of Eqs. (5.50, 5.51) as well as two-point functions

$$M_2^{\Lambda_2\Lambda_3}(p^2) = \int \frac{\mathrm{d}^4 q_2}{(2\pi)^4}\frac{1}{q^2-\Lambda_2^2}\frac{1}{(q+p)^2-\Lambda_3^2}. \tag{5.66}$$

Next we express the two-loop integrals in terms of the angular variables and invariants as discussed in Section 5.2.1. This yields the following representation of the two-particle discontinuities

$$\mathrm{Disc}_t^2 F_1^{\Lambda_1\Lambda_2\Lambda_3}(t) = -\frac{e^6|F(0,0,M^2)|^2}{16\pi}\beta_1 \int \mathrm{d}\cos\theta_1 \frac{N^{(1)}(q_1^2,m^2,t_1,t,\cos\theta_1)}{q_1^2+t_1-t-t\beta_1\beta\cos\theta_1} \tag{5.67}$$

and

$$\mathrm{Disc}_t^2 F_2^{\Lambda_1\Lambda_2\Lambda_3}(t) = -\frac{e^6|F(0,0,M^2)|^2}{16\pi}\beta_1 \int \mathrm{d}\cos\theta_1 N^{(2)}(q_1^2,m^2,t_1,t,\cos\theta_1) \tag{5.68}$$

with $q_1^2=\Lambda_1^2$ and $t_1^2=M^2$. The functions $N^{(1)}$ and $N^{(2)}$ are a linear combination of scalar functions $M_i^{\Lambda_j\Lambda_k}$ with polynomial functions of invariants and squared masses as coefficients. For instance, the numerator $N^{(1)}$ has the general decomposition

$$\begin{aligned}N^{(1)}(q_1^2,m^2,t_1,t,\cos\theta_1) =& M_3^{\Lambda_2\Lambda_3}(M^2,(q_1^2+t_1-t-t\beta_1\beta\cos\theta_1)/2,m^2)N_1(q_1^2,m^2,t_1,t,\cos\theta_1)\\ &+M_2^{\Lambda_2\Lambda_3}(0)N_2(q_1^2,m^2,t_1,t,\cos\theta_1)+M_2^{\Lambda_2 m}(0)N_3(q_1^2,m^2,t_1,t,\cos\theta_1)\\ &+M_2^{\Lambda_3 m}(0)N_4(q_1^2,m^2,t_1,t,\cos\theta_1)+M_2^{\Lambda_2 m}(m^2)N_5(q_1^2,m^2,t_1,t,\cos\theta_1)\\ &+M_2^{\Lambda_2\Lambda_3}(M^2)N_6(q_1^2,m^2,t_1,t,\cos\theta_1)\\ &+M_2^{\Lambda_3 m}(q_1^2+t_1-t-t\beta_1\beta\cos\theta_1)/2)N_7(q_1^2,m^2,t_1,t,\cos\theta_1)\\ &+N_8(q_1^2,m^2,t_1,t,\cos\theta_1).\end{aligned} \tag{5.69}$$

The integrals of Eqs. (5.67, 5.68) may be subsequently performed by means of numerical algorithms.

5.3.2 Three-particle discontinuity of Pauli form factor

The contribution to the discontinuity of the two-loop functions of Eqs. (5.32, 5.33) from the three-particle cuts are given next. For the first three-particle cut in Fig. 5.14 we have:

$$\begin{aligned}\mathrm{Disc}_t^3 F_1^{\Lambda_1\Lambda_2\Lambda_3}(t) = e^6|F(0,0,M^2)|^2 \int \frac{\mathrm{d}^4q_1}{(2\pi)^4}\int\frac{\mathrm{d}^4q_2}{(2\pi)^4} \\ \times (2\pi i)^3\delta(q_1^2-\Lambda_1^2)\delta(q_2^2-\Lambda_2^2)\delta((k-q_1-q_2)^2-\Lambda_3^2) \\ \times \frac{1}{(k-q_1)^2-M^2}\frac{1}{(p+q_1)^2-m^2}\frac{1}{(p+k-q_2)^2-m^2} \\ \times T_1(q_1,q_2,p,k)\end{aligned} \tag{5.70}$$

The trace $T_1(q_1,q_2,p,k)$ can be written in such a way that the hadronic and leptonic parts are factorized, in other words:

$$T_1(q_1,q_2,p,k) = L^{\mu\nu\lambda\rho}(p,p',q_1,q_2,k-q_1-q_2)\Pi^{\pi^0(2)}_{\mu\nu\lambda\rho}(k,q_1,q_2,k-q_1-q_2). \tag{5.71}$$

Here we introduced notation for the leptonic tensor

$$\begin{aligned}&L_{\mu\nu\lambda\rho}(p,p',q_1,q_2,k-q_1-q_2) \\ &\quad = \mathrm{Tr}\left[(\not p+m)\Lambda_\rho(p+k,p)(\not p+\not k+m)\gamma^\lambda(\not p+\not k-\not q_2+m)\gamma^\nu(\not p+\not q_1+m)\gamma^\mu\right]\end{aligned} \tag{5.72}$$

and

$$\Pi^{(2)}_{\mu\nu\lambda\rho}(k,q_1,q_2,k-q_1-q_2) = \frac{\mathcal{M}_{\mu\rho}(k^2,q_1^2,(k-q_1)^2)\mathcal{M}_{\nu\lambda}((k-q_1-q_2)^2,q_2^2,(k-q_1)^2)}{(k-q_1)^2-M^2}. \tag{5.73}$$

In order to correctly isolate the pole contribution to the HLbL tensor we need to explicitly formulate it in terms of the helicity amplitudes. Using completeness relation for the electromagnetic field polarization tensors

$$\sum_\lambda(-1)^\lambda\varepsilon^{\mu*}(q,\lambda)\varepsilon^\nu(q,\lambda) = g^{\mu\nu}-\frac{q^\mu q^\nu}{q^2} \tag{5.74}$$

and taking into account gauge invariance of the photon amplitude $q^\mu\Pi_{\mu\nu\lambda\rho}=0$ one can represent the photon propagators as

$$\Delta_{\mu\nu}(q) = \frac{-i}{q^2}\sum_\lambda(-1)^\lambda\varepsilon^{\mu*}(q,\lambda)\varepsilon^\nu(q,\lambda). \tag{5.75}$$

we can write

$$\begin{aligned}T_1(q_1,q_2,p,k) &= L_{\mu\nu\lambda\rho}(p,p',q_1,q_2,k-q_1-q_2)g^{\mu\mu'}g^{\nu\nu'}g^{\lambda\lambda'}g^{\rho\rho'}\Pi^{(1)}_{\mu'\nu'\lambda'\rho'}(k,q_1,q_2,k-q_1-q_2) \\ &= \sum_\lambda\sum_{\lambda_1}\sum_{\lambda_2}\sum_{\lambda_3}(-1)^{\lambda+\lambda_1+\lambda_2+\lambda_3}L_{\lambda\lambda_1\lambda_2\lambda_3}\Pi^{(2)}_{\lambda\lambda_1\lambda_2\lambda_3}\end{aligned} \tag{5.76}$$

with

$$\begin{aligned}&L_{\lambda\lambda_1\lambda_2\lambda_3}(p,p',q_1,q_2,k-q_1-q_2) = \epsilon^*(k,\lambda)\epsilon(q_1,\lambda_1)\epsilon(q_2,\lambda_2)\epsilon(k-q_1-q_2,\lambda_3) \\ &\quad\times\mathrm{Tr}\left[(\not p+m)\Lambda_\rho(p+k,p)(\not p+\not k+m)\gamma^\lambda(\not p+\not k-\not q_2+m)\gamma^\nu(\not p+\not q_1+m)\gamma^\mu\right]\end{aligned} \tag{5.77}$$

The pole contribution to the HLbL helicity amplitudes $\Pi^{(i)}_{\lambda\lambda_1\lambda_2\lambda_3}$ is given by Eq. (5.13). In the case of a pseudoscalar meson production, due to Lorentz and crossing symmetries the only non-zero $\gamma^*\gamma^* \to M$ helicity amplitudes, which we define in the rest frame of the produced meson, are given by:

$$\mathcal{M}_{\lambda_1=+1,\lambda_2=+1} = -\mathcal{M}_{\lambda_1=-1,\lambda_2=-1} = -e^2\sqrt{X}\,F_{P\gamma^*\gamma^*}(q_1^2,q_2^2) \tag{5.78}$$

where

$$X \equiv (q_1\cdot q_2)^2 - q_1^2q_2^2 = \frac{1}{4}(s-q_1^2-q_2^2)^2 - q_1^2q_2^2. \tag{5.79}$$

The non-vanishing independent helicity amplitudes $\Pi^{(i)}_{\lambda_1\lambda_2\lambda_3\lambda_4}$ are listed below

$$\Pi^{\pi^0(1,2,3)}_{++++},\ \Pi^{\pi^0(1,2,3)}_{----},\ \Pi^{\pi^0(1)}_{++--},\ \Pi^{\pi^0(1)}_{--++},\ \Pi^{\pi^0(2)}_{+--+},\ \Pi^{\pi^0(2)}_{-++-},\ \Pi^{\pi^0(3)}_{+-+-},\ \Pi^{\pi^0(3)}_{-+-+}. \tag{5.80}$$

Using Eq. (5.78) they can be written explicitly. For instance

$$\Pi^{\pi^0(1)}_{++++}(k^2,q_2^2,q_1^2,(k-q_1-q_2)^2,(k-q_2)^2) \tag{5.81}$$

$$= \frac{\mathcal{M}_{++}(k^2,q_2^2,M^2)\mathcal{M}_{++}(q_1^2,(k-q_1-q_2)^2,M^2)}{(k-q_2)^2-M^2}. \tag{5.82}$$

As a result the contribution of the three-particle cut to the discontinuity for the first topology is given by

$$\begin{aligned}\mathrm{Disc}^3_t F_1^{\Lambda_1\Lambda_2\Lambda_3}(t) = e^6|F(0,0,M^2)|^2 &\int\frac{\mathrm{d}^4q_1}{(2\pi)^4}\int\frac{\mathrm{d}^4q_2}{(2\pi)^4}\\ &\times(2\pi i)^3\delta(q_1^2-\Lambda_1^2)\delta(q_2^2-\Lambda_2^2)\delta((k-q_1-q_2)^2-\Lambda_3^2)\\ &\times\frac{1}{(k-q_1)^2-M^2}\frac{1}{(p+q_1)^2-m_1^2}\frac{1}{(p+k-q_2)^2-m_2^2}\\ &\times\sum_\lambda\sum_{\lambda_1}\sum_{\lambda_2}\sum_{\lambda_3}L_{\lambda\lambda_1\lambda_2\lambda_3}\tilde{\Pi}^{\pi^0(2)}_{\lambda\lambda_1\lambda_2\lambda_3}.\end{aligned} \tag{5.83}$$

Similarly to the case of scalar two-loop functions, for the second diagram in Fig. 5.10, there are two three-particle cut diagrams which contribute to the discontinuity (see second row in Fig. 5.14). In order to generalize our computation for both three-particle cuts appearing in this case we consider the leptons to have different masses m_1 and m_2. The first (three-photon) cut contribution (left panel in the second row of Fig. 5.14) is given by

$$\begin{aligned}\mathrm{Disc}^{3,1}_{\mathrm{t}} F_2^{\Lambda_1\Lambda_2\Lambda_3}(t) = e^6|F(0,0,M^2)|^2 &\int\frac{\mathrm{d}^4q_1}{(2\pi)^4}\int\frac{\mathrm{d}^4q_2}{(2\pi)^4}\\ &\times(2\pi i)^3\delta(q_1^2-\Lambda_1^2)\delta(q_2^2-\Lambda_2^2)\delta((k-q_1-q_2)^2-\Lambda_3^2)\\ &\times\frac{1}{(q_1+q_2)^2-M^2}\frac{1}{(p+q_1)^2-m_1^2}\frac{1}{(p+k-q_2)^2-m_2^2}\\ &\times\sum_\lambda\sum_{\lambda_1}\sum_{\lambda_2}\sum_{\lambda_3}L_{\lambda\lambda_1\lambda_2\lambda_3}\tilde{\Pi}^{\pi^0(3)}_{\lambda\lambda_1\lambda_2\lambda_3}.\end{aligned} \tag{5.84}$$

where the sum over helicities is performed in correspondence with the list of Eq. (5.80). The second (meson-lepton-lepton) cut contribution (right panel in the second row of Fig. 5.14) is

given by

$$\begin{aligned}\mathrm{Disc}_{\mathrm{t}}^{3,2}F_2^{\Lambda_1\Lambda_2\Lambda_3}(t) &= e^6|F(0,0,M^2)|^2\int\frac{\mathrm{d}^4q_1}{(2\pi)^4}\int\frac{\mathrm{d}^4q_2}{(2\pi)^4}\\ &\times(2\pi i)^3\delta(q_1^2-m^2)\delta(q_2^2-m^2)\delta((k-q_1-q_2)^2-M^2)\\ &\times\frac{1}{(q_1+q_2)^2-\Lambda_3^2}\frac{1}{(p+q_1)^2-\Lambda_1^2}\frac{1}{(p+k-q_2)^2-\Lambda_2^2}\\ &\times\sum_{\lambda}\sum_{\lambda_1}\sum_{\lambda_2}\sum_{\lambda_3}L_{\lambda\lambda_1\lambda_2\lambda_3}\tilde{\Pi}^{\pi^0(3)}_{\lambda\lambda_1\lambda_2\lambda_3}.\end{aligned}\tag{5.85}$$

In the angular coordinates, the three-particle discontinuity for the first topology is given by

$$\begin{aligned}\mathrm{Disc}_t^3F_1^{\Lambda_1\Lambda_2\Lambda_3}(t) &= -\frac{ie^6|F(0,0,M^2)|^2}{32t}\int\mathrm{d}q_1^2\int\mathrm{d}q_2^2\int\mathrm{d}t_1\int\mathrm{d}t_2\int\mathrm{d}t_{12}\frac{1}{t_1-M^2}\\ &\times\delta(q_1^2-\Lambda_1^2)\delta(q_2^2-\Lambda_3^2)\delta(t_{12}+t_1+t_2-t-q_1^2-q_2^2-\Lambda_2^2)\\ &\times\int\limits_0^{\pi}\mathrm{d}\cos\theta_1\int\limits_0^{2\pi}\mathrm{d}\theta_2\,\frac{2}{2m^2-2m_1^2+q_1^2+t_1-t-t\beta_1\beta\cos\theta_1}\\ &\times\frac{2}{2m^2-2m_2^2+q_2^2-t+t_2+t\beta_2\beta(\sin\theta_1\cos\theta_2\sin\theta+\cos\theta_1\cos\theta)}\\ &\times\sum_{\lambda}\sum_{\lambda_1}\sum_{\lambda_2}\sum_{\lambda_3}L_{\lambda\lambda_1\lambda_2\lambda_3}\tilde{\Pi}^{\pi^0(2)}_{\lambda\lambda_1\lambda_2\lambda_3}\end{aligned}\tag{5.86}$$

or

$$\begin{aligned}\mathrm{Disc}_t^3F_1^{\Lambda_1\Lambda_2\Lambda_3}(t) &= -\frac{ie^6|F(0,0,M^2)|^2}{32t}\int\mathrm{d}t_1\int\mathrm{d}t_2\frac{1}{t_1-M^2}\\ &\times\int\limits_0^{\pi}\mathrm{d}\cos\theta_1\int\limits_0^{2\pi}\mathrm{d}\theta_2\,\frac{2}{2m^2-2m_1^2+q_1^2+t_1-t-t\beta_1\beta\cos\theta_1}\\ &\times\frac{2}{2m^2-2m_2^2+q_2^2-t+t_2+t\beta_2\beta(\sin\theta_1\cos\theta_2\sin\theta+\cos\theta_1\cos\theta)}\\ &\times\sum_{\lambda}\sum_{\lambda_1}\sum_{\lambda_2}\sum_{\lambda_3}L_{\lambda\lambda_1\lambda_2\lambda_3}\tilde{\Pi}^{\pi^0(2)}_{\lambda\lambda_1\lambda_2\lambda_3}.\end{aligned}\tag{5.87}$$

For the three-particle contributions to the discontinuity of the diagram with the second topology we have

$$\begin{aligned}\mathrm{Disc}_t^{3,1}F_2^{\Lambda_1\Lambda_2\Lambda_3}(t) &= -\frac{ie^6|F(0,0,M^2)|^2}{32t}\int\mathrm{d}t_1\int\mathrm{d}t_2\frac{1}{t+\Lambda_1^2+\Lambda_2^2+\Lambda_3^2-t_1-t_2-M^2}\\ &\times\int\limits_0^{\pi}\mathrm{d}\cos\theta_1\int\limits_0^{2\pi}\mathrm{d}\theta_2\,\frac{2}{2m^2-2m_1^2+q_1^2+t_1-t-t\beta_1\beta\cos\theta_1}\\ &\times\frac{2}{2m^2-2m_2^2+q_2^2-t+t_2+t\beta_2\beta(\sin\theta_1\cos\theta_2\sin\theta+\cos\theta_1\cos\theta)}\\ &\times\sum_{\lambda}\sum_{\lambda_1}\sum_{\lambda_2}\sum_{\lambda_3}L_{\lambda\lambda_1\lambda_2\lambda_3}\tilde{\Pi}^{\pi^0(3)}_{\lambda\lambda_1\lambda_2\lambda_3}\end{aligned}\tag{5.88}$$

wheres the second discontinuity $\mathrm{Disc}_t^{3,2}F_2^{\Lambda_1\Lambda_2\Lambda_3}(t)$ may be easily obtained by a substitutions $m_1\leftrightarrow\Lambda_1$, $m_2\leftrightarrow\Lambda_2$, $M\leftrightarrow\Lambda_3$ similarly to the case of scalar two-loop functions.

The angular integral may be performed analogously to the case of scalar functions. The expression may be firstly simplified by canceling the angle dependent terms throughout the numerator against corresponding terms in the denominator. This yields a decomposition in terms of a set angular integrals similar to the one appearing in the case of scalar two-loop functions. They can be computed in an analogous way. The subsequent integration over t_1 and t_2 can be performed by means of numerical integration.

5.4 Discussion

In this chapter, we have presented the general dispersion formalism for the HLbL contribution to $(g-2)_\mu$. This formalism has the advantage that no uncontrollable extrapolation outside the mass-shell for the hadronic intermediate state has to be performed. We have shown explicitly how the HLbL contribution to $(g-2)_\mu$ can be expressed as a sum of two- and three-particle cuts. For the case of the dominant π^0 as hadronic state, we have shown that for the simplified model of vector meson (VM) poles for the π^0 transition FF, one can reduce the calculation to scalar integrals.

We subsequently worked out the case of two-loop scalar vertex functions for three different "photon" masses (corresponding with vector meson poles to describe the π^0 transition FF). We have shown explicitly that the discontinuities due to two- and three-particle cuts add up exactly to the result of the direct two-loop calculation, which can be performed unambiguously in this case.

The next step is to apply this dispersive formalism to the explicit calculation of the π^0 pole contribution. To this end, we presented in this work the explicit formulas necessary for the dispersive evaluation of the corresponding two- and three-particle cuts.

For the further development of the dispersive formalism for the HLbL contribution to $(g-2)_\mu$ we can foresee several steps :

1. A first step in this program is to extend the numerical evaluation from the scalar field theory case, presented in this work, to the dispersive evaluation of the HLbL contribution due to the π^0, when using VM poles for the π^0 transition FF.

2. Secondly, we can apply the dispersive formalism to directly include the phenomenological input for the meson transition FFs, e.g. by separating the FF in a VM pole + non-resonant background part.

3. A further extension will entail the inclusion of heavier hadronic intermediate states, most importantly the 2π intermediate states.

Chapter 6

Conclusion

In this thesis we considered a wide spectrum of problems related to processes of two-photon electromagnetic production. These processes are of tremendous importance for understanding QCD, for constraining the hadronic uncertainties in the precision measurements and in searches for new physics. At first, we systematically discussed the experimental approaches and methods of extraction of the phenomenological information on two-photon processes from the experimental data. We highlighted the main experimental results in this field and discussed relevant directions for further progress. From the theoretical point of view two-photon processes are very complicated and except for a few limited asymptotic regions, it cannot at present be rigorously described from first principles. To study non-perturbative features of two-photon production we use dispersion theory in this work. Such approach allows to rigorously constrain the energy behavior of the two-photon correlation functions. We derived several constraints in the form of superconvergent sum rules. These sum rules are the integral relations which involve energy weighted integrals of $\gamma^*\gamma$ fusion cross sections, measurable at e^+e^- colliders, which integrate to zero (super-convergence relations):

$$
\begin{aligned}
0 &= \int\limits_{s_0}^{\infty} ds \frac{1}{(s+Q_1^2)} \left[\sigma_0 - \sigma_2\right]_{Q_2^2=0}, \\
0 &= \int\limits_{s_0}^{\infty} ds \, \frac{1}{(s+Q_1^2)^2} \left[\sigma_{\parallel} + \sigma_{LT} + \frac{(s+Q_1^2)}{Q_1 Q_2} \tau_{TL}^a \right]_{Q_2^2=0}, \\
0 &= \int\limits_{s_0}^{\infty} ds \, \left[\frac{\tau_{TL}}{Q_1 Q_2}\right]_{Q_2^2=0}.
\end{aligned}
$$

Furthermore, we derived a set of integral relations which allow to define the low-energy structure of the elastic light-by-light scattering amplitudes in terms of integrals over fusion cross sections.

These sum rules were tested and verified exactly at tree and one-loop level in scalar and spinor QED for the case of two (quasi-)real photons, as well as for the case of one virtual and one (quasi-)real photons. We have observed that for larger values of the photon's virtuality the higher energy contributions are required for cancellations to take place. Another observation is that for the helicity difference sum rule the helicity-0 cross section dominates at lower energies while with increasing energies the helicity-2 cross section overtakes. A similar pattern is observed in the production of the hadronic states showing a deep relation between perturbative production of $q\bar{q}$ pairs and hadronic resonances. Furthermore, we have tested the criterium of the tree-level unitarity imposed by the sum rules on the example of the massive spin-1 QED. We have observed that when applied to the processes of higher spin particles production the sum rules hold for the natural values of the corresponding electromagnetic moments only.

Next, we have studied the consequences of causality constraints imposed by the helicity-difference sum rule for the forward light-by-light scattering process within the ϕ^4 scalar quantum field theory. Within this theory, we have performed a non-perturbative resummation of

bubble graphs. We have demonstrated that depending on the value of the renormalized self-interaction coupling of the ϕ^4 theory, three different regimes emerge. In a first regime, the perturbative series is convergent and the sum rule as calculated from the continuum states in the theory holds exactly. In a second regime for the renormalized coupling, the resummed amplitude acquires additional singularities: a dynamically generated bound state below the two-particle production threshold and a K-matrix pole above the two-particle production. It was shown that when evaluating the light-by-light sum rule, the bound state contribution exactly cancels the continuum contribution, so as to verify the sum rule. Furthermore, we found a third regime of the renormalized coupling where a tachyonic solution with negative invariant mass squared appears, signaling that in this regime the vacuum is unstable and that the considered non-perturbative resummation is essentially inconsistent.

The results within the considered model relativistic quantum field theory have demonstrated that such sum rules provide a very powerful tool to quantitatively connect dynamically generated bound states with the continuum region of the theory. As such this can be a first step, to apply such a tool e.g. to the study meson bound states produced in the $\gamma\gamma$-fusion process presently under study at different e^+e^- collider facilities.

Subsequently, we have performed a detailed quantitative study of the new sum rules for the case of the production of light quark mesons as well as for the production of mesons in the charm quark sector. Using the empirical $\gamma\gamma \to X$ information in evaluating the sum rules, we have found that the helicity-difference sum rule requires cancellations between different mesons, implying non-perturbative relations. For the light quark isovector mesons, the π^0 contribution was found to be compensated to around 70% by the contribution of the lowest lying isovector tensor meson $a_2(1320)$. For the isoscalar light quark mesons, the η and η' contributions were found to be entirely compensated within the experimental accuracy by the two lowest-lying tensor mesons $f_2(1270)$ and $f_2'(1525)$. In the charm quark sector, the situation is different as it involves the narrow resonance contributions below $D\bar{D}$ threshold, and the continuum contribution above $D\bar{D}$ threshold. For the narrow resonances, the η_c was found to give by far the dominant contribution. When using a duality estimate for the continuum contribution, we found that it entirely cancels the narrow resonance contributions, verifying the sum rule, and pointing to large tensor strength (helicity 2) in the cross sections above $D\bar{D}$ threshold. It will be interesting to test this property experimentally.

The helicity difference sum rule has also been applied for the case of one real and one virtual photon. In this case the $\gamma^*\gamma$ fusion cross sections depend on the meson transition form factors (FFs). We have reviewed the general formalism and parameterization for the $\gamma^*\gamma \to$ meson transition FFs for (pseudo-) scalar, axial-vector, and tensor mesons. Because for scalar and tensor mesons the $\gamma^*\gamma$ transition FFs have not yet been measured, a direct test of the sum rules for finite virtuality is not possible at present. However, we were able to show that the helicity-difference sum rule allows to provide an estimate for the $f_2(1270)$ tensor FF in terms of the η, and η' FFs, and for the $a_2(1320)$ tensor FF in terms of the π^0 FF. Since empirical information on pseudo-scalar meson FFs is available, these relations provide predictions for tensor meson FFs which will be interesting to confront with experiment.

The sum rules involving the $\sigma_{\parallel}, \sigma_{LT}$, and τ^a_{TL} $\gamma^*\gamma$ response functions, have also been tested for the case of quasi-real photons. As pseudo-scalar mesons cannot contribute to this sum rule, a cancellation between scalar and tensor mesons on one hand and axial-vector mesons on the other hand is at work. Using the existing empirical information for quasi-real photons, the contribution of the two lowest lying axial-vector mesons $f_1(1285)$ and $f_1(1420)$ was found to be entirely cancelled, within error bars, by the contribution of the dominant tensor meson $f_2(1270)$. When applying this sum rule to the case of one virtual photon, it again allows one to relate the $f_2(1270)$ tensor FF, this time to the transition FFs for the $f_1(1285)$ and $f_1(1420)$ mesons, which have both been measured. The predictions from the two different sum rules for

the $f_2(1270)$ FF were found to agree within 20% for a virtuality below 1 GeV^2, and within 35% up to about 2 GeV^2. The sum rules which express the coefficients in a low-energy expansion of the forward light-by-light scattering amplitude in terms of $\gamma^*\gamma \to X$ cross sections may be used as a cross-check for models of the non-forward light-by-light scattering which are applied to evaluate the hadronic LbL contribution to $(g-2)_\mu$.

On the experimental side, the ongoing $\gamma\gamma$ physics programs by the BABAR and Belle Collaborations, as well as the upcoming $\gamma\gamma$ physics program by the BES-III Collaboration, will allow to further improve the data situation significantly. In particular, the extraction of the $\gamma^*\gamma$ response functions through their different azimuthal angular dependencies, and the measurements of multi-meson final states ($\pi\pi$, $\pi\eta$, ...) promise to access besides the pseudo-scalar meson FFs also the scalar, axial-vector and tensor meson FFs, thus allowing direct tests of the sum rule predictions presented in this thesis.

In the second part of this thesis we have presented the formalism to calculate the HLbL contribution to the muon's anomalous magnetic moment a_μ due to axial-vector, scalar and tensor meson poles. In this way, we have extended the framework of Ref. [140], where the leading HLbL contribution due to pseudo-scalar mesons was evaluated. To allow for the different Lorentz structures of the $\gamma^*\gamma^* \to$ meson vertex, we have performed a combined analytical and numerical technique, where the angular integrals over the virtual photon momenta were performed analytically using the Legendre polynomial technique, and where the resulting four-dimensional integral for a_μ was performed numerically. We validated our method by reproducing the known result for pseudo-scalar mesons. To estimate the HLbL contribution to a_μ from axial-vector, scalar and tensor mesons, we incorporated available experimental input as well as constraints from light-by-light scattering sum rules. For those mesons which have the largest known couplings to two virtual photons, we obtained as estimates :

$$\begin{aligned} a_\mu(f_1, f_1') &= (6.4 \pm 2.0) \times 10^{-11}, \\ a_\mu(f_0, f_0', a_0) &= [(-0.9 \pm 0.2) \text{ to } (-3.1 \pm 0.8)] \times 10^{-11}, \\ a_\mu(f_2, f_2', a_2, a_2') &= (1.1 \pm 0.1) \times 10^{-11}. \end{aligned} \tag{6.1}$$

The size of such contributions is about an order of magnitude smaller than the dominant π^0 HLbL contribution. Given a new muon $g-2$ experiment at Fermilab, which aims to reduce the experimental uncertainty to $\delta a_\mu \approx 16 \times 10^{-11}$, it is however crucial to further constrain the theoretical uncertainty due to the HLbL contribution. In this respect, it would be particularly helpful to have $\gamma^*\gamma^* \to$ meson transition form factor measurements with one and two virtual photons for axial-vector, scalar and tensor states. As such information will become available, in particular from future measurements from BES-III, the formalism developed in this thesis can be used to further improve on the estimate of the HLbL contribution to a_μ.

The adopted approach has one significant disadvantage though. In the developed representation the HLbL correction is defined in terms of the off-shell hadronic amplitudes. Therefore, due to the absence of the phenomenological information we had to assume a constant behavior of the form factors in the meson mass. This, of course, might be a source of a larger uncertainty of such estimates compared to errors given in Eq. (6.1). In order to overcome this uncertainty, we developed a novel dispersive formalism for calculation of the hadronic light-by-light contribution to $(g-2)_\mu$. We showed that in this approach the inconsistency of the conventional framework does not emerge. This is due to the fact, that in the dispersion formalism the Pauli form factor is expressed in terms of on-shell hadronic matrix elements which can be directly measured in experiments.

As a first step the formalism was applied to the calculation of a single pseudo-scalar meson pole contribution to $(g-2)_\mu$. It was shown that for the case of the monopole form factors the pole contribution may be expressed in terms of two-loop scalar three-point functions. The

properties of the scalar amplitudes were studied in detail in the dispersion framework. We have subsequently computed one among those which appear in the $(g-2)_\mu$ and verified our result by the direct two-loop calculation using the Gegenbauer polynomial expansion. A crucial distinctive feature of the dispersion approach is that it allows extension to implement the form factors beyond the simplest monopole or dipole approximations and to include multi-meson channels. Especially, the next step will be to include the two-pion channel. The currently running measurements by the BES III collaboration are of a crucial importance for further developments in this field.

Appendix A

Kinematics and cross sections of the $e^{\pm} + e^{-} \to e^{\pm} + e^{-} + X$ process

In this Appendix we detail the kinematics of the $e^{\pm} + e^{-} \to e^{\pm} + e^{-} + X$ process, and show how the cross sections accessible in experiments are expressed in terms of the $\gamma^*\gamma^* \to X$ cross sections, which enter in the sum rules discussed in the present work.

The kinematics of the process $e(p_1) + e(p_2) \to e(p_1') + e(p_2') + X$, with X the produced hadronic state, in the lepton c.m. system, i.e. the c.m. system of the colliding beams (which we denote by *c.m. ee*) is characterized by the four-vectors of the incoming leptons :

$$p_1(E, \vec{p}_1), \qquad p_2(E, -\vec{p}_1), \tag{A.1}$$

with beam energy $E = \sqrt{s}/2$, and $s = (p_1 + p_2)^2$.
The kinematics of the outgoing leptons can be related to the virtual photon four-momenta as :

$$q_1 = p_1 - p_1', \qquad q_2 = p_2 - p_2'. \tag{A.2}$$

The kinematics of the outgoing leptons then determines five kinematical quantities :

- the energies of both virtual photons :

$$\omega_1 \equiv q_1^0 = E - E_1', \qquad \omega_2 = q_2^0 \equiv E - E_2', \tag{A.3}$$

  with E_1' and E_2' the energies of both outgoing leptons;

- the virtualities of both virtual photons :

$$Q_1^2 \equiv -q_1^2 = 4EE_1' \sin^2\theta_1/2 + Q_{1,\,min}^2\,, \qquad Q_2^2 \equiv -q_2^2 = 4EE_2' \sin^2\theta_2/2 + Q_{2,\,min}^2 \tag{A.4}$$

  where θ_1 and θ_2 are the (polar) angles of the scattered electrons relative to the respective beam directions, and where the minimal values of the virtualities are given by (in the limit where $E_1' >> m$ and $E_2' >> m$, with m the lepton mass) :

$$Q_{1,\,min}^2 \simeq m^2 \frac{\omega_1^2}{EE_1'}, \qquad Q_{2,\,min}^2 \simeq m^2 \frac{\omega_2^2}{EE_2'}; \tag{A.5}$$

- the azimuthal angle ϕ between both lepton planes, which in the lepton c.m. frame can be obtained as :

$$\big(\cos\phi\big)_{c.m.ee} \equiv -\frac{p_{1\perp}' \cdot p_{2\perp}'}{\big[(p_{1\perp}')^2\ (p_{2\perp}')^2\big]^{1/2}}, \tag{A.6}$$

  where $p_{1\perp}'$ and $p_{2\perp}'$ denote the components of the outgoing lepton four-vectors which are perpendicular to the respective beam directions, and are defined in the lepton c.m. frame as :

$$\big(p_{1\perp}'\big)^{\mu} = -R^{\mu\nu}(p_1, p_2)\ \big(p_1'\big)_{\nu}\,, \qquad \big(p_{2\perp}'\big)^{\mu} = -R^{\mu\nu}(p_1, p_2)\ \big(p_2'\big)_{\nu}\,, \tag{A.7}$$

with

$$R^{\mu\nu}(p_1, p_2) = -g^{\mu\nu} + \frac{1}{[(p_1 \cdot p_2)^2 - m^4]} \tag{A.8}$$

$$\times \left\{ (p_1 \cdot p_2) \, (p_1^{\mu} \, p_2^{\nu} + p_2^{\mu} \, p_1^{\nu}) - m^2 \, (p_1^{\mu} \, p_1^{\nu} + p_2^{\mu} \, p_2^{\nu}) \right\}. \tag{A.9}$$

In the following it will also turn out to be useful to determine kinematical quantities in the c.m. system of the virtual photons (which we denote by *c.m.* $\gamma\gamma$). In particular, the azimuthal angle between both lepton planes, in the $\gamma\gamma$ c.m. frame, which we denote by $\tilde{\phi}$ is given by :

$$\cos\tilde{\phi} \equiv -\frac{\tilde{p}_{1\perp} \cdot \tilde{p}_{2\perp}}{[(\tilde{p}_{1\perp})^2 \, (\tilde{p}_{2\perp})^2]^{1/2}}, \tag{A.10}$$

where $\tilde{p}_{1\perp}$ and $\tilde{p}_{2\perp}$ denote the transverse components of the incoming lepton four-vectors in the $\gamma\gamma$ c.m. frame and are defined in a covariant way as :

$$(\tilde{p}_{1\perp})^{\mu} = -R^{\mu\nu}(q_1, q_2) \, (p_1)_{\nu} \, , \qquad (\tilde{p}_{2\perp})^{\mu} = -R^{\mu\nu}(q_1, q_2) \, (p_2)_{\nu} \, , \tag{A.11}$$

with

$$R^{\mu\nu}(q_1, q_2) = -g^{\mu\nu} + \frac{1}{\left[(q_1 \cdot q_2)^2 - q_1^2 q_2^2\right]} \tag{A.12}$$

$$\times \left\{ (q_1 \cdot q_2) \, (q_1^{\mu} \, q_2^{\nu} + q_2^{\mu} \, q_1^{\nu}) - q_1^2 \, q_2^{\mu} \, q_2^{\nu} - q_2^2 \, q_1^{\mu} \, q_1^{\nu} \right\}. \tag{A.13}$$

As the *rhs* of Eq. (A.10) is expressed in a Lorentz invariant way, one can then evaluate all four-momenta in the lepton c.m. frame, to obtain the expression of $\cos\tilde{\phi}$ in terms of the lepton c.m. kinematics.

The cross section for the process $e(p_1) + e(p_2) \to e(p_1') + e(p_2') + X$, with X the produced hadronic state, can be expressed in terms of eight cross sections for the $\gamma^*\gamma^* \to X$ process, which where defined in Eq. (2.12), as :

$$d\sigma = \frac{\alpha^2}{16\pi^4 \, Q_1^2 \, Q_2^2} \, \frac{2\sqrt{X}}{s(1 - 4m^2/s)} \cdot \frac{d^3\vec{p}_1'}{E_1'} \cdot \frac{d^3\vec{p}_2'}{E_2'}$$

$$\times \left\{ 4 \, \rho_1^{++} \, \rho_2^{++} \, \sigma_{TT} + \rho_1^{00} \, \rho_2^{00} \, \sigma_{LL} + 2 \, \rho_1^{++} \, \rho_2^{00} \, \sigma_{TL} + 2 \, \rho_1^{00} \, \rho_2^{++} \, \sigma_{LT} \right.$$

$$+ 2 \, \left(\rho_1^{++} - 1\right) \, \left(\rho_2^{++} - 1\right) \, \left(\cos 2\tilde{\phi}\right) \, \tau_{TT} \tag{A.14}$$

$$\left. + 8 \left[\frac{\left(\rho_1^{00} + 1\right) \, \left(\rho_2^{00} + 1\right)}{\left(\rho_1^{++} - 1\right) \, \left(\rho_2^{++} - 1\right)} \right]^{1/2} \left(\cos\tilde{\phi}\right) \, \tau_{TL} \right.$$

$$+ h_1 h_2 \, 4 \left[\left(\rho_1^{00} + 1\right) \, \left(\rho_2^{00} + 1\right) \right]^{1/2} \, \tau_{TT}^{a} \tag{A.15}$$

$$\left. + \, h_1 h_2 \, 8 \left[\left(\rho_1^{++} - 1\right) \, \left(\rho_2^{++} - 1\right) \right]^{1/2} \left(\cos\tilde{\phi}\right) \, \tau_{TL}^{a} \right\}, \tag{A.16}$$

where $h_1 = \pm 1$ and $h_2 = \pm 1$ are both lepton beam helicities, and where we have defined kinematical coefficients :

$$\begin{aligned}
\rho_1^{++} &= \frac{1}{2} \left\{ 1 - \frac{4m^2}{Q_1^2} + \frac{1}{X} \, (2 \, p_1 \cdot q_2 - \nu)^2 \right\} , \\
\rho_2^{++} &= \frac{1}{2} \left\{ 1 - \frac{4m^2}{Q_2^2} + \frac{1}{X} \, (2 \, p_2 \cdot q_1 - \nu)^2 \right\} , \\
\rho_1^{00} &= \frac{1}{X} \, (2 \, p_1 \cdot q_2 - \nu)^2 - 1 \, , \\
\rho_2^{00} &= \frac{1}{X} \, (2 \, p_2 \cdot q_1 - \nu)^2 - 1 \, .
\end{aligned} \tag{A.17}$$

Appendix B

Tree-level $\gamma^*\gamma^*$ cross sections in QED

B.1 Scalar QED

The $\gamma^*\gamma^* \to \mathcal{S}\bar{\mathcal{S}}$ cross sections (with $\mathcal{S}$ an electrically charged structureless scalar particle) to lowest order in α are given by :

$$\sigma_0 + \sigma_2 = \sigma_\parallel + \sigma_\perp = \alpha^2 \frac{\pi}{2} \frac{s^2\nu^3}{X^3} \left\{ \sqrt{a} \left[2 - a + \left(1 - \frac{2X}{s\nu} \right)^2 \right] \right. \tag{B.1}$$

$$\left. - (1-a) \left(3 - \frac{4X}{s\nu} + a \right) L \right\}, \tag{B.2}$$

$$\sigma_\parallel - \sigma_\perp = \alpha^2 \frac{\pi}{4} \frac{s^2\nu^3}{X^3} \left\{ \sqrt{a} \left[1 - a + 2 \left(1 - \frac{2X}{s\nu} \right)^2 \right] - (1-a) \left(3 - \frac{8X}{s\nu} + a \right) L \right\}, \tag{B.3}$$

$$\sigma_0 - \sigma_2 = \alpha^2 2\pi \frac{s\nu^2}{X^2} \left\{ -\sqrt{a} \left(1 - \frac{X}{s\nu} \right) + (1-a)\, L \right\}, \tag{B.4}$$

$$\sigma_{LL} = \alpha^2 \pi Q_1^2 Q_2^2 \frac{s^2\nu}{X^3} \left\{ \sqrt{a} \left[2 + \frac{1}{1-a} \left(1 - \frac{X}{s\nu} \right)^2 \right] - \left(3 + \frac{X}{s\nu} \right) \left(1 - \frac{X}{s\nu} \right) L \right\}, \tag{B.5}$$

$$\sigma_{LT} = \alpha^2 \frac{\pi}{2} Q_1^2 \frac{s\nu(\nu - Q_2^2)^2}{X^3} \left\{ -3\sqrt{a} + (3-a)\, L \right\}, \tag{B.6}$$

$$\tau_{TL} = \alpha^2 \frac{\pi}{2} Q_1 Q_2 \frac{s\nu}{X^2} \left\{ -\sqrt{a} + \left(1 - \frac{2X}{s\nu} + a \right) L \right\}, \tag{B.7}$$

$$\tau_{TL}^a = \alpha^2 \frac{\pi}{2} Q_1 Q_2 \frac{s^2\nu^2}{X^3} \left\{ \sqrt{a} \left(3 - \frac{4X}{s\nu} \right) - \left[1 - a + 2 \left(1 - \frac{X}{s\nu} \right)^2 \right] L \right\}, \tag{B.8}$$

with

$$L \equiv \ln \left(\frac{1 + \sqrt{a}}{\sqrt{1-a}} \right), \qquad a \equiv \frac{X}{\nu^2} \left(1 - \frac{4m^2}{s} \right). \tag{B.9}$$

B.2 Spinor QED

The $\gamma^*\gamma^* \to q\bar{q}$ cross sections (with q an electrically charged structureless spin-1/2 particle) to lowest order in α are given by :

$$\sigma_0 + \sigma_2 = \sigma_\parallel + \sigma_\perp = \alpha^2\pi\frac{s^2\nu^3}{X^3}\left\{\sqrt{a}\left[-4\left(1-\frac{X}{s\nu}\right)^2 - (1-a)\right.\right. \tag{B.10}$$

$$\left. + \frac{Q_1^2Q_2^2}{\nu^2}\left(2 - \frac{1}{(1-a)}\,\frac{4X^2}{s^2\nu^2}\right)\right]$$

$$\left. + \left[3 - a^2 + 2\left(1-\frac{2X}{s\nu}\right)^2 - \frac{2Q_1^2Q_2^2}{\nu^2}(1+a)\right]\, L\right\}, \tag{B.11}$$

$$\sigma_\parallel - \sigma_\perp = \alpha^2\frac{\pi}{2}\frac{s^2\nu^3}{X^3}\left\{\sqrt{a}\left[-(1-a) - 2\left(1-\frac{2X}{s\nu}\right)^2\right]\right.$$

$$\left. + \left[-(1-a)^2 + 4(1-a)\left(1-\frac{2X}{s\nu}\right) + \frac{Q_1^2Q_2^2}{\nu^2}\,\frac{8X^2}{s^2\nu^2}\right]\, L\right\}, \tag{B.12}$$

$$\sigma_0 - \sigma_2 = \alpha^2 4\pi\frac{s\nu^2}{X^2}\left\{\sqrt{a}\left[2 - \frac{X}{s\nu} - \frac{Q_1^2Q_2^2}{\nu^2}\frac{1}{(1-a)}\,\frac{X}{s\nu}\right] - 2\left(1-\frac{X}{s\nu}\right)\, L\right\}, \tag{B.13}$$

$$\sigma_{LL} = \alpha^2 2\pi Q_1^2Q_2^2\frac{s^2}{\nu X^2}\left\{\sqrt{a}\left[-2 - \frac{(3-2a)}{(1-a)}\,\frac{Q_1^2Q_2^2}{X}\right] + \left(2 + \frac{3Q_1^2Q_2^2}{X}\right)\, L\right\}, \tag{B.14}$$

$$\sigma_{LT} = \alpha^2\pi Q_1^2\frac{s}{\nu X^2}\left\{\sqrt{a}\left[(\nu - Q_2^2)^2\left(2 + \frac{3Q_1^2Q_2^2}{X}\right) - 2\nu Q_2^2 + Q_2^4\frac{(3-a)}{(1-a)}\right]\right.$$

$$+ \left[(\nu - Q_2^2)^2\left(-2(1-a) - (3-a)\frac{Q_1^2Q_2^2}{X}\right)\right. \tag{B.15}$$

$$\left.\left. + \; 2\nu Q_2^2(1+a) - Q_2^4(3+a)\right]\, L\right\}, \tag{B.16}$$

$$\tau_{TL} = \alpha^2 2\pi\left(Q_1Q_2\right)^3\frac{s}{\nu X^2}\left\{\frac{\sqrt{a}}{1-a} - L\right\}, \tag{B.17}$$

$$\tau_{TL}^a = \alpha^2\pi Q_1Q_2\frac{s^2\nu^2}{X^3}\left\{-\sqrt{a}\left(3 - \frac{4X}{s\nu}\right) + \left(3 - \frac{4X}{s\nu} - a\right)\, L\right\}, \tag{B.18}$$

with

$$L \equiv \ln\left(\frac{1+\sqrt{a}}{\sqrt{1-a}}\right), \qquad a \equiv \frac{X}{\nu^2}\left(1 - \frac{4m^2}{s}\right). \tag{B.19}$$

Appendix C

Radiative corrections in a scalar ϕ^4 theory

The action describing electrodynamics of the charged scalar particle in the dimensional regularization scheme is defined by :

$$\mathcal{S} = \int \mathrm{d}^d x \left[(\partial_\mu \phi)(\partial^\mu \phi)^* - m^2 \phi \phi^* - \frac{1}{4} F_{\mu\nu} F^{\mu\nu} + \right. \tag{C.1}$$

$$\left. ie(\phi \partial_\mu \phi^* - \phi^* \partial_\mu \phi) A^\mu + e^2 A_\mu A^\mu \phi \phi^* - \frac{\lambda}{4} \mu^{4-d} (\phi \phi^*)^2 \right], \tag{C.2}$$

where A_μ and $F_{\mu\nu}$ are the electromagnetic field and its strength tensor, μ is a mass dimension constant and d is a number of dimensions.

C.1 One-loop correction to the scalar propagator

Figure C.1: One-loop correction to the scalar propagator.

According to Feynman rules the contribution of a graph on Fig.(C.1) can be written as

$$i\Pi = -i\lambda\mu^{4-d} \int \frac{d^d p}{(2\pi)^d} \frac{i}{p^2 - m^2} = i \frac{\lambda m^2}{(4\pi)^2} \frac{2}{4-d} + i \frac{\lambda m^2}{(4\pi)^2} \left(1 - \gamma + \ln \frac{4\pi\mu^2}{m^2} \right), \tag{C.3}$$

which is absorbed by a renormalization of mass.

C.2 One-loop correction to the three particle vertex

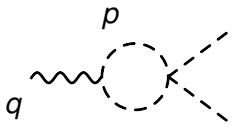

Figure C.2: One-loop correction to the three-point vertex.

Applying Feynman rules to a graph on Fig.(C.2) we obtain

$$i\Gamma_\mu = -e\lambda\mu^{4-d} \int \frac{d^d p}{(2\pi)^d} \frac{(q-2p)_\mu}{(p^2 - m^2)((q-p)^2 - m^2)}. \tag{C.4}$$

Using Feynman parametrization one can transform the loop integral to a spherically symmetric form and perform Wick's rotation which allows to integrate over the momenta in hyper spherical coordinates. As a result we obtain :

$$i\Gamma_\mu = -\frac{\lambda e}{(4\pi)^2} q_\mu \left(\frac{2}{4-d} - \gamma\right) \int_0^1 dz\,(1-2z) \left(\frac{\Delta}{4\pi\mu^2}\right)^{d/2-2}, \tag{C.5}$$

here $\Delta = m^2 + z(1-z)Q^2$ and $Q^2 = -q^2$. It is easy to show that the integral over the Feynman parameter is equal to zero

$$\begin{aligned} &\int_0^1 \mathrm{d}z\,(1-2z) - \frac{4-d}{2} \int_0^1 dz\,(1-2z) \ln\left(\frac{m^2 + Q^2 z(1-z)}{4\pi\mu^2}\right) \\ &\qquad = \frac{4-d}{2} \int_{-1/2}^{1/2} dz\,(-2z) \ln\left(\frac{m^2}{4\pi\mu^2} + \frac{Q^2}{4\pi\mu^2}\left(z+\frac{1}{2}\right)\left(\frac{1}{2}-z\right)\right) = 0, \end{aligned} \tag{C.6}$$

since the integrand is an antisymmetric function of z.

C.3 One-loop correction to the four-scalar vertex

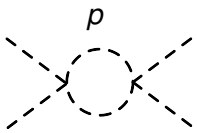

Figure C.3: The one-loop correction to the four-point vertex

In accordance with Feynman rules one can obtain for the graph on Fig. (C.3)

$$-i\lambda^2 \tilde{\mathrm{B}}(s) = \lambda^2 (\mu^2)^{4-d} \int \frac{\mathrm{d}^d p}{(2\pi)^d} \frac{1}{(p^2-m^2)((q_1+q_2-p)^2-m^2)}, \tag{C.7}$$

here we isolate $(-i\lambda)^2$ for convenience. Calculating the loop momentum integral we obtain :

$$\tilde{\mathrm{B}}(s) = -\frac{1}{(4\pi)^2} \left(\frac{2}{\epsilon} - \gamma_E - \int_0^1 \mathrm{d}x \ln\frac{m^2 - sx(1-x)}{4\pi\mu^2}\right). \tag{C.8}$$

The integral over x gives :

$$\begin{aligned} \tilde{\mathrm{B}}(s) = &-\frac{1}{(4\pi)^2}\left(\frac{2}{\epsilon} - \gamma_E + 2 + \ln\frac{4\pi\mu^2}{m^2}\right) \\ &+ \frac{1}{(4\pi)^2}\sqrt{1-\frac{4m^2}{s}}\left(-i\pi + 2\,\mathrm{arctanh}\sqrt{1-\frac{4m^2}{s}}\right). \end{aligned} \tag{C.9}$$

Recollecting the $i\varepsilon$-prescription we ascertain that the physical amplitude is defined on the upper edge of the right-hand cut of the s-plane.

C.4 One-loop correction to the $\gamma\gamma \to S\bar{S}$ vertex

The non-vanishing one-loop corrections to the $\gamma\gamma \to \phi^*\phi$ vertex are shown on Fig. (C.4)

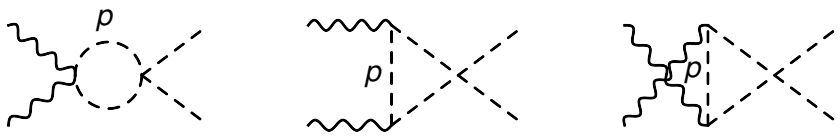

Figure C.4: The $\gamma\gamma \to S\bar{S}$ vertex correction.

The contribution of the first diagram on a Fig. (C.4) is :

$$iM^{\circ}_{\mu\nu} = -2\lambda e^2 \mu^{4-d} g_{\mu\nu} \int \frac{d^d p}{(2\pi)^d} \frac{1}{(p^2 - m^2)((q_1 + q_2 - p)^2 - m^2)}. \tag{C.10}$$

Integrating over the loop momentum we obtain

$$iM^{\circ}_{\mu\nu} = -\frac{2i\lambda e^2}{(4\pi)^2} g_{\mu\nu} \left(\frac{2}{4-d} - \gamma \right) + \frac{2i\lambda e^2}{(4\pi)^2} g_{\mu\nu} \int_0^1 dx \ln \frac{m^2 - sx(1-x)}{4\pi\mu^2}. \tag{C.11}$$

The contribution of the second graphs given by :

$$iM^{\triangle}_{\mu\nu} = \lambda e^2 \mu^{4-d} \int \frac{d^d p}{(2\pi)^d} \frac{(2p + q_1)_\mu (2p - q_2)_\nu}{((q_1 + p)^2 - m^2)((q_2 - p)^2 - m^2)(p^2 - m^2)} \tag{C.12}$$

Integration over the loop momentum gives :

$$\begin{aligned} iM^{\triangle}_{\mu\nu} = \frac{i\lambda e^2}{(4\pi)^2} \int_0^1 dx \int_0^{1-x} dy \Bigg\{ & 2g^{\mu\nu} \left(\frac{2}{4-d} - \gamma - \ln \frac{\Delta}{4\pi\mu^2} \right) \\ & - ((2x-1)q_1^\mu - 2yq_2^\mu)(2xq_1^\nu - (2y-1)q_2^\nu) \frac{1}{\Delta} \Bigg\}, \end{aligned} \tag{C.13}$$

with $\Delta = m^2 - 2xy\nu + Q_1^2 x(1-x) + Q_2^2 y(1-y)$.

In the Lorentz gauge only terms proportional $g^{\mu\nu}$ and $q_1^\nu q_2^\mu$ contribute to the matrix element thus we will omit all not relevant terms in further calculations. The third and the second diagrams on Fig.(**??**) give equal contributions. The total contribution of three diagrams is given by :

$$\begin{aligned} iM^{(1)}_{\mu\nu} = & \frac{4\lambda i e^2}{(4\pi)^2} \int_0^1 dx \int_0^{1-x} dy \left\{ -g_{\mu\nu} \ln \frac{\Delta}{4\pi\mu^2} + q_{2\mu} q_{1\nu} \frac{2xy}{\Delta} \right\} \\ & + \frac{2\lambda i e^2}{(4\pi)^2} g_{\mu\nu} \int_0^1 dx \ln \frac{m^2 - sx(1-x)}{4\pi\mu^2}. \end{aligned} \tag{C.14}$$

Integrating the first term by parts

$$\int_0^{1-x} dy \ln \frac{\Delta}{4\pi\mu^2} = (1-x) \ln \frac{m^2 - sx(1-x)}{4\pi\mu^2} + \int_0^{1-x} dy \frac{y(2x\nu - Q_2^2(1-2y))}{\Delta}, \tag{C.15}$$

one can rearrange this expression as follows

$$\begin{aligned} iM^{(1)}_{\mu\nu} = & -\frac{2\lambda i e^2}{(2\pi)^2} (g_{\mu\nu}\nu - q_{2\mu} q_{1\nu}) \int_0^1 dx \int_0^{1-x} dy \frac{xy}{\Delta} \\ & + \frac{4\lambda i e^2}{(4\pi)^2} Q_2^2 g_{\mu\nu} \int_0^1 dx \int_0^{1-x} dy \frac{y(1-2y)}{\Delta} - \\ & - \frac{2\lambda i e^2}{(4\pi)^2} g_{\mu\nu} \int_0^1 dx (1-2x) \ln \frac{m^2 - sx(1-x)}{4\pi\mu^2}. \end{aligned} \tag{C.16}$$

The third term in (C.16) vanish for the same arguments as (C.6). Thus finally we obtain

$$iM^{(1)}_{\mu\nu} = -ie^2\lambda\,(q_1\cdot q_2 g_{\mu\nu} - q_{2\mu}q_{1\nu})\,\mathrm{I}_1 + ie^2\lambda\, q_1\cdot q_2 g_{\mu\nu}\mathrm{I}_2, \tag{C.17}$$

where the integrals I_1 and I_2 are defined as follows

$$\mathrm{I}_1 = \frac{2}{(2\pi)^2}\int_0^1 dx\int_0^{1-x} dy \frac{xy}{m^2 - 2xy\nu + Q_1^2 x(1-x) + Q_2^2 y(1-y)}, \tag{C.18}$$

$$\mathrm{I}_2 = \frac{Q_2^2}{(2\pi)^2\nu}\int_0^1 dx\int_0^{1-x} dy \frac{y(1-2y)}{\Delta}. \tag{C.19}$$

Introducing form factors

$$F^T = -\mathrm{I}_1 + \mathrm{I}_2 \qquad \text{and} \qquad F^L - F^T = \frac{X}{Q_1^2 Q_2^2}\mathrm{I}_2 \tag{C.20}$$

one can define the amplitude for the $\gamma^*\gamma \to \bar{S}S$ production at one-loop level by :

$$\begin{aligned} iM^{(1)}_{\mu\nu} &= ie^2\lambda\, F^T(\nu, Q_1^2, Q_2^2)\,(q_1\cdot q_2 g_{\mu\nu} - q_{2\mu}q_{1\nu}) \\ &+ ie^2\lambda\,\frac{Q_1^2 Q_2^2}{X}\left(F^L(\nu, Q_1^2, Q_2^2) - F^T(\nu, Q_1^2, Q_2^2)\right) q_{2\mu}q_{1\nu} \end{aligned} \tag{C.21}$$

When one of photons is quasi-real (i.e. $Q_2^2 \to 0$) the integrals (C.18) and (C.19) can be evaluated analytically, which gives the following expressions for form-factors (C.20)

$$\begin{aligned} F^T(s, Q_1^2, 0) = \frac{1}{(2\pi)^2(s+Q_1^2)^2}\Bigg\{ & s + Q_1^2 + 4m^2 \mathrm{arctanh}^2\frac{1}{\beta} + \\ & + 2Q_1^2\beta\,\mathrm{arctanh}\frac{1}{\beta} - m^2\ln^2\frac{\kappa+1}{\kappa-1} - Q_1^2\kappa\ln\frac{\kappa+1}{\kappa-1}\Bigg\}, \end{aligned} \tag{C.22}$$

$$\begin{aligned} F^L(s, Q_1^2, 0) = & \frac{1}{4(2\pi)^2(s+Q_1^2)^2}\Bigg\{ 8(s+Q_1^2) + 4\,\mathrm{arctanh}\frac{1}{\beta}\left[-4s\beta + (s-Q_1^2)\mathrm{arctanh}\frac{1}{\beta}\right] - \\ & - (s-Q_1^2)\ln^2\frac{\kappa+1}{\kappa-1} + 4(s-Q_1^2)\kappa\ln\frac{\kappa+1}{\kappa-1}\Bigg\}, \end{aligned} \tag{C.23}$$

here $\kappa = \sqrt{1 + 4m^2/Q_1^2}$.

Appendix D

Angular integration in $(g-2)_\mu$

In this Appendix we give a complete summary of the three- and four- dimensional angular integration technique.

D.1 Four-dimensional angular integration

The generating function of the Gegenbauer polynomials $C_n^{(1)}(x)$ (hereinafter we use the notation $C_n^{(1)}(x) \equiv C_n(x)$) is given by

$$\frac{1}{z^2-2xz+1} = \sum_{n=0}^{\infty} z^n\, C_n(x), \quad -1 \le x \le 1,\ |z|<1. \tag{D.1}$$

From Eq. (D.1) we immediately obtain the following property under parity transformations $C_n(-x) = (-1)^n C_n(x)$. Furthermore we get $C_n(1) = n+1$. The Gegenbauer polynomials obey the orthogonality conditions

$$\int \mathrm{d}\Omega(\hat{K}) C_n(\hat{Q}_1\cdot\hat{K}) C_m(\hat{K}\cdot\hat{Q}_2) = 2\pi^2 \frac{\delta_{nm}}{n+1} C_n(\hat{Q}_1\cdot\hat{Q}_2) \tag{D.2}$$

$$\int \mathrm{d}\Omega(\hat{K}) C_n(\hat{Q}\cdot\hat{K}) C_m(\hat{K}\cdot\hat{Q}) = 2\pi^2 \delta_{nm}, \tag{D.3}$$

where, for instance, $(\hat{Q}_1\cdot\hat{K})$ is the cosine of the angle between the four-dimensional vectors Q_1 and K. Some low-order cases of the polynomials are listed below

$$C_0(x) = 1, \tag{D.4}$$

$$C_1(x) = 2x, \tag{D.5}$$

$$C_2(x) = 4x^2 - 1, \tag{D.6}$$

$$C_3(x) = 8x^3 - 4x, \tag{D.7}$$

$$C_4(x) = 16x^4 - 12x^2 + 1, \tag{D.8}$$

and therefore

$$Q\cdot K = \frac{1}{2}|Q||K| C_1(\hat{Q}\cdot\hat{K}), \tag{D.9}$$

$$(Q\cdot K)^2 = \frac{1}{4} Q^2K^2 \left[C_2(\hat{Q}\cdot\hat{K}) + 1\right], \tag{D.10}$$

$$(Q\cdot K)^3 = \frac{1}{8} Q^3K^3 \left[C_3(\hat{Q}\cdot\hat{K}) + 2C_1(\hat{Q}\cdot\hat{K})\right], \tag{D.11}$$

$$(Q\cdot K)^4 = \frac{1}{16} Q^4K^4 \left[C_4(\hat{Q}\cdot\hat{K}) + 3C_2(\hat{Q}\cdot\hat{K}) + 2\right]. \tag{D.12}$$

From the generating function, we obtain the following representation of the propagators in Euclidean space:

$$\frac{1}{(K-L)^2+M^2} = \frac{Z^M_{KL}}{|K||L|}\sum_{n=0}^{\infty}\left(Z^M_{KL}\right)^n C_n(\hat{K}\cdot\hat{L}) \tag{D.13}$$

$$\frac{1}{(K+L)^2+M^2} = \frac{Z^M_{KL}}{|K||L|}\sum_{n=0}^{\infty}\left(-Z^M_{KL}\right)^n C_n(\hat{K}\cdot\hat{L}) \tag{D.14}$$

$$Z^M_{KL} = \frac{K^2+L^2+M^2-\sqrt{(K^2+L^2+M^2)^2-4K^2L^2}}{2|K||L|} \tag{D.15}$$

$$\tag{D.16}$$

Note that we have to choose the negative sign in front of the square root in Z^M_{KL} in order that $|Z^M_{KL}|<1$. For a massless propagator these expressions simplify as follows:

$$\frac{1}{(K-L)^2} = \frac{1}{K^2}\sum_{n=0}^{\infty}\left(\frac{|L|}{|K|}\right)^n C_n(\hat{K}\cdot\hat{L}),\ \text{for}\ |K|>|L| \tag{D.17}$$

A set of simplest integrals similar to the one considered in Section 4.2.3 is listed below

$$\begin{aligned} I^M_1 &= \int\frac{\mathrm{d}\Omega(Q_1)}{2\pi^2}\int\frac{\mathrm{d}\Omega(Q_2)}{2\pi^2}\frac{1}{D_m D_4 D_5} = -\frac{1}{P^2Q_1^2Q_2^2}\ln\left(1-Z^M_{Q_1Q_2}Z^m_{PQ_1}Z^m_{PQ_2}\right)\\ &= \frac{1}{m^2Q_1^2Q_2^2}\ln\left[1+\frac{(M^2+Q_1^2+Q_2^2-R^M)(Q_1^2-R_1^m)(Q_2^2-R_2^m)}{8m^2Q_1^2Q_2^2}\right], \end{aligned} \tag{D.18}$$

$$\begin{aligned} I_2 &= \int\frac{\mathrm{d}\Omega(Q_1)}{2\pi^2}\int\frac{\mathrm{d}\Omega(Q_2)}{2\pi^2}\frac{1}{D_4 D_5} = \frac{Z^m_{PQ_1}Z^m_{PQ_2}}{P^2Q_1Q_2}\\ &= \frac{(Q_1^2-R_1^m)(Q_2^2-R_2^m)}{4m^4Q_1^2Q_2}, \end{aligned} \tag{D.19}$$

$$\begin{aligned} I^M_3 &= \int\frac{\mathrm{d}\Omega(Q_1)}{2\pi^2}\int\frac{\mathrm{d}\Omega(Q_2)}{2\pi^2}\frac{1}{D_M D_4} = \frac{Z^M_{Q_1Q_2}Z^m_{PQ_1}}{PQ_1^2Q_2}\\ &= \frac{(M^2+Q_1^2+Q_2^2-R^M)(Q_1^2-R_1^m)}{4m^4Q_1^2Q_2}, \end{aligned} \tag{D.20}$$

$$\begin{aligned} I^M_4 &= \int\frac{\mathrm{d}\Omega(Q_1)}{2\pi^2}\int\frac{\mathrm{d}\Omega(Q_2)}{2\pi^2}\frac{1}{D_M D_5} = \frac{Z^M_{Q_1Q_2}Z^m_{PQ_2}}{PQ_1Q_2^2}\\ &= \frac{(M^2+Q_1^2+Q_2^2-R^M)(Q_2^2-R_2^m)}{4m^4Q_1^2Q_2}, \end{aligned} \tag{D.21}$$

$$I_5 = \int\frac{\mathrm{d}\Omega(Q_1)}{2\pi^2}\int\frac{\mathrm{d}\Omega(Q_2)}{2\pi^2}\frac{1}{D_4} = \frac{Z^m_{PQ_1}}{PQ_1} = -\frac{Q_1^2-R_1^m}{2m^2Q_1^2}, \tag{D.22}$$

$$I_6 = \int\frac{\mathrm{d}\Omega(Q_1)}{2\pi^2}\int\frac{\mathrm{d}\Omega(Q_2)}{2\pi^2}\frac{1}{D_5} = \frac{Z^m_{PQ_2}}{PQ_2} = -\frac{Q_2^2-R_2^m}{2m^2Q_2^2}, \tag{D.23}$$

$$I_7 = \int\frac{\mathrm{d}\Omega(Q_1)}{2\pi^2}\int\frac{\mathrm{d}\Omega(Q_2)}{2\pi^2}\frac{1}{D_M} = \frac{Z^M_{Q_1Q_2}}{Q_1Q_2} = \frac{M^2+Q_1^2+Q_2^2-R^M}{2Q_1^2Q_2^2} \tag{D.24}$$

where the following abbreviations for the propagators in the loop integral are introduced:

$$D_1 = Q_1^2, \qquad D_2 = Q_2^2, \qquad D_3 = (Q_1+Q_2)^2, \qquad D_4 = (P+Q_1)^2+m^2, \tag{D.25}$$

$$D_5 = (P-Q_2)^2+m^2, \qquad D_M = (Q_1+Q_2)^2+M^2. \tag{D.26}$$

Other integrals that occur during the calculation, involve extra scalar products in the numerator. First, the integrands may be reduced by noting that $D_3 = Q_1^2 + Q_2^2 + 2(Q_1 \cdot Q_2)$, $D_4 = Q_1^2 + 2(P \cdot Q_1)$ and $D_5 = Q_2^2 - 2(P \cdot Q_2)$. After that using Eq. (D.9), (D.9) we may rewrite the residual scalar products in the numerator in terms of Gegenbauer polynomials. As a result, with the help of the identities

$$\begin{aligned}(Z^M_{Q_1Q_2})^2 &= \frac{M^2+Q_1^2+Q_2^2}{Q_1Q_2} Z^M_{Q_1Q_2} - 1,\\ (Z^m_{PQ_i})^2 &= \frac{m^2+P^2+Q_i^2}{PQ_i} Z^m_{PQ_i} - 1,\end{aligned} \tag{D.27}$$

we can reduce the integrals to the basic ones. In this way we obtain, for $P^2 = -m^2$:

$$\begin{aligned}\int \frac{\mathrm{d}\Omega(Q_1)}{2\pi^2} \int \frac{\mathrm{d}\Omega(Q_2)}{2\pi^2} \frac{Q_1\cdot P\, Q_2\cdot P}{D_\Lambda} &= -\frac{\left(Z^\Lambda_{Q_1Q_2}\right)^2 P^2}{8}\\ &= \frac{m^2}{8}\left[\left(\Lambda^2+Q_1^2+Q_2^2\right) I_7^\Lambda - 1\right], \end{aligned} \tag{D.28}$$

$$\int \frac{\mathrm{d}\Omega(Q_1)}{2\pi^2} \int \frac{\mathrm{d}\Omega(Q_2)}{2\pi^2} \frac{(Q_1\cdot P)}{D_5 D_\Lambda} = -\frac{\left(Z^\Lambda_{Q_1Q_2} Z^m_{PQ_2}\right)^2 |Q_1||P|}{4Q_2^2}, \tag{D.29}$$

$$\int \frac{\mathrm{d}\Omega(Q_1)}{2\pi^2} \int \frac{\mathrm{d}\Omega(Q_2)}{2\pi^2} \frac{Q_1\cdot P}{D_\Lambda} = 0, \tag{D.30}$$

$$\int \frac{\mathrm{d}\Omega(Q_1)}{2\pi^2} \int \frac{\mathrm{d}\Omega(Q_2)}{2\pi^2} \frac{Q_1\cdot P}{(P-Q_2)^2+m^2} = 0, \tag{D.31}$$

$$\begin{aligned}\int \frac{\mathrm{d}\Omega(Q_1)}{2\pi^2} \int \frac{\mathrm{d}\Omega(Q_2)}{2\pi^2} \frac{(Q_1\cdot P)^2}{D_5 D_\Lambda} &= \frac{Z^\Lambda_{Q_1Q_2} Z^m_{PQ_2}|Q_1||P|}{4Q_2^2}\left[\frac{\left(Z^\Lambda_{Q_1Q_2} Z^m_{PQ_2}\right)^2}{3} + 1\right]\\ &= \frac{1}{12}\left[\frac{1}{Q_2^2}\left(\left(\Lambda^2+Q_1^2+Q_2^2\right)^2\left(M^2+Q_2^2\right)\right.\right.\\ &\quad - Q_1^2Q_2^4\left(1+4M^2/Q_2^2\right)\Big) I_4^\Lambda\\ &\quad -\frac{1}{Q_2^2}\left(\left(\Lambda^2+Q_1^2+Q_2^2\right)^2 - Q_1^2Q_2^2\right) I_7^\Lambda\\ &\quad - \left(\Lambda^2+Q_1^2+Q_2^2\right)\left(\frac{M^2}{Q_2^2}+1\right) I_6\\ &\quad \left.+\frac{\Lambda^2+Q_1^2+Q_2^2}{Q_2^2}\right], \end{aligned} \tag{D.32}$$

$$\int \frac{\mathrm{d}\Omega(Q_1)}{2\pi^2} \int \frac{\mathrm{d}\Omega(Q_2)}{2\pi^2} \frac{(Q_1\cdot P)^2}{D_\Lambda} = \frac{Z^\Lambda_{Q_1Q_2}|Q_1|P^2}{4|Q_2|} = \frac{P^2|Q_1|^2}{4} I_7^\Lambda, \tag{D.33}$$

$$\begin{aligned}\int \frac{\mathrm{d}\Omega(Q_1)}{2\pi^2} \int \frac{\mathrm{d}\Omega(Q_2)}{2\pi^2} \frac{(Q_1\cdot P)^3}{D_5 D_\Lambda} &= -\frac{|Q_1|^2|P|^2}{8Q_2^2}\left(Z^\Lambda_{Q_1Q_2} Z^m_{PQ_2}\right)^2\\ &\quad \times\left[\frac{\left(Z^\Lambda_{Q_1Q_2} Z^m_{PQ_2}\right)^2}{4} + 1\right], \end{aligned} \tag{D.34}$$

$$\int \frac{\mathrm{d}\Omega(Q_1)}{2\pi^2} \int \frac{\mathrm{d}\Omega(Q_2)}{2\pi^2} \frac{(Q_1\cdot P)^3}{D_\Lambda} = 0, \tag{D.35}$$

$$\int \frac{\mathrm{d}\Omega(Q_1)}{2\pi^2} \int \frac{\mathrm{d}\Omega(Q_2)}{2\pi^2} \frac{(Q_1\cdot P)^4}{D_5 D_\Lambda} = \frac{|Q_1|^3|P|^3}{16Q_2^2} \left(Z^\Lambda_{Q_1Q_2} Z^m_{PQ_2}\right) \times \left[\frac{\left(Z^\Lambda_{Q_1Q_2} Z^m_{PQ_2}\right)^4}{5} + \left(Z^\Lambda_{Q_1Q_2} Z^m_{PQ_2}\right)^2 + 2\right], \tag{D.36}$$

$$\int \frac{\mathrm{d}\Omega(Q_1)}{2\pi^2} \int \frac{\mathrm{d}\Omega(Q_2)}{2\pi^2} \frac{(Q_1\cdot P)^4}{D_\Lambda} = \frac{Z^\Lambda_{Q_1Q_2}|Q_1|^3P^4}{8|Q_2|}, \tag{D.37}$$

$$\int \frac{\mathrm{d}\Omega(Q_1)}{2\pi^2} \int \frac{\mathrm{d}\Omega(Q_2)}{2\pi^2} \frac{(Q_1\cdot P)^4}{(P-Q_2)^2+\Lambda^2} = \frac{Z^\Lambda_{PQ_2}|Q_1|^4P^3}{8|Q_2|}. \tag{D.38}$$

D.2 Three-dimensional angular integration

The Legendre polynomials obey the orthogonality relations which read

$$\int \frac{\mathrm{d}\Omega(\hat{\mathbf{Q}})}{4\pi} P_n(\hat{\mathbf{Q}}_1\cdot\hat{\mathbf{K}}) P_m(\hat{\mathbf{K}}\cdot\hat{\mathbf{Q}}_2) = \delta_{nm}\frac{P_n(\hat{\mathbf{Q}}_1\cdot\hat{\mathbf{Q}}_2)}{2n+1} \tag{D.39}$$

and

$$\int \frac{\mathrm{d}\Omega(\hat{\mathbf{Q}})}{4\pi} P_n(\hat{\mathbf{Q}}_1\cdot\hat{\mathbf{Q}}_2) P_m(\hat{\mathbf{Q}}_1\cdot\hat{\mathbf{Q}}_2) = \frac{\delta_{nm}}{2n+1} \tag{D.40}$$

where, for instance, $(\hat{\mathbf{Q}}_1\cdot\hat{\mathbf{K}})$ is the cosine of the angle between the three-dimensional vectors $\mathbf{Q}_1$ and $\mathbf{K}$. Some low-order cases of the Legendre polynomials and functions are given below

$$Q_0(x) = \frac{1}{2}\ln\frac{x+1}{x-1}, \tag{D.41}$$

$$Q_1(x) = \frac{x}{2}\ln\frac{x+1}{x-1} - 1, \tag{D.42}$$

$$Q_2(x) = \frac{1}{4}(3x^2-1)\ln\frac{x+1}{x-1} - \frac{3}{2}x, \tag{D.43}$$

$$Q_3(x) = \frac{1}{4}(5x^2-3)x\ln\frac{x+1}{x-1} - \frac{1}{6}(15x^2-4), \tag{D.44}$$

showing the even order functions to be odd in x and conversely, and

$$P_0(x) = 1, \tag{D.45}$$

$$P_1(x) = x, \tag{D.46}$$

$$P_2(x) = \frac{1}{2}(3x^2-1), \tag{D.47}$$

$$P_3(x) = \frac{1}{2}(5x^3-3x). \tag{D.48}$$

The expansion of the denominator in Eq. (4.82) may be derived by exploiting the orthogonality property. Our task here is to calculate

$$\frac{1}{\Delta - (\hat{\mathbf{K}}\cdot\hat{\mathbf{L}})} = \sum_{n=0}^{\infty} C_n(\Delta) P_n(\hat{\mathbf{K}}\cdot\hat{\mathbf{L}}). \tag{D.49}$$

Using the orthogonality we can write:

$$C_n(\Delta) = \frac{2n+1}{4\pi} \int \mathrm{d}\Omega(\hat{L}) \frac{P_n(\hat{\mathbf{K}} \cdot \hat{\mathbf{L}})}{\Delta - \hat{\mathbf{K}} \cdot \hat{\mathbf{L}}} = (2n+1) Q_n(\Delta), \tag{D.50}$$

where we used the integral

$$\int_{-1}^{1} \mathrm{d}x \frac{P_n(x)}{x - z} = -2 Q_n(z), \tag{D.51}$$

for $z \notin [-1, 1]$. Here $Q_n(x)$ is a Legendre function of the second kind. The integral representation for $Q_n(z)$ is

$$Q_n(z) = \frac{1}{2} \int_{-1}^{1} \frac{\mathrm{d}t}{(z-t)} \left[\frac{1-t^2}{2(z-t)} \right]^n. \tag{D.52}$$

With the help of Eq. (D.50) we can write:

$$\frac{1}{\Delta - (\hat{\mathbf{K}} \cdot \hat{\mathbf{L}})} = \sum_{n=0}^{\infty} (2n+1) Q_n(\Delta) P_n(\hat{\mathbf{K}} \cdot \hat{\mathbf{L}}), \tag{D.53}$$

Applied to a denominator of a propagator together with the orthogonality relation (D.40), this gives

$$\begin{aligned} \int \frac{\mathrm{d}\Omega(\mathbf{Q_1})}{4\pi} \frac{P_i(\hat{\mathbf{Q}}_\mathbf{1} \cdot \hat{\mathbf{Q}}_\mathbf{2})}{(Q_1+Q_2)^2 + \Lambda^2} &= \int \frac{\mathrm{d}\Omega(\mathbf{Q_1})}{4\pi} \frac{P_i(\hat{\mathbf{Q}}_\mathbf{1} \cdot \hat{\mathbf{Q}}_\mathbf{2})}{2(\mathbf{Q_1} \cdot \mathbf{Q_2}) + 2E_1E_2 + Q_1^2 + Q_2^2 + \Lambda^2} \\ &= \int \frac{\mathrm{d}\Omega(\mathbf{Q_1})}{4\pi} \sum_{n=0}^{\infty} (-1)^n \frac{2n+1}{2|\mathbf{Q_1}||\mathbf{Q_2}|} Q_n\left(R_\Lambda\right) P_n(\hat{\mathbf{Q}}_\mathbf{1} \cdot \hat{\mathbf{Q}}_\mathbf{2}) P_i(\hat{\mathbf{Q}}_\mathbf{1} \cdot \hat{\mathbf{Q}}_\mathbf{2}) \\ &= \frac{(-1)^i}{2|\mathbf{Q_1}||\mathbf{Q_2}|} Q_i\left(R_\Lambda\right) = \frac{(-1)^i}{2Q_1Q_2 \sin\psi_1 \sin\psi_2} Q_i\left(R_\Lambda\right) \end{aligned} \tag{D.54}$$

with

$$R_\Lambda = \frac{2E_1E_2 + Q_1^2 + Q_2^2 + \Lambda^2}{2|\mathbf{Q_1}||\mathbf{Q_2}|} = \frac{2Q_1Q_2\cos\psi_1\cos\psi_2 + Q_1^2 + Q_2^2 + \Lambda^2}{2Q_1Q_2\sin\psi_1\sin\psi_2}. \tag{D.55}$$

The second type of integrals involves factors $\left[(Q_1 \cdot Q_2)^2 - Q_1^2 Q_2^2\right]^{-2}$. In this case the answer can be obtained as a derivative of the known integral over a parameter:

$$\frac{1}{[(Q_1+Q_2)^2 + \Lambda^2]^2} = -\frac{\partial}{\partial \Lambda^2} \frac{1}{(Q_1+Q_2)^2 + \Lambda^2}. \tag{D.56}$$

For example:

$$\int \frac{\mathrm{d}\Omega(\mathbf{Q_1})}{4\pi} \frac{P_i(\hat{\mathbf{Q}}_\mathbf{1} \cdot \hat{\mathbf{Q}}_\mathbf{2})}{[(Q_1+Q_2)^2 + \Lambda^2]^2} = \frac{(-1)^{i+1}}{2|\mathbf{Q_1}||\mathbf{Q_2}|} \lim_{\Lambda \to 0} \frac{\partial}{\partial \Lambda^2} Q_i \left(\frac{2E_1E_2 + Q_1^2 + Q_2^2 + \Lambda^2}{2|\mathbf{Q_1}||\mathbf{Q_2}|} \right). \tag{D.57}$$

A full list of the integrals appearing in the calculation is written out below:

$$\int \frac{\mathrm{d}\Omega(\mathbf{Q_1})}{4\pi} \frac{1}{(Q_1+Q_2)^2+\Lambda^2} = \frac{1}{4|\mathbf{Q_1}||\mathbf{Q_2}|} \ln\left(\frac{R_\Lambda+1}{R_\Lambda-1}\right), \tag{D.58}$$

$$\int \frac{\mathrm{d}\Omega(\mathbf{Q_1})}{4\pi} \frac{P_1(\hat{\mathbf{Q_1}}\cdot\hat{\mathbf{Q_2}})}{(Q_1+Q_2)^2+\Lambda^2} = -\frac{1}{4|\mathbf{Q_1}||\mathbf{Q_2}|} \left[-2+R_\Lambda \ln\left(\frac{R_\Lambda+1}{R_\Lambda-1}\right)\right], \tag{D.59}$$

$$\int \frac{\mathrm{d}\Omega(\mathbf{Q_1})}{4\pi} \frac{P_2(\hat{\mathbf{Q_1}}\cdot\hat{\mathbf{Q_2}})}{(Q_1+Q_2)^2+\Lambda^2} = \frac{1}{8|\mathbf{Q_1}||\mathbf{Q_2}|} \left[-6R_\Lambda+(3R_\Lambda^2-1)\ln\left(\frac{R_\Lambda+1}{R_\Lambda-1}\right)\right], \tag{D.60}$$

$$\begin{aligned}\int \frac{\mathrm{d}\Omega(\mathbf{Q_1})}{4\pi} \frac{P_3(\hat{\mathbf{Q_1}}\cdot\hat{\mathbf{Q_2}})}{(Q_1+Q_2)^2+\Lambda^2} &= -\frac{1}{24|\mathbf{Q_1}||\mathbf{Q_2}|} \left[8-30R_\Lambda^2\right. \\ &\left.+3R_\Lambda(5R_\Lambda^2-3)\ln\left(\frac{R_\Lambda+1}{R_\Lambda-1}\right)\right],\end{aligned} \tag{D.61}$$

$$\int \frac{\mathrm{d}\Omega(\mathbf{Q_1})}{4\pi} \frac{1}{[(Q_1+Q_2)^2+\Lambda^2]^2} = \frac{1}{4|\mathbf{Q_1}|^2|\mathbf{Q_2}|^2} \frac{1}{R_\Lambda^2-1}, \tag{D.62}$$

$$\int \frac{\mathrm{d}\Omega(\mathbf{Q_1})}{4\pi} \frac{P_1(\hat{\mathbf{Q_1}}\cdot\hat{\mathbf{Q_2}})}{[(Q_1+Q_2)^2+\Lambda^2]^2} = \frac{1}{8|\mathbf{Q_1}|^2|\mathbf{Q_2}|^2} \left[\ln\left(\frac{R_\Lambda+1}{R_\Lambda-1}\right)-\frac{2R_\Lambda}{R_\Lambda^2-1}\right], \tag{D.63}$$

$$\begin{aligned}\int \frac{\mathrm{d}\Omega(\mathbf{Q_1})}{4\pi} \frac{P_2(\hat{\mathbf{Q_1}}\cdot\hat{\mathbf{Q_2}})}{[(Q_1+Q_2)^2+\Lambda^2]^2} &= -\frac{1}{8|\mathbf{Q_1}|^2|\mathbf{Q_2}|^2} \left[-6+3R_\Lambda \ln\left(\frac{R_\Lambda+1}{R_\Lambda-1}\right)\right. \\ &\left.-\frac{2}{R_\Lambda^2-1}\right],\end{aligned} \tag{D.64}$$

$$\begin{aligned}\int \frac{\mathrm{d}\Omega(\mathbf{Q_1})}{4\pi} \frac{P_3(\hat{\mathbf{Q_1}}\cdot\hat{\mathbf{Q_2}})}{[(Q_1+Q_2)^2+\Lambda^2]^2} &= \frac{1}{16|\mathbf{Q_1}|^2|\mathbf{Q_2}|^2} \left[-30R_\Lambda\right. \\ &\left.+(15R_\Lambda^2-3)\ln\left(\frac{R_\Lambda+1}{R_\Lambda-1}\right)-\frac{4R_\Lambda}{R_\Lambda^2-1}\right].\end{aligned} \tag{D.65}$$

The integrations appearing when performing the averaging over the direction of K may be performed in a similar way. We can rearrange the denominators by partial fraction decomposition, with the result that

$$\frac{1}{(Q_1\cdot Q_2)^2-Q_1^2Q_2^2} = \frac{1}{2Q_1Q_2}\left[\frac{1}{(Q_1\cdot Q_2)-Q_1Q_2}-\frac{1}{(Q_1\cdot Q_2)+Q_1Q_2}\right] \tag{D.66}$$

and

$$\frac{(Q_1\cdot Q_2)}{(Q_1\cdot Q_2)^2-Q_1^2Q_2^2} = \frac{1}{2}\left[\frac{1}{(Q_1\cdot Q_2)-Q_1Q_2}+\frac{1}{(Q_1\cdot Q_2)+Q_1Q_2}\right]. \tag{D.67}$$

We next exploit Eqs. (D.48) to express the numerator of the integrand in terms of the Legendre polynomials. Finally, a straightforward calculation yields:

$$\int \frac{\mathrm{d}\Omega(\hat{\mathbf{K}})}{4\pi} \frac{(Q_1\cdot k)(Q_2\cdot k)}{(Q_2\cdot k)^2-K^2Q_2^2} = \frac{|\mathbf{Q_1}|}{|\mathbf{Q_2}|}\left[1-\frac{Q_2}{2|\mathbf{Q_2}|}\ln\left(\frac{Q_2+|\mathbf{Q_2}|}{Q_2-|\mathbf{Q_2}|}\right)\right] P_1(\hat{\mathbf{Q_1}}\cdot\hat{\mathbf{Q_2}}), \tag{D.68}$$

$$\int \frac{\mathrm{d}\Omega(\hat{\mathbf{K}})}{4\pi} \frac{(Q_1\cdot k)^2}{(Q_2\cdot k)^2 - K^2Q_2^2} = \frac{1}{6}\frac{|\mathbf{Q_1}|^2}{Q_2|\mathbf{Q_2}|}\left[-\ln\left(\frac{Q_2+|\mathbf{Q_2}|}{Q_2-|\mathbf{Q_2}|}\right) + 6\frac{Q_2}{|\mathbf{Q_2}|}P_2(\hat{\mathbf{Q_1}}\cdot\hat{\mathbf{Q_2}})\right.$$
$$\left. - \frac{3Q_2^2-|\mathbf{Q_2}|^2}{|\mathbf{Q_2}|^2}\ln\left(\frac{Q_2+|\mathbf{Q_2}|}{Q_2-|\mathbf{Q_2}|}\right)P_2(\hat{\mathbf{Q_1}}\cdot\hat{\mathbf{Q_2}})\right], \tag{D.69}$$

$$\int \frac{\mathrm{d}\Omega(\hat{\mathbf{K}})}{4\pi}\frac{1}{k^2}\frac{(Q_2\cdot k)(Q_1\cdot k)^3}{(Q_2\cdot k)^2 - K^2Q_2^2} = \frac{3}{10}\frac{|\mathbf{Q_1}|^3}{|\mathbf{Q_2}|}\left[\frac{Q_2}{|\mathbf{Q_2}|}\ln\left(\frac{Q_2+|\mathbf{Q_2}|}{Q_2-|\mathbf{Q_2}|}\right) - 2\right]P_1(\hat{\mathbf{Q_1}}\cdot\hat{\mathbf{Q_2}})$$
$$+\frac{1}{30}\frac{|\mathbf{Q_1}|^3}{|\mathbf{Q_2}|}\left[3\frac{Q_2}{|\mathbf{Q_2}|}\frac{5Q_2^2-3|\mathbf{Q_2}|^2}{|\mathbf{Q_2}|^2}\ln\left(\frac{Q_2+|\mathbf{Q_2}|}{Q_2-|\mathbf{Q_2}|}\right)\right.$$
$$\left.+\frac{8|\mathbf{Q_2}|^2-30Q_2^2}{|\mathbf{Q_2}|^2}\right]P_3(\hat{\mathbf{Q_1}}\cdot\hat{\mathbf{Q_2}}). \tag{D.70}$$

For squared denominators we use the same approach as previously. In other words, we exploit relation

$$\begin{aligned}\frac{1}{\left[(Q_1\cdot Q_2)^2 - Q_1^2Q_2^2\right]^2} &= \lim_{\Lambda\to 0}\frac{1}{\left[(Q_1\cdot Q_2)^2 - Q_1^2(Q_2+\Lambda)^2\right]^2}\\ &= \frac{1}{2Q_1^2Q_2}\lim_{\Lambda\to 0}\frac{\partial}{\partial\Lambda}\frac{1}{(Q_1\cdot Q_2)^2 - Q_1^2(Q_2+\Lambda)^2}.\end{aligned} \tag{D.71}$$

Applied to the integrands, this gives

$$\int \frac{\mathrm{d}\Omega(\hat{\mathbf{K}})}{4\pi}\frac{(Q_1\cdot k)(Q_2\cdot k)k^2}{\left[(Q_2\cdot k)^2 - K^2Q_2^2\right]^2} = \frac{|\mathbf{Q_1}|}{2Q_2|\mathbf{Q_2}|^2}P_1(\hat{\mathbf{Q_1}}\cdot\hat{\mathbf{Q_2}})\left[\frac{1}{2}\ln\left(\frac{Q_2+|\mathbf{Q_2}|}{Q_2-|\mathbf{Q_2}|}\right)\right.$$
$$\left. - \frac{|\mathbf{Q_2}|Q_2}{Q_2^2-|\mathbf{Q_2}|^2}\right], \tag{D.72}$$

$$\int \frac{\mathrm{d}\Omega(\hat{\mathbf{K}})}{4\pi}\frac{(Q_1\cdot k)^2k^2}{\left[(Q_2\cdot k)^2 - K^2Q_2^2\right]^2} = -\frac{|\mathbf{Q_1}|^2}{6Q_2^3|\mathbf{Q_2}|}\left[\frac{1}{2}\ln\left(\frac{Q_2+|\mathbf{Q_2}|}{Q_2-|\mathbf{Q_2}|}\right) + \frac{Q_2|\mathbf{Q_2}|}{Q_2^2-|\mathbf{Q_2}|^2}\right.$$
$$- \frac{3Q_2^2+|\mathbf{Q_2}|^2}{|\mathbf{Q_2}|^2}\frac{1}{2}\ln\left(\frac{Q_2+|\mathbf{Q_2}|}{Q_2-|\mathbf{Q_2}|}\right)P_2(\hat{\mathbf{Q_1}}\cdot\hat{\mathbf{Q_2}})$$
$$\left. + \frac{3Q_2^2-|\mathbf{Q_2}|^2}{|\mathbf{Q_2}|^2}\frac{Q_2|\mathbf{Q_2}|}{Q_2^2-|\mathbf{Q_2}|^2}P_2(\hat{\mathbf{Q_1}}\cdot\hat{\mathbf{Q_2}})\right], \tag{D.73}$$

$$\int \frac{\mathrm{d}\Omega(\hat{\mathbf{K}})}{4\pi}\frac{(Q_2\cdot k)(Q_1\cdot k)^3}{[(Q_2\cdot k)^2 - K^2Q_2^2]^2} = -\frac{3}{10}\frac{|\mathbf{Q_1}|^3}{|\mathbf{Q_2}|^2Q_2}\left[\frac{1}{2}\ln\left(\frac{Q_2+|\mathbf{Q_2}|}{Q_2-|\mathbf{Q_2}|}\right)\right.$$
$$\left. - \frac{|\mathbf{Q_2}|Q_2}{Q_2^2-|\mathbf{Q_2}|^2}\right]P_1(\hat{\mathbf{Q_1}}\cdot\hat{\mathbf{Q_2}})$$
$$- \frac{1}{20}\frac{|\mathbf{Q_1}|^3}{|\mathbf{Q_2}|^3}\left[3\frac{5Q_2^2-|\mathbf{Q_2}|^2}{|\mathbf{Q_2}|Q_2}\ln\left(\frac{Q_2+|\mathbf{Q_2}|}{Q_2-|\mathbf{Q_2}|}\right)\right.$$
$$\left. -2\frac{15Q_2^2-13|\mathbf{Q_2}|^2}{Q_2^2-|\mathbf{Q_2}|^2}\right]P_3(\hat{\mathbf{Q_1}}\cdot\hat{\mathbf{Q_2}}). \tag{D.74}$$

Appendix E

Two-loop scalar vertex function in the Hyperspherical approach

Hyperspherical approach. The contribution of the first diagram on Fig.(E.1) is

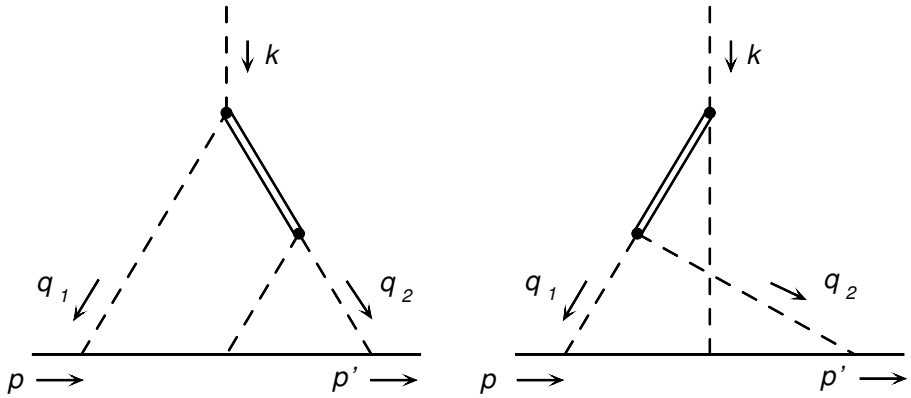

Figure E.1: The two-loop correction to a vertex function in a scalar ϕ^3 theory.

$$F(0) = -i \int \frac{\mathrm{d}^4 q_1}{(2\pi)^4} \int \frac{\mathrm{d}^4 q_2}{(2\pi)^4} \frac{1}{q_1^2 - M^2} \frac{1}{q_1^2 - \Lambda_1^2} \frac{1}{q_2^2 - \Lambda_2^2} \times \frac{1}{(p+q_1)^2 - m^2} \frac{1}{(p-q_2)^2 - m^2} \frac{1}{(q_1+q_2)^2 - \Lambda_3^2}. \tag{E.1}$$

After Wick rotation $E_i^0 \to i E_i^0$:

$$F(0) = i \int \frac{\mathrm{d}^4 Q_1}{(2\pi)^4} \int \frac{\mathrm{d}^4 Q_2}{(2\pi)^4} \frac{1}{Q_1^2 + M^2} \frac{1}{Q_1^2 + \Lambda_1^2} \frac{1}{Q_2^2 + \Lambda_2^2} \times \frac{1}{(P+Q_1)^2 + m^2} \frac{1}{(P-Q_2)^2 + m^2} \frac{1}{(Q_1+Q_2)^2 + \Lambda_3^2}. \tag{E.2}$$

Changing integral measure to the hypesherical coordinates:

$$F(0) = \frac{i}{4(2\pi)^4} \int \mathrm{d}Q_1\, Q_1^3 \int \mathrm{d}Q_2\, Q_2^3 \int \frac{\mathrm{d}\Omega(Q_1)}{2\pi^2} \int \frac{\mathrm{d}\Omega(Q_2)}{2\pi^2} \frac{1}{Q_1^2 + M^2} \frac{1}{Q_1^2 + \Lambda_1^2} \frac{1}{Q_2^2 + \Lambda_2^2} \times \frac{1}{(P+Q_1)^2 + m^2} \frac{1}{(P-Q_2)^2 + m^2} \frac{1}{(Q_1+Q_2)^2 + \Lambda_3^2}. \tag{E.3}$$

Using properties of Gegenbauer polynomials we have for the first diagram:

$$F(0) = \frac{i}{4(2\pi)^4}\int \mathrm{d}Q_1 \int \mathrm{d}Q_2 \, \frac{Q_1^3}{Q_1^2+\Lambda_1^2}\frac{Q_2^3}{Q_2^2+\Lambda_2^2}\frac{1}{Q_1^2+M^2} \times\frac{1}{m^2Q_1^2Q_2^2}\ln\left[1+\frac{(\Lambda_3^2+Q_1^2+Q_2^2-R^{\Lambda_3})(Q_1^2-R_1^m)(Q_2^2-R_2^m)}{8m^2Q_1^2Q_2^2}\right]. \tag{E.4}$$

For the third diagram it takes form:

$$\begin{aligned} F(0) =& \frac{i}{4(2\pi)^4}\int \mathrm{d}Q_1 \int \mathrm{d}Q_2 \int \frac{\mathrm{d}\Omega(Q_1)}{2\pi^2}\int \frac{\mathrm{d}\Omega(Q_2)}{2\pi^2} Q_1^3Q_2^3 \frac{1}{Q_1^2+\Lambda_1^2}\frac{1}{Q_2^2+\Lambda_2^2} \\ &\times \frac{1}{(P+Q_1)^2+m^2}\frac{1}{(P-Q_2)^2+m^2}\frac{1}{(Q_1+Q_2)^2+\Lambda_3^2}\frac{1}{(Q_1+Q_2)^2+M^2}. \end{aligned} \tag{E.5}$$

Fractional decomposition of the denominator yields

$$\begin{aligned} F(0) =& \frac{i}{4(2\pi)^4}\int \mathrm{d}Q_1 \int \mathrm{d}Q_2 \int \frac{\mathrm{d}\Omega(Q_1)}{2\pi^2}\int \frac{\mathrm{d}\Omega(Q_2)}{2\pi^2} Q_1^3Q_2^3 \frac{1}{Q_1^2+\Lambda_1^2}\frac{1}{Q_2^2+\Lambda_2^2} \\ &\times \frac{1}{(P+Q_1)^2+m^2}\frac{1}{(P-Q_2)^2+m^2}\frac{1}{M^2-\lambda^2}\left[\frac{1}{(Q_1+Q_2)^2+\Lambda_3^2}-\frac{1}{(Q_1+Q_2)^2+M^2}\right] \end{aligned} \tag{E.6}$$

which can be easily integrated using orthogonality relations of Eq. D.2 and power expansions of Eq. (D.13, D.14)

$$\begin{aligned} F(0) = \frac{i}{4(2\pi)^4}\int \mathrm{d}Q_1 \int \mathrm{d}Q_2 \, & \frac{Q_1^3}{Q_1^2+\Lambda_1^2}\frac{Q_2^3}{Q_2^2+\Lambda_2^2}\frac{1}{M^2-\Lambda_3^2}\frac{1}{m^2Q_1^2Q_2^2} \\ & \times\left[\ln\left[1+\frac{(\Lambda_3^2+Q_1^2+Q_2^2-R^{\Lambda_3})(Q_1^2-R_1^m)(Q_2^2-R_2^m)}{8m^2Q_1^2Q_2^2}\right]\right. \\ & \left.-\ln\left[1+\frac{(M^2+Q_1^2+Q_2^2-R^{M})(Q_1^2-R_1^m)(Q_2^2-R_2^m)}{8m^2Q_1^2Q_2^2}\right]\right]. \end{aligned} \tag{E.7}$$

Obtained two-dimensional representation may be integrated numerically.

Appendix F

Angular integration in the three-particle phase space integral

The angular integral of interest is given by

$$\begin{aligned}\Omega = \int_0^{\pi} \mathrm{d}\cos\theta_1 \int_0^{2\pi} \mathrm{d}\theta_2 \, \frac{2}{2m^2 - 2m_1^2 + q_1^2 + t_1 - t - t\beta_1\beta\cos\theta_1} \\ \times \frac{2}{2m^2 - 2m_2^2 + q_2^2 - t + t_2 + t\beta_2\beta(\sin\theta_1\cos\theta_2\sin\theta + \cos\theta_1\cos\theta)}.\end{aligned} \tag{F.1}$$

It can be simplified as follows

$$\Omega = -\frac{4}{\beta_1\beta_2\beta^2 t^2} \int_0^{\pi} \mathrm{d}\cos\theta_1 \int_0^{2\pi} \mathrm{d}\theta_2 \, \frac{1}{\cos\theta_2\sin\theta_1\sin\theta + \cos\theta_1\cos\theta + b} \frac{1}{\cos\theta_1 + a} \tag{F.2}$$

with

$$\begin{aligned} a &= -\frac{2m^2 - 2m_1^2 + q_1^2 - t + t_1}{t\beta_1\beta}, \\ b &= \frac{2m^2 - 2m_2^2 + q_2^2 - t + t_2}{t\beta_2\beta}. \end{aligned} \tag{F.3}$$

The integral over the azimuthal angle θ_2 gives

$$\int_0^{2\pi} \mathrm{d}\theta_2 \, \frac{1}{\cos\theta_2\sin\theta_1\sin\theta + \cos\theta_1\cos\theta + b} = -\frac{2\pi}{\sqrt{(b + \cos\theta_1\cos\theta)^2 - \sin^2\theta_1\sin^2\theta}} \tag{F.4}$$

Introducing a change of variables $\cos\theta_1 = z$ we obtain

$$\Omega = \frac{8\pi}{\beta_1\beta_2\beta^2 t^2} \int_{-1}^{1} \mathrm{d}z \frac{1}{\sqrt{(b + z\cos\theta)^2 - (1 - z^2)\sin^2\theta}} \frac{1}{z + a}. \tag{F.5}$$

It is convenient to rearrange the integrand of the latter equation as

$$\frac{1}{\sqrt{(b + z\cos\theta)^2 - (1 - z^2)\sin^2\theta}} = \frac{1}{\sqrt{(z + b\cos\theta)^2 - (1 - b^2)\sin^2\theta}}. \tag{F.6}$$

Here $(z + b\cos\theta)^2 - (1 - b^2)\sin^2\theta > 0$. A shift of variable $z \to z - b\cos\theta$ yields

$$\int_{-1}^{1} \mathrm{d}z \frac{1}{\sqrt{(b + z\cos\theta)^2 - (1 - z^2)\sin^2\theta}} \frac{1}{z + a} = \int_{-1-b\cos\theta}^{1-b\cos\theta} \mathrm{d}z \frac{1}{\sqrt{z^2 - (1 - b^2)\sin^2\theta}} \frac{1}{z + a - b\cos\theta}. \tag{F.7}$$

The latter integral may be easily performed which gives

$$\begin{aligned}\Omega = -\frac{4}{\beta_1\beta_2\beta^2 t^2}\frac{2\pi}{\sqrt{(a+b)^2-2ab(1+\cos\theta)-\sin^2\theta}}\Bigg\{&\log\frac{a-1}{a+1}\\ &+\log\Big[(a+b)(1-b)-b(1+\cos\theta)+ab(1+\cos\theta)+\sin^2\theta\\ &\qquad+(\cos\theta+b)\sqrt{(a+b)^2-2ab(1+\cos\theta)-\sin^2\theta}\Big]\\ &-\log\Big[-(a+b)(1+b)+b(1+\cos\theta)+ab(1+\cos\theta)+\sin^2\theta\\ &\qquad-(\cos\theta-b)\sqrt{(a+b)^2-2ab(1+\cos\theta)-\sin^2\theta}\Big]\Bigg\}.\end{aligned} \tag{F.8}$$

Bibliography

[1] J. Beringer et al. Review of Particle Physics (RPP). *Phys.Rev.*, D86:010001, 2012.

[2] In an interview of Caltech professor Harvey Newman by Computerworld UK - Gaudin, Sharon. "Collider test called a 'great milestone of mankind'". *Computerworld UK.*, Retrieved 18 February 2013.

[3] Serguei Chatrchyan et al. Observation of a new boson at a mass of 125 GeV with the CMS experiment at the LHC. *Phys.Lett.*, B716:30–61, 2012.

[4] Georges Aad et al. Observation of a new particle in the search for the Standard Model Higgs boson with the ATLAS detector at the LHC. *Phys.Lett.*, B716:1–29, 2012.

[5] F. Englert and R. Brout. Broken Symmetry and the Mass of Gauge Vector Mesons. *Phys.Rev.Lett.*, 13:321–323, 1964.

[6] Peter W. Higgs. Broken Symmetries and the Masses of Gauge Bosons. *Phys.Rev.Lett.*, 13:508–509, 1964.

[7] G.S. Guralnik, C.R. Hagen, and T.W.B. Kibble. Global Conservation Laws and Massless Particles. *Phys.Rev.Lett.*, 13:585–587, 1964.

[8] Carl D. Anderson. The Apparent Existence of Easily Deflectable Positives. *Science*, 76:238–239, 1932.

[9] Lev Davidovich Landau and Evgeny Mikhailovich Lifschitz. Production of electrons and positrons by a collision of two particles. *Phys.Z.Sowjetunion*, 6:244, 1934.

[10] Hermann Kolanoski and Peter M. Zerwas. Two photon physics. 1987.

[11] D. Williams et al. Production of the pseudoscalars π^0, η, and η' in the reaction $\gamma\gamma \to \gamma\gamma$. 1988.

[12] G.M. Shore. The U(1)(A) Anomaly and QCD Phenomenology. *Lect.Notes Phys.*, 737:235–288, 2008.

[13] S. Scherer. Chiral Perturbation Theory: Introduction and Recent Results in the One-Nucleon Sector. *Prog.Part.Nucl.Phys.*, 64:1–60, 2010.

[14] Bernard Aubert et al. Measurement of the $\gamma\gamma^* \to \pi^0$ transition form factor. *Phys.Rev.*, D80:052002, 2009.

[15] D.M. Asner, T. Barnes, J.M. Bian, I.I. Bigi, N. Brambilla, et al. Physics at BES-III. *Int.J.Mod.Phys.*, A24:S1–794, 2009.

[16] E. Czerwinski, S. Eidelman, C. Hanhart, B. Kubis, A. Kupsc, et al. MesonNet Workshop on Meson Transition Form Factors. 2012.

[17] P. Roy. Exact sum rules for the decay constant of the neutral pion. *Phys.Rev.*, D9:2631–2635, 1974.

[18] S.B. Gerasimov and J. Moulin. Check of Sum Rules for Photon Interaction Cross-Sections in Quantum Electrodynamics and Mesodynamics. *Yad.Fiz.*, 23:142–153, 1976.

[19] Stanley J. Brodsky and Ivan Schmidt. Classical photoabsorption sum rules. *Phys.Lett.*, B351:344–348, 1995.

[20] S.B. Gerasimov. A Sum rule for magnetic moments and the damping of the nucleon magnetic moment in nuclei. *Sov.J.Nucl.Phys.*, 2:430–433, 1966.

[21] S.D. Drell and Anthony C. Hearn. Exact Sum Rule for Nucleon Magnetic Moments. *Phys.Rev.Lett.*, 16:908–911, 1966.

[22] Vladimir Pascalutsa and Marc Vanderhaeghen. Sum rules for light-by-light scattering. *Phys.Rev.Lett.*, 105:201603, 2010.

[23] K.S. Kumar, Sonny Mantry, W.J. Marciano, and P.A. Souder. Low Energy Measurements of the Weak Mixing Angle. *Ann.Rev.Nucl.Part.Sci.*, 63:237–267, 2013.

[24] Randolf Pohl, Ronald Gilman, Gerald A. Miller, and Krzysztof Pachucki. Muonic hydrogen and the proton radius puzzle. *Ann.Rev.Nucl.Part.Sci.*, 63:175–204, 2013.

[25] P.A.M. Dirac. The Quantum theory of electron. 2. *Proc.Roy.Soc.Lond.*, A118:351, 1928.

[26] Paul A.M. Dirac. The Quantum theory of electron. *Proc.Roy.Soc.Lond.*, A117:610–624, 1928.

[27] H.M. Foley and P. Kusch. On the Intrinsic Moment of the Electron. *Phys.Rev.*, 73:412–412, 1948.

[28] Julian S. Schwinger. On Quantum electrodynamics and the magnetic moment of the electron. *Phys.Rev.*, 73:416–417, 1948.

[29] Fred Jegerlehner and Andreas Nyffeler. The Muon $g-2$. *Phys.Rept.*, 477:1–110, 2009.

[30] A. X. Klebnikov V. B. Berestetskii, O. N. Krokhin. *Zh. Eksp. Teor. Fiz.*, 30:788, 1956. [Sov. Phys. JETP 3 (1956) 761].

[31] W.S. Cowland. On schwinger's theory of the muon. *Nuclear Physics*, 8(0):397 – 401, 1958.

[32] J. Bailey et al. Final Report on the CERN Muon Storage Ring Including the Anomalous Magnetic Moment and the Electric Dipole Moment of the Muon, and a Direct Test of Relativistic Time Dilation. *Nucl.Phys.*, B150:1, 1979.

[33] G.W. Bennett et al. Final Report of the Muon E821 Anomalous Magnetic Moment Measurement at BNL. *Phys.Rev.*, D73:072003, 2006.

[34] G.W. Bennett et al. Measurement of the negative muon anomalous magnetic moment to 0.7 ppm. *Phys.Rev.Lett.*, 92:161802, 2004.

[35] Tatsumi Aoyama, Masashi Hayakawa, Toichiro Kinoshita, and Makiko Nio. Complete Tenth-Order QED Contribution to the Muon $g-2$. *Phys.Rev.Lett.*, 109:111808, 2012.

[36] Tatsumi Aoyama, Masashi Hayakawa, Toichiro Kinoshita, and Makiko Nio. Tenth-Order QED Contribution to the Lepton Anomalous Magnetic Moment – Sixth-Order Vertices Containing an Internal Light-by-Light-Scattering Subdiagram. *Phys.Rev.*, D85:093013, 2012.

[37] K. Fujikawa, B.W. Lee, and A.I. Sanda. Generalized Renormalizable Gauge Formulation of Spontaneously Broken Gauge Theories. *Phys.Rev.*, D6:2923–2943, 1972.

[38] Andrzej Czarnecki, Bernd Krause, and William J. Marciano. Electroweak corrections to the muon anomalous magnetic moment. *Phys.Rev.Lett.*, 76:3267–3270, 1996.

[39] Marc Knecht, Santiago Peris, Michel Perrottet, and Eduardo De Rafael. Electroweak hadronic contributions to the muon (g-2). *JHEP*, 0211:003, 2002.

[40] Andrzej Czarnecki, William J. Marciano, and Arkady Vainshtein. Refinements in electroweak contributions to the muon anomalous magnetic moment. *Phys.Rev.*, D67:073006, 2003.

[41] M. Davier, S. Eidelman, Andreas Hocker, and Z. Zhang. Confronting spectral functions from e^+e^- annihilation and tau decays: Consequences for the muon magnetic moment. *Eur.Phys.J.*, C27:497–521, 2003.

[42] M. Benayoun, P. David, L. DelBuono, O. Leitner, and H.B. O'Connell. The Dipion Mass Spectrum In e^+e^- Annihilation and tau Decay: A Dynamical (ρ, ω, ϕ) Mixing Approach. *Eur.Phys.J.*, C55:199–236, 2008.

[43] M. Benayoun, P. David, L. DelBuono, and O. Leitner. A Global Treatment Of VMD Physics Up To The ϕ: I. e^+e^- Annihilations, Anomalies And Vector Meson Partial Widths. *Eur.Phys.J.*, C65:211–245, 2010.

[44] M. Davier, A. Hoecker, B. Malaescu, C.Z. Yuan, and Z. Zhang. Reevaluation of the hadronic contribution to the muon magnetic anomaly using new $e^+e^- \to \pi^+\pi^-$ cross section data from BABAR. *Eur.Phys.J.*, C66:1–9, 2010.

[45] M. Davier, A. Hoecker, G. Lopez Castro, B. Malaescu, X.H. Mo, et al. The Discrepancy Between tau and e^+e^- Spectral Functions Revisited and the Consequences for the Muon Magnetic Anomaly. *Eur.Phys.J.*, C66:127–136, 2010.

[46] Michel Davier, Andreas Hoecker, Bogdan Malaescu, and Zhiqing Zhang. Reevaluation of the Hadronic Contributions to the Muon $g-2$ and to $\alpha(M_Z)$. *Eur.Phys.J.*, C71:1515, 2011.

[47] Fred Jegerlehner and Robert Szafron. $\rho^0 - \gamma$ mixing in the neutral channel pion form factor F_π^e and its role in comparing e^+e^- with τ spectral functions. *Eur.Phys.J.*, C71:1632, 2011.

[48] Kaoru Hagiwara, Ruofan Liao, Alan D. Martin, Daisuke Nomura, and Thomas Teubner. $(g-2)_\mu$ and $\alpha(M_Z^2)$ re-evaluated using new precise data. *J.Phys.*, G38:085003, 2011.

[49] M. Benayoun, P. David, L. DelBuono, and F. Jegerlehner. An Update of the HLS Estimate of the Muon $g-2$. *Eur.Phys.J.*, C73:2453, 2013.

[50] Fred Jegerlehner. Application of Chiral Resonance Lagrangian Theories to the Muon $g-2$. *Acta Phys.Polon.*, B44(11):2257–2266, 2013.

[51] Joaquim Prades, Eduardo de Rafael, and Arkady Vainshtein. Hadronic Light-by-Light Scattering Contribution to the Muon Anomalous Magnetic Moment. 2009.

[52] Thomas Blum, Achim Denig, Ivan Logashenko, Eduardo de Rafael, B. Lee Roberts, et al. The Muon $g-2$ Theory Value: Present and Future. 2013.

[53] B. Lee Roberts. The Fermilab muon $g-2$ project. *Nucl.Phys.Proc.Suppl.*, 218:237–241, 2011.

[54] Hiromi Iinuma. New approach to the muon $g-2$ and EDM experiment at J-PARC. *J.Phys.Conf.Ser.*, 295:012032, 2011.

[55] Vladimir Pascalutsa, Vladyslav Pauk, and Marc Vanderhaeghen. Light-by-light scattering sum rules constraining meson transition form factors. *Phys.Rev.*, D85:116001, 2012.

[56] W. Heisenberg and H. Euler. Consequences of Dirac's theory of positrons. *Z.Phys.*, 98:714–732, 1936.

[57] Robert Karplus and Maurice Neuman. Non-Linear Interactions between Electromagnetic Fields. *Phys.Rev.*, 80:380–385, 1950.

[58] V.M. Budnev, I.F. Ginzburg, G.V. Meledin, and V.G. Serbo. The Two photon particle production mechanism. Physical problems. Applications. Equivalent photon approximation. *Phys.Rept.*, 15:181–281, 1975.

[59] L.G. Landsberg. Electromagnetic Decays of Light Mesons. *Phys.Rept.*, 128:301–376, 1985.

[60] Johan Bijnens and Fredrik Perrsson. Effects of different form-factors in meson photon photon transitions and the muon anomalous magnetic moment. 1999.

[61] M.R. Whalley. A Compilation of data on two photon reactions. *J.Phys.*, G27:A1–A121, 2001.

[62] D. Morgan, M.R. Pennington, and M.R. Whalley. A Compilation of data on two photon reactions leading to hadron final states. 1994.

[63] M.P. Locher and B.S. Zou. Multi - pion production in photon-photon collisions. *Z.Phys.*, C56:103–106, 1992.

[64] Christoph Berger and W. Wagner. Photon-Photon Reactions. *Phys.Rept.*, 146:1, 1987.

[65] Johan Bijnens, Albert Bramon, and Fernando Cornet. Pseudoscalar Decays Into Photon-photon in Chiral Perturbation Theory. *Phys.Rev.Lett.*, 61:1453, 1988.

[66] Stefan Scherer. Introduction to chiral perturbation theory. *Adv.Nucl.Phys.*, 27:277, 2003.

[67] P. Aguar-Bartolome et al. A new determination of the η transition form factor in the Dalitz decay $\eta \to e^+e^-\gamma$ with the Crystal Ball/TAPS detectors at the Mainz Microtron. 2013.

[68] M.N. Achasov, V.M. Aulchenko, K.I. Beloborodov, A.V. Berdyugin, A.G. Bogdanchikov, et al. Study of Conversion Decays $\phi \to \eta e^+e^-$ and $\eta \to \gamma e^+e^-$ in the Experiment with SND Detector at the VEPP-2M Collider. *Phys.Lett.*, B504:275–281, 2001.

[69] R.R. Akhmetshin et al. Study of the processes $e^+e^- \to \eta\gamma\pi 0\gamma \to 3\gamma$ in the c.m. energy range 600-MeV to 1380-MeV at CMD-2. *Phys.Lett.*, B605:26–36, 2005.

[70] J. Gronberg et al. Measurements of the meson - photon transition form-factors of light pseudoscalar mesons at large momentum transfer. *Phys.Rev.*, D57:33–54, 1998.

[71] J.P. Lees et al. Measurement of the $\gamma\gamma^* \to \eta_c$ transition form factor. *Phys.Rev.*, D81:052010, 2010.

[72] H.J. Behrend et al. A Measurement of the π^0, η and η' electromagnetic form-factors. *Z.Phys.*, C49:401–410, 1991.

[73] P. del Amo Sanchez et al. Measurement of the $\gamma\gamma^* \to \eta$ and $\gamma\gamma^* \to \eta'$ transition form factors. *Phys.Rev.*, D84:052001, 2011.

[74] Amand Faessler, C. Fuchs, and M. I. Krivoruchenko. Dilepton spectra from decays of light unflavored mesons. *Phys. Rev. C*, 61:035206, Feb 2000.

[75] Masayasu Harada and Koichi Yamawaki. Hidden local symmetry at loop: A new perspective of composite gauge boson and chiral phase transition. *Physics Reports*, 381(1–3):1 – 233, 2003.

[76] C. Terschluseen, Diploma Thesis, Gießen, 2010, http://www.fysast.uu.se/leupold/research-presentation/carla-terschluesen-Dipl.pdf.

[77] Thimo Petri. Anomalous decays of pseudoscalar mesons. 2010.

[78] J.J. Sakurai. Theory of strong interactions. *Annals Phys.*, 11:1–48, 1960.

[79] Ulf G. Meissner. Low-Energy Hadron Physics from Effective Chiral Lagrangians with Vector Mesons. *Phys.Rept.*, 161:213, 1988.

[80] L. Ametller, J. Bijnens, A. Bramon, and F. Cornet. Transition form-factors in pi0, eta and eta and eta-prime couplings to gamma gamma. *Phys.Rev.*, D45:986–989, 1992.

[81] Roland Kaiser and H. Leutwyler. Pseudoscalar decay constants at large N(c). 1998.

[82] Rafel Escribano and Jean-Marie Frere. Study of the eta - eta-prime system in the two mixing angle scheme. *JHEP*, 0506:029, 2005.

[83] B. Borasoy and R. Nissler. Two photon decays of pi0, eta and eta-prime. *Eur.Phys.J.*, A19:367–382, 2004.

[84] R. Arnaldi et al. Study of the electromagnetic transition form-factors in $\eta \to \mu^+\mu^-\gamma$ and $\omega \to \mu^+\mu^-\pi^0$ decays with NA60. *Phys.Lett.*, B677:260–266, 2009.

[85] M. Poppe. Exclusive Hadron Production in Two Photon Reactions. *Int.J.Mod.Phys.*, A1:545–668, 1986.

[86] G.A. Schuler, Frits A. Berends, and R. van Gulik. Meson photon transition form-factors and resonance cross-sections in e^+e^- collisions. *Nucl.Phys.*, B523:423–438, 1998.

[87] Chen-Ning Yang. Selection Rules for the Dematerialization of a Particle Into Two Photons. *Phys.Rev.*, 77:242–245, 1950.

[88] P. Achard et al. $f_1(1285)$ formation in two photon collisions at LEP. *Phys.Lett.*, B526:269–277, 2002.

[89] P. Achard et al. Study of resonance formation in the mass region 1400-MeV to 1500-MeV through the reaction $\gamma\gamma \to K^0_S K^\pm \pi^\mp$. *JHEP*, 0703:018, 2007.

[90] Robert N. Cahn. Production of Spin 1 Resonances in $\gamma\gamma$ Collisions. *Phys.Rev.*, D35:3342, 1987.

[91] Robert N. Cahn. Cross-sections for Single Tagged Two Photon Production of Resonances. *Phys.Rev.*, D37:833, 1988.

[92] V.M. Budnev, V.L. Chernyak, and I.F. Ginzburg. Kinematics of gamma gamma scattering. *Nucl.Phys.*, B34:470–476, 1971.

[93] Steven D. Bass, Stanley J. Brodsky, and Ivan Schmidt. The Spin structure of a polarized photon. *Phys.Lett.*, B437:417–424, 1998.

[94] Duane A. Dicus, Chung Kao, and Wayne W. Repko. Effective Lagrangians and low-energy photon-photon scattering. *Phys.Rev.*, D57:2443–2447, 1998.

[95] John M. Cornwall, David N. Levin, and George Tiktopoulos. Derivation of gauge invariance from high-energy unitarity bounds on the <math><mi>s</mi></math> matrix. *Phys. Rev. D*, 10:1145–1167, Aug 1974.

[96] E. Llanta and R. Tarrach. Polarizability Sum Rules in QED. *Phys.Lett.*, B78:586, 1978.

[97] Duane A. Dicus and Roberto Vega. The Drell-Hearn sum rule at order alpha**3. *Phys.Lett.*, B501:44–47, 2001.

[98] J. Sucher and C.H. Woo. Arbitrariness of Coupling Constants in Asymptotically Free Theories. *Lett.Nuovo Cim.*, 10:111, 1974.

[99] Abdus Salam and J.A. Strathdee. Sum rules in asymptotically free theories. *Lett.Nuovo Cim.*, 10:113–114, 1974.

[100] Haim Goldberg. Gravitons and the Drell-Hearn-Gerasimov sum rule: Support for large extra dimensions? *Phys.Lett.*, B472:280–286, 2000.

[101] Hovhannes R. Grigoryan. Analyticity, Unitarity and One-loop Graviton Corrections to Compton Scattering. *JHEP*, 1210:030, 2012.

[102] Sidney R. Coleman, R. Jackiw, and H. David Politzer. Spontaneous Symmetry Breaking in the O(N) Model for Large N*. *Phys.Rev.*, D10:2491, 1974.

[103] L.F. Abbott, J.S. Kang, and Howard J. Schnitzer. Bound States, Tachyons, and Restoration of Symmetry in the 1/N Expansion. *Phys.Rev.*, D13:2212, 1976.

[104] F.J. Dyson. Divergence of perturbation theory in quantum electrodynamics. *Phys.Rev.*, 85:631–632, 1952.

[105] E. Brezin, J.C. Le Guillou, and Jean Zinn-Justin. Perturbation Theory at Large Order. 1. The phi**2N Interaction. *Phys.Rev.*, D15:1544–1557, 1977.

[106] L.N. Lipatov. Divergence of the Perturbation Theory Series and the Quasiclassical Theory. *Sov.Phys.JETP*, 45:216–223, 1977.

[107] Lev Landau. Niels bohr and the development of physics.

[108] L.D. Landau, A.A. Abrikosov, and I.M. Khalatnikov. The electron mass in quantum electrodynamics. 1954.

[109] David J. Gross and Andre Neveu. Dynamical Symmetry Breaking in Asymptotically Free Field Theories. *Phys.Rev.*, D10:3235, 1974.

[110] R. B. Dingle, *Asymptotic Expansions: Their Derivation and Interpretation*, Academic Press, New York, (1973).

[111] H. Kleinert and V. Schulte-Frohlinde. Critical properties of phi**4-theories. 2001.

[112] T. Mori et al. High statistics measurement of the cross sections of $\gamma\gamma \to \pi^+\pi^-$ production. *Journal of the Physical Society of Japan*, 76(7):074102, 2007.

[113] S. Uehara et al. High-statistics measurement of neutral pion-pair production in two-photon collisions. *Phys.Rev.*, D78:052004, 2008.

[114] S. Uehara et al. High-statistics study of eta pi0 production in two-photon collisions. *Phys.Rev.*, D80:032001, 2009.

[115] M.R. Pennington, T. Mori, S. Uehara, and Y. Watanabe. Amplitude Analysis of High Statistics Results on $\gamma\gamma \to pi^+pi^-$ and the Two Photon Width of Isoscalar States. *Eur.Phys.J.*, C56:1–16, 2008.

[116] V.A. Novikov, L.B. Okun, Mikhail A. Shifman, A.I. Vainshtein, M.B. Voloshin, et al. Charmonium and Gluons: Basic Experimental Facts and Theoretical Introduction. *Phys.Rept.*, 41:1–133, 1978.

[117] Stephen Godfrey and Stephen L. Olsen. The Exotic XYZ Charmonium-like Mesons. *Ann.Rev.Nucl.Part.Sci.*, 58:51–73, 2008.

[118] Stanley J. Brodsky and Toichiro Kinoshita. Theoretical results for sixth order contributions to the anomalous magnetic moment of the muon and electron. 1970.

[119] Stanley J. Brodsky and Glennys R. Farrar. Scaling Laws for Large Momentum Transfer Processes. *Phys.Rev.*, D11:1309, 1975.

[120] G. Ecker, J. Gasser, A. Pich, and E. de Rafael. The Role of Resonances in Chiral Perturbation Theory. *Nucl.Phys.*, B321:311, 1989.

[121] G. Ecker, J. Gasser, H. Leutwyler, A. Pich, and E. de Rafael. Chiral Lagrangians for Massive Spin 1 Fields. *Phys.Lett.*, B223:425, 1989.

[122] Avinash Dhar, R. Shankar, and Spenta R. Wadia. Nambu-Jona-Lasinio Type Effective Lagrangian. 2. Anomalies and Nonlinear Lagrangian of Low-Energy, Large N QCD. *Phys.Rev.*, D31:3256, 1985.

[123] M. Bando, T. Kugo, S. Uehara, K. Yamawaki, and T. Yanagida. Is rho Meson a Dynamical Gauge Boson of Hidden Local Symmetry? *Phys.Rev.Lett.*, 54:1215, 1985.

[124] Masako Bando, Taichiro Kugo, and Koichi Yamawaki. Nonlinear Realization and Hidden Local Symmetries. *Phys.Rept.*, 164:217–314, 1988.

[125] Masayasu Harada and Koichi Yamawaki. Hidden local symmetry at loop: A New perspective of composite gauge boson and chiral phase transition. *Phys.Rept.*, 381:1–233, 2003.

[126] Steven see also Weinberg. Nonlinear realizations of chiral symmetry. *Phys.Rev.*, 166:1568–1577, 1968.

[127] Gerard 't Hooft. A Planar Diagram Theory for Strong Interactions. *Nucl.Phys.*, B72:461, 1974.

[128] Edward Witten. Baryons in the 1/n Expansion. *Nucl.Phys.*, B160:57, 1979.

[129] A.V. Manohar. Hadrons in the 1/N expansion. 2001.

[130] H. Leutwyler. On the 1/N expansion in chiral perturbation theory. *Nucl.Phys.Proc.Suppl.*, 64:223–231, 1998.

[131] Johan Bijnens, Elisabetta Pallante, and Joaquim Prades. Hadronic light by light contributions to the muon g-2 in the large N(c) limit. *Phys.Rev.Lett.*, 75:1447–1450, 1995.

[132] Johan Bijnens, Elisabetta Pallante, and Joaquim Prades. Analysis of the hadronic light by light contributions to the muon g-2. *Nucl.Phys.*, B474:379–420, 1996.

[133] M. Hayakawa, T. Kinoshita, and A.I. Sanda. Hadronic light by light scattering effect on muon g-2. *Phys.Rev.Lett.*, 75:790–793, 1995.

[134] M. Hayakawa, T. Kinoshita, and A.I. Sanda. Hadronic light by light scattering contribution to muon g-2. *Phys.Rev.*, D54:3137–3153, 1996.

[135] M. Hayakawa and T. Kinoshita. Pseudoscalar pole terms in the hadronic light by light scattering contribution to muon g - 2. *Phys.Rev.*, D57:465–477, 1998.

[136] Vernon D. Barger, W.F. Long, and M.G. Olsson. New Evaluation of Muon (G-2) Hadronic Anomaly. *Phys.Lett.*, B60:89, 1975.

[137] J. Calmet, Stephan Narison, M. Perrottet, and E. de Rafael. Higher Order Hadronic Corrections to the Anomalous Magnetic Moment of the Muon. *Phys.Lett.*, B61:283, 1976.

[138] J. Calmet, Stephan Narison, M. Perrottet, and E. de Rafael. The Anomalous Magnetic Moment of the Muon: A Review of the Theoretical Contributions. *Rev.Mod.Phys.*, 49:21–29, 1977.

[139] L. Martinovic and S. Dubnicka. Hadronic Part of the Muon Anomalous Magnetic Moment: An Improved Evaluation. *Phys.Rev.*, D42:884–892, 1990.

[140] Marc Knecht and Andreas Nyffeler. Hadronic light by light corrections to the muon $g-2$: The Pion pole contribution. *Phys.Rev.*, D65:073034, 2002.

[141] Stephan Narison. Scalar mesons and the muon anomaly. *Phys.Lett.*, B568:231–236, 2003.

[142] Kirill Melnikov and Arkady Vainshtein. Hadronic light-by-light scattering contribution to the muon anomalous magnetic moment revisited. *Phys.Rev.*, D70:113006, 2004.

[143] Andreas Nyffeler. Hadronic light-by-light scattering in the muon $g-2$: A New short-distance constraint on pion-exchange. *Phys.Rev.*, D79:073012, 2009.

[144] Janis Aldins, Toichiro Kinoshita, Stanley J. Brodsky, and A.J. Dufner. Photon - photon scattering contribution to the sixth order magnetic moments of the muon and electron. *Phys.Rev.*, D1:2378, 1970.

[145] Stanley J. Brodsky and Jeremiah D. Sullivan. W boson contribution to the anomalous magnetic moment of the muon. *Phys.Rev.*, 156:1644–1647, 1967.

[146] Jonathan L. Rosner. Higher-order contributions to the divergent part of Z(3) in a model quan tum electrodynamics. *Annals Phys.*, 44:11–34, 1967.

[147] Michael J. Levine and R. Roskies. Hyperspherical approach to quantum electrodynamics - sixth-order magnetic moment. *Phys.Rev.*, D9:421–429, 1974.

[148] Michael J. Levine, E. Remiddi, and R. Roskies. Analytic contributions to the g factor of the electron in sixth order. *Phys.Rev.*, D20:2068–2076, 1979.

[149] F. Oberhettinger W. Magnus and R.P. Soni. Formulas and Theorems for the Special Functions of Mathematical Physics . *Springer, New York.*, page p. 218, 1966.

[150] M. Abramowitz and I. A. Stegun. Handbook of mathematical functions. *Dover Publications, New York*, page p. 771, 1970.

[151] J. Kuipers, T. Ueda, J.A.M. Vermaseren, and J. Vollinga. FORM version 4.0. *Comput.Phys.Commun.*, 184:1453–1467, 2013.

[152] S. Laporta. Hyperspherical integration and the triple cross vertex graphs. *Nuovo Cim.*, A107:1729–1738, 1994.

[153] James P. Miller, Eduardo de Rafael, and B. Lee Roberts. Muon (g-2): Experiment and theory. *Rept.Prog.Phys.*, 70:795, 2007.

[154] B. Moussallam. Unified dispersive approach to real and virtual photon-photon scattering at low energy. 2013.

[155] Gerard 't Hooft and M.J.G. Veltman. Scalar One Loop Integrals. *Nucl.Phys.*, B153:365–401, 1979.

[156] O.Yudilevich, Master Thesis, Utrecht, 2009, http://www.nikhef.nl/pub/theory/masters-theses/ori_yudilevich.pdf.